भौतिक अनुसंधान प्रयोगशाला, अहमदाबाद
Physical Research Laboratory, Ahmedabad

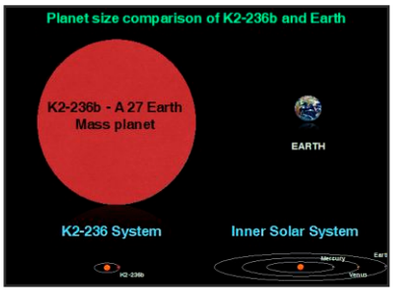

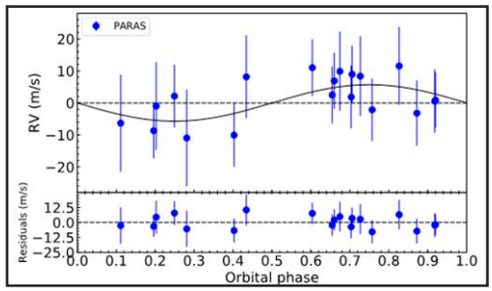

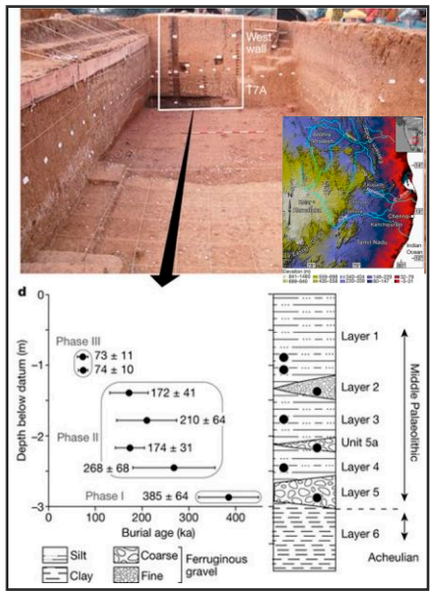

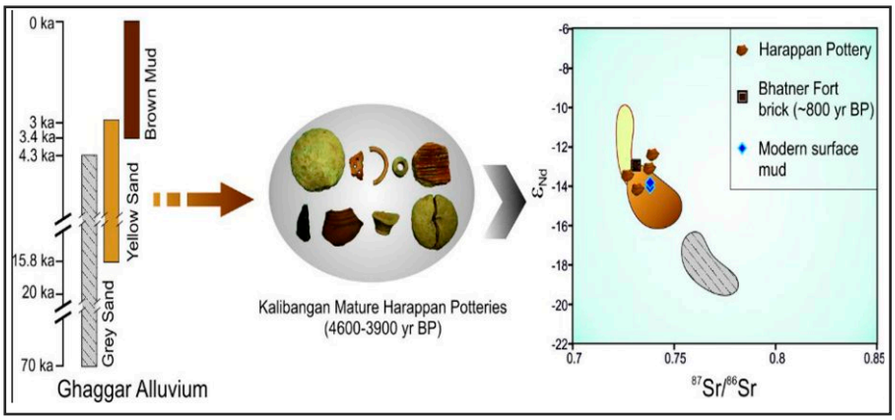

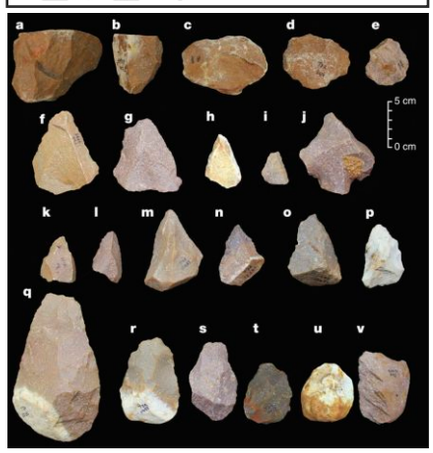

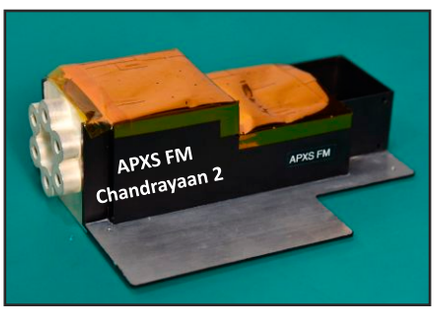

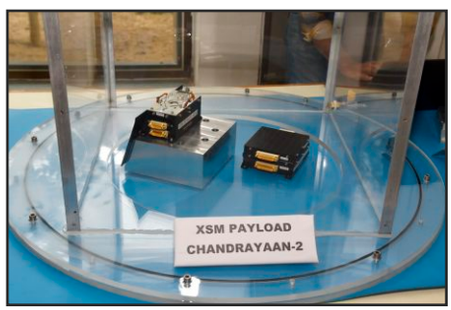

वार्षिक प्रतिवेदन
Annual Report
2017-2018

Front cover page: Top Panel: Planet Size Comparison of K2-236b & Earth and Radial Velocity (RV) data points of K2-236, observed by PARAS with 1.2m telescope of PRL at Mt. Abu. Black solid curve represents the modeled RV curve. The model shows the wobbling of the host star and its amplitude gives us the mass of the exoplanet K2-236b.

Middle Panel: Dating Ghaggar Kalibangan Potteries

Bottom Panel: APXS and XSM Payloads for Chandrayaan-2

Back cover page: Top Image: Dr. Vikram Sarabhai statue at PRL

Middle images : APXS and XSM Model details.

Bottom Image: Chandrayaan 2 payload flag off moment: December 2017

Compilation and Layout by:
Office of the Dean, PRL.

Published by:
Physical Research Laboratory, Ahmedabad.

Contact:
Physical Research Laboratory
Navrangpura
Ahmedabad - 380 009, India
Phone: +91-79-2631 4000 / 4855
Fax: +91-79-2631 4900
Cable: RESEARCH
Email: info@prl.res.in
Website: https://www.prl.res.in/

Contact

Website

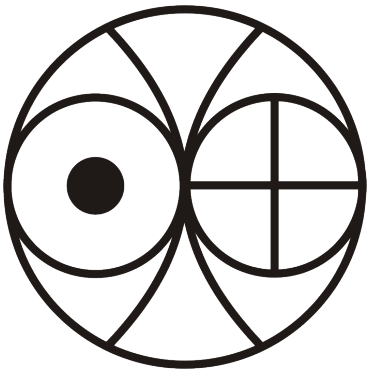

Annual Report

2017 – 2018

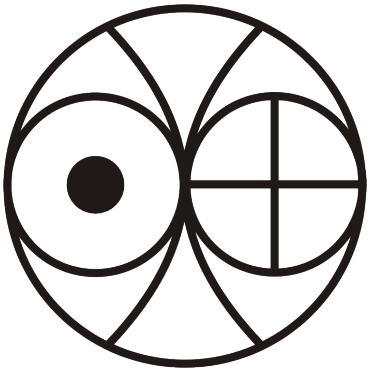

PRL research

encompasses

the Earth, the Sun

Immersed in the fields

and radiations

reaching from and to infinity,

all that man's curiosity

and intellect can reveal

PRL Council of Management

Three nominees of the Government of India

Professor U.R. Rao Antariksh Bhavan, New BEL Road Bengaluru-560231	Chairman (till 24 July 2017)
Shri A. S. Kiran Kumar Antariksh Bhavan, New BEL Road Bengaluru-560231	Chairman (from 25 July 2017)
Dr. K. Sivan, Secretary, Department of Space, Govt. of India Chairman, ISRO Bengaluru-560231	Member
Mrs. Vandita Sharma, AS & FA, DoS Antariksh Bhavan, New BEL Road Bengaluru-560231	Member (till 27 November 2017)
Shri Anoop Srivastava, JS & FA, DoS Antariksh Bhavan, New BEL Road Bengaluru-560231	Member

A nominee of the Karmakshetra Education Foundation

Shri Kartikeya V. Sarabhai Director, Centre for Environment Education Ahmedabad-380054	Member

A nominee of Ahmedabad Education Society

Shri Sanjay S. Lalbhai Chancellor & Chairman, Board of Governors, Ahmedabad University, Ahmedabad-380009	Member

A nominee of the Govt. of Gujarat, Gandhinagar

Smt. Anju Sharma, I.A.S. The Principal Secretary, Higher and Technical Education Government of Gujarat, Gandhinagar	Member

Director, Physical Research Laboratory

Dr. Anil Bhardwaj	Member (Ex-Officio)

Registrar, Physical Research Laboratory

Prof. J. S. Ray	Member (Ex-Officio) (till 8 October 2017)
Mr. C. V. R. G. Deekshitulu	Member (Ex-Officio)

Contents

Areas of Scientific Research & Activities

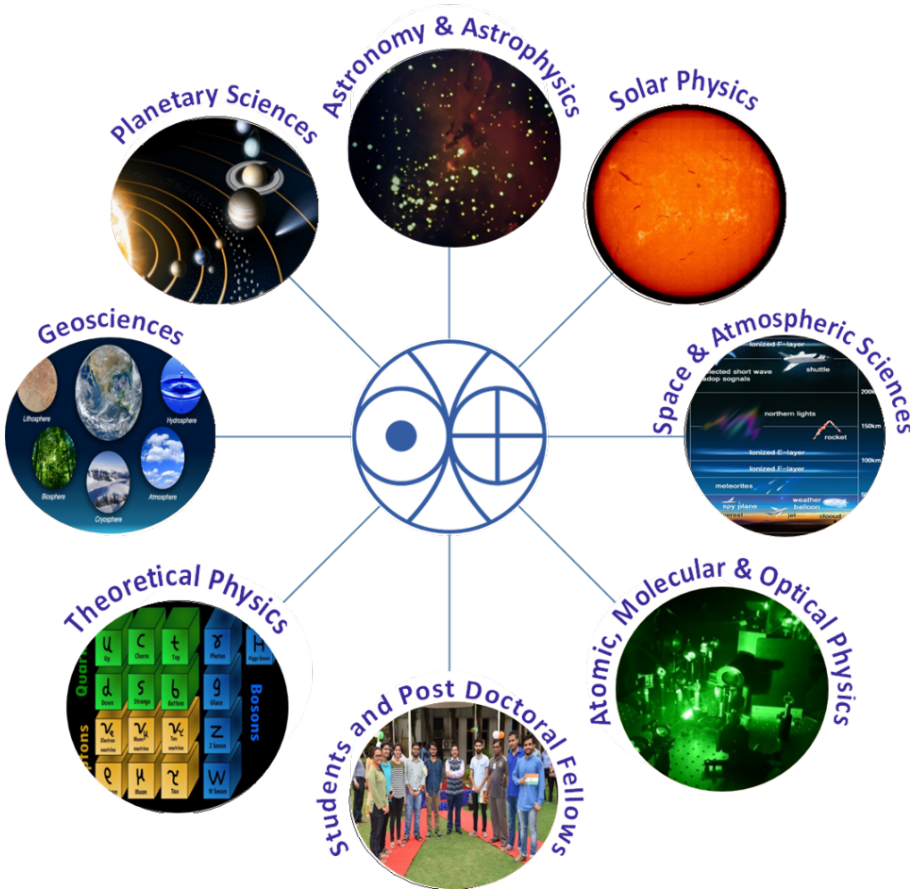

From The Director's Desk

At the outset I must record my deep sense of loss at the passing away of Prof. U. R. Rao on 24 July 2017. Prof. Rao steered PRL as it's Council Chairman for over two and half decades. My fellow colleagues and I at PRL are indebted to his vision and guidance that has held PRL as one of the leading research institutes in India, and also globally as a well-recognized research laboratory. It is important to state here that Prof. U. R. Rao was an alumni of PRL and completed his Ph.D. in year 1960 under the supervision of Prof. Vikram Sarabhai.

The PRL, under the aegis of the Department of Space, Government of India, conducts cutting-edge research in many domains of Astronomy and Astrophysics, Solar Physics, Space and Atmospheric Sciences, Atomic-Molecular and Optical Physics, Astrochemistry, Geosciences, Planetary Sciences, and Theoretical Physics, as well as well as design and development of new ground-based research instruments and space mission-based scientific experiments (payloads). The mandate of the Laboratory is to carry out fundamental research, publish scientific papers in the respective fields of expertise, and to design and develop appropriate instrumentation and experiments to enable realization of specific science goals. With over two hundred research publications in high-impact peer-reviewed journals, and 11 Ph.D. theses in the last one year, I can say with pride that PRL is carrying out its scientific and socital obligations through producing high quality research and producing competent and highly trained researchers through its academic and outreach programs. Moreover all this is done by the PRL members with a very high level of commitment, dedicated efforts, and sincerity.

During the one year, several of new and important scientific findings have been reported by PRL scientists in the frontier areas of research mentioned above; a few selected of which are briefly mentioned in this report. Very significant progress has been made in initiatives on the large projects, like the establishment of a new 2.5 m telescope facility at Mt. Abu, along with the development of back-end instruments, femto-second laser Lab, establishing a facility for hard X-ray focusing optics, and the like. A 1 MeV Accelerator Mass Spectrometer – Accelerator Unit for Radioisotope Studies (PRL-AURiS) has been installed at Thaltej Campus of PRL and tuned for the measurement of rare isotopes such as ^{14}C, ^{10}Be and ^{26}Al.

One of the major scientific highlights of the year is the discovery of a sub-Saturn or super-Neptune size planet (mass about 27 Earth Mass, and size 6 Earth Radii) around a Sun-like star. The new planet is known as EPIC 211945201b or K2-236b. This discovery is made by measuring the mass of the planet using the indigenously designed "PRL Advance Radial-velocity Abu-sky Search" (PARAS) spectrograph integrated with 1.2 m Telescope at PRL's Gurushikhar Observatory in Mount Abu, India. Only 23 such exo-planetary systems (including this discovery) are known to this date with masses between 10 and 70 Earth mass and size of 4 to 8 Earth radii with such precision. This discovery is important for understanding the formation mechanism of such super-Neptune or sub-Saturn size planets that are too close to the host star, as well as planet formation around Sun-like stars. With this discovery, India has joined a handful of countries, which have discovered planets around stars beyond our solar system. Further, PARAS is the first of it's kind of spectrograph in Asia, and among a very few spectrographs that exist around the world, which can measure, with such precision, the mass of a planet going around a star. This discovery has been acclaimed by the global scientific community and applauded by ISRO-DOS and the Honourable Prime Minister of India.

Using the CZT-Imager onboard the Indian multi-wavelength astronomy satellite AstroSat, the most sensitive hard X-ray polarization measurements of the Crab nebula and pulsar have been made. These are the very first results on the variation of the hard X-ray polarization properties of the Crab pulsar as a function of its pulse phase. The observations cannot be explained by any of the present pulsar X-ray emission models and is likely to result in completely new understanding of the X-ray emission from the pulsars.

Decimetric emission was detected from a solar flare located 500 arcsec away from a flaring site. This was shown to be due to the wave ducting effect, as observed from the first high time cadence Giant Meterwave Radio Telescope (GMRT) solar images at 610 MHz. Numerical simulations using the PRL's 100 TF cluster computing facility (Vikram-100) are carried out to understand the physics behind generation of spontaneous current ribbons, possible candidates for coronal heating. The study revealed the autonomous generation of current ribbons with the chaoticity of magnetic field lines, ubiquitous in complexly structured plasma of coronal active regions.

The payloads - Solar X-ray Monitor (XSM), Alpha Particle X-rays Spectrometer (APXS), and Chandra's Thermophysical Experiment (ChaSTE) for the upcoming Chandrayaan-2 Orbiter, Rover, and Vikram Lander missions, respectively, are delivered to project and integarted with the Chandrayaan-2 spacecraft. Development of the ASPEX payload for the Aditya-L1 mission is progressing well. The work on design and development of payloads for the future planetary and space missions is also going on smoothly.

Mukundpura is a new CM chondrite which fell in Mukundpura village near Jaipur, Rajasthan, India on June 6, 2017 at 5:15 IST. According to eyewitnesses, the stony object was fragmented into several pieces once it hit the ground. Based on petrography, mineralogy and bulk composition, Mukundpura is classified as CM2 chondrite. This rare type of specimen is the fifth carbonaceous meteorite fall in India since 1890.

It was believed until recently that modern human ancestors moved out of Africa and settled in various places around the world where they left their mark by introducing small tools, around 140,000—120,000 years ago. However, our recent study has revealed stunning new evidence that small tools — as opposed to larger ones that characterised early human species — were being made at this site way before — nearly 385,000 years ago, suggesting that humans have settled in Southern India much earlier than believed till now.

The ephemeral Ghaggar-Hakra River of northwestern India has been considered to be the remnant of an ancient perennial glacier-fed river (Vedic Saraswati). The exact reason and timing of major hydrological change of this river remains speculative. New study by PRL indicated that the river did have glacial sources during the early Holocene period. However, during the time of the Mature Harappans the Ghaggar had already become a foothill-fed river. The hygroscopic growth factors derived based on aerosol scattering coefficient measurements made with an indigenously developed adsorption based diffusion dryer system show a strong linear dependence on relative humidity which has implications to aerosol radiative properties and forcing.

A comprehensive analysis of neutrino decay was performed in the context of the India-based Neutrino Observatory (INO) experiment. A full three flavour framework and matter effect was included in the study for the first time. It was shown that atmospheric neutrinos at INO can constrain the decay parameter better than the long-baseline experiments. To explain both neutrino mass and dark matter, the Standard Model was extended by singlet fermions and scalars, respectively. It was shown that these two sectors get connected when we consider the stability of the vacuum. Parameter spaces consistent with neutrino oscillation data, Dark Matter and vacuum stability/meta-stability was delineated. The existing conflict between the measurements of matter perturbation peer spectrum determined from cosmic microwave background and LSS was resolved by invoking a cosmological viscosity of dark matter. The bounds on neutrino mass in this case is further constrained compared to the standard LCDM cosmology.

A detailed observational analysis of a hot molecular core in the high-mass star-forming region using Atacama Large Millimeter/submillimeter Array data showed many complex organic molecules in the source including a pre-biotic species among the COMs in the source.

A compact, simple and robust high brightness entangled photon source at room temperature was produced based on a 30-mm-long periodically poled Potassium titanyl phosphate crystal. The source produces non-collinear, type-0, phase-matched, degenerate photons at 810 nm with spectral brightness as high as $\sim$0.41$\pm$0.02 ($\sim$0.025$\pm$0.02) MHz/mW/nm for multi (single) mode fiber coupling. So far, this is the highest number of degenerate photons generated using a continuous-wave laser pumped bulk crystal and detected using multimode fiber. A simple generic experimental scheme is developed to generate hybrid entangled states in polarization and orbital angular momentum through direct transfer of classical non-separable states of the pump beam in parametric down conversion process.

As a part of societal commitment and capacity building, PRL contributes by providing highly skilled researchers through its vibrant Doctoral and Post-Doctoral programmes. In addition, PRL conducts a Visiting Scientist programme for university teachers, and project training for graduate and post graduate students in both science and engineering to conduct project work. PRL organizes intensive summer programmes for students as well as college and university teachers every year and also partake through its association with similar programmes conducted by the Indian Science Academies.

Around sixty graduate and undergraduate students were trained this year in the PRL Summer Research Programme. PRL is entrusted with the responsibility of conducting United Nations CSSTEAP course on Space and Atmospheric Sciences for the Asia-Pacific region for more than two decades. The tenth course with twelve students was completed on 30 April 2017. The new course, eleventh in series, has started in August 2018. PRL continues its strong academic association with many universities and institutes in Gujarat and allover the country.

PRL scientists continue to get recognized at both national and international academic fora. This year the recognitions include ISRO's Outstanding Achievement Award, Fellowship of Indian National Science Academy, Decennial Award of Indian Geophysical Union, Membership to Indian National Young Academy of Science, Young Associate of Indian Academy of Sciences, Vice-President of Indian National Science Academy, Vice-Chairman of United Nations Group of Experts on Scientific Aspects of Marine Environmental Protection,

Member C11 Commission of particles and fields of International Uniuon of Pure and Applied Physics. PRL faculty members serve on the Editorial Board of many leading national and International journals, and have received Certificate of Outstanding Contribution in Reviewing from international journals. They are member of the Governing Council and Scientific Advisory Committees of several academic and research institutions, and government departments, such as SERB, DST, CSIR and MoES. Several PRL research scholars have also received best paper awards for their presentation in national and international scientific meetings, and a research scholar has won CHARUSAT inspired Gujarat Science Academy best thesis award in the category of Physical Sciences. PRL faculty have received invitations to give more than a hundred and seventy lectures at conferences, symposia, workshops, universities and other academic and research institutions.

Significant steps have been taken to ensure use of Hindi in all areas of administration and official communications. The new bilingual website of PRL with enhanced security features is operational now. Work done at PRL in implementation of Hindi in various domains has been recognized by the Town Official Language Committee and DOS. PRL also has a effervescent outreach programmes, including celebration of World Space Week in October 2017, and a two-day long open house in February 2018 that attracted over 3000 children, young school, college, and university students, and a host of other visitors across almost every social background and profession.

I am indebted to all the members of the PRL Council for their constant encouragement, invaluable advice and whole-hearted support for all the scientific activities pursued at PRL. In particular, I am grateful to Shri A. S. Kiran Kumar, Chairman, PRL Council of Management, and Dr. K. Sivan, Chairman, ISRO and Secretary Department of Space for their sage advices, unstinted support and encouragement.

Anil Bhardwaj
Director

PRL in News

1. Decimetric emission 500 arcseconds away from a flaring site: Possible scenarios from GMRT solar radio observations. This work appeared as a Community of European Solar Radio Astronomers (CESRA) “Science Nugget”, Sept 2018, accessible at https://bit.ly/2OFbPNE.
2. The work of Mr. Sanjeev Kumar Mishra and Dr. K. Durga Prasad, Planetary Science Division, PRL has been reported as a “Research Highlight” in “Nature India” on 16 July 2018. Their study assesses the spacecraft landing induced lunar surface damage by numerically evaluating the hovering time, altitude, velocity and mass of dust ejected during landing. A link to the “Nature India” report is https://go.nature.com/2y5Ftlk.
3. Prime Minister’s Tweet on Discovery of a Sub-Saturn Exoplanet around a Sun-like star (July 3, 2018).

   “Immensely proud of our scientists, who created history by discovering a sub-Saturn size planet 600 light years away from the Earth. Congratulations to them. The discovery puts India among select countries.

   https://bit.ly/2E3SvFJ”, Narendra Modi, Prime Minister of India, Through Twitter, 8:22 AM - 3 Jul 2018 (https://twitter.com/narendramodi/status/1014167536122974209).

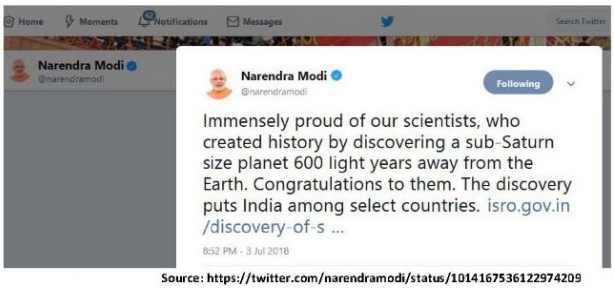

Source: https://twitter.com/narendramodi/status/1014167536122974209

4. In a landmark discovery, a team of scientists of Astronomy & Astrophysics division of PRL has discovered an exo-planet approximately 6 times larger than the earth and orbiting a Sun-like star about 600 light year away. The planet star system has been named EPIC, thereby making this an ”epic” Indian discovery. With this discovery India has joined a handful of countries which have discovered planets around stars. Significantly, the discovery was made using the PRL Advanced Radial Velocity Abu Sky (PARAS) spectrograph coupled to PRL’s 1.2 meter telescope at Mount Abu. PARAS was designed and developed at PRL, Ahmedabad and was used to measure & confirm the mass & radius of the new planet.

   This work was published as “Story of the Week” by ISRO through its web site;

   https://bit.ly/2E3SvFJ.

   ISRO also made a Press Release of this discovery on June 22, 2018 https://bit.ly/2RvJ1FP.
5. AstroSat, India’s multi-wavelength space telescope, has successfully accomplished the extremely difficult task of measuring X-ray polarisation. In a paper published in ’Nature Astronomy’, the team has documented the results of their eighteen- month study of the Crab pulsar in the Taurus constellation and measured the variations of polarisation as this highly magnetised object spins around 30 times every second. This landmark measurement puts up a strong challenge to prevailing theories of high energy X-ray emission from pulsars.AstroSat discovers strange polarisation in the Crab Nebula.

   this work was highlighted by IUCAA, Pune through a press note;

   https://bit.ly/2NqX4t7. This work was also highlighted as ISRO Story of the week.
6. A new angle on the effects of solar wind Physicists have developed a method for predicting how the interactions between fast-moving and slow-moving solar wind streams influence the Earth’s atmosphere1, particularly magnetosphere and ionosphere which have a significant effect on satellite-based technology, such as mobile communications. Scientists from the Physical Research Laboratory, Ahmedabad in India studied 43 CIR events and analysed their potential to impact the Earth’s atmosphere. When solar winds moved at angles less than 6 degrees, they formed CIR events that adversely impacted the Earth’s atmosphere. This method will be helpful for forecasting geomagnetic storms. This, in turn, allows ground stations to take appropriate measures to prevent damage to ground- and space-based communication systems.

   This research was highlighted in Nature India, in September 2017 https://go.nature.com/2RynrjR.
7. Indian scientists show how chaotic magnetic field lines result in stronger current sheets and extreme heating of the sun’s corona. It is known that the sun’s corona – the outermost layer of the sun’s atmosphere – is roughly 100 times hotter than its photosphere – the sun’s visible layer. The reason for this mysterious heating of the solar coronal plasma, however, is not yet entirely understood. A research team in Udaipur Solar Observatory, PRL has developed a set of numerical computations to shed light on this phenomenon, and this work was presented in Physics of Plasmas, from AIP Publishing, analysis examining the role of chaotic magnetic fields in potential heating mechanisms.

   https://bit.ly/2OFbomu.

Science Highlights

Astronomy and Astrophysics

- We report here strong evidence for a sub-Saturn around EPIC 211945201 and confirm its planetary nature. EPIC 211945201b was found to be a planetary candidate from *K2* photometry in Campaigns 5 & 16, transiting a bright star ($V_{mag} = 10.15$, G0 spectral type) in a 19.492 day orbit. However, the photometric data combined with false positive probability calculations using VESPA was not sufficient to confirm the planetary scenario. Here we present high-resolution spectroscopic follow-up of the target using the PARAS spectrograph (19 radial velocity observations) over a time-baseline of 420 days. We conclusively rule out the possibility of an eclipsing binary system and confirm the 2-σ detection of a sub-Saturn planet. The confirmed planet has a radius of 6.12$\pm$0.1 $R_\oplus$, and a mass of $27^{+14}_{-12.6}$ $M_\oplus$. We also place an upper limit on the mass (within the 3-σ confidence interval) at 42 $M_\oplus$ above the nominal value. This results in the Saturn-like density of $0.65^{+0.34}_{-0.30}$ g cm^{-3}. Based on the mass and radius, we provide a preliminary model-dependent estimate that the heavy element content is 60-70 % of the total mass. This detection is important as it adds to a sparse catalog of confirmed exoplanets with masses between 10-70 $M_\oplus$ and radii between 4-8 $R_\oplus$, whose masses and radii are measured to a precision of 50% or better (only 23 including this work).
- Understanding solar active region is extremely important to unravel the mystery of the million degree Kelvin atmosphere of the Sun. Active regions are clearly identified in the ultraviolet/X-ray images of the sun. They are bright compared to their surrounding and consist several loop like structures. Various dynamic features are observed in the active regions including flows and frequent transient brightenings. We study such active regions by means of various spacecraft observations and through numerical simulations, using High-Performance Computing facility of PRL. Our present studies show we can numerically model various magnetohydrodynamic waves of the active regions in three dimensions. These waves get generated after solar flares. Nature of such modeled waves resembles spacecraft observations very well. In another work, we model a phenomenon called chromospheric evaporation. Using the simulated data we also forward model the intensity dynamics of an active region loop. Comparing such intensity with the real observed intensity of a transient brightening associated loop, we conclude that chromospheric evaporation is responsible for the dynamics of such loops.
- The role of filaments in the formation of dense massive star-forming clumps and clusters is still poorly understood. Furthermore, one of the key problems in star formation research is how the filaments fragment into dense clumps/cores that produce star. We have carried out an extensive multi-wavelength study of four star-forming sites, S242, IRAS 05480+2545, IRAS 05463+2652, and Sh 2-53. These sites contain embedded filaments, which are associated with star-forming clumps. The sites, IRAS 05480+2545 and Sh 2-53 have been investigated at the junction of filaments (i.e. hub-filament system). In the site S242, the most massive clumps are observed at both the elongated filamentary structure (length $\sim$25 pc) ends, while the S242 H $_{II}$ region is located at one filamentary structure end. In the site S242, the observed results are consistent with the prediction of a star formation scenario of the end-dominated collapse driven by the higher acceleration of gas.
- The formation mechanisms of massive stars ($\gtrsim$ 8 $M_\odot$) and their feedback processes are still being debated. In recent years, the theoretical and observational studies of the cloud-cloud collision process have drawn considerable attention, which can produce massive OB stars and young stellar clusters at the junction of molecular clouds. We have found observational signatures of cloud-cloud collision in four galactic star-forming regions. These regions are G35.20-0.74,

S235, bubble N49, and bubble N37. In each site, our analysis reveals that two molecular clouds are physically connected in both space and velocity. In these regions, the collision of the molecular clouds appears to be operated, and may have triggered the formation of embedded protostars and massive stars.

- The investigation of the role of magnetic fields in the formation of large-scale structures in massive star-forming regions is a very challenging task. We have studied the molecular cloud associated with the G35.673-00.847 site (hereafter MCG35.6). Based on the multi-wavelength images, we have investigated an embedded face-on ring-like feature in the molecular cloud MCG35.6. At least five clumps seem to be distributed in an almost regularly spaced manner along the ring-like feature and contain noticeable young protostars. The starlight polarization traces the plane-of-sky magnetic field, which is oriented parallel to the major axis of the ring-like feature. Three subregions containing the clumps are found to be magnetically supercritical in the ring-like feature. Altogether, the existence of the ring-like feature and the star formation activities on its edges can be explained by the magnetic field mediated process as simulated by Li & Nakamura (2002).
- A series of near-infrared spectra of Nova Ophiuchus 2017 in the K band was obtained to record the evolution of the first overtone CO emission in unprecedented detail. Starting from 11.7d after maximum, when CO is first detected at great strength, the spectra track the CO emission to +25.6d by which time it is found to have rapidly declined in strength by almost a factor of $\sim$ 35. The cause for the rapid destruction of CO is examined in the framework of different mechanisms for CO destruction viz. an increase in photoionizating flux, chemical pathways of destruction or destruction by energetic non-thermal particles created in shocks. From LTE modelling of the CO emission, the ^{12}C/^{13}C ratio is determined to be 1.6 $\pm$ 0.3 which constitutes one of the most secure estimates of this ratio in a classical nova.
- Most sensitive hard X-ray polarization measurement for the Crab nebula and pulsar has been carried out with the CZT-Imager instrument onboard the Indian multi-wavelength astronomy satellite, AstroSat. These has yielded the very first results on the variation of the hard X-ray polarization properties of the Crab pulsar as function of its pulse phase. It has been observed that the phase dependent polarization show significant variation during the off-pulse period. This observation can not be explained by any of the present pulsar X-ray emission models and is likely to result in completely new understanding of the X-ray emission from the pulsars.
- Broad-band timing and spectral studies of accretion powered X-ray pulsars provide important information regarding the geometry, magnetic field and emission mechanism of the neutron star in the binary systems. Temporal and spectral properties of newly discovered transient X-ray pulsar Swift J0243.6+6124 were investigated by using a $NuSTAR$ observation in 2017 October when the source flux was $\sim$280 mCrab. Pulsations at 9.8542 s were detected in the X-ray light curves of the pulsar. Pulse profiles of the pulsar were found to be strongly energy dependent. Broad-band continuum spectrum of the pulsar was well described with a negative and positive exponential cutoff or high-energy cutoff power-law models modified with a hot blackbody at $\sim$3 keV. An iron emission line was also detected at 6.4 keV in the source spectrum. Results obtained from time-resolved spectroscopy suggested that the pulsar continuum was evolving with luminosity and showing effect of mass accretion rate.
- Multifrequency observation campaign of AGNs provides an opportunity to investigate different emitting regions of the central engine. An intense monitoring programme of Seyfert 1 galaxy NGC 4593 over a duration of a month with Swift observatory has been used to study the variability in six ultraviolet/optical and two soft (0.3–1.5 keV) and hard X-ray (1.5–10 keV) bands. The amplitude of the observed variability is found to decrease from high energy to low energy (X-ray to optical) bands. The variations observed in the ultraviolet/optical emission are strongly correlated with the hard X-ray band. Cross-correlation analysis provides the lags for the longer wavelengths compared to the hard X-rays which suggests that the changes in the ultraviolet/optical bands follow the variations in the hard X-ray band. This implies that the observed variation in longer wavelengths is due to X-ray reprocessing. Though, the measured lag spectrum is well described by the standard disc model, the observed lags are found to be longer than the predicted values. This implies that the actual size of the disc of NGC 4593 is larger than the estimated size of standard thin disc.
- A detailed broad-band spectral variability study of the Seyfert 1 galaxy 1H 0419-577 was carried out using six XMM-Newton observations in 2002-2003. These observations covered a large amplitude variability event during which the soft X-ray count rate increased by a factor of $\sim$4. The X-ray spectra are well described by a model consisting of a power law, blurred and distant reflection. The 2–10 keV power-law flux varied by a factor of $\sim$7 while the 0.3–2 keV soft X-ray excess flux varied only by a factor of $\sim$2. The variability event was also observed in the optical and UV bands at a variability amplitudes level of 6-10%. During the rising phase, the optical bands lagged behind the UV band but during the declining phase, the optical bands led the UV band. Such behaviour is not expected in the reprocessing models where the optical/UV emission is the result of reprocessing of X-ray emission in the accretion disc. The delayed contribution of the broad emission lines in the UV band or the changes in the accretion disc/corona geometry combined with X-ray reprocessing may give rise to the observed behaviour of the variations.
- A comprehensive timing and spectral studies of Be/X-ray binary pulsar EXO 2030+375 has been carried out by using extensive RXTE observations from 1995 till 2011. Pulse profiles of the pulsar were found to be strongly luminosity dependent. Comparison of pulse profiles showed that the features at a particular luminosity are independent of type of X-ray outbursts. This indicates that the emission geometry is solely a function of mass accretion rate. Any signature of cyclotron resonance scattering feature was absent in the spectra obtained from all the observations. Depending on source luminosity, the power-law photon index was found to be distributed in three distinct regions suggesting the phases of spectral transition from sub-critical to super-critical regimes in the pulsar.
- The observations of galaxy assemblies at higher-redshifts is very important to understand the galaxy formation in the early phase of the universe. With the aim to understand the AGN and galaxy formation at higher redshifts we have carried out deep radio survey of few extragalactic fields with Giant

Metrewave Radio Telescope (GMRT). These extragalactic fields are chosen such that they possess deep observations in the optical (VLT and Subaru), IR (Spitzer) and X-ray (XMM-N) wavelengths. Using our deep radio surveys in combination with the auxiliary multiwavelength data we have found a new population of active galactic nuclei (AGN). These galaxies are primarily radio galaxies at z $\sim$ 0.5 $-$ 4.0 which are bright in radio but faint in optical and IR wavelengths. Our study based on the small-area deep surveys also acts as a test-bed for the upcoming large-area deep surveys from Square Kilometre Array (SKA) and Large Synoptic Survey Telescope (LSST).

- Blazars, a sub-class of AGN, are extreme sources with powerful jets and violently variable flux and polarization. Since they do not have emission/absorption lines in their spectra, it is very difficult to estimate the mass of supermassive black hole (SMBH). They are also very compact and at large distances and hence un-resolvable. Mt Abu InfraRed Observatory (MIRO) 1.2m telescope was used to monitor blazar 3C66A for more than 10 years to determine intra-night (micro-variability), short term and long term variations. Using these tools, size of the emission region and mass of the SMBH were estimated as 6.92$\times 10^{14}$ cm and 3.7$\times 10^{8}\mathrm{M}_{\odot}$, respectively, taking that rapid variation of 37 mins originate near the event horizon. Blazars 3C66A was found to show short lived quasi-periodicity with 1.4 hr as period.

Solar Physics

- Using Multi-Application Solar Telescope (MAST), simultaneous images in G-band and H-alpha for studying photospheric and chromospheric coupling were obtained. Simultaneous imaging in FeI 617.3 nm and CaII 854.2 nm, and Stokes, I, Q, U and V measurements (for deriving vector magnetic field and line-of-sight velocities) and chromospheric line-of-sight velocity measurements in solar active regions have also been initiated using MAST.
- The study of the evolution of solar surface mean velocity flows over the Solar Cycle 23 and 24 shows variations of these velocity flows with the progress of the solar activity cycle, which illustrates the dynamical changes in the convective sources at the surface and sub-surface layers of the Sun.
- Observational analysis and modeling of coronal blowout jet revealed opening of previously closed magnetic field lines in the jet region. The study also shows that the jet perturbed pre-existing 'X-type' magnetic configuration of the active region that resulted a C-class solar flare.
- Formation, activation, and eruption of a flux rope from the sigmoid active region NOAA 11719 by analyzing EUV, X-ray, and radio measurements was studied. The analysis shows deviation from the standard flare model.
- A comparative study of the eruptive and confined flares produced by AR 12192 suggests that the critical decay index for the onset of torus instability was achieved at a higher height (52 Mm) over the non-eruptive core region, as compared to that over eruptive region, where it was achieved at lower height (35 Mm). The change in Lorentz force per unit area for the eruptive flare was about 4040 dyne/cm^2, which is almost three times larger than that found in the four confined cases.
- Kinematics of two CMEs observed on 13 and 14 June 2012 which originated from the same active region was studied using SECCHI/STEREO observations. The analysis reveals their interaction at a distance of 100 solar radii from the Sun. The signatures of the interaction based on the in situ observations by ACE shows that it led a moderate geomagnetic storm (Dst index $\sim$ -86 nT) with the strongest sudden storm commencement (SSC) ($\sim$150 nT) of the present solar cycle 24.
- Numerical simulations using the 100 TF cluster facility (Vikram-100) were carried out to understand the physics behind generation of spontaneous current ribbons which are believed to be possible candidates for coronal heating. The study shows the autonomous generation of current ribbons with the chaoticity of magnetic field lines, ubiquitous in complexly structured plasma of coronal active regions.

Planetary Sciences and PLANEX Program

- We have developed a model for the calculation of flare and non-flare electron density profiles due to impact of X-rays (0.5-90 Å) and Galactic Cosmic Rays (GCR) in the D and E regions of Mars' ionosphere simultaneously. In the non-flare profile case, D layer is produced at 25 km due to impact of GCR and hard X-rays (0.5-3 Å) with electron densities $1.0 \times 10^2 cm^{-3}$ and $8 \times 10^2 cm^{-3}$ respectively while E layer is produced at 100 -110 km due to impact of soft X-rays (3-90 Å) with electron density $\sim 4 - 5 \times 10^4 cm^{-3}$. The D peak density produced by hard X-rays is larger by about an order than that produced by GCR.
- Comparison of morphology of gullies is carried out within two high-latitude Martian craters (Domoni- 51.38° N; 234.41° E, and Maricourt- 53.34° N; 288.92° E) in the northern hemisphere of Mars with (1) the debris flow gully systems in the Ladakh Himalaya (34° N; 78° E) and (2) Istok Crater (45.11° S; 274.2° E) in the southern mid-latitudes of Mars where water-bearing debris-flow deposits have been previously reported. The study findings led us to suggest that the debris-flow landforms preserved on gully and alluvial fans in the Ladakh Himalaya are potential analogues for the deposits preserved over the equator-facing slopes of Domoni and Maricourt Craters.
- Mukundpura is a new CM chondrite which fell in Mukundpura village near Jaipur, Rajasthan, India on June 6, 2017 at 5:15 IST. According to eyewitnesses, the stony object was fragmented into several pieces once it hit the ground. Based on petrography, mineralogy and bulk composition, Mukundpura is classified as CM2 chondrite. This rare type of specimen is the fifth carbonaceous meteorite fall in India since 1890.
- Beni M'hira, fell on Jan. 8, 2001 in Tunisia is classified as L6 chondrite. Noble gases and nitrogen were studied in this meteorite with the objective of finding cosmic ray exposure age, as well as to look for pre-atmospheric size. Beni M'hira has trapped gases of both primordial and solar type. The latter (solar) component could be implanted either in at the time of formation in early solar system duration or during exposure at regolith. The cosmic ray exposure age of this meteorite is 15.6 Ma, and falls at the peak in ordinary chondrite histogram.
- The objective of APXS instrument is to acquire the spectral response of several soil/rock samples along the rover track in the high latitude south polar region for the major elements giving fluorescent X-rays in the energy region 1 to 25 keV.

The development of the Qualification Model (QM) and Flight Model (FM) of the APXS instrument has been completed. The developed instrument provides energy resolution of $\sim$140 eV at 5.9 keV with low energy cut-off of about 0.8 keV. The QM and FM version of the APXS has been tested for various environmental conditions and successfully passed all the tests with desired performance.

- The primary scientific objective of Solar X-ray Monitor (XSM) onboard Chandrayaan-2 Orbiter is to provide the real time solar X-ray spectrum for quantitative interpretation of lunar X-ray fluorescence spectra measured by a companion instrument Chandra's Large Area Soft X-ray Spectrometer (CLASS). The development of the Qualification Model (QM) and Flight Model (FM) of the XSM instrument has been completed. The developed instrument provides the energy resolution of $\sim$180 eV at 5.9 keV with low energy cut-off of about 0.8 keV.
- Aditya Solar wind Particle EXperiment (ASPEX) is one of the seven scientific experiments onboard the Aditya - L1 mission (the forthcoming Indian solar mission), ASPEX will carry out the in-situ, multi-directional measurements of the slow and fast solar wind, supra-thermal particles and solar energetic particles in the energy range of 100 eV to 20 MeV/n with its two sub-systems namely Solar Wind Ion Spectrometer (SWIS) and Supra Thermal & Energetic Particle Spectrometer (STEPS). The development of engineering model of STEPS, and thermal & structural analysis of the STEPS packages are being carried out presently.

Space and Atmospheric Sciences

- Nighttime black carbon concentration contributes 60% to total over an urban region, while day-night contributions are almost equal over a remote, background site owing to transport of anthropogenic emissions from the source regions. Measurements-model comparison revealed that model significantly underestimates black carbon mass over an urban source region, while over a background region the agreement is good suggests the lack of/absence of proper representation of black carbon aerosols in emission inventories over source regions.
- The hygroscopic growth factors derived based on aerosol scattering coefficient measurements made with an indigenously developed adsorption based diffusion dryer system show a strong linear dependence on relative humidity which has implications to aerosol radiative properties and forcing.
- Observations show that aerosols in higher size range ($>$100nm) are more externally mixed whereas aerosols in lower size ranges ($<$100 nm) are more internally mixed, and refractory black carbon aerosols are found to suppress the hygroscopic growth of aerosols at higher relative humidity.
- Estimation of biomass burning and photo-oxidation sources to ambient volatile organic compounds (VOCs) is ambiguous mainly due to the coexistence of a variety of emission sources in India. Analysis of high time-resolution data of atmospheric VOCs obtained from PTR-TO-FMS instrument indicates the increasing trends of biomass burning and photochemical oxidation sources during winter to summer transition in western India.
- Enhancements of carbon monoxide (CO) mixing ratio in the upper free troposphere during convective days of the tropical cyclone Nilam over peninsular India. Convective dynamics in the post-monsoon season over peninsular India lead to efficient vertical mixing and redistributions of trace gases.
- A quasi-27-day oscillation is observed at Southern hemispheric low latitude stations. The solar radiation as well as lower atmospheric convective activity are found to excite the oscillation.
- Mesospheric temperature inversions (MTIs) refer to the narrow thermal layers showing an inversion of the vertical temperature gradient from negative to positive. Several causes for the MTI occurrences have been proposed, however, due to lack of detailed statistics there has been no convergence on the mechanisms. Detailed statistical analyses of MTIs based on around five years of O_2 and OH nightglow emission intensities and temperatures data obtained from Gurushikhar, Mount Abu suggesting that chemical heating of the atmosphere due to the exothermic chemical reactions as a more probable cause as compared to the dynamical processes.
- Low latitude upper atmospheric processes are influence by equatorial processes during geomagnetic quiet conditions. During periods of geomagnetic disturbances the influence can also be from the traveling atmospheric disturbances triggered due to joule heating at high latitudes. Our investigations on geomagnetic storms that occurred during different seasons, show that although the influence of high latitude processes on low-latitude upper atmospheric behaviour is stronger during solstices, during equinoxes, the equatorial processes continue to have a strong influence on the low latitude behaviour and the associated neutral wave dynamics.

Geosciences

- The ephemeral Ghaggar-Hakra River of northwestern India has been considered to be the remnant of an ancient perennial glacier-fed river (Vedic Saraswati). The exact reason and timing of major hydrological change of this river remains speculative. Our results indicate that the river did have glacial sources during the early Holocene.
- We suggest that the method of mass fractionation is critical to accurate ^{142}Nd analysis by TIMS. Power-normalised exponential law for fractionation correction is most appropriate. ^{142}Nd/^{144}Nd ratios of Ames and JNdi-1 standards differ at least by 6 ppm.
- Marwar Supergroup of India is found to have been deposited during 700–540 Ma. There exists a depositional hiatus of $\sim$100 Ma between the lower and middle Marwars. The hiatus marks a major change in sediment provenance.
- Our stable isotope analysis of rainwater samples suggest the northeast Indian rivers carry water derived from isotopically depleted high altitude rainfall and snow melt. A hump in the d-excess time series during August suggest enhanced contribution of vapour derived from wetlands.
- Another study suggests that the southwest monsoon prominently enter the Kashmir Valley from southwest, crossing over the Pir Panjal Mountain which does not seem to be an effective orographic barrier for monsoon winds.

- Lakhshadweep coral study suggests stressed condition for coral growth after 1995 is due to increased sea surface temperature.
- Newly installed AURiS (Accelerator Unit for Radio Isotope Studies) is capable of making routine radiocarbon measurements with high precision.
- Most of the significant shifts in monsoon activity during mid-Holocene seems to have occurred within few decades followed by multi-centennial prolonged droughts.
- Highest Oxidative potential of ambient particulate matter over Mount Abu were found during post-monsoon (October-November), which is attributable to long-range transport of anthropogenically emitted pollutants brought by the NE air masses.
- In rivers draining highly populated urban centers, lower reaches and tributaries tended to exhibit higher levels of organic C and the partial pressure of CO_2 than less impacted upstream reaches and eutrophic impounded reaches, often plagued by frequent algal blooms and pulsatile CO_2 emissions from urban tributaries delivering high loads of wastewater.
- Enriched isotope tracers experiments suggests that the overall consumption of both NH_4^+ and NO_3^- exceeded the production rates in the Western Ghat's soils, even with the presence of high ambient nutrient concentrations. This indicates the presence of a nutrient conservation mechanism, especially for NH_4^+, adapted by the microbes present in these systems.
- Comparing the bulk elemental composition especially the REE abundances of Mukundpura shows good agreement with the CM carbonaceous chondrite.
- Recommendations are made for improvements in N deposition estimation through changes in observations, modelling and model–observation comparison procedures.

Theoretical and Computational Physics

- Superconductivity is the phenomenon in which at very low temperatures (typically below 30 K) certain metals show no resistance to the flow of electric current. The phenomenon was discovered by Kammerling Onnes in 1911, and was theoretically explained by John Bardeen, Leon Cooper, and Robert Schrieffer in 1957(the BCS paradigm). In 1986, superconductivity was discovered in unexpected materials called cuprates which superconduct at comparatively higher temperatures (of the order of 100 K). These materials go beyond the BCS paradigm, and at present, we do not have the understanding of the mechanism of superconductivity in these materials. The normal state out of which superconductivity emerges is very unconventional, and is not understood. This field, now popularly known as the field of unconventional superconductivity experiences another revival with the discovery of pnictide materials in 2008. The field has seen many different paradigms like RVB, magnetic spin fluctuation mechanisms, and the paradigm of quantum criticality. But there are problems with these paradigms. We present a survey of these developments. An objective critical analysis of the facts shows that the right direction is already there in the literature, however, much needs to be done. We will present an overview of our recent investigations in that direction, and summarize the open problems.
- The effect of non-standard interactions (NSI) on the propagation of neutrinos through matter was studied. It was found that for the special case when the diagonal NSI parameter cancels the standard matter effect, though the hierarchy sensitvity is seriously compromised the discovery of CP violation is not affected due to this degeneracy. This study was done in the context of the proposed DUNE experiment.

  In an attempt to explain both neutrino mass and Dark Matter the Standard model was extended by singlet fermions and scalars respectively. It was shown that these two sectors get connected when we consider the stability of the vacuum. Parameter spaces consistent with neutrino oscillation data, Dark Matter and vacuum stability/meta-stability was delineated.

  A comprehensive analysis of neutrino decay was perforemd in the context of the India-based Neutrino Observatory (INO) experiment. A full three flavour framework and matter effect was included in the study for the first time. It was shown that atmospheric neutrinos at INO can constrain the decay parameter better than the long-baseline experiments.
- Since the last and remaining piece of the standard model of particle physics is discovered, efforts went into measuring at the properties of this Higgs boson. Even more importantly, primary focus is now on finding any indication for the physics beyond this established model of standard model (BSM).

  Large Hadron Collider (LHC) already collected a significant amount of high energy data to push the exclusion limits quite high at the range of TeV energy scale for many of the popular existing BSM scenario. Hence, the significant amount of theoretical study is focused into two primary directions. First one is to find the different scenario with the exotic production and their decay which can possibly evade such strong exclusion limits. Compressed nature of mass spectra within a BSM model can bring one such possibility. Comprehensive study is carried out for different compressed region of parameter space and proposed different search strategy and also suitable kinematic variables to uncover such hidden events.

  Second class of study is involving some of the new class of observables and analysis which can bring out yet unexplored new events into our study. Fat-jet, jet-substructure and machine learning techniques are some of them we are seriously exploring in this context.
- Did the science study for the 3 meter Terahetz telescope proposal. The mapping of the galactic CO with terahertz observations can lead to the determination of a more accurate rotation curve of the Milky Way which will in turn map the density of dark matter in the galaxy.
- The existing conflict between the measurements of matter perturbation peer spectrum determined from CMB and LSS was resolved by a invoking a cosmological viscosity of dark matter. The bounds on neutrino mass in this case is further constrained compared to the standard LCDM cosmology.

Atomic, Molecular and Optical Physics

- The NGC 1333 IRAS 4A, a protostellar binary, hosts to core A1 and A2. A number of complex organic molecules (COMs) have been observed in A2 and it shows hot-corino activities. The other core shows star formation activities but no COMs have been reported till now. For the first time, we have discovered

traces of COMs in the A1 core and speculate that it shows hot-corino activity. Till now only a few known hot-corino are there, using high resolution ALMA observation we discovered a new hot-corino, NGC 1333 IRAS 4A1.

- We report a detail observational analysis of a hot molecular core (HMC) in the high-mass star-forming region G31.41+0.31. Using ALMA data , we report many complex organic molecules (COMs) in the source. For the first time, we report a pre-biotic species among the COMs in the source G31.41+0.31, outside the Galactic center. Our observation show COMs produce in the hot-dense medium in the HMC, G31.41+0.31.
- We report the first time collection of more than 1000 fragments of a meteorite within one meter of the impact crater. This has implications in understanding the impactor fragmentation and projectile survival from impact events.
- In order to understand the physico-chemical nature of benzonitrile ices at astrochemical icy conditions, the spectroscopic details of benzonitrile ices are imperative. Here, we present the VUV and IR spectra of nano-blocks of benzonitrile formed in astrochemical icy conditions.
- The finding of reversible phase change in astrochemical ices demanded more experiments to examine the reversible phase change in ice layers/mixtures containing ethanethiol. In the follow up experiments using ethanethiol – water layered ices, it is clearly observed that the reversible phase change does occur under a layer of water ice. Therefore, it is evident that the reversible phase change may not due to liquefaction of crystalline ices at higher temperatures and ultrahigh vacuum conditions.
- Estimation of thermal history of North Almora Thrust fault using newly established thermochronology technique.
- Study of luminescence response of amorphous glasses for very high radiation doses (100Gy to 50kGy)
- Establishing chronology of oldest archaeological tools in India.
- The simulation of electron and ion trajectories in electrostatic lens have been performed for development of velocity map imaging spectrometer. The simulated results are recently published in IEEE journal.
- The cis and trans isomers identification using the Coulomb Explosion Imaging (CEI) method has been performed on $C_2H_2Br_2$, $C_2H_2CL_2$ and difluoroiodobenzene molecules. This method is successful for identification of isomers. This work is appeared in IOP Journal.
- We have demonstrated that in spontaneous parametric down conversion (SPDC) process amplitude distribution of the pump beam could be obtained simply by spatial filtering of individual (signal or idler) photons from the total SPDC distribution.
- We have addressed the possibility of using even/odd states of orbital angular momentum (OAM) of photons for the quantum information tasks.
- We have provided a method for complete experimental Stokes characterization of a broad range of random fields.
- We have reported linear and nonlinear generation of ultrafast hollow Gaussian beams (HGBs). Using only two spiral phase plates (SPPs) having phase variation corresponding to vortex orders, l=1 and 2, and an experimental scheme, we have generated high power, ultrafast HGBs of orders up to 3 at 1064 nm.
- We have reported on single-pass optical parametric generation for high power, high repetition rate (RR), ultrafast broadband optical radiation in the mid-IR.
- We have reported a simple generic experimental scheme to generate hybrid entangled states in polarization and OAM through direct transfer of classical non-separable states of the pump beam in parametric down conversion process.
- We have reported on a compact, simple and robust high brightness entangled photon source at room temperature. Based on a 30-mm-long PPKTP crystal, the source produces non-collinear, type-0, phase-matched, degenerate photons at 810 nm with spectral brightness as high as $\sim 0.41 \pm 0.02 (\sim 0.025 \pm 0.02)$ MHz/mW/nm for multi (single) mode fiber coupling. So far, this is the highest number of degenerate photons generated using a continuous-wave laser pumped bulk crystal and detected using multimode fiber.

Awards and Honors

A. S. Kiran Kumar

1. HK Firodia Vijnan Ratna Award by HK Firodia Foundation in 2017
2. Special Achievement Award 2017 by Geospatial World Forum
3. India's Global Icon Award 2017 by Times Now Global
4. One Globe Award 2017

Anil Bhardwaj

5. "Outstanding Achievement Award" of ISRO, 2017.
6. "Decennial Award" of Indian Geophysical Union, 2017.
7. "Letter of Felicitation", by the Uttar Pradesh (UP) State Government, at First UP Divas, for "Distinguished work in Science and Technology", 2018.
8. "Lunar and Planetary Society's Endowment Lecture" , Gujarat Science Academy, 2018.

A.K. Singhvi

9. Elected, Vice President, Indian National Science Academy 2018-2020.
10. Marwar Ratna Award by the Mehrangarh Museum Trust, Jodhpur.

M. M. Sarin

11. Vice-Chairman (2017-18), United Nations Group of Experts on Scientific Aspects of Marine Environmental Protection - An interagency advisory body of the United Nations.

S. Goswami

12. Elected as the Fellow of Indian National Science Academy, 2018.
13. Selected as a member of the C11 Commission of Particles and Fields of International Union of Pure and Applied Physics, 2018.

Som Kumar Sharma

14. Elected Vice-Chairman Indian Meteorological Society, Ahmedabad chapter.

B. Sivaraman

15. Elected as member of the Indian National Young Academy of Science (INYAS) – 2017.

B. Joshi

16. Awarded grants for Indo-Austrian DST- BMWFW bilateral research project entitled "Onset of solar flares and flare-CME associations" which will be implemented during 2017–2019.

A. Singh

17. Elected Young Associate, Indian Academy of Sciences (IAS), Bangalore, 2017.

Recognition, Best paper & Thesis awards

Anil Bhardwaj

1. Represented India at the "CIENCIA 2017", National Science Summit of Portugal, Lisbon, July 3-5, 2017.
2. Moderator of "Space Exploration Session", in the 24^{th} Session of the Asia-Pacific Regional Space Agency Forum (APRSAF-24), Bengaluru, India, 14-17 November, 2017.
3. Member, Science Organizing Committee,"International Conference On Mars Aeronomy, Boulder, Colorado, USA", 15-19 May, 2017.
4. Member, Scientific Organizing Committee, International Astronomical Union (IAU) Symposia 335 on "Space Weather of the Heliosphere: Processes and Forecast, University of Exeter, UK, 17-21 July, 2017.
5. Co-Convener, Session PS12 "Future Space Missions and Instrumentation for Space and Planetary Science, AOGS 14^{th} Annual Meeting, Singapore", 6–11 August, 2017.
6. Co-Convener, Session PS16 "Science and Exploration of the Moon", AOGS 14^{th} Annual Meeting, Singapore, 6–11 August, 2017.
7. Member, Research Council,"CSIR-National Geophysical Research Laboratory(CSIR-NGRI), Hyderabad, 2017".
8. Member,"Research Council, CSIR-National Institute of Oceanography (CSIR-NIO), Goa, 2017".
9. Associate Editor of "Advances in Space Research" (Elsevier Publications).
10. Member ,"TIFR Balloon Facility Management Board,2018".
11. Member ,"AOGS Publication Committee, 2017".

A.K. Singhvi

12. Honoured as Associate-Editor, Quaternary, MDPI Publication, Switzerland.
13. Distinguished Lecturer, Beijing University, Beijing.
14. Honoured as Subject Editor, Earth Sciences for the Proceedings of Indian National Science Academy.

M. M. Sarin

15. Co-Convener, Special Session on "Air-sea exchanges: Impacts on Biogeochemistry and Climate", European Geophysical Union-2017 Vienna, Austria, 25 - 26 April, 2017.
16. Co-Chair, UN/GESAMP Annual Session hosted by World Meteorological Organization (WMO), Geneva (Switzerland), 4 - 8 September, 2017.
17. Member, National Scientific Steering Committee (NSSC) for Cloud -Aerosol Interaction & Precipitation Enhancement Experiment (CAIPEEX), IITM (Pune).
18. Secretary & Convener (2017-18), INSA-Sectional Committee for Earth & Planetary Sciences.
19. Special Invitee, "3^{rd} Interdisciplinary Biomass Burning Initiative (IBBI)" workshop, University of Colorado, Boulder, sponsored by International Global Atmospheric Chemistry (IGAC) Project, USA, 10-12 July, 2017.
20. Member, Scientific Advisory Committee - Atmospheric Sciences, ARIES, Manora Peak (Nainital)
21. Secretary & Convener (2017-18), INSA-Sectional Committee for Earth & Planetary Sciences.

D. Pallamraju

22. Member, Scientific Organizing Committee, 10^{th} Workshop on long term changes and trends in the atmosphere, Hefei, China, 14-18 May 2018.

23. Member, Scientific Organizing Committee, 3^{rd} International Conference on Environmental Management, Jawaharlal Nehru Technological University, Hyderabad, India, 27-30 November 2017.
24. Member, Editorial Board, Earth, Planets and Space, Springer Verlag journal, 2018-2021.

Nandita Srivastava

25. Member, Scientific Advisory Committee for Astronomy and Astrophysics, ARIES, Nainital.
26. Session Chair, Sun and Solar System, Astronomical Society of India meeting, Hyderabad, 5−9 February, 2018.
27. Session Chair, Indices of Solar Cycle from Photosphere to the Heliosphere, IAU symposium 340, Jaipur, 19-23 February, 2018.
28. SOC member, International Study of Earth Affecting Transients (ISEST) 2017, at Jeju island, South Korea, 18−22 September, 2017.
29. SOC member, 4^{th} Asia Pacific Solar Physics Meeting, Kyoto, Japan, 7−10 November, 2017.
30. SOC member, IAU symposium 340 on "Long-term datasets for the understanding of solar and stellar magnetic cycles", Jaipur, 19−23 February, 2018.

Varun Sheel

31. Main Convener:"Science and Exploration of Mars and Venus", 14^{th} annual meeting of the Asia Oceania Geosciences Society (AOGS), Singapore, 6-11 August 2017.

Som Kumar Sharma

32. Convener, "Exploration and Science of the Earth's Lower and Middle Atmosphere: Past, Present and Future perspectives", 14^{th} annual meeting of the Asia Oceania Geosciences Society (AOGS), Singapore, 6-11 August 2017.
33. Member of Board of Studies (Physical Sciences), Academy of Scientific and Innovative Research (AcSIR) of CSIR, India.
34. Member of Board of Studies (Physics), Pandit Deendayal Petrolium University (PDPU), Gandinagar, India.

Kuljeet Kaur Marhas

35. Co-convener, Workshop on "Role of sample return in addressing major outstanding questions in Planetary Sciences", International Space Science Institute, Bern, Switzerland, 5-9 February, 2018.
36. Co-convener, Goldschmidt conference, for session titled "Presolar Grains and Isotopic Heterogeneity in Planetary Materials", Paris, France, July 2017.

B. Joshi

37. Member of Scientific Advisory Committee for 32nd National Symposium on Plasma Science & Technology (PLASMA-2017) organized by Plasma Science Society of India (PSSI), Institute for Plasma Research (IPR), Gandhinagar, Gujarat, 7-10 November, 2017.

Amit Basu Sarbadhikari

38. Editor, Section (Mineralogy, Petrology and Geochemistry of the surface of the Moon), "Encyclopedia of Lunar Science", Springer Publishing.

Neeraj Srivastava

39. Member, Judge Panel, Touch the Jovian Moon Contest,"Pearl Jubilee Celebrations of Liquid Propulsion System Centre (LPSC), ISRO, Valiamala, Trivandrum".

Best, Paper & Thesis, Awards

Deepak Kumar Karan

40. Won CHARUSAT inspired Gujarat Science Academy Best Thesis Award in the category of Physical Sciences for the year 2017.

Jabir M. V.

41. Best poster award, Incubic / Milton Chang travel grant for the paper, Generation of hybrid entangled two photon state using classical non-separable state of the pump beam." in Frontiers in Optics Conference in Washington DC, USA, September, 2017

P. K. Mitra

42. Best Poster award for poster entitled "Flux Rope Eruption from a Sigmoidal Active Region: Triggering Mechanism and Large-Scale Magnetic Reconnection" in the category "Astrophysical Plasma", Plasma Science Society of India (PSSI) meeting,Gandhinagar, Gujarat, 7 − 10 November, 2017.

Human Resource Development

Human Resource Development at PRL The laboratory has a strong Human Resource Development (HRD) component with Doctoral, Post–Doctoral, Visiting Scientist programs. In addition we have an Associate program for university teachers and project training for graduate and post graduate students in both science and engineering. PRL organizes intensive summer programmes for students as well as college teachers every year. The purpose is to provide them an insight into current research activities being pursued at PRL which they can continue even after returning back to their colleges. It is also aimed at motivating them to take up research in basic sciences. Brief details of scientific output and staff details in numbers during the reporting year are reported here.

Research Programmes One of the important aims of the laboratory is to serve as a post-graduate and post-doctoral study centre in physics, earth & planetary sciences and chemistry to train research students in experimental and theoretical physics. With this in view, PRL offers a graduate programme through Research Fellowship leading to Ph. D. degree. It also provides opportunities for carrying out post-doctoral research. The strength of fellows under these programmes are presented in figure 1.

Figure 1: Research Programmes.

Training Opportunities PRL provides summer training programme to students doing their Bachlor's and Master's degree in Physics,Chemistry,Earth Sciences to acquaint them with the research programmes and opportunities available at PRL. This includes the internship of students selected through three national science academies and Indian Institute of Space Science and Technology, Thiruvananthapuram. Following is the list of students who did their B.Sc./M.Sc./M.Phil projects at PRL during this year.

1. Mr. SOUVIK BERA, Indian Inst. Of Tech, Mumbai, "Emission Mechanisms in Active Galactic Nuclei", [Supervisor: Dr. Veeresh Singh]
2. Mr. ADITYA NARENDRA, National Inst Of Tech, Rourkela, "Infrared studies of Be/X-ray binary system X Persei", [Supervisor: Dr. S. Naik]
3. Mr. HARI K, National Inst Of Tech, Tiruchirapall, "Study on Designing an SLR(Satellite Laser Ranging) station", [Supervisor: Mr. R. R. Shah]
4. Mr. SWAPNESH KHADE, Pune University, "The study of broad band spectral energy distribution of Active Galactic Nuclei", [Supervisor: Dr. Veeresh Singh]
5. Mr. JIBANJYOTI ROUTRAY , Annamalai University, "Luminescence dating technique and its application", [Supervisor: Dr. Naveen Chauhan]
6. Ms. AKANKSHA GAUTAM, Devi Ahilya Vishwavidyalaya, "Generation of an Optical Vortex", [Supervisor: Prof. R. P. Singh]
7. Mr. ROHAN PRAMANICK, Indian Inst. Of Tech, Kharagpur ,"Generation of Airy beam by Comatic aberration", [Supervisor: Dr. Goutam K. Samanta]
8. Ms. MONIKA KUSUMBHI, Indian Inst. Of Tech, Madras, "Collision of dust particle with ice", [Supervisor: Dr. Bhalamurugan Sivaraman]
9. Mr. BRAJESH RAJESH BHAGAT, Devi AhilyaVishwavidyalaya, "Impact Induced Plasma", [Supervisor: Dr. Bhalamurugan Sivaraman]
10. Ms. NAMROTA SAHA, Indian School Of Mines, "Inferring Climate-Culture relationship in the Western Great Rann of Kachchh using Luminescence Dating of Fluvial sediments" [Supervisor: Dr. Navin Juyal]
11. Ms. ARUNIMA MISHRA, Annamalai University, "DIC(Dissolved Inorganic Carbon) in water samples", [Supervisor: Dr. M. G. Yadava].
12. Mr. CHANDAN PATTNAIK, Banaras Hindu University, "Carbonaceous aerosol in atmosphere", [Supervisor: Mr. A. K. Sudheer]
13. Ms. ARCHANA TRIPATHY, Central University Of Rajasthan , "Characteristics of carbonaceous aerosols from north east-Himalayas", [Supervisor: Dr. Neeraj Rastogi]
14. Ms. GAYATHRI E M, Cochin University Of Science & Technology, "Isotopic Analysis of Rain Water", [Supervisor: Dr. M. G. Yadava]
15. Ms. RISHIKA NAIR , Gujarat University, "Extreme events of microorganisms in the Pacific Ocean, [Supervisor: Dr. Arvind Singh]

16. Mr. ASHU YADAV, Indian Insitute Of Technology, Kharagpur, “Paleoerosion over Himalaya: Impact of Climate” [Supervisor: Dr. Sunil Kumar Singh]
17. Ms. ARPITA DASH, Manipal Academy Of Higher Education, Manipal, “Stable Isotopic Composition of Hailstone” [Supervisor: Dr. M. G. Yadava]
18. Ms. AISWARYA P K, Periyar University, “Paleotemperature Reconstruction using Stable Isotope from Fossils”, [Supervisor: Dr. Sanjeev Kumar]
19. Mr. NAGA SANTOSH SREE BHUVAN G, Pondicherry University, “Trace Element modelling in magnetic processes: A case study of Andaman Ophiolites”, [Supervisor: Dr. J.S. Ray]
20. Mr. SUDEB SARKAR, Amity University , Uttar Pradesh ,GautamBudh Nagar , “Simple Models of Galactic Chemical Evolution and Oxygen Isotopes”, [Supervisor: Dr. Kuljeet Kaur Marhas]
21. Ms. VENEELA MANDALA, Andhra University, “Topographic Data Processing of some important Sites on the Moon” [Supervisor: Dr. Durga Prasad]
22. Mr. DINESH KUMAR V R , BITS, Pilani , “Prototype of Lightning Detector for future Venus Mission”, [Supervisor: Dr. Jayesh Pabari]
23. Mr. DINESH SINGH BHATI, Central University Of Rajasthan, “Geomorphology of SirenumTholus region on Mars” [Supervisor: Dr. Neeraj Srivastava]
24. Mr. SHAMBHARKAR SHILBHUSHAN, IIser Pune, [Supervisor: Dr. Kuljeet Kaur Marhas]
25. Mr. HARSHITH BACHIMANCHI, IIser Pune , “Compact Optical Tweezer Using a DVD Optical Pickup” [Supervisor: Dr. Goutam K Samanta]
26. Ms. VALLI DIVYA R, Indian Institute Of Technology, Bhubaneswar, “Cosmic Ray Exposure Ages of Eucrite and Diogenite Meteorites”, [Supervisor: Mr. Ramakant Mahajan]
27. Mr. PIYUSH SRIWASTAVA, Indian Institute Of Technology, Mumbai, “Mineralogical Association Surrounding Recurring Slope Lineae (RSL) on Mars”, [Supervisor: Dr. Amit Basu Sarbadhikari]
28. Ms. NEENA PICARDO, Indian Institute Of Technology, Mumbai, “A study on the layered deposits within a crater in the Elysium Volcanic Province, Mars using HiRISE and CRISM data”, [Supervisor: Dr. S. Vijayan]
29. Mr. MD SOYEB ALLAM, Indian Institute Of Technology, Roorkee, “Spectral Reflectance Study of Orientale Basin Using CHANDRAYAN-1, M3 Data”, [Supervisor: Dr. Neeraj Srivastava]
30. Mr. ADITYA PATKAR, Indian Institute Of Technology, Roorkee, “Petrography, Mineralogy, Thermal and Shock History of Ordinary Chondrites”, [Supervisor: Dr. Dwijesh Ray]
31. Ms. SANTILATA SAHOO, Pondicherry University, Synthetic Dust Data Generation And Parameter Retrieval for Future Mars Mission, [Supervisor: Dr. Jayesh Pabari]
32. Mr. YASH SRIVASTAVA, University Of Delhi, “Cr-Spinel in Sinus Aestuum of the Moon”, [Supervisor: Dr. Amit BasuSarbadhikari]
33. Ms. SAMIKSHA BAJAJ, Amity University Noida, “Emission and Dispersion of Volatile Organic Compound from a landfill site in Ahmedabad”, [Supervisor: Dr. Lokesh Sahu]
34. Ms. REGINA A, Bharathiar University, “Characteristic Features of aerosol size distribution over an urban area”, [Supervisor: Dr. S. Ramachandran]
35. Mr. MAHARSHI BHATT, Sardar Patel University, “Characteristics of Black carbon aerosol mass concentration in western India”, [Supervisor: Mr. T. A. Rajesh]
36. Ms. KOMAL JANI , Saurashtra University, “Study of stratospheric ozone and solar UV radiations, over Ahmedabad” [Supervisor: Dr. Som Kumar Sharma]
37. Mr. VIVEK SINGH , SHUATS, Allahabad, “Impact of Solar Disturbance on Earth’s Middle Atmosphere”, [Supervisor: Dr. Som Kumar Sharma]
38. Ms. SWETHA S, University of Madras,“ Study of Atmospheric Aerosols using Sunphotometer”, [Supervisor: Dr. S. Ramachandran]
39. Ms. UDITA SEHGAL ,MNIT, Jaipur,”General Relativity and Standard Model of Cosmology”, [Supervisor: Dr. Raghavan Rangaranjan]
40. MS. SMRUTIBEN PARIKH,SPU,”Bose-Einstein condensate in symmetric double-well potential”, [Supervisor: Dr. Angom Dilipkumar Singh]
41. MR. SHREYASH GARG , SVNIT, Surat,”The fluctuation - dissipation theorem and the Callen-Welton formalism (OR) Kelvin water dropper: Measuring the temporal development of charge”, [Supervisor: Dr. Navinder Singh]
42. MR. RISHABHPORWAL ,IASc , ”Dynamics of Quantum Particle in double well”, [Supervisor: Dr. Angom Dilipkumar Singh]
43. MS. S. ABJASREE,NIT, Trichy, ”Study of Gamma-Ray Flares in Blazars”, [Supervisor: Prof. K. S. Baliyan]
44. MR. NOOMBULAAVINASH ,IASc, ”Thermal Analysis of Lunar Soil along the Length of Thermal Probe for ChaSTE payload of Chandrayaan-2, [Supervisor: Dr. Anil Bhardwaj]
45. MS. BHAGYASHREE SAHOO, Utkal University, Bhubaneswar, ”Geochemical approach for marine paleoclimatic reconstruction on AMS radiocarbon dated sediment core”, [Supervisor: Dr. Ravi Bhushan]
46. MR. RAKHIL DEV,Central University Of Karnataka, ”Understanding hydrometeorological processes governing precipitation in Jorhat using stable water isotopes”, [Supervisor: Dr. R. D. Deshpande]
47. MR. AMRUTHA KRISHNA, National institute of Technology, Tiruchirappalli, “A study of Neutrino Oscillation”, [Supervisor: Dr. Namit Mahajan]
48. MR. RAJESH KUMAR RATH, IIT, Bhubaneswar, “Track the migration of the Yamuna River by studying down-core variation of chemical Compositions, $^{87}Sr/^{86}Sr$ and εNdin sediments”, [Supervisor: Dr. Sunil Kumar Singh]
49. MS. V MIDHILA VARNA, Cochin Uni. Of Sci. & Tech,Kochi, ”Sea surface salinity in the Arabian Sea”, [Supervisor: Dr. Arvind Singh]
50. MR. NIKHIL TANWAR, IISER, Mohali, ”Noise in the optical signal detection” , [Supervisor: Prof. R P Singh]
51. MR. ANAND YADAV ,IIT-Gn,”Dual axis Hybrid Sun Tracking System”, [Supervisor: Mr. T.A. Rajesh]
52. Ms. L. MADHULIKA ,IIT-Gn ,”Temperature control of Peltier Coolers”, [Supervisor: Dr. Shanmugam M]

53. MS. KINJAL CHAUHAN, IIST ,"On the study of Estimation of mass of Black hole in AGN", [Supervisor: Dr. K.S. Baliyan]
54. MS. PRACHI PRAJAPATI ,IIST ,"Studies on Starburst Galaxies", [Supervisor: Dr. Shashikiran Ganesh]
55. MR. SWAPNIL SINGH ,IIST ,"Study of Globular Clusters in the Milky Way", [Supervisor: Dr. Shashikiran Ganesh]
56. MS. BHAGYASHREE PAGARE, IIST ,"Coronal Seismology using Numerical Simulation", [Supervisor: Dr. Aveek Sarkar]
57. MS. SHREEYA NATARAJAN ,IIST ,"Study of organics essential for life within interplanetary dust particles, meteorites and Cometary sample", [Supervisor: Dr. K. K. Marhas]
58. MS. ARUNITAKUMARI, IIST ,"Conceptualisation and design of extreme ultraviolet window/ filter for the pass-band of 50-110 nm", [Supervisor: Dr. Kinsuk Acharyya]
59. MR. SHIVAM MISHRA ,M.J.P. Rohilkhand University, Bareilly, "Shock Processing on Ice", [Supervisor: Dr. Bhalamurugan Sivaraman]
60. MS. NANDITAKUMARI, Anna University, Chennai ,"Crater Chronology of Selected Lacus Basalts on The Moon", [Supervisor: Dr. Anil Bhardwaj]

PRL also provides project training in engineering disciplines like computer engineering, electronics & communication, instrumentation & control, information technology to graduate/post-graduate students. Details of the same are presented in figure 2. Following is a list of students who did their B.Tech. final semester projects at PRL during the Financial year April 2017-March 2018.

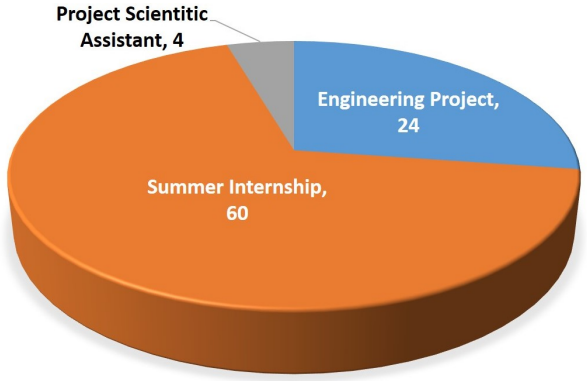

Figure 2: Internship Training Programmes.

1. MR. PARTHSINH CHAUHAN, Dharmsinh Desai University, Nadiad, Gujarat, "Development of compact mechanical structure for photonic source", [Supervisor:Dr. Goutam K Samantha].
2. MS. SHERIN EAPEN, Government Engineering College Patan, Gujarat Technological University, "Lightning Detector for Future Planetary Mission", [Supervisor: Dr. Jayesh Pabari].
3. MR. VATSAL SHAH ,CSPIT, Charotar University Of Science & Technology , Anand, Gujarat, "Characterizing Secondary Ejecta due to Hypervelocity Impact on Moon", [Supervisor: Dr. Jayesh Pabari].
4. MR. JAY PATEL ,CSPIT, Charotar University Of Science & Technology , Anand, Gujarat, "Developing Tool for Simulation of Solar Wind Particles on Detector Target", [Supervisor: Dr. Jayesh Pabari].
5. MR. SAGAR DASWANI, Dharmsinh Desai University, Nadiad, Gujarat, "Developing Tool for Simulation of Solar Winds Particles on Detector Target", [Supervisor: Dr. Jayesh Pabari]
6. MS. POOJA KUMARI, U. V. Patel College Of Engineering, Ganpat University, Mehsana, Gujarat, "Radiometer",[Supervisor: Dr. Kinsuk Acharyya]
7. MS. DEVANSHI ADHVARYU, L.D College Of Engineering, Ahmedabad, "Polarization Nephelometer for Planetary missions", [Supervisor: Dr. Kinsuk Acharyya]
8. MR. KALPAN MEHTA, Institute Of Technology, Ahmedabad, "Tunable Diode Laser Spectrometer for in-situ Study of Atmosphere",[Supervisor: Dr. Kinsuk Acharyya]
9. MR. SHIVAM YEMULWAR, U. V. Patel College Of Engineering, Ganpat University, Mehsana, Gujarat, [Supervisor: Dr. Navinder Singh]
10. MS. NIKITABEN PRAJAPATI, U V Patel College Of Engineering, Ganpat University, Mehsana, Gujarat, "Measurement of the Non-Equlibrium Electronic Transport", [Supervisor:Dr. Navinder Singh]
11. MS. AISHWARIYA BHATT, CSPIT, Charotar University Of Science & Technology, Anand, Gujarat,"Digital Image Processing andAnalysis of Planetary Datasets", [Supervisor: Dr. Neeraj Srivastava]
12. MR. YASH SHETH, CSPIT, Charotar University Of Science & Technology, Anand, Gujarat, "Digital Image Processing andAnalysis of Planetary Datasets", [Supervisor: Dr. Neeraj Srivastava]
13. MR. RONIT PATEL, Dharmsinh Desai University, Nadiad, Gujarat,"Digital Image Processing andAnalysis of Planetary Datasets", [Supervisor: Dr. Neeraj Srivastava]
14. MR. ABHINAV ANTANI, Dharmsinh Desai University, Nadiad, Gujarat,"Shadow Removal from the Craters of the Moon", [Supervisor:Dr. S. Vijayan]
15. MS. SWETA GADHIYA, CSPIT, Charotar University Of Science & Technology, Anand, Gujarat, "Development of Software for Visualization of the Earth's Atmospheric Parameters using Satellite data and Ground Based Observations", [Supervisor: Dr. Som Kumar Sharma]
16. MR. SAMIP THAKKAR, CSPIT, Charotar University Of Science & Technology, Anand, Gujarat, "Development of Software for Visualization of the Earth's Atmospheric Parameters using Satellite data and Ground Based Observations", [Supervisor:Dr. Som Kumar Sharma]
17. MR. PARTHIT SARDHARA, Dharmsinh Desai University, Nadiad, Gujarat, "Synthetic Data simulation for Radio Occultation", [Supervisor: Dr. Varun Sheel]
18. MR. HENIL PATEL, Dharmsinh Desai University ,Nadiad, Gujarat,"Customisation and developing visualisation software of WRF model", [Supervisor: Dr. Varun Sheel]
19. MS. KRISHNA PATEL, CSPIT, Charotar University Of Science & Technology, Anand, Gujarat, "Design and Evaluation of FE electronics for Space Plasma Sensors", [Supervisor: Dr. K. Durga Prasad]

20. MR. VISHWAS SARAGIA, Nirma University, Ahmedabad, “Design of a Nephelometer Prototype for Future Space Exploration”, [Supervisor:Dr. K. Durga Prasad]

21. MR. JAY PAREKH, Dharmsinh Desai University, Nadiad, Gujarat,“Design of an anemometer prototype for planetary wind velocity measurements”, [Supervisor:Dr. K. Durga Prasad]

22. MR. MAHARSHI KANSARA, CSPIT, Charotar University Of Science & Technology, Anand, Gujarat, “Antenna design and evaluation for Space based wireless sensor networks (WSN)”, [Supervisor:Dr. K. Durga Prasad]

23. MR.MALKAUSH GADHAVI, L.D College Of Engineering, Ahmedabad, [Supervisor:Dr.M.Shanmugan]

24. MS. ANEE DUDHIA , Indus University, Indus International University, Ahmedabad, Gujarat,“High Speed Sampling for the Time of Flight Mass Spectrometer“, [Supervisor:Mr. Shiv Kumar Goyal]

25. MS. PRIYAM CHAUHAN, Vishwakarma Government Engineering College, Chandkheda., Gujarat Technological University , “High Speed Sampling for the Time of Flight Mass Spectrometer”, [Supervisor:Mr. Shiv Kumar Goyal]

PRL also offers training programmes in computers, electronics, library science, engineering and administrative services (Fig. 3).

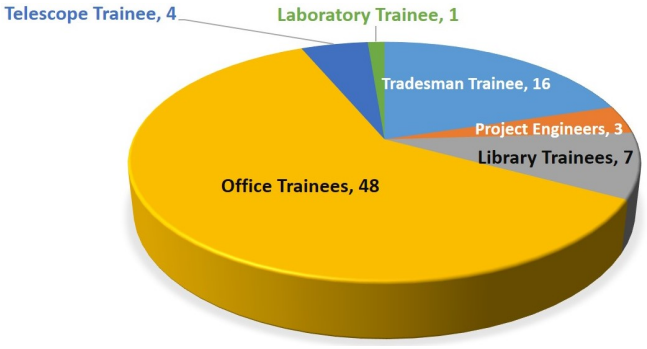

Figure 3: Training Programmes in technical and administrative areas.

Research Contributions The research work carried out by PRL scientists are published in reputed and peer reviewed national and international journals. Few of our scientists are also invited to write review articles in the field of their specialization. Some of our scientists have also edited books.

Many of our scientists attend conferences and symposia at home and abroad where they present the results of their research investigations. Some of them are invited to present review talks. Few of them serve as chairmen and members of scientific committees for organizing national conferences and symposia. They are also invited to convene and chair sessions during symposia and meetings. The research output during the reporting year are shown in figure 4.

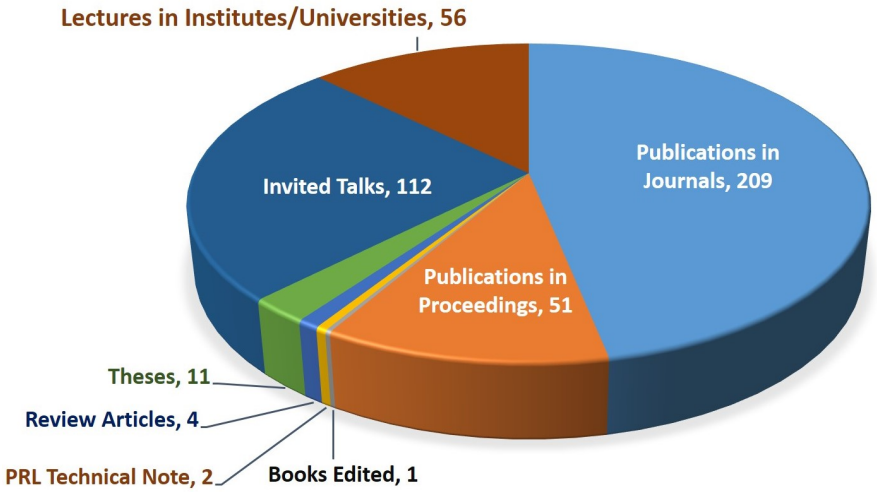

Figure 4: Research Contributions.

Administrative Support

Behind the scientific achievements of PRL is the able and efficient support given by the administrative and the technical staff.

The administrative section of our laboratory continues to plays a pivotal role in providing an excellent management support to carry out our scientific activities. In addition, it also provides management support to the Solar Observatory at Udaipur and the Infrared Observatory al Mt. Abu. The staff structure of PRL are shown in figure 5.

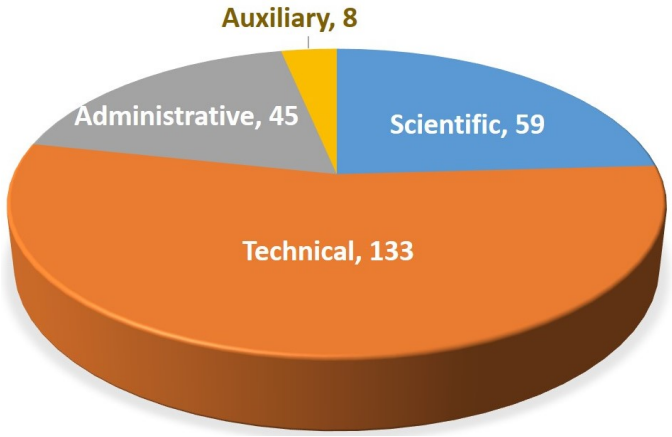

Figure 5: The distribution of PRL staff.

Ph.D. Awarded

Abhaya Kumar Swain

1. "Mass Determination Methods at Large Hadron Collider", Mohanlal Sukhadia University, Udaipur, July, 2017. [Supervisor: Dr Partha Konar]

Diptiranjan Rout

2. "Investigations of Magnetosphere-Ionosphere-Thermosphere systems under varying space weather conditions", Mohanlal Sukhadia University, Udaipur, July, 2017. [Supervisor: Dr Dibyendu Chakrabarty]

Anirban Chatterjee

3. "Provenance of late Quaternary continental sediments in western India: Insights from trace element and isotope geochemistry", Maharaja Sayajirao University of Baroda, Vadodara, September, 2017. [Supervisor: Dr J S Ray]

Deepak Kumar Karan

4. "Investigations of Daytime Thermospheric Wave Dynamics Over Low-latitudes Using Ground-based Optical Techniques", Indian Institute of Technology, Gandhinagar, October, 2017. [Supervisor: Dr D. Pallamraju]

Ikshu Gautam

5. "Sm-Nd isotope systematic of continental igneous rocks of India: implications for early evolution of the silicate Earth", Maharaja Sayajirao University of Baroda, Vadodara, October, 2017. [Supervisor: Dr J S Ray]

Bivin Geo George

6. "Evolution of the Proterozoic sedimentary basins of India: A geochemical perspective", Maharaja Sayajirao University of Baroda, Vadodara, October, 2017. [Supervisor: Dr J S Ray]

Navpreet Kaur

7. "Understanding the structure and emission processes in AGN using blazar variability", Indian Institute of Technology, Gandhinagar, November, 2017. [Supervisor: Dr K S Baliyan]

Ravindra Pratap Singh

8. "Investigations of Interactions in The Earth's Upper Atmosphere Using Optical and Radio Wave Techniques", Sardar Patel University, Vallabh Vidyanagar, November, 2017. [Supervisor: Dr D. Pallamraju]

Chandana K.R.

9. "Reconstruction of Paleoclimatic History of the northern Indian Ocean using isotopic and geochemical proxies", Mohanlal Sukhadia University, Udaipur, February, 2018. [Supervisor: Dr R Bhushan]

Karanam Durga Prasad

10. "Thermophysical Behaviour of the Surface of Moon from Laboratory Experiments and Numerical Modelling", Pondicherry University, January, 2018. [Supervisor: Dr Vinai Rai]

A. K. Sudheer

11. "Chemical and Isotopic Studies of Atmospheric Aerosol: Sources, Deposition Fluxes and Surface Ocean Biogeochemistry", Mohanlal Sukhadia University, Udaipur, March, 2018. [Supervisor: Dr S K Singh]

Colloquia/Public Lectures by Visitors

1. **Mr. Satishchandra C. Wani**
   TeamIndus, Bengaluru, India
   TeamIndus GLXP Mission
   26 April 2017

2. **Dr. Rohan Eugene Louis**
   Leibniz-Institute for Astrophysics Potsdam (AIP), Germany
   Investigating magnetic flux emergence through multi-wavelength observations
   17 May 2017

3. **Dr. Nissim Kanekar**
   National Centre for Radio Astrophysics, Pune, India
   Do the Fundamental Constants change with Time?
   27 June 2017

4. **Prof. Sreerup Raychaudhuri**
   Tata Institute of Fundamental Research, Mumbai, India
   Early Days of Particle Physics in India
   26 July 2017

5. **Dr. Urbasi Sinha**
   Raman Research Institute, Bengaluru, India
   Fascinating world of photons, superposition and entanglement
   30 August 2017

6. **Prof. Jens Biegert**
   The Institute of Photonic Sciences, Barcelona, Spain
   Teaching electrons to take a selfie - Public Lecture
   01 September 2017

7. **Shri S. Somanath**
   Liquid Propulsion Systems Centre, Thiruvananthpuram, India
   Innovation in Launch Vehicle & Propulsion System - Enablers of Exploration - Public Lecture
   08 November 2017

8. **Prof. Amita Das**
   Institute for Plasma Research, Gandhinagar, India
   Electron Transport in Plasmas
   15 November 2017

9. **Dr. Swadesh M Mahajan**
   University of Texas, Austin, USA
   Beating the Magnetic Barrier: Relativistically Induced Escape of Low Frequency Electromagnetic Radiation
   11 December 2017

10. **Prof. Girish S. Agarwal**
    Texas A & M University, Texas, USA
    Super Resolution Microscopy
    15 December 2017

11. **Prof. H. C. Verma**
    Former Professor, Indian Institute of Technology, Kanpur, India
    Neutrino Katha
    25 January 2018

12. **Prof. P. C. Deshmukh**
    Indian Institute of Technology, Tirupati, India
    Time, and Time Delay, in Atomic Dynamics
    07 February 2018

13. **Prof. B. M. Azizur Rahman**
    City University, London, UK
    Photonics: From its emergence to becoming a Key Enabling Technology - Public Lecture
    16 February 2018

14. **Prof. Mark G. Lawrence**
    Institute for Advanced Sustainability Studies, Potsdam, Germany
    Air Pollution in Southern Asia: a Case Study of Steps Towards a More Sustainable Atmosphere for the Kathmandu Valley
    20 February 2018

15. **Dr. Kishore Dutta**
    Handique Girl's College, Guwahati, India
    Critical phenomena in Uranium Ferromagnetic superconductors
    14 March 2018

Conference/Symposium/Workshop organized by PRL

Planetary Sciences and PLANEX Program

1. "Brainstorming Session on Vision & Exploration for Planetary Sciences in Decades 2020-2060", 8-10 November, 2017.

Space and Atmospheric Sciences

2. "ISRO Structured Training Programme (STP)", on "Space Science Programme: ISRO & Global Scenario", 05-09 March, 2018.

Theoretical Physics

3. "Annual Theory Discussion Days (ATDD 2018)", 6-8 February, 2018.
4. "Young Physicists' Meet (YPM 2017)", 22-24 March, 2017.

Atomic, Molecular and Optical Physics

5. "SCOP-the Students' Conference in Optics and Photonics", 1-2 September, 2017.
6. "Cassini-Huygens", Cassini-Huygens @ PRL, 13 September, 2017.

Administration

7. Workshop on "Reservation in Services For Central Government Employees", 1-2 February, 2018.

Invited Talks at Conference / Symposia / Workshops

Astronomy and Astrophysics

Janardhan, P.

1. "Long-term datasets for the understanding of solar and stellar magnetic cycles", IAU Symposium 340, Jaipur, India, 19-24 Feb, 2018.

Kiran S Baliyan

2. "Compact Objects: What does variability in blazars tell us", RETCO-3 meeting, IIST, Trivandrum, India, 05-07 June, 2017.
3. "Understanding the Universe using ground based telescopes", ISRO's STP-2018, PRL, Ahmedabad, India, 5-9 March, 2018.

S. V. Vadawale

4. "Future X-ray Astronomy experiments", Brainstorming meeting, Physical Research Laboratory, Ahmedabad, 8 - 10 November, 2017.
5. "Hard X-ray polarimetry with CZTI", AstroSat Science Meet, ISRO-HQ, Bangalore, 26-27 Septemer, 2017.
6. "New Results from Astrosat", New Initiatives in Fundamental Science and Experiments, Udaipur, 11-14 September, 2017.
7. "Polarisation measurements using AstroSat CZTI", Workshop on Gamma-ray Bursts: Prompt to Afterglow, NCRA, Pune, 4 - 7 July, 2017.

Shashikiran Ganesh

8. "Dust in the Solar System and the Milky Way", BINA meeting at the Royal Observatory of Belgium, Brussells, 12th October 2017.
9. "Distribution of dust in the Galactic plane", Meeting on 'Piercing the Galactic Darkness', Max Planck Institute of Astronomy, Heidelberg, 16th October 2017.

Srivastava, Mudit K.

10. "MFOSC-P : Mount Abu Faint Object Spectrograph-Camera V Pathfinder on PRL 1.2m Telescope - Optical and Opto-Mechanical Designs", International Topical Meeting on Applied and adaptive optics (INTOPMAA-17), Indian Institute of Space Science & Technology (IIST) Thiruvananthapuram, India, 11-13 August, 2017.
11. "Optical Instrumentation in Astronomy : An Engineering Perspective", Workshop on New Avenues of interface between Astronomy and Engineering, Model Engineering College, Ernakulam, Kerala, 4-6 January, 2018.

Veeresh Singh

12. "AGN-jets : radio power, morphology and scales", Astrophysical jets workshop at 36th meeting of Astronomical Society of India, Osmania University, Hyderabad, India, 5th February, 2018.
13. "Unconventional radio-loud AGN with less massive SMBH", 36th meeting of Astronomical Society of India, Osmania University, Hyderabad, 6-9 February, 2018.

Dewangan, L.K.

14. "Observational Signatures of Cloud-Cloud Collision in the Galactic Star-Forming Regions", 36th meeting of Astronomical Society of India, Osmania University, Hyderabad, India, 5-9 February, 2018.

Vishal Joshi

15. "Evolution of nova ejecta: A near-infrared perspective", Dynamic Infrared Sky, Caltech, Pasadena, CA, USA, 18-20 September, 2017.

Mithun N. P. S

16. "Data analysis with AstroSat-CZTI", AstroSat Data Analysis Workshop, IUCAA, Pune, 26th November 2017.
17. "Hard X-ray spectroscopy AstroSat-CZTI", AstroSat Science Meet, ISRO-HQ, Bangalore, 26-27 September, 2017.

Navpreet Kaur

18. "Multi-wavelength study of Blazars", 3rd National Conference on High Energy Emission from Active Galactic Nuclei, University of Calicut, India, 28-30 November, 2017.

Prahlad Epili

19. "Decade long RXTE monitoring observations of Be/X-ray binary pulsar EXO 2030+375", International Conference 'Be/X-ray Binary 2017, Heraklion, Greece, 11-13 September, 2017.

Aarthy E.

20. "Measuring GRB Polarization using AstroSat CZTI", Workshop on Gamma-Ray Bursts: Prompt to Afterglow, NCRA, Pune, 4-7 July, 2017.
21. "Hard Xray Mirrors-A new saga in high energy astrophysics", Student conference on optics and photonics (SCOP-17), PRL, Ahmedabad, 1-2 September 2017.

Archita Rai

22. "Near-Infrared Imaging Spectro-Polarimeter (NISP) instrument for PRL 2.5-m telescope", 36th meeting of Astronomical Society of India, Osmania University, Hyderabad, 5-9 February, 2018.

Solar Physics

Nandita Srivastava

23. "Solar physics research using ground and spacebased observations", Structured Training Program (STP), PRL, Ahmedabad, 5−9 March, 2018.

B. Joshi

24. "Large-scale eruptive phenomena on the Sun and their interplanetary consequences", Symposium on Advances in Physics from small to large scales, Department of Physics (UGC-centre of advanced study), Kumaun University, Nainital, Uttarakhand, 27 − 28 Mar, 2018.

A. Raja Bayanna

25. "A Low-order Adaptive Optics System for Multi-Application Solar Telescope : Current Status", International Topical Meeting On Applied and Adaptive Optics (INTOPMAA-17), IIST, Thiruvananthapuram, 11 − 13 Aug, 2017.

Planetary Sciences and PLANEX Program

Anil Bhardwaj

26. "Space Sciences and Planetary Exploration", 3rd Indian Society of Systems for Science and Engineering National Conference – 2017, National Conference on Complex Engineering Systems of National Importance: Current Trends & Future Perspective, Indian School of Business, Mohali, 12 Oct, 2017.
27. "A New View on Solar Wind Interaction with Moon", PLASMA-2017, PLASMA-2017, 32nd National Symposium on Plasma Science & Technology, Gandhinagar, Gujarat, 07 Nov − 10 Dec, 2017.
28. "Science of the Outer Planets and their Moons", Brainstorming session on Vision & Exploration for Planetary Sciences in Decades 2020-2060, PRL, Ahmedabad, 08 Nov − 10 Nov, 2017.
29. "Indian Planetary Exploration Program", National Vijyoshi Camp, IISER, Kolkata, 10 Dec, 2017.

S A Haider

30. "Effects of X-ray flares on the ionosphere and human exploration to Mars ", Asia Oceanic Geo-sciences Society, 14th Annual Meeting, Singapore, 06 Aug − 11 Aug, 2017.
31. "Science and exploration of Indian Mars mission: MOM 2 ", Asia Oceanic Geo-sciences Society, 14th Annual Meeting, Singapore, 06 Aug − 11 Aug, 2017.

Debabrata Banerjee

32. "Science of Mars using gamma ray spectrometer", Brainstorming session on Vision & Exploration for Planetary Sciences in Decades 2020-2060, PRL, Ahmedabad, PRL, Ahmedabad, 08 Nov − 10 Nov, 2017.

Varun Sheel

33. "Radio Occultation Experiment for future Indian Space Missions", 14th annual meeting of the Asia Oceania Geosciences Society (AOGS), Singapore, 06 Aug − 11 Aug, 2017.
34. "Exploration of Europa: Search of Ingredients for Life", 14th annual meeting of the Asia Oceania Geosciences Society (AOGS), Singapore, 06 Aug − 11 Aug, 2017.

Kuljeet Kaur Marhas

35. "Asteroid Sample Return", Vision & Explorations for Planetary Sciences in Decades 2020-2060, PRL, Ahmedabad, 08 Nov — 10 Nov, 2017.
36. "Short lived nuclides and Irradiation Scenario", Role of sample return in addressing major outstanding questions in Planetary Sciences, Bern, Switzerland, 05 Feb — 09 Feb, 2018.

J. P. Pabari

37. "Mars Orbit Dust Experiment for Mars Orbiter Mission-2", Brainstorming Session on Vision & Exploration for Planetary Sciences in Decades 2020-2060, PRL, Ahmedabad, 08 Nov — 10 Nov, 2017.
38. "Research Opportunities in Wireless Sensor Network", STTP on "Smart Engineering, Parul Institute of Engineering and Technology, Waghodia, 16 Feb, 2018.

Shanmugam M

39. "Advances in Aerospace Engineering", IETE workshop, Udaipur, 01 Sep, 2017.

Amit Basu Sarbadhikari

40. "Melting and Differentiation in Planetary Bodies of the Solar System", CAPS-2017, IISc, Bangalore, 08 Nov — 10 Nov, 2017.
41. "Geology of the landing site using a lunar rover", Brainstorming Session on "Vision & Explorations for Planetary Sciences in Decades 2020-2060, PRL, Ahmedabad, 08 Nov — 10 Nov, 2017.

Dwijesh Ray

42. "Meteorites-A Messenger from outer Space", ., Centre for Earth Studies at IISc, Bangalore, 18 Sep, 2017.
43. "The Lonar crater, India-An analog for Mars and its basaltic alteration", 14th Annual Meeting of Asia Oceania Geosciences Society, SUNTEC, Singapore, 06 Aug — 11 Aug, 2017.

Neeraj Srivastava

44. "Lunar Sample Return Mission", Brainstorming Session on"Vision & Explorations for Planetary Sciences" in decades 2020 -2060, PRL. Ahmedabad, 08 Nov — 10 Nov, 2017.
45. "Remote Sensing of the Moon", Challenges and Advances in Planetary Science (CAPS), Indian Institute of Science (IISC), Bengaluru, 18 Sep — 22 Sep, 2017.

Shiv Kumar Goyal

46. "Aditya Solar wind & Particle Experiment (ASPEX) onboard Aditya-L1 mission", 14th Asia Oceania Geosciences Society (AOGS) meeting, Singapore, 06 Aug — 11 Aug, 2017.
47. "Alpha Particle X-ray Spectrometer for the Chandrayaan-2 Rover", 14th Asia Oceania Geosciences Society (AOGS) meeting, Singapore, 06 Aug — 11 Aug, 2017.
48. "Development of STEPS for Aditya-L1 mission", Brainstorming session on Vision & Exploration for planetary sciences in decades 2020-2060, PRL, Ahmedabad, 08 Nov — 10 Nov, 2017.
49. "Supra Thermal & Energetic Particle Spectrometer (STEPS), onboard Aditya-L1 mission", 36th Annual meeting of the Astronomical Society of India (ASI), Osmania University, Hyderabad, 08 Feb, 2018.

Karanam Durga Prasad

50. "Planetary Exploration: Opportunities and Challenges", Planetary Exploration: Opportunities and Challenges, Indian Institute of Information Technology (IIIT)-Srikakulam, 27 Feb — 28 Feb, 2018.
51. "Prototype Development of Langmuir Probe and Electric Field Experiment for Future Mars Mission", AOGS-2017, SUNTEC, Singapore, 06 Aug — 11 Aug, 2017.

Space and Atmospheric Sciences

S. Ramachandran

52. "Atmospheric aerosols: Science and Techniques", ISRO Structured Training Programme (STP) on Space Science Porgramme: ISRO & Global Scenario, Physical Research Laboratory, Ahmedabad, 5-9 Mar, 2018.
53. "Air pollution and climate change: Challenges", National Seminar on Environment, Pollution and Climate Change, Vallabh Vidyanagar, 30 Jan, 2018.
54. "Ozone and Climate", International Ozone Day, Science City, Ahmedabad, 16 Sep, 2017.
55. "Observations and Simulations of Aerosols: Challenges", Keynote Address, International conference on Understanding, Predicting and projecting Climate change over Asian Region, National Atmospheric Research Laboratory, Gadanki, 26-28 June, 2017.
56. "Volcanic analog for geoengineering", National Roundtable Discussion on Geoengineering and India: Science and Policy, Indian Institute of Technology, New Delhi, 23 June, 2017.
57. "Climate change and aerosols", Workshop on Atmospheric constituents and climate change implications under the aegis of National Carbonaceous Aerosol Program sponsored by MoEFCC, IIT Kharagpur, 20 June, 2017.

D. Pallamraju

58. "Space Environment", 3^{rd} International Conference on Environmental Management, Jawaharlal Nehru Technological University, Hyderabad, India, 27-30 Nov, 2017.
59. "Remote sensing of the upper atmosphere through optical techniques", Structured Training Program, Physical Research Laboratory, Ahmedabad, 5-9 Mar, 2018.

Som Kumar Sharma

60. "Raman Lidar for Atmospheric Investigations", National Symposium on Multidimensional Aspects of Spectroscopy (NSMAS)-2017, Deen Dayal Upadhyaya University, Gorakhapur, 17-18 Nov, 2018.
61. "Atmospheric Studies using Rayleigh - Mie - Raman Lidar in India", Seminar on Space & Atmospheric Physics, Saurashtra University, Rajkot, 12 Mar, 2018.
62. "Investigations of the Earth's Atmosphere using Lidar: Indian Perspectives", 105^{th} Indian Science Congress, Imphal, India, 16-20 Mar, 2018.

Harish Gadhavi

63. "Role of black carbon particles in Earth's climate", and acted as guest of honour at Institute of Infrastructure, Technology, Research and Management (IITRAM)), Ahmedabad on occasion of celebration of Engineer's Day, Ahmedabad, 15 Sep, 2017.

A. Guharay

64. "Diurnal tide and planetary wave interactions at low latitude MLT region", 15^{th} International Workshop on Technical and Scientific Aspects of MST radar (MST15/iMST2), National Institute of Polar Research, Tokyo, Japan, 26-31 May, 2017.

Geosciences Division

J.S. Ray

65. "Bound on time-variation of Fine Structure Constant from Radioactive Decay Ages", Conference on New Initiatives in Fundamental science Experiments (NIFE), Physical Research Laboratory, Udaipur, 12 -14 Sept, 2017.
66. "Cretaceous continental magmatism in North-Eastern India", 83^{rd} Annual Meeting of the Indian Academy of Sciences, Bangalore, Shillong, 4 Nov, 2017.
67. "Geochemical evolution of Amba Dongar carbonatite, complex", International Seminar on Carbonatites-Alkaline Rocks and Associated Economic Mineral Deposits, Vadodara, 8 - 11 Dec, 2017.
68. "Bitter Springs δ13C anomaly in the Vindhyan Supergroup, Rajasthan, India", National Seminar on 'Dynamics of surface and subsurface geological processes', Pondicherry, 8 - 9 Feb, 2018.
69. "Third Rock from the Sun", DST-INSPIRE talk at National Institute of Science and Technology, Berhampur, 24 March, 2018.

R.D. Deshpande

70. "submarine ground water discharge (SGD)", Brainstorming meeting,National Centre for Earth Science Studies (NCESS), Ministry of Earth Sciences (MOES), Thiruvananthapuram, Kerala, India, 31 Aug - 01 Sept, 2017.
71. "Advancements in Space-based earth observations and services for weather and climate", International tropical meteorology symposium (intromet-2017), SAC, Ahmedabad, 7 -10 Nov, 2017.
72. "vision & explorations for planetary sciences in decades 2020-2060", Brainstorming session, PRL, Ahmedabad, 8 - 10 Nov , 2017.
73. "Water Conservation and Related Issues", National Workshop organized by Central Ground Water Board, West-Central Region, Ahmedabad, Sardar Patel National Museum, Shahibaug, Ahmedabad, 15 Nov, 2017.

R. Bhushan

74. "Role of radiocarbon in ocean sciences,", National Seminar on 'Dynamics of Surface and Subsurface Geological Processes', Pondicherry University, Pondicherry, 09 Feb, 2018.

M.G.Yadava

75. "Paleoclimate reconstruction from Speleothem", Symposium on 'Advances in Modern Earth System Sciences', IISER, Kolkata, 25 - 26 March, 2017.

N. Rastogi

76. "Chemistry of Secondary Aerosol over India", Keynote address, International conference on "Understanding, Predicting and Projecting Climate Change over Asian Region (UPCAR)", jointly organized, National Atmospheric Research Laboratory (NARL) and S.V. University, Tirupati, 26 - 28 June, 2017.
77. "Particulate Pollutants in Ambient Air: Effects on Environment and Human Health", Environmental Researchers' Meet-2017, Gujarat Environmental Gujarat Environment Management Institute (GEMI), Gandhinagar, 5 June, 2017.
78. "Aerosol Chemistry: Organic Aerosol", DST's National Workshop on 'Aerosols: Science and Application' as part of proposed National Network Programme on Climate Change and Aerosols, IIT-Kanpur, 11-12 May, 2017.

S. Kumar

79. "Effect of a tidal cycle on biogeochemistry of mangrove dominated tropical estuary (Sundarbans, India)", The Second International Workshop on Human Impacts on Carbon Fluxes in Asian River Systems, Dhaka, Bangladesh, 9 - 11 Feb, 2018.
80. "The flow of nitrogen through the land-atmosphere system", Fifth Integrated Land Ecosystem-Atmosphere Processes Study (iLEAPS) conference, Oxford, UK, 11 - 14 Sept, 2017.

Theoretical and Computational Physics

S. Mohanty

81. "Supergravity models consistent with LHC and Inflation", III Saha Theory Workshop, SINP, Kolkata, 16 Jan — 20 Jan, 2017.

82. “Overview of Astroparticle Physics”, Candles of Darkness Conference, ICTS, Bengaluru, 5 Jun — 9 Jun, 2017.

83. “Supergravity Inflation”, 13th International Workshop on Dark Side of the Universe, Daejeon, Korea, 10 Jul — 14 Jul, 2017.

H. Mishra

84. “Transport coefficients in Polyakov loop quark meson coupling model”, International conference on Critical point and onset of deconfinement (CPOD2017), Stony Brook University, USA, 7 Aug — 11 Aug, 2017.

85. “Transport coefficients for hot and dense matter: a relaxation time approximation”, Workshop on High Energy Physics Phenomenology, (WHEPP-XV), IISER Bhopal, 14 Dec — 23 Dec, 2017.

S. Goswami

86. “Neutrino Phenomenology”, 18th Lomonosov Conference on Elementary Particle Physics, Moscow, Russia, 2 Aug, 2018.

87. “Neutrinoless double beta decay”, NuHorizons, HRI, Allahabad, 22 Feb, 2018.

Angom D. K. Singh

88. “Interacting BECs and introduction to Bose-Hubbard Model”, SERB School on Frontiers in Quantum Optics, IIT Guwahati, 1 Dec — 19 Dec, 2017.

89. “Quantum Hall states in optical lattices”, ISAMP-TC7, IISER Tirupati, 6 Jan — 8 Jan, 2018.

90. “Coupled-cluster theory in atomic calculations”, Ultrafast and many-body atomic physics, IIT Tirupati, 8 Mar — 9 Mar, 2018.

91. “Bosonic quantum Hall states in single layer 2D optical lattices”, Recent Trends in Cold and Ultracold Matter, IIT Guwahati, 27 Mar — 29 Mar, 2018.

R. Rangarajan

92. “Current Status of Warm Inflation”, 18th Lomonosov Conference on Elementary Particle Physics at Moscow State University, Lomonosov Moscow State University, 24 Aug — 30 Aug, 2017.

P. Konar

93. “Jet on the top”, Workshop on Top physics, IISER Kolkata, 27 Jan — 30 Jan, 2018.

94. “Machine Learning”, Annual Theory Discussion Days 2018 (ATDD’18), PRL, Ahmedabad, 6 Feb — 8 Feb, 2018.

95. “Overview on Jet physics”, WG-1, WG-III joint session, WHEPP, IISER Bhopal, 14 Dec — 23 Dec, 2017.

96. “Demystifying compressed top squark region with kinematic variables”, International Conference on Supersymmetry and the Unification of Fundamental Interactions (SUSY’17),, TIFR, Mumbai, 11 Dec — 15 Dec, 2017.

A. R. Prasanna

97. “Story of our Universe”, Invited talk at the British Council, Ahmedabad, British Council, Ahmedabad, 13 May, 2017.

98. “Our Universe and the new astronomies”, Invited special talk at PDPU, Gandhinagar, PDPU, Gandhinagar, 10 Nov, 2017.

Atomic, Molecular and Optical Physics

K. P. Subramanian

99. “LTE condition validation by plume characterization in laser produced plasmas”, 7^{th} Topical Conference of the Indian Society of Atomic and Molecular Physics, IISER & IIT Tirupati, 6—8 January 2018.

R. P. Singh

100. “Recovering the lost vorticity of scattered optical vortex”, International Conference on Advances in Optics and Photonics (ICAOP-2017, XLI Conference of the Optical Society of India) Guru Jambheshwar, University of Science and Technology, Hisar, Haryana, 23 Nov — 26 Nov, 2017.

101. “Using non-separable state of light to find the “lost” phase structure”, International Conference on Quantum Foundations – 2017 (ICQF-17), NIT, Patna, 04 Dec — 09 Dec , 2017.

G. K. Samanta

102. “High repetition rate, ultrafast parametric sources of structured beams.”, UFS-2017, University of Hyderabad, Hyderabad, 02 Nov — 04 Nov, 2017.

B. Sivaraman

103. “Astrochemistry - Fate of Molecules Deep in Space”, Kurukshetra 2018,, Anna University, Chennai, 03 Feb, 2018.

104. “Shock Processing of Astromaterials - From astrochemical ices to meteorites”, National Shock Wave Symposium, Terminal Ballistics Research Laboratory, Chandigarh, 26 Feb — 28 Feb, 2018.

R. K. Kushawaha

105. “Photoionization of polyatomic molecules: multi-slits type interferences, molecular fragmentation and ultrafast dynamics”, 7th Topical Conference of the Indian Society of Atomic and Molecular Physics, IISER & IIT, Tirupati, 6 Jan — 8 Jan, 2018.

106. “Probing the Structure and Ultrafast Dynamics in polyatomic molecules: Towards Molecular Movies”, Workshop on Ultrafast and many-body atomic physics, IIT, Tirupati, 8 Mar — 9 Mar, 2018.

A.K. Singhvi

107. “Land -sea correlations: some thoughts”, During the International conference on Loess Research, Loessfest -2017, Gorgon, Iran, 07 Oct – 11 Oct, 2017.

108. “Annual Convention of the Indian Association for Sedimentologists, Correlation of Terrestrial and Marine Sedimentation Records”, During the Quaternary: Some Conceptual Issues, Amravati University, Amravati, 19 Dec – 21 Dec, 2017.

B. G. Vaishnav

109. “ACID-AstroChemical Ices Database”, 2nd Solid Spectroscopy Hosting Architecture of Databases and Expertise (SSHADE) partners meeting, IPAG, Grenoble, France, 4-5 December 2017.

Swetapuspa Soumyashree

110. “LIBS algorithm for multi-element samples employing synthetic generated spectra”, 7th Topical Conference of the Indian Society of Atomic and Molecular Physics, IISER & IIT Tirupati, 6—8 January 2018.

111. “Concentration estimation of brass sample using the synthetic generated LIBS spectra”, 2nd Meghnad Saha Memorial International Symposium-cum-Workshop on ‘Laser Induced Breakdown Spectroscopy’(MMISLIBS-II) 2018”, Physics Department, University of Allahabad 19-21 February 2018.

E. Nageswara Rao

112. “Quantitative analysis of geological rock samples using LIBS”, 2nd Meghnad Saha Memorial International Symposium-cum-Workshop on ‘Laser Induced Breakdown Spectroscopy’ 2018”, Physics Department, University of Allahabad 19-21 February 2018.

Lectures at Universities / Institutions

Astronomy and Astrophysics

Srivastava, Mudit K

1. "Optical Instrumentation for Ground Based Telescopes and its Challenges", Seminar delivered at Institution of Engineers, Udaipur India, 16th September 2017
2. "Design of MFOSC-P: A Spectrometer-Camera for Mt. Abu 1.2m Telescope", Seminar delivered at Indian Institute of Astrophysics, Bengaluru, 8th January 2018

Veeresh Singh

3. "Unvieling new population of Active Galactic Nuclei using deep multiwavelength surveys", Talk delivered at Aryabhatt research institute of observational sciences (ARIES), Nainital, India, May 31st 2017

A.S. Rajpurohit

4. "Constraining the fundamental parameters of M dwarfs", Talk delivered at Tautenburg Observatory, Jena, Germany, 24th Ocotober 2017.

Vishal Joshi

5. "Astronomical fireworks", Talk delivered at Ganpat University, Kherva, Gujarat, India, February 28, 2018.
6. "Understanding Black holes", Talk delivered at D College of Engineering, Ahmedabad, India, March 24, 2018.

Solar Physics

A. Prasad

7. "Magnetohydrodynamics of the solar corona initiated with an extrapolated non-force-free magnetic field", Astrophysics Colloquium, Institute of Physics, University of Graz, Graz, Austria, November 22, 2017

Planetary Sciences and PLANEX Program

Anil Bhardwaj

8. "CSIR-CSIO Foundation Day Lecture", CSIR-CSIO Foundation Day Lecture, Central Scientific Instruments Organisation (CSIO-CSIR), Chandigarh, 30 October, 2017.
9. "Indian Planetary Exploration Program", IIG Mumbai, 22 Feb, 2018.
10. "Indian Planetary Mission and Exploration", National Science Day Lecture, Institute of Physics, Bhubaneswar, 28 Feb, 2018.

J. P. Pabari

11. "Role of Electronics in Space Science and Space Research", An Invited Talk at Parul Institute of Engineering and Technology, Waghodia, July 21, 2017

Space and Atmospheric Sciences

Diptiranjan Rout

12. "Space weather", Rajasthan English Higher Secondary School, Ahmedabad, India, 10 Feb, 2018
13. "Magnetosphere-Ionosphere-Thermosphere System Under Varying Space Weather Conditions", ISEE, Nagoya University, Japan, 10 Nov, 2017

Harish Gadhavi

14. "Delivered six lectures for a short course on atmospheric radiative transfer", St. Xavier's College, Ahmedabad, 26-28 Dec, 2017

H. Chandra

15. "Measurements from Langmuir probe", NARL, Gadanki, 16 Nov, 2017
16. "Radar Techniques to probe ionosphere and atmosphere", Saurashtra University, Rajkot, 12 Mar, 2018
17. "Seminar on Space and Atmospheric Physics", Saurashtra University, Rajkot, 12 Mar, 2018

L. K. Sahu

18. "Ozone in Earth's Atmosphere: Past, Present and Future", World Ozone Day, India Meteorological Society (IMS), National Institute Of Oceanography (NIO), Goa, India, 15 Sep, 2017.
19. "Study of volatile organic compounds (VOCs) in India: Anthropogenic vs Biogenic Sources", Indian Institute of Tropical Meteorology, Pune, India, 29 Sep, 2017
20. "Volatile organic compounds in contrasting chemical environments over South Asia", Max Planck Institute for Chemistry (MPIC), Mainz, Germany, 25 Oct, 2017
21. "Future challenges in Atmospheric Measurements", Webinar on Sun-Climate Space Education and Research Foundation (SERF), Ahmedabad, India, 01 Mar, 2018
22. "Volatile Organic Compounds (VOCs) in the Atmosphere: Sources and Role in Ozone Photochemistry", Ishwarbhai Ambalal Patel (Shertha) Visiting Professor Lecture Program, S. P. University: Dept. of Chemistry, Anand, India, 14 Mar, 2018

Som Kumar Sharma

23. "Atmospheric Ozone as Life Supporting Gas", Uttar Pradesh Council of Science and Technology (UPCST), Lucknow, 22 Sep, 2017
24. "Atmospheric Ozone Concentrations and Trends: Role of Good Ozone and Bad Ozone", Hindu College, Delhi University, Delhi, 6 Feb, 2018
25. "Solar Forcing on Climate and Environment", Space Education and Research Foundation (SERF), Ahmedabad, 28 Feb, 2018

Dr. D. Chakrabarty

26. "Various aspects of Space weather", Delivered four invited lectures in second PG Course of CSSTEAP in Global Navigation Satellite Systems (GNSS-2), 15-16 January, 2018

Geosciences Division

J.S. Ray

27. "Quaternary Volcanism in India: the tale of two Andaman Volcanoes:", Colloquium at School of Physical Sciences, Tata Institute of Fundamental Research, Mumbai, 12 April, 2017.

R. D. Deshpande

28. "Implementation of National Network Project on Mission – SGD (submarine ground water discharge) during 2018-2023", National Centre for Earth Science Studies (NCESS), Ministry of Earth Sciences (MOES), Thiruvananthapuram, Kerala, India, 21, 22 & 23 Feb, 2018.
29. "Isotope Characterization of various hydrological components concerning India: New insights and challenges", 2^{nd} National Geo-scholar's Research Meet, Wadia Institute of Himalayan Geology, Dehradun, May 17 - 19, 2017
30. "Isotope applications in aid of water conservation in India ", National Workshop on 'Water Conservation and Related Issues', at Sardar Patel National Museum, Shahibaug, Ahmedabad, Organized by Central Ground Water Board, West-Central Region, Ahmedabad, November 15, 2017
31. "Isotope Characterization of Water Resources of IndiaScientific and Societal Relevance", 4^{th} Information & Networking Event: European Union-India Call on Water, M.S. University of Baroda, Vadodara, January 11, 2018
32. "Isotope applications in Submarine Ground Water Discharge - Use of IWIN Isotope Data", Workshop on implementation of National Network Project on Mission - SGD (submarine ground water discharge) during 2018-2023, at National Centre for Earth Science Studies (NCESS), Ministry of Earth Sciences (MOES), Thiruvananthapuram, Kerala, February 21-23, 2018
33. "Hydrological Challenges and Options for IndiaImportance of Isotope Tracers", ISRO Structured Training Programme on Space Science ProgrammeISRO & Global Scenario, Physical Research Laboratory, Ahmedabad, March 5 - 9, 2018

R. Bhushan

34. "Challenging applications of radiocarbon in Earth Sciences ", National Centre for Earth Science Studies, Trivandrum, December 27, 2017

N. Rastogi

35. "Atmospheric Aerosol: Physico-chemical Characteristics and Effects", Ishwarbhai Ambalal Patel (Shertha) Visiting Professor Lecture Programme at Depart of Chemistry, Sardar Patel University, Vallabh Vidyanagar, Gujarat, 14 Mar, 2018.

A. Singh

36. "Climate Change Impacts Management", Gujarat University,Ahmedabad, Course lectures (20 lectures), May 2017 – February 2018
37. "International Earth Science Olympiad (IESO)", Anna University (one out of the four Indian students secured bronze medals for India during 20-28 Aug in IESO France, and secured gold medal in team event), 25-29 May, 2017 & 16-18 July, 2017

Theoretical and Computational Physics

S. Goswami

38. "Introduction to Particle Physics", Set of two lectures given in the three days lecture workshop at St. Anthony's college, Shillong, 7 Sept – 9 Sept, 2017

D. Angom

39. "Quantum Hall states in optical lattices", RIST popular talk at Manipur University, Imphal, November 17, 2017

P. Konar

40. "Fundamental building blocks of nature" Tarang'18", Space and Science Fest at LD college, Ahmedabad, March 24, 2018
41. "Demystifying compressed top squark region with kinematic variables", IMSC, Chennai, September 19, 2017

N. Singh

42. "A bird's-eye view of the field of unconventional superconductivity", PRL Colloquium, July 12, 2017

A.R. Prasanna

43. "History of the Universe as seen from different Windows", Invited lecture atIIAR, Gandhinagar, Jan 15, 2018
44. "Gravitational waves and the associated Physics of the Cosmos", Colloquium delivered in Institute of Astrophysics, Bangalore,, December 2, 2017

R. Rangarajan

45. "Enigma of the Matter-Antimatter Asymmetry of the Universe and Gravitinos", Novosibirsk State University, Novosikbirsk, Russia, September 4, 2017
46. "Gravitinos, Reheating and the Matter-Antimatter Asymmetry of the Universe ", SINP, Kolkata, October 30, 2017
47. "Gravitinos, Reheating and the Matter-Antimatter Asymmetry of the Universe ", Novosibirsk State University, Novosikbirsk, Russia, September 5, 2017
48. "Gravitinos, Reheating and the Matter-Antimatter Asymmetry of the Universe ", Joint Institute for Nuclear Research (JINR), Russia, September 7, 2017

Atomic, Molecular and Optical Physics

R. P. Singh

49. "Optical vortices and orbital angular momentum of light", NIT Warangal, October 29, 2017

Vinayak Kumar

50. "Thermochronology Studies ", Oral presentation on Thermochronology Studies in Alaknanda valley in International conference on Luminescence and ESR Dating (LED-2017), September 14, 2017.

A.K. Singhvi

51. "Recent developments in Luminescence dating", International lecture at the Beijing, Beijing University, Beijing, 06 Dec – 11 Dec , 2017.
52. "Some unexplored facets of luminescence dating", International lecture at Beijing, Beijing University, Beijing, 06 Dec – 11 Dec , 2017.
53. "Earth Sciences in India: some new initiatives", International lecture at Beijing, Beijing University, Beijing, 06 Dec – 11 Dec , 2017.
54. "The societal dimension of geosciences: The challenges ahead", International lecture at Beijing, Beijing University, Beijing, 06 Dec – 11 Dec , 2017.
55. "Land-sea correlation during the Quaternary: Are they real", Colloquium at the Institute of Geology and Geophysics, Chinese Academy of Sciences, Beijing, 09 Dec, 2017.

B. G. Vaishnav

56. "Science-Engineering-Technology", Tarang – Science fest, L. D. Enginnering College, Ahmedabad, 23 March, 2018.

Science

Astronomy and Astrophysics

GMRT decimetric observations during a long duration C1.4 solar flare

A study of decimetric radio emission, was carried out using the first high time cadence (0.5 s) images from the *Giant Meterwave Radio Telescope* (*GMRT*) at 610 MHz. The observed activity was associated with a *GOES* C1.4 class solar flare, an M1.0 class solar flares, and a coronal mass ejection (CME) onset that occurred on 20 June 2015. The high spatial resolution images from *GMRT* show a strong radio source during the C1.4 flare, located $\sim 500''$ away from the flaring site with no corresponding bright foot points or coronal features nearby. In contrast however, strong radio sources were found to be located near the flaring site during the M1.0 flare and around the CME onset time. Weak radio sources, located near the flaring site, were also found during the maximum of the C1.4 flare activity, which show a temporal association with metric type-III bursts identified by the Solar Broadband Radio Spectrometer at the Yunnan Astronomical Observatory, China. A multi-wavelength analysis, in combination with magnetic potential field source surface extrapolations, have been carried out to investigate the genesis of radio emitting electrons of the decimetric and metric bursts, which has revealed that the strong *GMRT* decimetric source is produced by an electron cyclotron maser emission process and the exciting agents of *GMRT* radio sources including that of metric type-III bursts originated from a common electron acceleration site.

This work was done in collaboration with NAO, China, and INPE, Brazil.

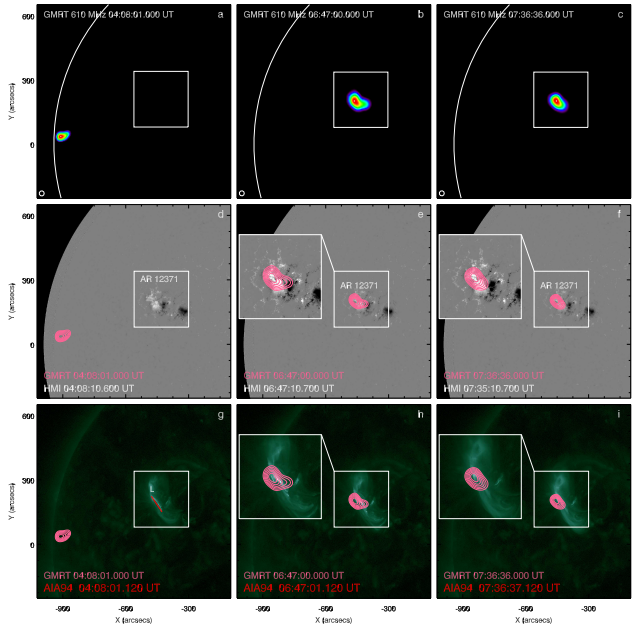

Figure no. 1: The columns, from left to right, show images, respectively, at the peak times of C1.4 and M1.0 flares, and at the onset of the CME, on 20 June 2015. The top row shows the *GMRT* 610 MHz snapshot maps, while the middle and bottom rows show their contour images (in pink) overlaid, respectively, on *HMI* photospheric and *AIA* 94 Å EUV images.

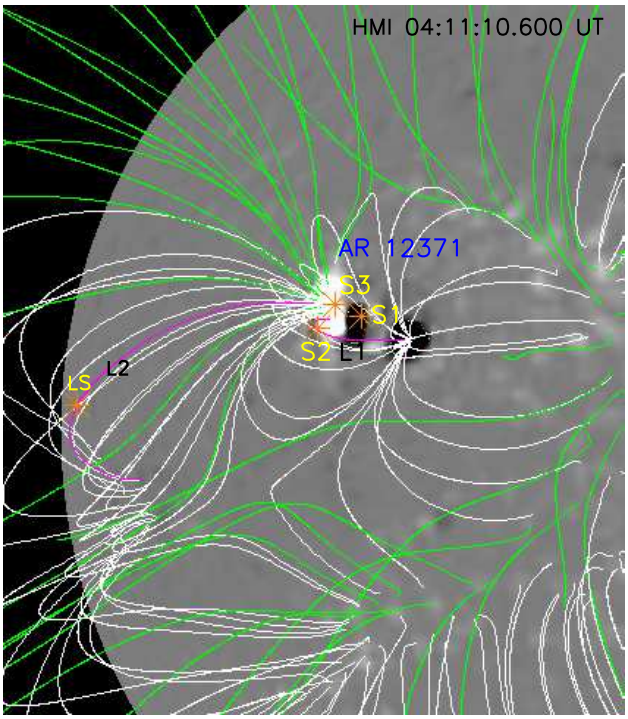

Figure no. 2: The PFSS computed coronal magnetic field lines are shown in white (for closed field lines) and green (for open field lines), overlaid on a background HMI image, at the radio flare maximum. Also, overplotted as star symbols in orange are centroids of $GMRT$ 610 MHz sources LS, S1, S2 and S3. The magnetic field loops associated with sources S2 and LS are shown by the solid pink curves, labelled as L1 and L2.

(Janardhan, P.)

Simulation of coronal loop implosion and magnetohydrodynamic oscillation

There is considerable observational evidence of implosion of magnetic loop systems inside solar coronal active regions following high-energy events like solar flares. We propose that such collapse can be modeled in three dimensions quite accurately within the framework of ideal magnetohydrodynamics. We furthermore argue that the dynamics of loop implosion is only sensitive to the transmitted disturbance of one or more of the system variables, e.g., velocity generated at the event site. This indicates that to understand loop implosion, it is sensible to leave the event site out of the simulated active region. Toward our goal, a velocity pulse is introduced to model the transmitted disturbance generated at the event site. Magnetic field lines inside our simulated active region are traced in real time, and it is demonstrated that the subsequent dynamics of the simulated loops closely resemble observed imploding loops. Our work highlights the role of plasma β in regards to the rigidity of the loop systems and how that might affect the imploding loops' dynamics. Compressible magnetohydrodynamic modes such as kink and sausage are also shown to be generated during such processes, in accordance with observations.

This work is done in collaboration with Bhargav Vaidya of IIT - Indore, Soumitra Hazra of IISER - Kolkata and Jishnu Bhattacharyya who is an independent scholar.

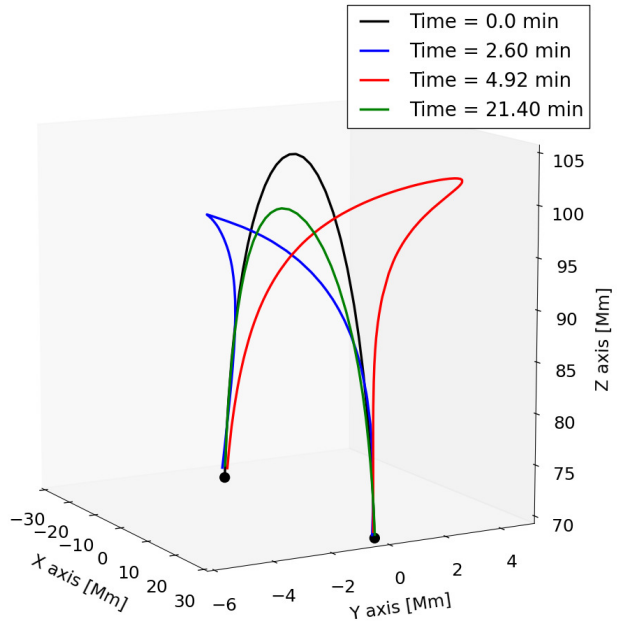

Figure no. 3: Orientation of a typical collapsing loop from our simulation at different moments (exact times in inset).

(Aveek Sarkar)

Understanding solar active region transient brightening through observation and modeling

Using the observations recorded by Atmospheric Imaging Assembly (AIA) on-board the Solar Dynamics Observatory (SDO), the Interface Region Imaging Spectrograph (IRIS) and the Extreme-ultraviolet Imaging Spectrometer (EIS) and X-Ray Telescope (XRT) both on-board Hinode, we find the evidence of chromospheric evaporation in a coronal loop after the occurrence of two active region transient brightenings (ARTBs). Such transient brightenings are often seen in the solar active region, but their association with chromospheric evaporation is hardly observed. We numerically model such scenario for better understanding of the loop dynamics and the evaporation process.

This work is done in collaboration with Girjesh Gupta and Durgesh Tripathi of IUCAA - Pune

(Aveek Sarkar)

Time and Phase resolved optical spectra of potentially hazardous asteroid 2014JO25

The double lobed contact binary asteroid 2014 JO25, considered to be "potentially hazardous" by the Minor Planet Center was spectroscopically followed during its close-Earth encounter on 19th

and 20th of April 2017. The optical spectra of the asteroid were taken with the low resolution spectrograph (LISA), mounted on the 1.2m telescope at the Mount Abu Infrared Observatory, India. Using the Johnson-Cousin BVR filter profile, synthetic photometry was carried out on the spectra. The optical reflectance and B-V color of the asteroid turns out to be a very sensitive function of the combined effective viewing area of the asteroid surface which depends on the rotational phase and the changing solar phase angle. The absolute magnitude H and the phase function slope parameter G were obtained for the asteroid by fitting the two parameter H-G phase function. Although, only the intermediate phase angles were covered during the two days of observation, we have tried fitting the Hapke parameters to the phase function.

The rotation period of the asteroid was determined from the V band light curve and was found to be roughly 3.1 hrs. The absolute magnitude H and the slope parameter G were determined for the asteroid in V and R filters using the IAU accepted standard two parameter H-G model. A peculiar rarely found result coming from this asteroid is its phase bluing trend. The relative B-V color index seems to increase with decreasing phase angle. Such a trend has never been reported for any of the asteroids. On the contrary, phase reddening in asteroids are very common due to reasons like space weathering. The asymmetry parameter g and the single scattering albedo w were estimated for the asteroid by fitting the hapke phase function to the observed data. The asteroid shows relatively large value for the single scattering albedo and it also seems to be highly backscattering.

(Kumar Venkataramani, Shashikiran Ganesh, Archita Rai, Kiran S Baliyan, Umesh C Joshi)

Masses and radii of four very low mass stars in F+M eclipsing binary systems

Eclipsing Binaries (EBs) with one of the companions as very low mass stars (VLMS or M dwarfs) are testbeds to substantiate stellar models and evolutionary theories. F+M EBs are important systems to be studied as they are the most commonly occurring EBs. For the present study, four EB candidates with F type primaries, namely, SAO 106989, HD 24465, EPIC 211682657 and HD 205403, were identified from different photometry missions, the ground-based photometry mission SuperWasp, and the space-based photometry missions, Kepler 2 (K2) and STEREO. Using the high-resolution spectrograph, PARAS, at the 1.2 m telescope at Mount Abu, Rajasthan, India, we hereby report the detection of four VLMS, SAO 106989B, HD 24465B, EPIC 211682657B and HD 205403B as companions to the four EBs. We performed spectroscopic analysis for these EBs and found the companion masses to be 0.255 ± 0.005, 0.233 ± 0.002, 0.599 ± 0.017, and 0.406 ± 0.005 $M_{\odot}$ for SAO 106989, HD 24465, EPIC 211682657 and HD 205403 respectively. We determined orbital periods of 4.39790 ± 0.00001 and 7.19635 ± 0.00002 d and eccentricity values of 0.248 ± 0.005 and 0.208 ± 0.002 for EBs SAO 106989 and HD 24465 respectively. The orbital period for the other two EBs, EPIC 211682657 and HD 205403, are determined as 3.142023 ± 0.000003 and 2.444949 ± 0.000001 d and the eccentricity values for the same sources are 0.0097 ± 0.0008 and 0.002 ± 0.002 respectively. The determination of radius for the VLMS companions is achieved by modeling the photometric and spectroscopic data. These values are 0.326 ± 0.012 $R_{\odot}$ for SAO 106989, 0.244 ± 0.001 $R_{\odot}$ for HD 24465, 0.566 ± 0.005 $R_{\odot}$ for EPIC 211682657, and 0.444 ± 0.014 $R_{\odot}$ for HD 205403. The radii of M dwarf for companion of HD 24465 and EPIC 211682657, have been measured by precise photometry observations from KEPLER and are consistent with theoretical predictions within error bars. However, for the companions of SAO 106989 and HD 205403 for which the M dwarf radii are measured by KELT and STEREO photometry, the radii derived here are 17-20% higher than those predicted by theory. A brief comparison of the results of the current work is made with the M dwarfs already studied in the literature.

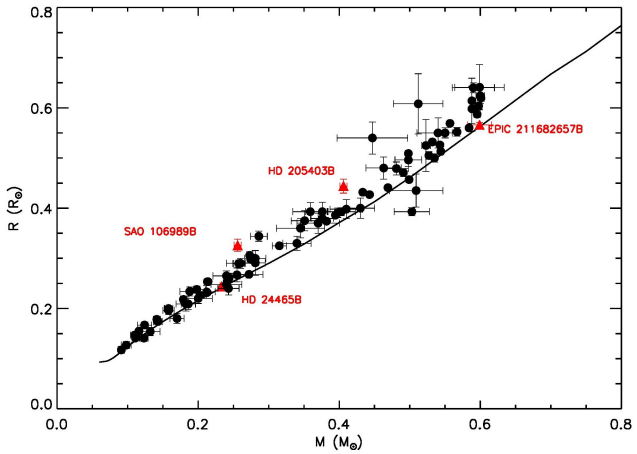

Figure no. 4: Mass-Radius diagram for M dwarfs based on Baraffe models for 1 Gyr isochrone and solar metallicity. Overplotted in black filled circles are the M dwarfs taken from literature and the ones in red filled triangles are studied as a part of this paper. The masses and radii are plotted with their respective error bars.

(Abhijit Chakraborty, Priyanka Chaturvedi, Rishikesh Sharma, Neelam J.S.S.V Prasad, B.G. Anandarao)

Evidence of a sub-Saturn around EPIC 2119452001

We at PRL have discovered a sub-Saturn exoplanet around a bright star (V =10.15, G0 spectral type), EPIC$\sim$211945201. EPIC 211945201b was found to be a planetary candidate from K2 photometry in Campaigns 5 & 16, transiting in a 19.492day orbit. The photometric data combined with FPP calculations was not sufficient to confirm the planetary scenario. Hence we did high-resolution spectroscopic follow-up of the target using the PARAS spectrograph (19 radial velocity observations) over a time-baseline of $\sim$1.5 years and conclusively ruled out the possibility of an eclipsing binary system and confirm the 2-σ detection of a sub-Saturn planet. The confirmed planet has a radius of 6.12$\pm$0.1 $R_{\odot}$, and a mass of 27$\pm$14 $M_{\odot}$ and Saturn-like density of 0.65$\pm$0.34 g cm-3. This detection is important as it adds to a sparse catalog of confirmed exoplanets with masses between 10-70 $M_{\odot}$ and radii between 4-8 $R_{\odot}$, whose masses and radii are measured to a precision of 50% or better (only 23 including this work). This is the first exoplanet discovery from the country.

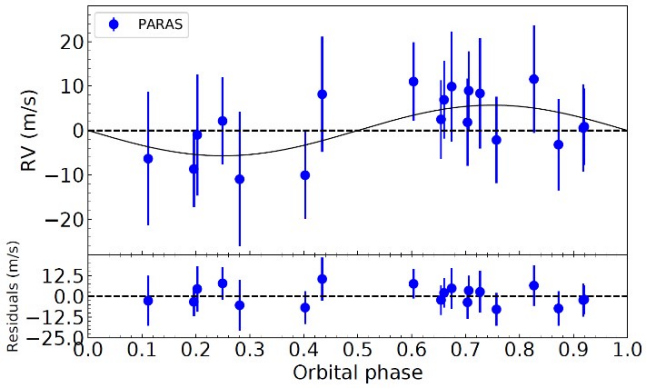

Figure: Radial Velocity (RV) data points of K2-236, observed by PARAS with 1.2m telescope of PRL at Mt. Abu. Black solid curve represents the modeled RV curve. The model shows the wobbling of the host star and its amplitude gives us the mass of the exoplanet K2-236b.

(A. Chakraborty, A. Roy, A. Sharma, S. Mahadevan, P. Chaturvedi, J. S. S. V Neelam Prasad, and B. G. Anandarao)

Star formation activities in the molecular cloud associated with S242

The role of filaments in the formation of dense massive star-forming clumps and clusters is still a matter of debate. We present a multi-wavelength study to probe the star formation processes on a larger scale ($\sim$1$\circ$.05 $\times$ 0$\circ$.56) around the S242 site. The S242 molecular cloud is depicted in a velocity range from $-$3.25 to 4.55 km s^{-1} and has spatially elongated appearance. Based on the virial analysis, the cloud is prone to gravitational collapse. The cloud harbors an elongated filamentary structure (length $\sim$25 pc) evident in the *Herschel* column density map and the filamentary structure has an observed mass per unit length of $\sim$200 M$_\odot$ pc^{-1} exceeding the critical value of $\sim$16 M$_\odot$ pc^{-1} (at T = 10 K). The filamentary structure contains a chain of *Herschel* clumps (M$_{clump}$ $\sim$150 to 1020 M$_\odot$), revealing the evidence of fragmentation along its length. The most massive clumps are observed at both the filamentary structure ends, while the S242 H II region is located at one filamentary structure end. Based on the radio continuum maps at 1.28 and 1.4 GHz, the S242 H II region is ionized by a B0.5V–B0V type star and has a dynamical age of $\sim$0.5 Myr. The photometric 1–5 μm data analysis of point-like sources traces young stellar objects toward the EFS and the clusters of young stellar objects are exclusively found at both the filamentary structure ends, revealing the star formation activities (see Figure no. 5). Considering the spatial presence of massive clumps and clusters of young stellar objects at both the filamentary structure ends, the observed results are consistent with the prediction of a star formation scenario of the end-dominated collapse driven by the higher accelerations of gas.

This work was done in collaboration with T. Baug (KIAA, China), D. K. Ojha (TIFR, India), P. Janardhan (PRL, India), R. Devaraj (INAOE, México), and A. Luna (INAOE, México).

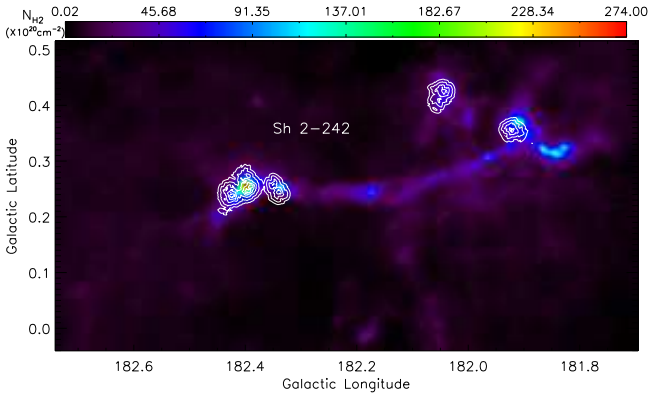

Figure no. 5: a) The *Herschel* column density map is overlaid with the surface density contours (in white) of the identified young stellar objects toward the elongated filamentary structure (length $\sim$25 pc) containing the S242 site. The contours are shown at 5, 10, 20, and 40 stars/pc^2, from the outer to the inner side. The map shows the presence of clusters of young stellar objects toward the ends of the filamentary structure

(Dewangan, L.K.)

New insights in the mid-infrared bubble N49 site: a clue of collision of filamentary molecular clouds

The formation mechanisms of massive stars ($\gtrsim$ 8 M$_\odot$) and young stellar clusters are still poorly understood. Furthermore, we do not have much knowledge of the physical processes of their interaction and feedback on the surrounding molecular environment. We investigate the star formation processes operating in a mid-infrared bubble N49 site, which harbors an O-type star in its interior, an ultracompact H II region, and a 6.7 GHz methanol maser at its edges. The ^{13}CO line data reveal two velocity components (at velocity peaks $\sim$88 and $\sim$95 km s^{-1}) in the direction of the bubble. An elongated filamentary feature (length $>$15 pc) is investigated in each molecular cloud component, and the bubble is found at the interface of these two filamentary molecular clouds (see Figure no. 6). The *Herschel* temperature map traces all these structures in a temperature range of $\sim$16–24 K. In the velocity space of ^{13}CO, the two molecular clouds are separated by $\sim$7 km s^{-1}, and are interconnected by a lower intensity intermediate velocity emission (i.e. a broad bridge feature). A possible complementary molecular pair at [87, 88] km s^{-1} and [95, 96] km s^{-1} is also observed in the velocity channel maps. These observational signatures are in agreement with the outcomes of simulations of the cloud-cloud collision process. There are also noticeable embedded protostars and *Herschel* clumps distributed toward the filamentary features including the intersection zone of the two molecular clouds. In the bubble site, different early evolutionary stages of massive star formation are also present. Together, these observational results suggest that in the bubble N49 site, the collision of the filamentary molecular clouds appears to be operated about 0.7 Myr ago, and may have triggered the formation of embedded protostars and massive stars.

This work was done in collaboration with D.K. Ojha (TIFR, India), and I. Zinchenko (IAPRAS, Russia).

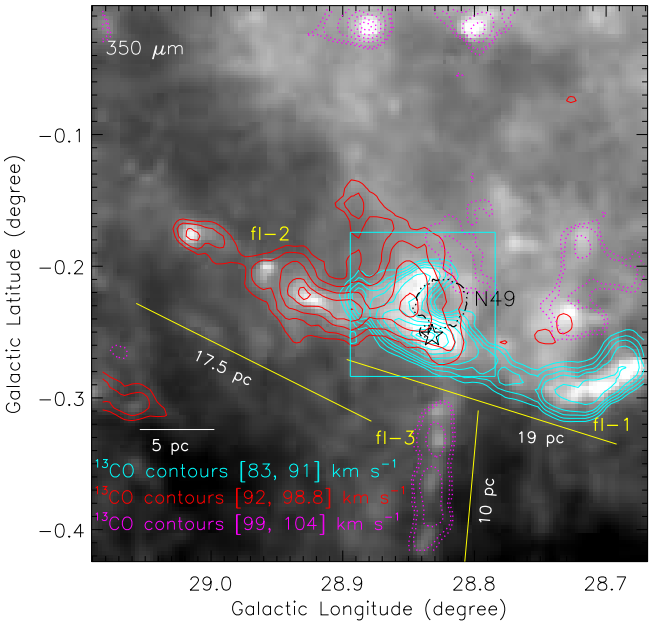

Figure no. 6: Overlay of the molecular clouds linked with the filamentary features on the *Herschel* 350 μm image. The ^{13}CO emissions integrated over three different velocity ranges are presented and the velocity ranges are also given in the figure. The ^{13}CO contours (in red) are 38.357 K km s^{-1} $\times$ (0.45, 0.55, 0.7, 0.85, 0.95), while the levels of cyan contours are 40.847 K km s^{-1} $\times$ (0.35, 0.4, 0.45, 0.5, 0.6, 0.7, 0.8, 0.9, 0.95). A broken contour at 20 cm (in black) represents the location of the bubble N49, and the contour level is 0.0024 Jy/beam. A position of the Class II 6.7 GHz methanol maser is shown by a black star. A scale bar corresponding to 5 pc is shown in the bottom left corner.

(Dewangan, L.K.)

The embedded ring-like feature and star formation activities in G35.673-00.847

The investigation of the role of magnetic fields in the formation of large scale structures in massive star-forming regions is a very challenging task. We present a multi-wavelength study to probe the star formation process in the molecular cloud linked with the G35.673-00.847 site (hereafter MCG35.6), which is traced in a velocity range of 53–62 km s^{-1}. Multi-wavelength images reveal a semi-ring-like feature (associated with ionized gas emission) and an embedded face-on ring-like feature (without the NVSS 1.4 GHz radio emission; where 1σ $\sim$0.45 mJy beam^{-1}) in the MCG35.6. The semi-ring-like feature is originated by the ionizing feedback from a star with spectral type B0.5V–B0V. The central region of the ring-like feature does not contain detectable ionized gas emission, indicating that the ring-like feature is unlikely to be produced by the ionizing feedback from a massive star. Several embedded *Herschel* clumps and young stellar objects are identified in the MCG35.6, tracing the ongoing star formation activities within the cloud (see Figure no. 7). The polarization information from the *Planck* and GPIPS data trace the plane-of-sky magnetic field, which is oriented parallel to the major axis of the ring-like feature. At least five clumps (having M_{clump} $\sim$740–1420 $M_{\odot}$) seem to be distributed in an almost regularly spaced manner along the ring-like feature and contain noticeable young stellar objects (see Figure no. 7). Based on the analysis of the polarization and molecular line data, three subregions containing the clumps are found to be magnetically supercritical in the ring-like feature. Altogether, the existence of the ring-like feature and the star formation activities on its edges can be explained by the magnetic field-mediated process as simulated by Li & Nakamura (2002).

This work was done in collaboration with R. Devaraj (INAOE, México) and D.K. Ojha (TIFR, India).

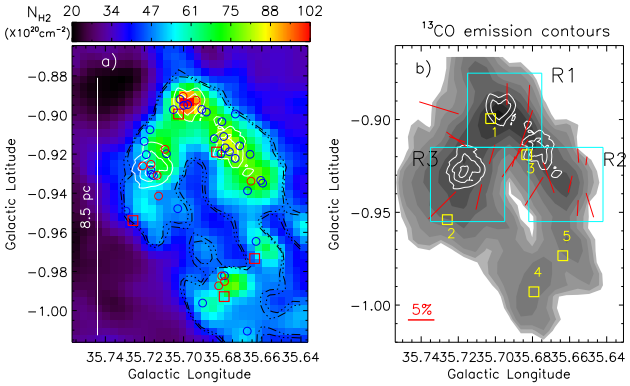

Figure no. 7: Zoomed-in view of the ring-like feature. a) *Herschel* column density map is superimposed with surface density contours (in white) of all the identified young stellar objects, *Herschel* clumps and selected young stellar objects. b) Overlay of GPIPS H-band polarization vectors (in red) of high quality background stars on the integrated ^{13}CO emission map. The map is also superimposed with surface density contours (in white) of all the identified young stellar objects and the *Herschel* clumps. A reference vector of 5% is highlighted in the lower left corner of the map.

(Dewangan, L.K.)

Optical to Near Infrared : A step towards consistent stellar parameters of M dwarfs

Being the most numerous and oldest stars in the galaxy, M dwarfs are the objects which are of great interest for exoplanet searches. As compared to our Sun, the presence of molecules in their cool atmospheres, complicates our understanding of their atmospheric properties including their fundamental stellar parameters. The aim of this study is to determine the fundamental parameters of M dwarfs using high resolution visible and near-infrared spectra observed with CARMENES spectrograph. The high spectral resolution of CARMENES spectra provides a unique opportunity to constrain chemical and physical processes that occur in a cool atmosphere, in particular the redistribution of energy from optical to NIR. We have performed the spectral synthesis using updated BT-Settl model atmosphere by comparing them with the high-resolution observed spectra both in the visible and NIR. We have derived the fundamental stellar parameters such as effective temperature, surface gravity, and metallicity (Teff , log g and [Fe/H]) respectively. (see Figure no. 9).

This work has been done in collabration with Prof. France Allard (ENS Lyon, France) and S. Rajpurohit of University of Gottingen, Germany, O. Mousis of LAM, Marseille, France

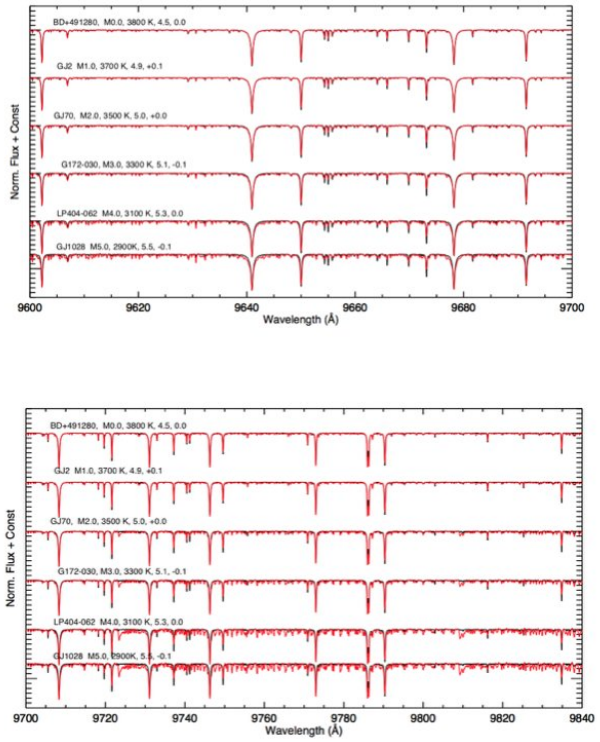

Figure no. 8: CARMENES spectra (black) is compared with the best-fit BT-Settl (red) model.

(A.S. Rajpurohit)

SPIRou Input Catalogue: global properties of 440 M dwarfs observed with ESPaDOnS at CFHT

In the framework of the preparation of the SPIRou Input Catalogue (SPIC), the CoolSnap program aims at screening M dwarfs in the solar neighbourhood against binarity, rapid rotation, activity, etc. To optimize the selection, this paper describes the methods used to compute effective temperature, metallicity, projected rotation velocity of a large sample of 440 M dwarfs observed in the visible with the high-resolution spectropolarimeter Echelle SpectroPolArimetric Device for the ObservatioN of Stars (ESPaDOnS) at Canada–France–Hawaii Telescope. It also summarizes known and newly discovered spectroscopic binaries, and stars known to belong to visual multiple systems. A calibration of the projected rotation velocity versus measured line widths for M dwarfs observed by the ESPaDOnS spectropolarimeter is derived, and the resulting values are compared to equatorial rotation velocities deduced from rotation periods and radii. A comparison of the derived effective temperatures and metallicities with literature values is also conducted. Finally, the radial-velocity uncertainty of each star in the sample is estimated, to narrow down the selection of stars to be included into the SPIC.

This work has been done in collaboration with Dr. Pascal Fouque and Claire Moutou of CFHT and Universite de Toulouse along with other international research institutes.

(A.S.Rajpurohit)

Nova Ophiuchus 2017 as a probe of ^{13}C nucleosynthesis and carbon monoxide formation and destruction in classical novae

Novae contribute almost all of the ^{13}C found in the Galaxy as predicted by nucleosynthesis theory of nova physics. Also the abundance of ^{13}C in novae ejecta can be so extreme that it is comparable to ^{12}C. Nova Ophiuchus 2017 was observed in near-infrared almost at daily cadance for two weeks after its discovery.

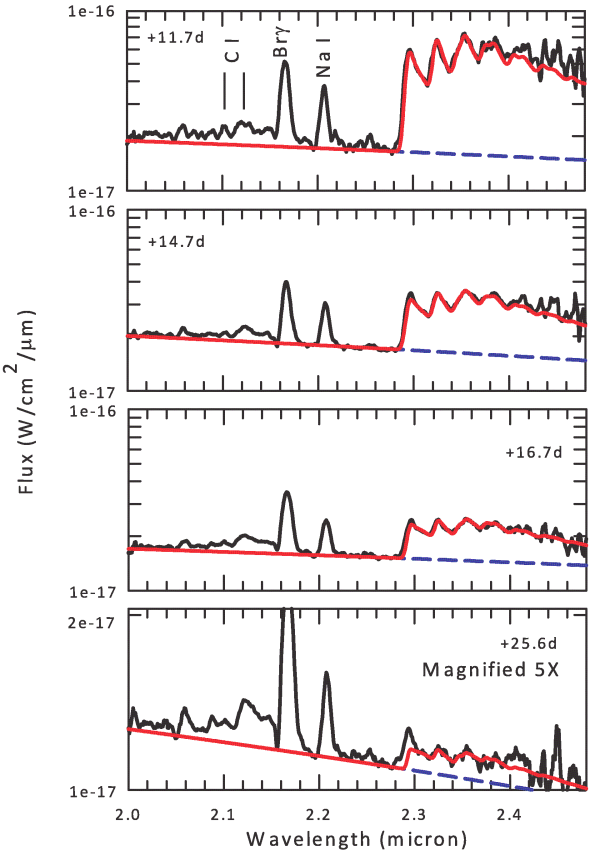

Figure no. 9: The rapid decline in the CO emission with time. All figures drawn to the same flux except when specified. Black, blue and red lines represent observed data, adopted continuum and model fit, respectively.

The K band spectrum obtained 3 days after discovery shows the strong emission feature of first overtone of carbon monoxide (CO) molecule which was almost vanished in next 14 days. LTE modeling of CO emission bands inferrs the ^{12}C/^{13}C ratio is determined to be 1.6 $\pm$ 0.3 assuming that the CO emission is optically thin. This is consistent with the expected value of this parameter from nucleosynthesis theory for a nova eruption occuring on a low mass ($\sim$ 0.6 M$_\odot$) carbon-oxygen core white dwarf. The present ^{12}C/^{13}C estimate constitutes one of the most secure estimates of this ratio in a classical nova. LTE modeling infers the temperature of CO molecules to be 2500 $\pm$ 200K. Figure no. 9 shows the observed K band spectra for four different epochs and best fit LTE models. The strength of CO emission was found to have rapidly declined by almost a factor of $\sim$35 in two weeks. In contrast, the strengths of Brγ and the NaI 2.2056, 2.2084 μm lines have remained fairly constant. The NaI lines were used as a probe to examine the rapid destruction of CO molecules in the framework of different mechanisms proposed for CO destruction viz. an increase in

photoionizating flux, chemical pathways of destruction or destruction by energetic non-thermal particles created in shocks. Sodium has a first ionization potential (IP) of 5.139 eV; the lowest among those elements whose lines are seen in the NIR spectrum of novae. A detailed analysis indicates that an increase in photoionizating flux or energetic non-thermal particles created in shocks are very unlikely to distruct CO and hence the surviving mechanism is the chemical pathways through which CO ahhinilates in the nova ejecta.

(Vishal Joshi, D.P.K Banerjee, Srivastava, Mudit K)

Remnant of Nova Sco 2014: a symbiotic star with too little circumstellar matter to decelerate the ejecta

Pre-outburst 2MASS and WISE photometry of Nova Sco 2014 (V1534 Sco) have suggested the presence of a cool giant at the location of the nova in the sky.

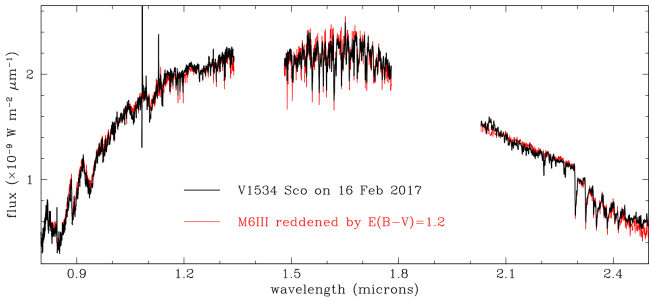

Figure no. 10: The IRTF-SpeX spectrum of V1534 Sco for 16 Feb 2017 is nearly perfectly fitted with that of an M6III template (HD 196610) reddened by E(B - V) = 1.2 following the standard R_V = 3.1 law as tabulated by Fitzpatrick (1999).

The spectral evolution recorded for the nova did not however support a direct partnership because no flash-ionized wind and no deceleration of the ejecta were observed, contrary to the behavior displayed by other novae which erupted within symbiotic binaries like V407 Cyg or RS Oph. We have therefore obtained an 0.8−2.5 μm spectra of the remnant of Nova Sco 2014 in order to ascertain if a cool giant is indeed present and if it is physically associated with the nova. As shown in the Figure no. 10 the spectrum shows the presence of a M6III giant, reddened by E(B-V)=1.20, displaying the typical and narrow emission-line spectrum of a symbiotic star, including HeI 1.0830 μm with a deep P-Cyg profile. This makes Nova Sco 2014 a new member of the exclusive club of novae that erupt within a symbiotic binary. Nova Sco 2014 shows that a nova erupting within a symbiotic binary does not always come with a deceleration of the ejecta, contrary to the common belief. Many other similar systems may lay hidden in past novae, especially in those that erupted prior to the release of the 2MASS all-sky infrared survey, which could be profitably cross-matched now against them.

This work was done in collaboration with Ulisse Munari, INAF Astronomical Observatory of Padova, Italy.

(D. P. K. Banerjee)

Phase-resolved hard X-ray polarimetry of Crab pulsar with *AstroSat* CZT-Imager

The Crab pulsar is a typical example of a young, rapidly spinning, strongly magnetized neutron star that generates broadband electromagnetic radiation by accelerating charged particles to near light speeds in its magnetosphere. Despite of the spectral-timing observations over decades, the mechanism of the emission in pulsars remains poorly understood. Measurement of polarization in X-rays, particularly as a function of pulse phase, is thought to be a key element necessary to understand the emission mechanism and geometry. However, there has been only few measurements of polarization of Crab pulsar so far and these were not sensitive enough to study the variation of polarization properties with pulse phase.

CZT-Imager on-board *AstroSat*, designed as coded-mask hard X-ray spectrometer, makes use of Compton scattering to measure the polarization of incident photons. Though not designed to be a polarimeter, the polarimetric capability of CZTI was well calibrated on ground. We use 800ks of observations of Crab with CZTI in the polarimeteric energy range of 100-380 keV to estimate polarization fraction of 32.7±5.8% with position angle of 143.5±2.8 degrees, which is the most sensitive measurement to date in hard X-rays. Analysis of off-pulse region suggests that the emission has slightly higher polarization with fraction of polarization 39.0±10%. The high significance of polarization detection enables to examine the dependence of polarization characteristics with pulse phase. Keeping in mind that optical polarization study of Crab shows rapid change in position angle within narrow phase intervals and it would not be possible to have sufficient signal in such narrow bins for X-ray data, we perform polarization analysis in dynamic phase bins of width 0.1 starting at all phases with an interval of 0.01. Figure no. 11 shows the resultant phase-dependant fraction of polarization and angle of polarization.

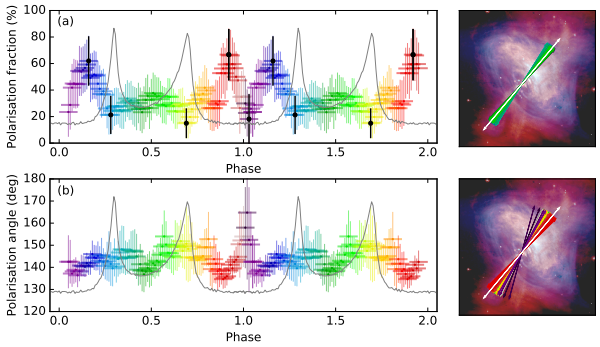

Figure no. 11: Phase-resolved polarization fraction (a) and polarization angle (b) of Crab. The light grey line indicate the pulse profile. Polarization angles are depicted as arrows in the sky planes plotted on the Chandra and Hubble composite images of the Crab nebula with colour representing the phase bin as shown in the plots of the polarization fraction.

Surprisingly, the polarization fraction shows variation within the off-pulse region with dip at around phase zero. Polarization fraction shows a decrease at the pulse peaks and further analysis indicates a hint of polarization angle swing across pulse peaks. These observations along with optical polarization studies poses challenge to the existing models of pulsar emission. Though some variants of Striped wind model is favoured by the results, they do not completely explain the observations, particularly the variation within

off-pulse region. Further observations with CZTI and that with future polarimetric missions are expected to put stronger constraints on the models of pulsar emission.

(Santosh Vadawale, N. P. S. Mithun)

Hard X-ray polarization measurement of Gamma Ray Bursts

Gamma Ray Bursts (GRBs) are the most powerful explosions observed so far in the universe and are believed to originate during the formation of black holes either by the collapse of massive Wolf-Rayet stars or by mergers of binary compact objects. GRB emission occurs in two distinct phases - the prompt and the afterglow. The initial burst of high energy emission or the prompt emission is widely accepted as to originate from a jet close to the black hole whereas the long-lasting multi-wavelength emission or the afterglow following the prompt phase happens far from the compact object when the GRB jet interacts with the ambient medium. In spite of the improvement in our understanding of these sources in the last decade the emission mechanism of the prompt phase have not been accurately traced down. These emission processes are associated with unique polarization signatures and therefore measurement of X-ray and Gamma ray polarization may lead to a proper understanding of the GRB prompt emission. Though there have been many attempts in the past to measure the polarization of GRBs, those were using instruments which are primarily spectroscopic but not optimized for polarimetry. Cadmium Zinc Telluride Imager (CZTI) is one of the five instruments on board AstroSat, which is capable of doing spectroscopy and imaging in the range of 20 keV - 200 keV, during ground calibration showed significant polarization measurement capability based on Compton scattering in 100 - 300 keV. Pixilated detectors have an inherent modulation pattern since the edge pixels has a different size. The azimuthal angle covered by the edge pixels is much larger and hence more number of photons are detected in edge pixels. This was corrected using the modulation pattern for unpolarized photons using AstroSat mass model.

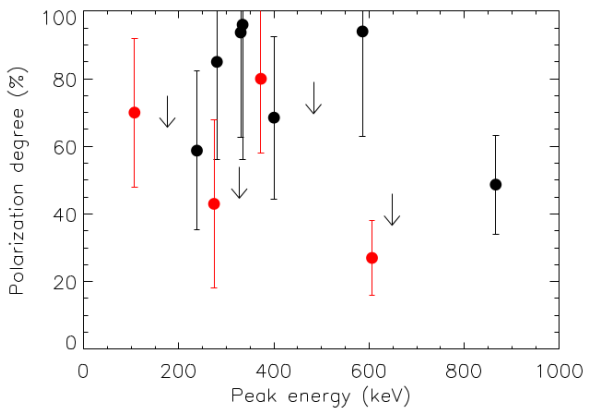

Figure no. 12: Polarization Fraction as a function of peak energies Epeak, for the GRBs for which polarizations have been estimated. The black points represent the GRBs detected by CZTI, whereas the red points stand for those detected by GAP and INTEGRAL

CZTI in the first one year of operation has detected a total of 47 GRBs, among which we attempted polarization measurements for 11 bright GRBs which had sufficient Compton events. Most of the GRBs show high polarization implying either synchrotron emission in a time independent uniform magnetic field or Compton drag to be the reason for the prompt emission and these results are the statistically significant polarization measurements so far. 7 GRBs were reported with polarization fractions with more than 3σ confidence level and an upper limit were given for 4. A recent study showed that statistical study of GRB polarization may provide critical inputs to constrain the possible emission mechanisms for the prompt emission. CZTI almost doubled the number of GRBs with polarization measurements in one year and is expected to measure polarization for more GRBs at the same rate. Though it is difficult to differentiate the various emission models with the current sample of polarization measurements, CZTI in its minimum lifetime of five years is expected to provide a large sample of polarization measurements which would lead to a better understanding of the prompt emission.

(Aarthy, E., N. P. S. Mithun, Santosh Vadawale)

Transient Localization with AstroSat-CZTI

Localization of short duration transients such as gamma-ray bursts (GRB) or fast radio bursts (FRB) is very important to identify and further study their counterparts at other wavebands. Because of the increasingly open nature of the CZTI instrument, it can be used to localize such transients or to put upper limits of hard X-ray emission for a transient with known location. This has been achieved using the AstroSat mass model which has been developed using Geant4 (version 4.10.03) a Monte Carlo based toolkit including all the payloads of AstroSat: UVIT, SXT, LAXPC, CZTI and the complete satellite structure. The mass model is also critical for the hard X-ray polarization measurements of GRBs and provides the modulation curves for unpolarized and 100% polarized photons for each GRB. It also aids in the off-axis spectroscopy of bright source by providing the response of CZTI as a function of off-axis position. The AstroSat Mass Model has been extensively used to investigate the electromagnetic counterparts of the gravitational wave events. Before the recent discovery of EM counterpart of GW170817, the previous GW170104 event had a multi-wavelength follow-up campaign by AstroSat CZTI and GROWTH collaboration. It was suspected that a newly detected source ATLAS17eau was EM counterpart of GW170104, however, using AstroSat Mass Model, it was proved that the ATLAS17eau was the afterglow of an unrelated long GRB170105A with only a fortuitous spatial coincidence with GW170104. Fast Radio Bursts (FRBs) are intense bright radio emissions whose origin remains a mystery unless it is localized. Recently following up Parkes discovered FRBs over a small time window CZTI gives an upper limit for source fluence and flux in the 20-200 keV band. For a given FRB the AstroSat Mass Model simulations are used to calculate the instrument response for the specific direction.

(Aarthy, E., N. P. S. Mithun, Santosh Vadawale)

Understanding the spectral and timing behaviour of a newly discovered transient X-ray pulsar Swift J0243.6+6124

Accretion powered X-ray pulsars, discovered in early seventies, are among the brightest transient sources in the Galaxy. These objects are known to be powered by accretion of mass into the enormous gravitational field of the neutron stars. Most of these transient pulsars

belong to the class of high-mass X-ray binaries (HMXBs) in which a magnetized neutron star (B$\sim 10^{12}$ G) corotates with a supergiant or a Be-type optical companion around the common center of mass. The strong field lines from the neutron star interact closely with the accreting plasma at the magnetospheric radius and channel the accreted matter on to the magnetic poles. This leads to the formation of hotspots or column-like structures at the magnetic poles of the neutron star which act as a source of immense high-energy radiations from the pulsars. The spin period of the neutron star in these systems ranges from a few seconds to 1000 s.

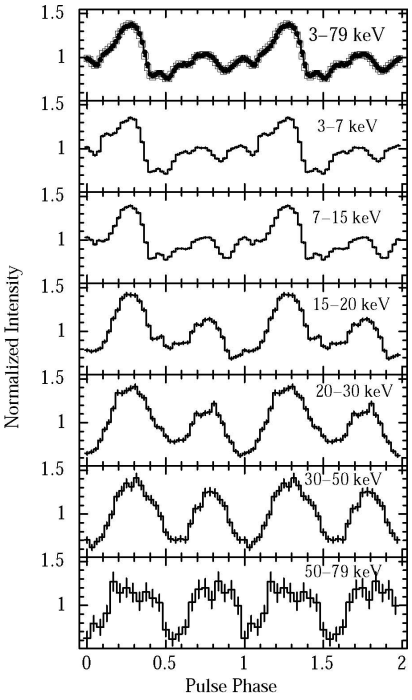

Figure no. 13: Pulse profiles of Swift J0243.6+6124 obtained from the background subtracted light curves of FPMA and FPMB detectors of $NuSTAR$ observation on 5 October 2017 are shown in the top panel. The data from FPMA and FPMB are consistent with each other and represented by solid dot and square in the panel, respectively. Energy resolved pulse profiles of the pulsar from FPMA detector are also shown in the figure. These profiles are found to show strong energy dependence. A broad profile seen at soft X-rays evolved into a double peaked profile at high energies. Pulsations were clearly detected in the light curves up to 79 keV. Two pulses in each panel are shown for clarity.

We have studied the new X-ray transient Swift J0243.6+6124 was discovered by Swift observatory on 3 October 2017 at a flux level of $\sim$80 mCrab. Detection of $\sim$9.86 s X-ray pulsations confirmed the nature of Swift J0243.6+6124 as a pulsating neutron star. Optical observations confirmed that the optical counterpart of Swift J0243.6+6124 is a Be star and the distance of the binary was estimated to be 2.5 kpc. Following the discovery, the pulsar was observed with several X-ray observatories. We carried out a detailed timing and spectral studies of the newly discovered accreting X-ray binary pulsar Swift J0243.6+6124 using Nuclear Spectroscopy Telescope Array (NuSTAR) observation in 2017 October at a flux level of $\sim$280 mCrab. Pulsations at 9.85423 s were detected in the X-ray light curves of the pulsar. Pulse profiles of the pulsar were found to be strongly energy dependent. A broad profile at lower energies was found to evolve into a double-peaked profile in $\geq$ 30 keV (Figure no. 13). The 3-79 keV continuum spectrum of the pulsar was well described with a negative and positive exponential cutoff or high-energy cutoff power-law models modified with a hot blackbody at $\sim$3 keV. An iron emission line was also detected at 6.4 keV in the source spectrum. We did not find any signature of cyclotron absorption line in our study.

This work was done in collaboration with Jerome Chenevez of National Space Institute, Technical University of Denmark, Denmark.

(Gaurava K. Jaisawal, Sachindra Naik)

Correlated X-ray/UV/optical emission and short-term variability in a Seyfert 1 galaxy NGC 4593

Active galactic nuclei (AGNs) are normally considered to have accreting supermassive black holes (SMBHs) at the heart of the host galaxies. The radiation from these AGNs covers almost entire range of electromagnetic spectrum – starting from X-ray to Radio bands. The X-ray continuum emission from these objects is considered to be dominated by the power law model, which is known to be due to the inverse Compton scattering of soft photons in an optically thin and hot electron plasma ($kT_e \sim$ 100 keV). The soft photons observed in these sources are believed to be emitted from the accretion disc around the SMBH. In Seyfert galaxies, radiation emitted from the accretion disc is dominated in the UV band. However, due to large Galactic absorption along the line of sight, the UV radiation peak is hardly detectable. The observed UV/optical emission shows different variabilities on various time-scales from days to years for 10^6–10^9 M$\odot$ black hole mass range. However, the cause of observed variabilities in UV/optical emission from the accretion disc is not very clear. The observed UV/optical emission variabilities in Seyfert galaxies are thought to be associated with the fluctuation in the mass accretion. However, such interpretation is unable to explain the observed disc variability on short (hours to days) time-scale. This time-scale is very much shorter compared to the expected time-scale of the density fluctuations in the accretion flow. The variations observed in X-ray emission are found to lead the variations in UV/optical band. This is difficult to explain by using the hypothesis that the cause of UV/optical variation is associated with accretion flow fluctuation. Thus, the correlation and variations between the emission in UV/optical and X-ray bands are complex and their intensive exploration is required.

We carried out a detailed multifrequency analysis of an intense monitoring programme of Seyfert 1 galaxy NGC 4593 over a duration of nearly for a month with Swift observatory. We used 185 pointings to study the variability in six ultraviolet/optical and two soft (0.3–1.5 keV) and hard X-ray (1.5–10 keV) bands. The amplitude of the observed variability is found to decrease from high energy to low energy (X-ray to optical) bands. Count-count plots of ultraviolet/optical bands with hard X-rays clearly suggest the presence of a mixture of two major components: (i) highly variable component such as hard X-ray emission, and (ii) slowly varying disc-like component. The variations observed in the ultraviolet/optical emission are strongly correlated with the hard X-ray band. Cross-correlation analysis provides the lags for the longer wavelengths compared to the hard X-rays. Such lags clearly suggest that the changes in the ultraviolet/optical bands follow the variations in the hard X-ray band. This implies that the observed variation in longer wavelengths is due to X-ray reprocessing. Though, the measured lag spectrum (lag versus wavelength) is well described by $\lambda^{4/3}$ as expected from the standard disc model, the observed lags are found to be longer than the predicted values from standard disc

model (Figure no. 14). This implies that the actual size of the disc of NGC 4593 is larger than the estimated size of standard thin disc.

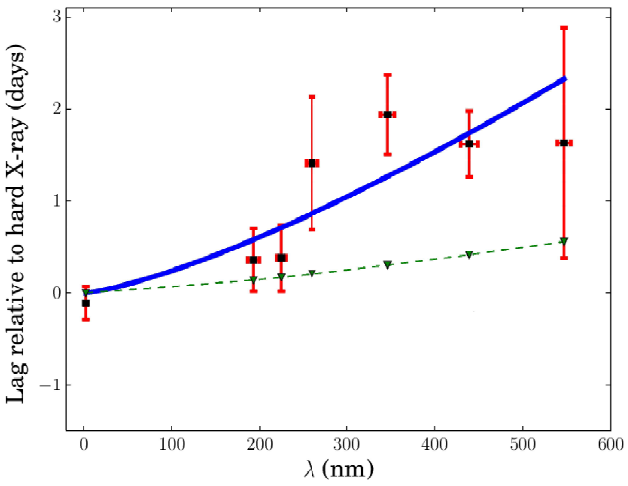

Figure no. 14: The lag spectrum with respect to the hard X-ray band. The fit for the lag spectrum (a) Blue curve - the best-fit power-law model $(1.8 \pm 0.02 \times 10^{-4}[(\lambda/0.49)^{4/3} - 1])$ (b) Green dashed curve : standard accretion thin disc theoretical model for NGC 4593.

(Sachindra Naik, Main Pal)

Complex optical/UV and X-ray variability of the Seyfert 1 galaxy 1H 0419-577

Active galactic nuclei (AGNs) exhibit variable and complex spectral energy distribution (SED). The central engine of an AGN is known to radiate in the luminosity range 10^{41-47} erg s^{-1} almost equally over the entire electromagnetic spectrum. In the brightest AGN, the intense radiation emitted from the central engine dominates the light coming from other constituents of the host galaxy such as stars. The huge energy release is attributed to accretion on to a supermassive black hole (SMBH). The emitting regions in the vicinity of an SMBH are too small to be identified separately by any available instruments on ground or space facilities. Therefore, the multiwavelength variability of spectral components, such as the big blue bump, power-law continuum, reflection components (i.e. Fe-Kα and reflection hump), soft X-ray excess and relationship between them are the most effective way to investigate the complex phenomenon in the exotic physical conditions in the nuclear environment of an AGN. Indeed, variability studies of AGNs over the last few decades have been important to understand the physical structure of emitting regions close to the SMBH. Thus, simultaneous observations in X-ray and UV/optical bands can provide important clues on the complex environment around the central engine. 1H 0419-577 is a unique AGN to investigate the complex mechanisms for the variability.

A detailed investigation on the broad-band UV/optical to X-ray spectral variability of the Seyfert 1 galaxy 1H 0419–577 using six XMM-Newton observations was performed during 2002–2003. These observations covered a large amplitude variability event in which the soft X-ray (0.3–2 keV) count rate increased by a factor of $\sim$4 in six months. The X-ray spectra during the variability are well described by a model consisting of a primary power law, blurred and distant reflection. The 2-10 keV power-law flux varied by a factor of $\sim$7 while the 0.3–2 keV soft X-ray excess flux derived from the blurred reflection component varied only by a factor of $\sim$2. The variability event was also observed in the optical and UV bands but the variability amplitudes were only at the 6–10 per cent level. The variations in the optical and UV bands appear to follow the variations in the X-ray band. During the rising phase, the optical bands appear to lag behind the UV band but during the declining phase, the optical bands appear to lead the UV band. Such behaviour is not expected in the reprocessing models where the optical/UV emission is the result of reprocessing of X-ray emission in the accretion disc. The delayed contribution of the broad emission lines in the UV band or the changes in the accretion disc/corona geometry combined with X-ray reprocessing may give rise to the observed behaviour of the variations.

This work was done in collaboration with G. C. Dewangan, A. K. Kembhavi and R. Mishra of Inter University Centre for Astronomy and Astrophysics, Pune, India.

(Main Pal, Sachindra Naik)

Decade long RXTE monitoring observations of Be/X-ray binary pulsar EXO 2030+375

Be/X-ray binaries, consisting of a compact object (neutron star) in orbit around the Be star, form the largest subclass of High Mass X-ray Binaries (HMXBs). The orbit of the neutron star (pulsar) in these systems is wide and highly eccentric. The pulsars in these binaries are generally X-ray quiescent. Transient X-ray outbursts seen in these objects are thought to be due to interactions between the neutron star and the circumstellar disk surrounding the Be star at the periastron passage. Among the 96 proposed HMXB pulsars, 67% of the identified systems are Be/X-ray systems and 33% of the systems have no known optical/IR counterparts. These Be/X-ray binary systems attract interests in several branches of astrophysics: stellar astrophysics, accretion theory, close binary evolution, etc. Progress towards the understanding of the physics of these systems depends on multiwavelength program of observations (in optical, infrared (IR) and X-ray wavebands). Using the IR and Optical observations of these objects, the physical conditions under which the neutron star accretes matter can be determined. In combination with the X-ray timing and flux observations, we can get a complete picture of the accretion process in these systems.

We carried out a comprehensive timing and spectral studies of Be/X-ray binary pulsar EXO 2030+375 by using extensive Rossi X-ray Timing Explorer observations from 1995 till 2011, covering numerous Type I and 2006 Type II (giant) X-ray outbursts. Pulse profiles of the pulsar were found to be strongly luminosity dependent. At low luminosity, the pulse profile consisted of a main peak and a minor peak that evolved into a broad structure at high luminosity with a significant phase shift (Figure no. 15). A narrow and sharp absorption dip, also dependent on energy and luminosity, was detected in the pulse profile. Comparison of pulse profiles showed that the features at a particular luminosity are independent of Type I or Type II (giant)

X-ray outbursts (Figure no. 15). This indicates that the emission geometry is solely a function of mass accretion rate. The broad-band energy spectrum was described with a partial covering high energy cutoff model as well as a physical model based on thermal and bulk Comptonization in accretion column. We did not find any signature of cyclotron resonance scattering feature in the spectra obtained from all the observations. A detailed analysis of spectral parameters showed that, depending on source luminosity, the power-law photon index was distributed in three distinct regions. It suggests the phases of spectral transition from sub-critical to super-critical regimes in the pulsar as proposed theoretically. A region with constant photon index was also observed in $\sim$(2-4) $\times$ 10^{37} erg s^{-1} range, indicating critical luminosity regime in EXO 2030+375.

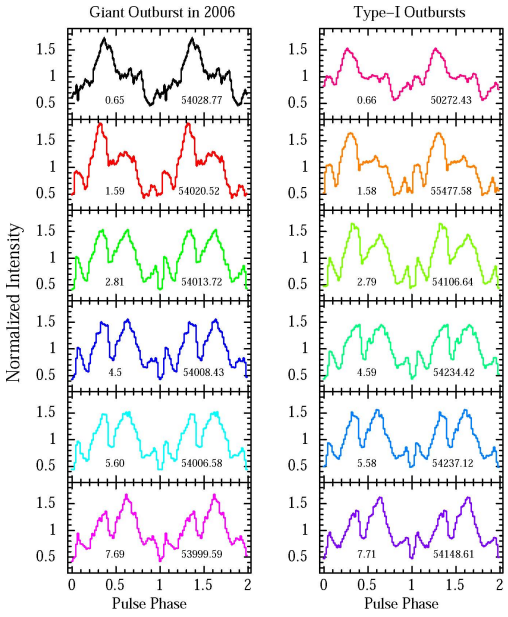

Figure no. 15: Pulse profiles of EXO 2030+375 during the Type II outburst in 2006 (left panels) and during normal Type I outbursts (right panels) in 2-60 keV range at comparable luminosities. The 3-30 keV luminosity of the pulsar (in 10^{37} erg s^{-1} units) and beginning of corresponding observation (in MJD) are quoted in left and right side of each panel. Two pulses are shown in each panel for clarity.

(Sachindra Naik, Prahlad Epili, Gaurava K. Jaisawal, Shivangi Gupta)

Investigating radio properties of the largest sample of narrow-line Seyfert galaxies

Narrow-line Seyfert 1 galaxies (NLS1s) are a subclass of Active Galactic Nuclei (AGN) that show relatively narrower broad permitted Balmer emission lines in their optical spectra, and are largely believed to be radio-quiet. In recent years, several Radio-Loud (RL) NLS1s possessing relativistic jets have come into attention with their detection in Very Large Baseline Array (VLBA) and in Gamma-ray observations. We attempt to understand the nature of radio-jets in NLS1s by examining the kpc-scale radio properties of, hitherto, the largest sample 11101 optically-selected NLS1s. Using 1.4 GHz Faint Images of Radio Sky at Twenty-cm survey we find the radio-detection of merely $\sim$ 4.5 per cent (498/11101) NLS1s, with majority (407/498 $\sim$ 81.7 per cent) of them being RL-NLS1s. Our study yields the largest sample of RL-NLS1s till date, and indicates the possible existence of a much larger population of RL-NLS1s. We find that the most of our radio-detected NLS1s are compact ($<$ 30 kpc), exhibit both flat as well as steep radio spectra, and are distributed across a wide range of 1.4 GHz radio luminosities ($10^{22} - 10^{27}$ W Hz^{-1}). At the high end of radio luminosity our NLS1s often tend to show blazar-like properties such as compact radio-size, flat/inverted radio spectrum, radio variability and polarization. The diagnostic plot of radio-luminosity versus radio-size, suggests that the radio-jets in NLS1s are either in the early evolutionary phase or possibly remain confined within the nuclear region due to low-power or intermittent AGN activity (Figure no. 16)).

This work has been done in collaboration with Dr. Hum Chand (ARIES, Nainital).

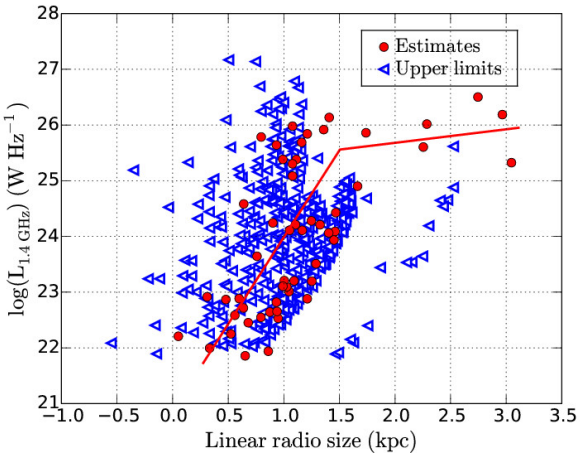

Figure no. 16: Projected linear radio-size versus 1.4 GHz radio luminosity radio-detected narrow-line Seyfert galaxies (NLS1s). It demonstrates that most of NLS1s possess compact radio jets which may be in the early phase of their evolution.

(Veeresh Singh)

Probing Intra-Night Optical Variability (INOV) in Narrow-Line Seyfert galaxies (NLS1s)

Based on the radio-loudness parameter *R*, which is defined as the ratio of 5 GHz radio flux density to the optical flux at λ4400Å, AGN are divided into radio-quiet (R $<$ 10) and radio-loud (R $\geq$ 10) categories. Radio studies suggest that NLS1s tend to be radio-quiet, and hence, possess radio-jets of low power. Also, unlike BL-AGN, a much smaller fraction of NLS1s is believed to be radio-loud. For instance, only 7 per cent of NLS1s are found to be radio-loud (Komossa et al. 2006), while 10 - 20 per cent BL-AGN are reported to be radio loud (Kellermann et al. 2016). In fact, the fraction of strong radio-loud NLS1s (R $>$ 100) is even much lower ($\sim$ 2.5 per cen). Therefore, the scarcity of RL-NLS1s is intriguing, and the nature of RL-NLS1s needs to be investigated. The presence of the relativistic jets motivates us to search for optical variability in RL-NLS1s, because of the well-known beaming effect (e.g., Wagner & Witzel 1995). Radio-loudness can be used as a proxy for the jet production efficiency. We are carrying out optical, IR monitoring of a sample of RL-NLS1s using 1.2m Mt. Abu telescope,

1.3m and 3.6m optical telescope at Devasthal, Nainital.

This work is being done in collaboration with Navpreet Kaur (PRL), Shashikiran Ganesh (PRL), K.S. Baliyan (PRL), Hum Chand (ARIES, Nainital) and Vineet Ojha (ARIES, Nainital).

(Veeresh Singh)

Unprecedented outburst in FSRQ CTA102: Rapid variation in optical and $\gamma-$ray detected

Blazars, a sub-class of AGN are interesting sources in themselves but when flaring, these become wonderful source of information about the structure and emission processes in AGN. It allows their detection across the electro-magnetic spectrum enabling correlation studies between fluxes at different energy regimes. It also gives the opportunity to sample small the flux in small bins, particularly at high energies.

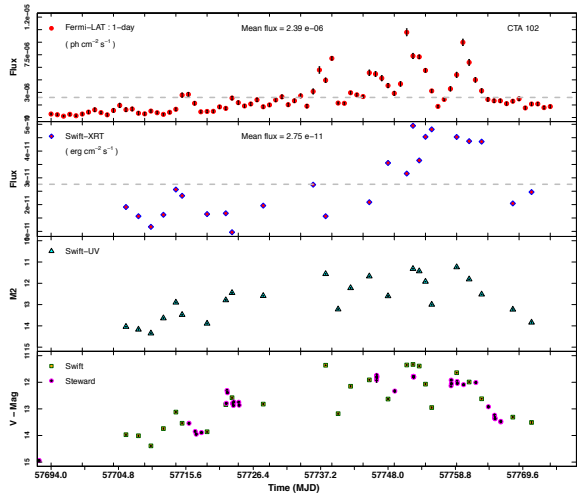

Figure no. 17: Multi-wavelength light curves for CTA 102 during 2016 November - 2017 January major outburst. From top to bottom: 1-day binned Fermi-LAT gamma-ray flux (E ¿ 100 MeV); X-ray flux (2.0 - 10.0 keV) from Swift-XRT; UV-band magnitude (M2) from Swift-UVOT, and optical V-band magnitudes from Swift-UVOT and Steward Observatory.

During 2016-17, flat spectrum radio quasar, blazar CTA 102 underwent historical outburst, surpassing all the past brightness levels. We obtained the high energy $\gamma-$ray data from Fermi/LAT (100 MeV- 300 GeV), UV/optical, X-ray data from Swift/XRT-UVOT, and 15 GHz data from OVRAO (Oven's Valley Radio Astronomy Observatory) during November 2016- January 2017 (please refer to Figure no. 17). The source was also observed from Mt Abu in optical and some data was used from Steward Observatory. The multi-wavelength data were analyzed, light-curves and spectral energy distribution were constructed to understand the spectral behaviour and structure of the source CTA 102. A number of short term (3 to 8 days) and long term ($>$ month) variability events are noticed across the EMS. Mt. Abu observations revealed more than 1.0 magnitude change (an increase of flux by more than a factor of two) within 24 hrs (December 18-19, 2016), unprecedented for this source! On 2016 December 29, the source attained the optical magnitude of R=10.92$\pm$0.01, which represents the historically brightest level ever achieved by the source. We infer a mild redder when brighter trend in general and a bluer when brighter one during a few optical flares. Based on the flux doubling timescale of 4.5 hrs, the size of the γ-ray emitting region is estimated as $\approx 7 \times 10^{15}$cm, located in the jet at a distance of about 1.47×10^{15} cm from the central engine.

(Navpreet Kaur, K S. Baliyan)

Infrared polarimetry with the NICS instrument

The Near Infrared Camera and Spectrograph (NICS) instrument is one of the back end instruments of the 1.2 m Cassegrain f/13 telescope located at the Mount Abu Infrared Observatory and has been extensively used for photometry and spectroscopy of a wide variety of celestial objects. We have recently added a polarimetric capability to this instrument which makes NICSPol the first imaging IR polarimeter in India. This allows to extend polarimetric measurements into the near-infrared wavelength domain complementing the facilities available at MIRO for optical polarimetry. The NICS imaging polarimetry mode offers a FOV of 4 arcmin x 4 arcmin at the same spatial resolution as available in the NICS imaging mode.

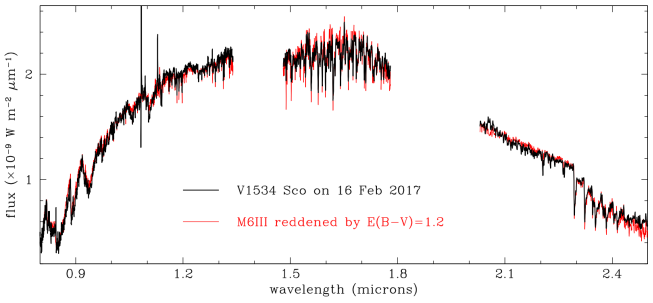

Figure no. 18: % polarization of polarization standard star HD 283809

The polarimetric module consists of a rotating wire-grid polarizer placed before the entrance aperture of NICS i.e. before the focal plane of the 1.2m telescope. Observations are taken at multiple steps of this rotating wire-grid polarizer (at 0, 45, 90 and 135 degrees). This allows us to compute the degree of polarization and the position angle of polarization over the field of view. The instrument was calibrated in the laboratory using an unpolarized light source. This allowed to check the instrumental polarization - found to be close to 0.5%. The instrument was also checked for 100% polarized light generated using a glan prism in front of the unpolarized light source used earlier. The instrument detected the 100% polarized light as $\sim$95-97%. This validates our instrument for polarimetric observations. After this laboratory characterization, we carried out measurements of polarized and unpolarized standard stars and Figure no. 18 shows the observed PF and PA over JHKs bands for HD 283809. The correction of the position angle to translate NICSPol's measurements to the equatorial coordinate system was estimated to be 110.45 deg. Observations have been carried out for various science targets since then, including infrared polarization mapping of the Crab Nebula. The instrument will be used for mapping the Northern Galactic plane as visible from MIRO. A pilot observation of a molecular cloud and some other regions in the plane has been initiated.

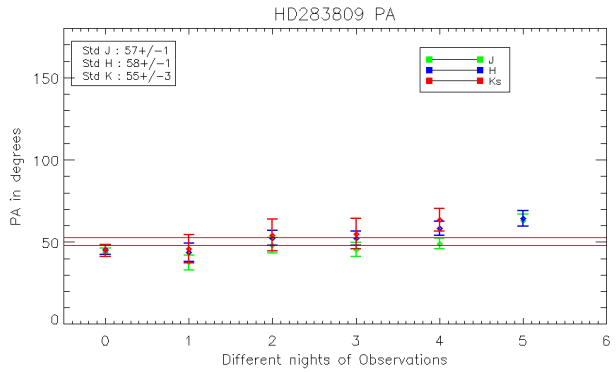

Figure no. 19: Polarization position angle of polarization standard HD 283809

The Crab pulsar and its nebula is one of the favourite and well studied sources over all the wavelengths. Radio, Optical and X-ray/Gamma ray polarization of the pulsar and nebula have been extensively studied over the past several decades. However, there is no proper study of the IR polarization of the Crab pulsar and its nebula. Hence using our IR polarimeter to study Crab bridges this gap. With the current read out time available for NICS, pulse phase resolved polarization study of the pulsar itself is not possible. Hence phase integrated polarization over J, H, K bands of the entire nebula is carried out. It can be seen that few filaments which are bright have low polarization. Figure no. 20 shows how the crab nebula looks like in the infrared false colour composite (left panel) with the polarization structures tracing well the filaments(right panel).

Figure no. 20: Image (left panel) of Crab Nebula in J - blue, H - Green, K - Red. Polarized image (right panel) of Crab Nebula in 0, 45, 90 degrees (0 - Red, 45 - Green, 90 - Blue)

(Aarthy E., Archita Rai, Shashikiran Ganesh, Santosh Vadawale)

Development of MFOSC-P : An Optical Imager-Spectrograph for Mt. Abu 1.2m Telescope - Structural Analysis, Fabrication and Control System

Mt. Abu Faint Object Spectrograph and Camera-Pathfinder (MFOSC-P) is being developed for PRL 1.2m telescope at Mt. Abu. The instrument is an imager spectrograph and has been designed to provide imaging over $\sim 6 \times 6 arc-min^2$ on a 1K $\times$ 1K Andor CCD detector in seeing limited conditions and slit limited spectroscopy with gratings. In the imaging mode the sampling of 3 pixels per arc-second is considered while in spectroscopy two modes of resolution ~ 2000 and ~ 1000 around ~ 6500 and ~ 5500 angstroms are provided. The base specifications, optical and mechanical designs were described in last annual report. Here we report on the mechanical structural design analysis and control system development of the instrument.

(A.) Structural Analysis and Fabrication of MFOSC-P

(This analysis was done by a team from ISRO-Space Application Centre (SAC), in collaboration with PRL MFOSC-P team.)

The First design configuration was designed and developed by PRL team. The structural modifications and iterative analysis were later carried out with a team from ISRO-Space Application Centre (SAC) which was periodically reviewed by PRL and SAC team to conclude the optimal design configuration of the instrument. The CAD model of the final design configuration is shown in Figure no. 21. Along with the instrument mechanics, other auxiliary support structure and devices e.g. electronics control system, control PC, coupling mechanism with the telescope etc. have also been considered for the structural analysis. The image quality requirements of the instrument demand that optics of the instrument need to be stable within $\pm$ 0.03 degree. This translates in to a deviation of 500 microns over the length of 1m. To decouple the instrument from the telescope the natural frequency of the instrument is required to be greater than 10 Hz. Total Mass of the instrument with support structure was required to be less than 125 kg. Self-load and acceleration load stresses in to the structural elements was to be less than the IS800 specifications of the materials used. All these specifications were simulated in the finite element (FE) model.

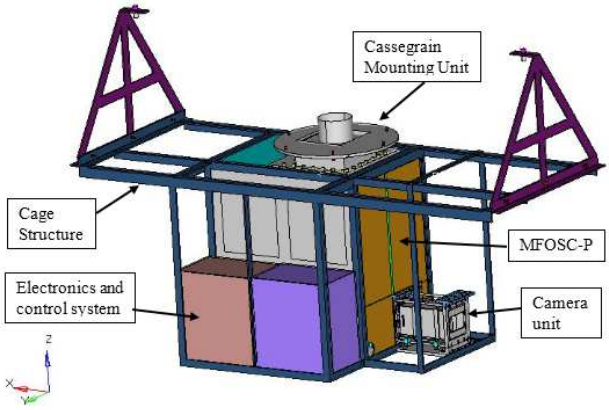

Figure no. 21: Structural system design of MFOSC-P along with all the interfaces as it would be mounted on the telescope.

After few design iterations, the final design configuration was analyzed for self-weight load and acceleration moments. The boundary conditions are imposed on the FE model for predicting normal modes, static deflections, and Von-mises stresses. First mode of assembly was determined at 24.1 Hz, next mode occurred at 36 Hz. Thus the instrument is safely decoupled with telescope's structure. Maximum absolute deflections of the structural system under self-weight static analysis in various orientation were estimated to be in range of 39-234 microns. This is good enough to insure the alignment of various optical sub systems within the instrument in various orientations of

the telescope. Maximum nominal stresses for various orientations were estimated within the range of 10.6-16.8 MPa. The stresses were also analyzed for dynamic rotation of instrument. In this case, the maximum absolute deflection and von-mises stress were estimated as 262 microns and 13.8 MPa respectively. All the estimated values were in compliance with the specified design requirements and had adequate margin of safety. Figure no. 22 shows the results of one such analysis.

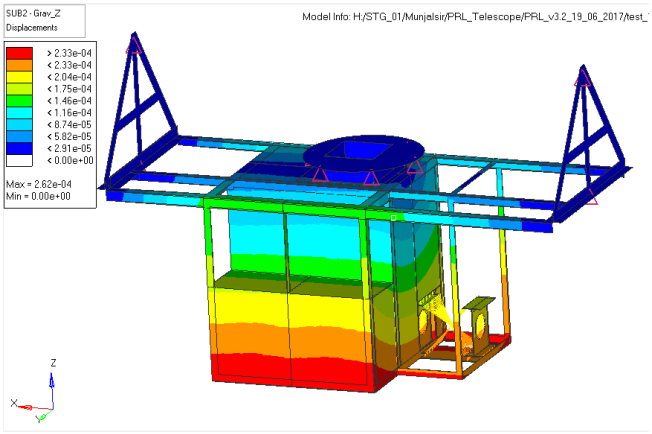

Figure no. 22: Deflection self load analysis of MFOSC-P under dynamic conditions. Maximum deflection of 262 microns was determined at the free end of the instrument.

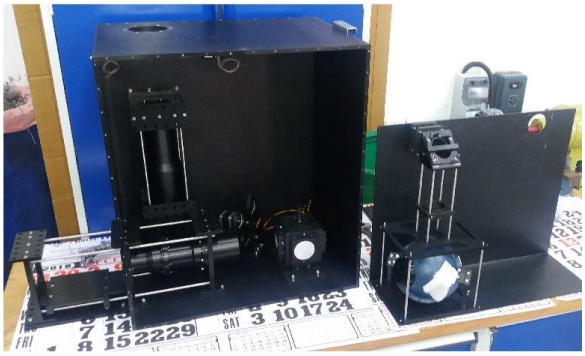

Figure no. 23: MFOSC-P mechanical system currently being assembled in the PRL workshop.

Having successfully analyzed the mechanical design model for structural integrity, the fabrication of various mechanical parts and subsystems were done within PRL workshop as well as by local manufacturers. The mechanical system fabrication is complete and individual sub systems are now being assembled and tested in the laboratory. Figure no. 23 shows the mechanical system of the instrument currently being assembled in PRL workshop.

(B.) Control System Development for MFOSC-P

MFOSC-P carries two stepper motor based linear stages and three stepper motors for the motion of various optical and mechanical components e.g. slits, gratings, filters etc. These motion systems are designed to work in closed loop motion using several limit switches and encoder sensors. In addition three calibration lamps are being used within the instrument for spectral calibration. These motion systems and calibration lamps would be used during the science run time operations of the instrument as per user's choice to use any specific observing mode. To enable an automated way of controlling these aspects of the instrument, a control system is being developed using off-the-shelf commercial components and devices. At the core of the control system are two Arcus make PMX series of controllers. Each of these controllers has provision to provide control pulses to four off-the-shelf stepper motors driver electronics and read their limit and encoder status. Based on these inputs a closed loop motion algorithm is being developed that would be used to control the motion aspects of MFOSC-P. The controllers also have several digital input-output pins which are being used to control the operation lamps using an relay based interface lamp driver electronics. There are two 24V and two 5V dc power supplies are used within the control system enclosure to meet the power requirements of the instrument. These power supplies draw the input power from AC mains. The control system takes commands from a PC based user's interface provided by Arcus using a USB communication link.

(Mudit K. Srivastava, Mohanlal Jangra, Ankita Patel, Vaibhav Dixit)

Science

Solar Physics

Study of the evolution of velocity flows on the solar surface over the Solar Cycles 23 and 24

The network of solar telescopes located at six sites around the globe in the Global Oscillation Network Group (GONG) program has been nearly-continuously observing the Sun since the last quarter of the year 1995 for Doppler imaging of the solar-disk aimed to study the oscillations and velocity flows on the solar surface. The solar full-disk Dopplergrams obtained by the GONG instrument for the period from 1 January, 1996 to 31 May, 2001 were by using a CCD camera of 256 $\times$ 256 pixels format giving a spatial sampling of about 8 arc-sec per pixel at a cadence of one minute. These full-disk Doppler observations from GONG were upgraded since 1 August, 2001 to provide a spatial sampling of about 2 arc-sec per pixel by using a CCD camera of 1024 $\times$ 1024 pixels format at a cadence of one minute.

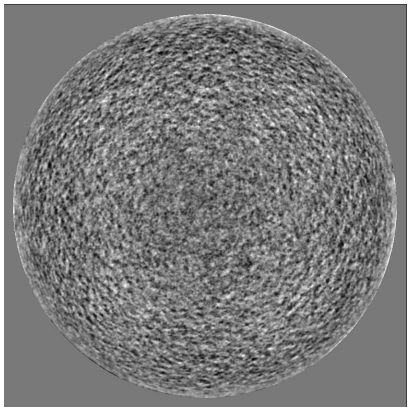

Figure 1.: Site-merged full-disk Dopplergram of the solar surface illustrating the photospheric velocity flows as observed with the GONG instrument.

Thus, the GONG observations of the solar photospheric velocity flows have now covered the complete Solar Cycle 23 and the ongoing Cycle 24. The site-merged full-disk Dopplergrams (c.f., Figure 1) from GONG aimed to study the velocity flows on the solar surface comprise of the velocity signals from various convective sources, viz., the oscillatory signals due to the p-modes, supergranular velocity flows, Evershed flows in the sunspots, and the meridional circulation flows. It is worthy to mention that the global velocity oscillations in the Sun, known as p-modes, are stochastically excited due to high turbulence in the convection zone of the Sun. The incoherent superposition of these p-modes peak in the 2-4 mHz frequency band.

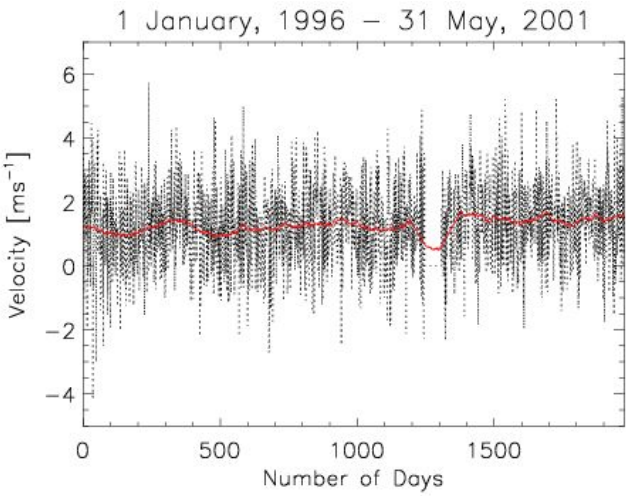

Figure 2.: Temporal evolution of the daily mean velocity flows (dashed lines) on the solar surface as observed with the GONG instrument for the period from 1 January, 1996 to 31 May, 2001 covering the ascending phase of Solar Cycle 23. The red solid line shows a smoothed fit applied to these velocity signals to illustrate the mean level of changes over the aforementioned period. The zero values indicate discontinuity in the observations.

These solar oscillation frequencies have shown variation over the solar activity cycle, which is believed to be the indicator of the structural

and magnetic changes taking place in the sub-surface layers of the Sun with the increase and decrease of the solar activity. Motivated with this example, in this work we study the evolution of daily mean velocity flows on the solar surface using the nearly continuous full-disk Doppler observations from the GONG network of telescopes for the Solar Cycles 23 and 24. In the Figures 2 and 3, we show the evolution of the mean velocity flows on the solar surface for the aforementioned two different epochs of full-disk Doppler observations from the GONG instrument covering nearly-continuously the Solar Cycles 23 and 24.

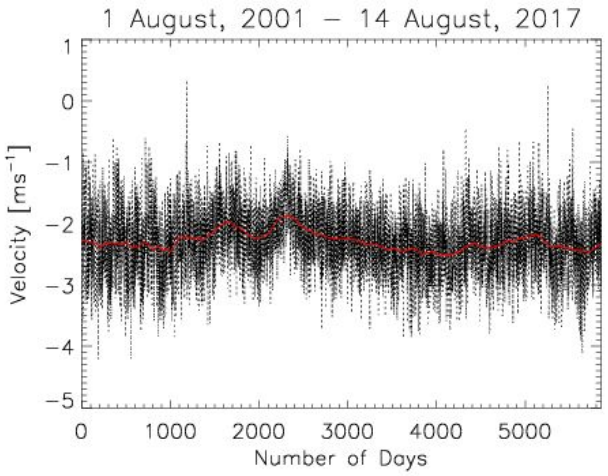

Figure 3.: Temporal evolution of the daily mean velocity flows (dashed lines) on the solar surface as observed with the upgraded GONG instrument from 1 August, 2001 to 14 August, 20017 covering the peak phase and the descending phase of Solar Cycle 23, and the ongoing Cycle 24. The red solid line shows a smoothed fit applied to these velocity signals to illustrate the mean level of changes over the aforementioned period.

We observe that the mean surface velocity flows do show evolution with the solar activity cycle, which indicate changes in the dynamics of the surface and sub-surface layers of the Sun. The correlation analysis of these solar mean velocity flows relative to the various solar activity indicators (viz., sunspot number, solar-disk integrated 10.7 cm radio flux, and the total solar irradiance) is also done in order to understand the relation between the changes in these solar photospheric velocity flows and the magnetic activity cycle of the Sun. However, we do not find a substantial correlation between the changes in the mean surface velocity flows and the various solar activity indices. The lack of correspondence between the evolution of solar surface mean velocity flows and the various activity proxies over the solar cycle is being further investigated.

This work is being done in collaboration with K. Jain, S.C. Tripathy, and Frank Hill of GONG Program, National Solar Observatory, University of Colorado Campus, Boulder, USA.

(Brajesh Kumar)

Study of magnetic-jerk driven waves in the solar atmosphere during large flares

We have investigated the abrupt changes in the solar magnetic fields associated with large flares employing the recently available high-cadence photospheric vector magnetograms obtained by the HMI instrument onboard Solar Dynamics Observatory. The analysis of these magnetograms show sudden and persistent magnetic field changes at different locations of the active regions during the flares.

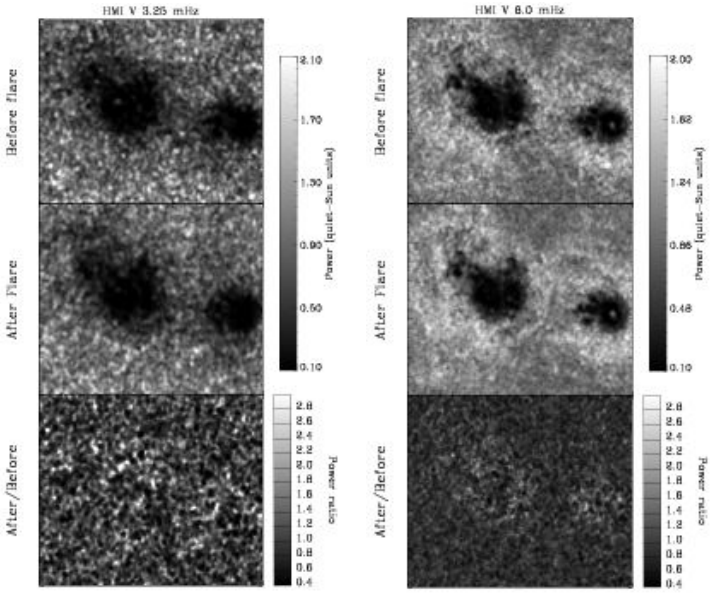

Figure 4.: Power Spectra of velocity oscillations in the active region NOAA 12371 estimated before and spanning an M6.5-class flare on 22 June 2015 using the Doppler observations from HMI instrument onboard SDO spacecraft. The left panel shows the power spectra estimated in the frequency band 3.0-3.5 mHz (p-mode band) while the right panel shows the same for the frequency band 5.75-6.25 mHz (high-frequency band). In both the cases, it is observed from the power ratio of the spectra spanning the flare to the spectra before the flare that oscillatory power is enhanced in the active region at different locations during the flare.

Using the simultaneous Dopplergrams and Intensity filtergrams obtained from HMI and AIA instruments at 6173 Å and 1600 Å, respectively; we have produced power spectra of these observations to study the acoustic power in these affected locations during the flare at different heights in the solar atmosphere. The power spectra of these observations show signatures of enhanced oscillatory power during the flare in the aforementioned locations of the active region in some cases (c.f., Figure 4). These results indicate that the transient Lorentz forces associated with the abrupt changes in the magnetic fields during the flare could drive the localized oscillations in the active region. We are also working on the cross-power and cross-phase analysis of the multi-height power spectra to understand the propagation of wave energy from the surface to the higher solar atmospheric layers during the transient activities in the Sun. This study will be extended to multi-height observations in the solar atmosphere from the Multi-Application Solar Telescope (MAST) of USO/PRL.

This work is being done in collaboration with S.P. Rajaguru and P. Vemareddy of Indian Institute of Astrophysics, Bengaluru (India).

(Brajesh Kumar)

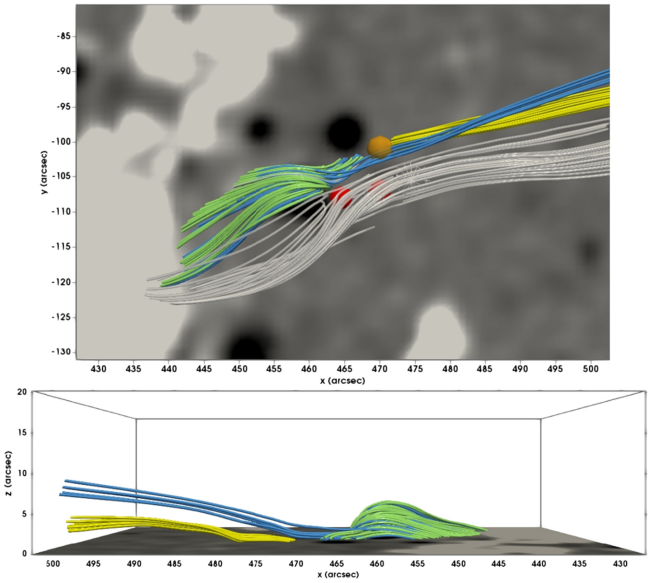

Figure 6.: Pre-jet (green and yellow lines) and post-jet (at blue lines) coronal model magnetic field structure. The gray lines are shown to complete the representation of the jet-related structure as a whole. The grayscale background resembles the pre-jet vertical magnetic field at the lower model boundary, scaled to $\pm$100 G. The orange sphere marks the location of the first compact loop-like brightening observed in AIA 304 Å . The red spheres mark the position of flare kernels observed in AIA 1600 Å . The units are arc-sec from solar disk center. Bottom panel: side view along the solar-y direction. The units are arc-sec.

Observational and Model Analysis of a Two-ribbon Flare Possibly Induced by a Neighboring Blowout Jet

We explore unique observations of a blowout coronal jet that possibly triggered a two-ribbon confined C1.2 flare in bipolar solar active region NOAA 12615 on 2016 December 5.

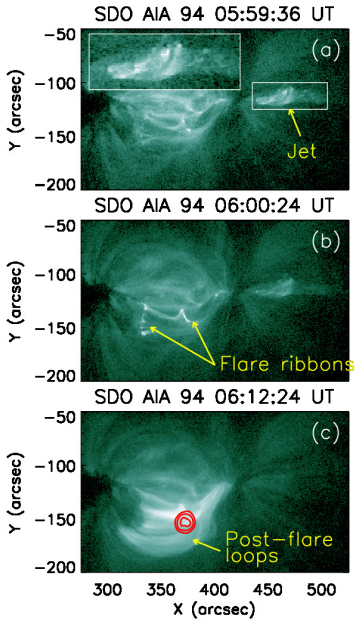

Figure 5.: Sequence of AIA 94 Å images showing the coronal jet and subsequent flare emission. The red contours in panel (c) represent X-ray images at 6-12 keV with contour levels as 40%, 60%, and 90% of the peak flux. The inset in panel (a) shows zoomed-in image of the selected region (shown by smaller rectangular area).

The jet activity initiated at chromospheric/transition region heights with a small brightening that eventually increases in volume, with well developed standard morphological jet features, viz., base and spire. The spire widens up with a collimated eruption of cool and hot plasma components, observed in the 304 Å and 94 Å channels of AIA, respectively. The speed of the plasma ejection, which forms the jet's spire, was higher for the hot component ($\approx$200 km s^{-1}) than the cooler one ($\approx$130 km s^{-1}). The NLFF model of coronal fields at the pre- and post-jet phases successfully reveals openings of previously closed magnetic field lines with a rather inclined/low-lying jet structure.

The peak phase of the jet emission is followed by the development of a two-ribbon flare that shows coronal loop emission in HXRs up to $\approx$25 keV energy. The coronal magnetic fields rooted at the location of EUV flare ribbons, derived from the NLFF model, demonstrate the pre-flare phase to exhibit an "X-type" configuration, while the magnetic fields at the post-flare phase are more or less oriented parallel. Comparisons of multi-wavelength measurements with the magnetic field extrapolations suggest that the jet activity likely triggered the two-ribbon flare by perturbing the field in the interior of the active region (see Figures 5 and 6).

This work has been done in collaboration with Julia Thalmann, Astrid Veronig of University of Graz, Austria) and Ramesh Chandra of Kumaun University, India.

(B. Joshi and P. K. Mitra)

Characteristics & kinematics of Stealth Coronal Mass Ejections

Coronal Mass Ejections (CMEs) are the most energetic events on the Sun in which hot coronal plasma is ejected out from the Sun into the interplanetary space. During the eruption process, these CMEs are usually accompanied by various phenomena such as flares, filament eruptions, coronal jets etc. However, there are many observational evidence where CMEs are not associated with any of the above phenomena. These CMEs are called 'stealth CMEs'. Non association of any distinct lower coronal feature makes it more difficult to estimate the CME arrival time on earth causing unexpected geomagnetic storms (problem storms) for the earth directed events. This silent behaviour make stealth CMEs more mysterious and different from other normal CMEs.

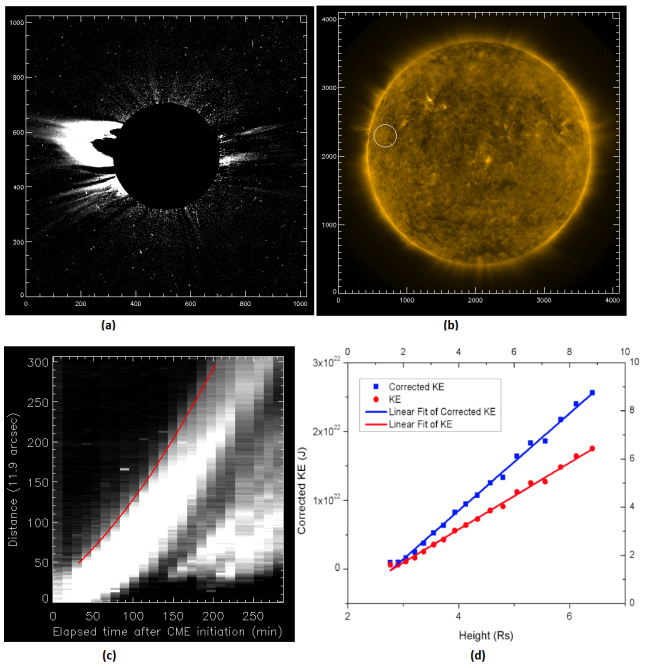

Figure 7.: (a) shows the LASCO C2 image of the stealth CME on Jan-17-2017. The corresponding AIA 171? image is shown in (b), the white circle encircles the extrapolated CME direction. (c) shows the time-slice diagram of this event where the red curve depicts the height time profile. The kinetic energy (KE) is plotted in (d), with red and blue line indicating the KE derived from projected and deprojected parameters respectively.

Stealth CMEs can only be observed in solar corona with white light coronagraphs. We use AIA/SDO, SECCHI/STEREO and LASCO/SOHO coronagraph observations to identify four CMEs which do not show any distinct lower coronal signature in AIA images. Using the multi-viewpoint data from the LASCO and STEREO-A, we determine the orientation of CME in three-dimensional space. We also estimate the plane of sky projected mass and velocity of these selected CMEs. Using the directional parameters from the CME orientation, we calculate the 'true' (deprojected) mass and velocity of these CMEs.

From our analysis we confirm that all these events are front sided. Fitting a 2nd order polynomial on the time-slice diagram (Figure 7(c)), we obtain velocity and acceleration of the CME of Jan-17-2017. Our study shows that these stealth CMEs are slow CMEs with velocity less than 350 km/s, except for the Oct-5-2012 event which propagated with 510 km/s. Due to their slow speed, these CMEs are dragged by solar wind and get accelerated. This can be inferred from the height-time profile. The true mass andenergy of the stealth CMEs reported here, are of the order of 1015 g and 1021 J respectively. These values lie close to the lower range of the mass and energy of normal CMEs.

This work is done in collaboration with Suvadip Sinha at CESSI, IISER Kolkata

(Nandita Srivastava)

Geometric and magnetic properties of near-Sun coronal flux ropes and the associated magnetic clouds at 1 AU

Predicting the strength and orientation of the magnetic field associated with the interplanetary coronal mass ejections (ICMEs) is one of the key challenges in space weather physics. Study of both the remote-sensing and in-situ data are required in order to infer the magnetic properties of ICMEs in advance. Recent studies reveal that the magnetic properties of near-Sun coronal flux ropes are well-correlated with that of the ICMEs at 1 AU. In this work, we examine the geometric and magnetic properties of near-Sun coronal flux-ropes and that of ICMEs in order to understand the geo-effectiveness of the associated magnetic clouds (MCs).

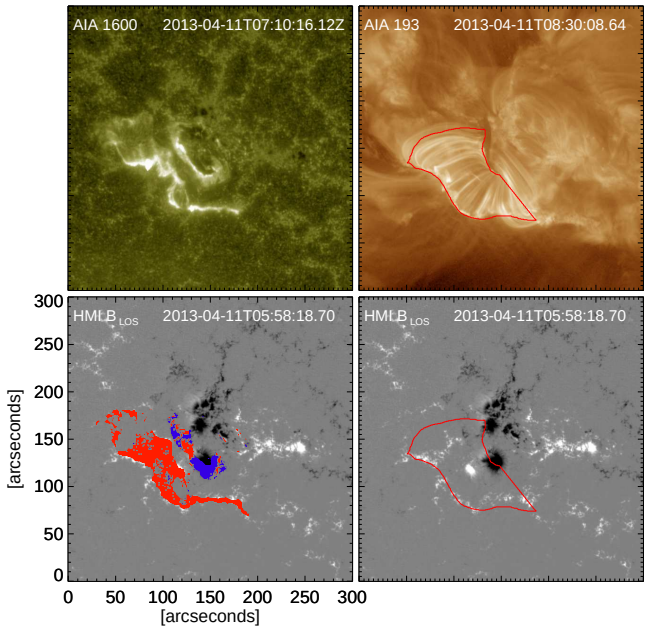

Figure 8.: Upper-left panel depicts the flare ribbons in AIA 1600 Å image for the M6.5-class flare on 11th April 2013. The red boundary line in upper-right panel marks the post eruption arcade in AIA 193 Å image. Lower panels illustrate the HMI line-of-sight magnetic field. The red and blue regions in lower-left panel depict the cumulative flare ribbon area overlying the positive and negative magnetic field respectively.The red boundary in lower-right panel is the over-plotted PEA region.

Estimating the reconnection flux underlying the post eruptive arcades (PEA) and the cumulative flare ribbon area (FRA)(Figure 8), we have calculated the near-Sun properties of the coronal flux-ropes using the FRED model for four CMEs. The CME morphology observed in the white-light coronagraphic images has been geometrically

fitted using the Graduated Cylindrical Shell (GCS) model (Figure 9).

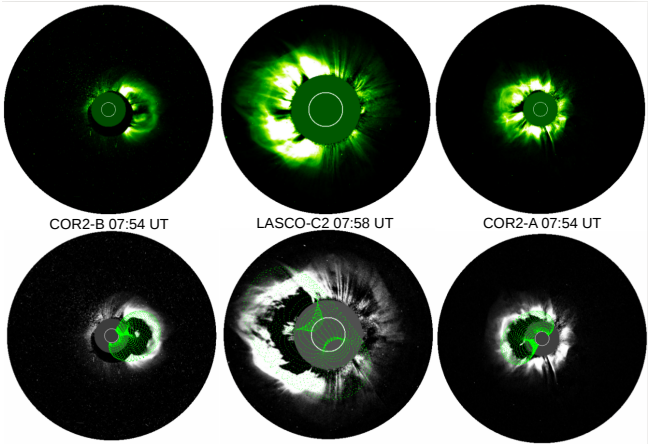

Figure 9.: Top panels depict the CME morphology observed from COR2-B, LASCO-C2, and COR2-A, respectively at around 07:54 UT on 2013 April 11. Bottom panels illustrate the overplot of the bestfitted wireframe of the magnetic flux rope in the GCS model.

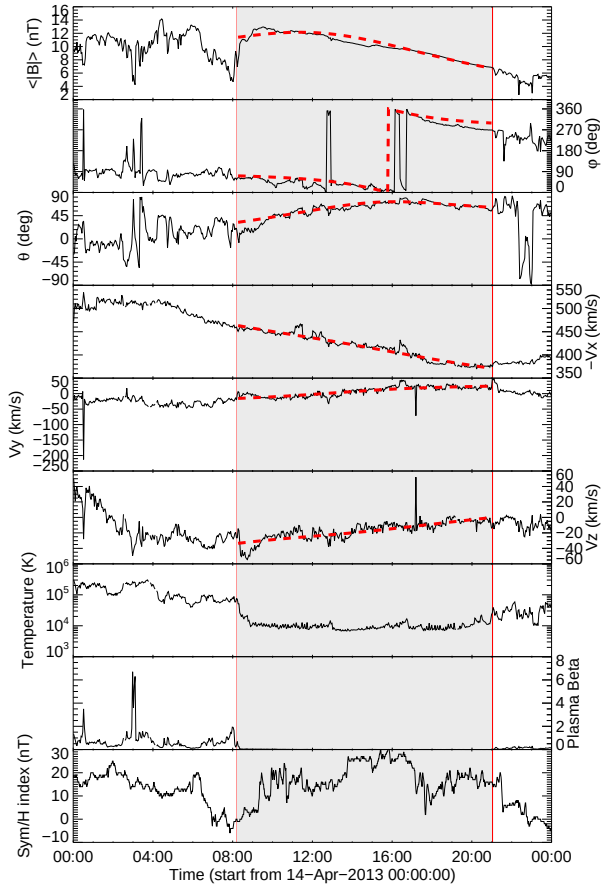

Figure 10.: Magnetic cloud fitting for 14th April ICME event in 2013. The two red vertical lines denote the magnetic cloud boundary. The red solid and blue dashed lines denote the modeled parameters obtained from the uniformly twisted cylindrical flux-rope solution.

B_0 of the coronal flux ropes at 10 R_S for the four events ranges between 12 to 130 mG for both the PEA and FRA methods, whereas using the MC fitting method (Figure 10) we have found that B_0 of the associated MCs at 1 AU ranges between 9 to 43 nT. The average observed value of B_0 for the MCs at 1 AU is $\approx$ 23nT for the four events. This value is almost two times larger than the average inferred value of B_0 ($\approx$ 10 nT) at 1 AU assuming the self-similar expansion of the CMEs. Comparing the orientation of the flux-rope axis we have found that the MCs at 1 AU show 15° to 100° deviation from the initial orientation near the Sun. This significant deviation in the axis orientation of the MCs suggests that the interplanetary deflection and rotation of the CMEs need to be quantified in order to predict the geo-effectiveness of the associated ICMEs.

(R. Sarkar and Nandita Srivastava)

Solar cycle variation of coronal mass ejections contribution to solar wind mass flux

Coronal Mass Ejections (CMEs) contributes to the perturbation of solar wind in the heliosphere. Thus, depending on the different phases of the solar cycle and the rate of CME occurrence, the contribution of CMEs to solar wind parameters near the Earth changes. In our study, the long term occurrence rate of CMEs, their angular size, speeds and mass are estimated based on LASCO onboard SOHO observations. The occurrence rate of Interplanetary counterparts of CMEs (ICMEs) near the Earth, their speeds and solar wind mass flux determined are based on the in in-situ observations of ACE and WIND. We attempt to find correlation between near sun parameters, determined using white light images from coronagraphs, with solar wind measurements near the Earth from in-situ instruments. Our analysis shows that although the occurrence rate of CMEs is higher for solar cycle 24 than 23, the speeds of CMEs and ICMEs are lower in solar cycle 24 than those during solar cycle 23.

The occurrence rate of CMEs tends to track the solar activity cycle 23 and 24, in both amplitude and phase except in the descending phase of cycle 23. Although sunspot numbers in solar cycle 24 are half of that in previous cycle, the rate of CMEs is little higher in solar cycle 24 than that in the corresponding phase of previous cycle 23. In contrast to the total number of CMEs, their total mass is dominated mainly by larger events and we find that the mass loss rate at any solar latitude is lesser for solar cycle 24 than cycle 23. During the solar maximum, CMEs are wider and more uniformly distributed in latitude than during the solar minimum. Based on our analysis, we find that in the ecliptic region, the contribution of CMEs to the solar wind mass flux is negligibly small during the solar minimum but increased to $\sim$5% at the maximum for both the solar cycles 23 and 24. It is also noted that the fractional contribution of CMEs to the solar wind mass flux closely tracks the solar cycle. In ecliptic near the Earth, averaged solar wind flux is relatively constant compared to the CME flux during different phases of the solar cycle 23 and 24 (Figure 11).

This work is carried out in collaboration with Wageesh Mishra and Yuming Wang of USTC, China and Z. Mirtoshev of Samarkand University, Uzbekistan.

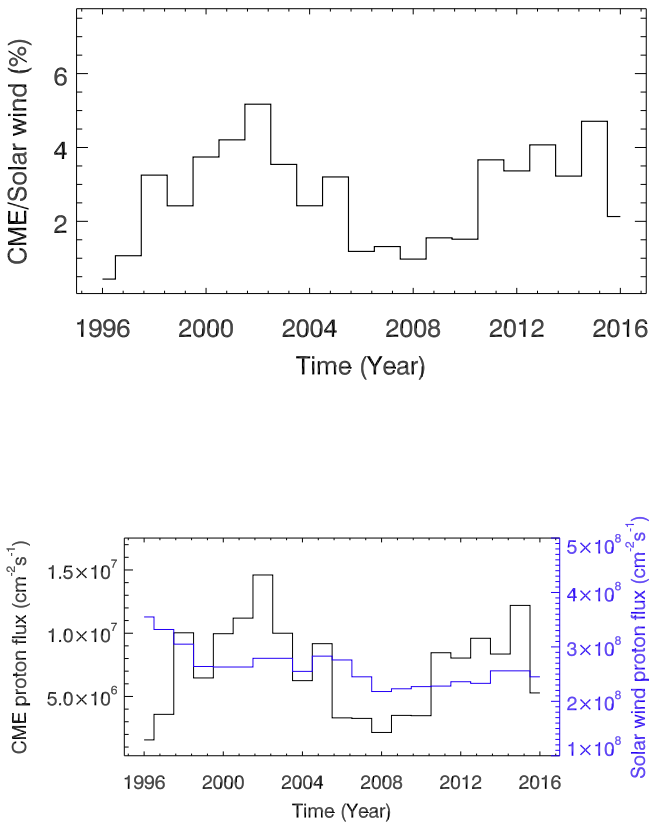

Figure 11.: The variation of the CMEs and solar wind proton fluxes at 1 AU in the near-ecliptic region is shown in the top panel. The ratio of CME to solar wind mass flux is shown in the bottom panel.

(Nandita Srivastava)

Magnetohydrodynamic simulation of magnetic null-point reconnections in NOAA AR12192 initiated with an extrapolated non-force-free-field

The solar active region (AR) 12192 was one of the most flare productive region of solar cycle 24, which produced many X-class flares; the most energetic being an X3.1 confined flare on October 24, 2014 at 21:10 UT. Customarily, such events are believed to be triggered by magnetic reconnection in coronal magnetic fields. Here we use the vector magnetograms from solar photosphere, obtained from Heliospheric Magnetic Imager to investigate the magnetic field topology prior to the X3.1 event, and ascertain the conditions that might have caused the flare. To infer the coronal magnetic field, a novel non-force-free field (NFFF) extrapolation technique of the photospheric field is used, which suitably mimics the Lorentz forces present in the photospheric plasma.

Particularly, we identify and focus on a circular brightening that appears in the extreme-ultraviolet/ultraviolet channels following the peak of the flare. The extrapolated field lines show the presence of a three-dimensional (3D) null near one of the polarity inversion lines—where the flare was observed (Figure 12a). In the simulation, we find magnetic reconnections occurring near the 3D null, which provides a possible triggering mechanism for the flare. Importantly, the post-flare circular brightening observed at the chromospheric and coronal heights co-locates with footpoints of the dome-shaped field lines inherent to the 3D null (see Figure 12b) which strengthens the viability of the initial non-force-free field along with the dynamics it initiates. Moreover, the initial field and its simulated evolution is found to be devoid of any flux rope, which is in congruence with the confined nature of the flare.

This work is done in collaboration with Q. Hu of The University of Alabama in Huntsville, USA., and S. Kumar of Patna University, India.

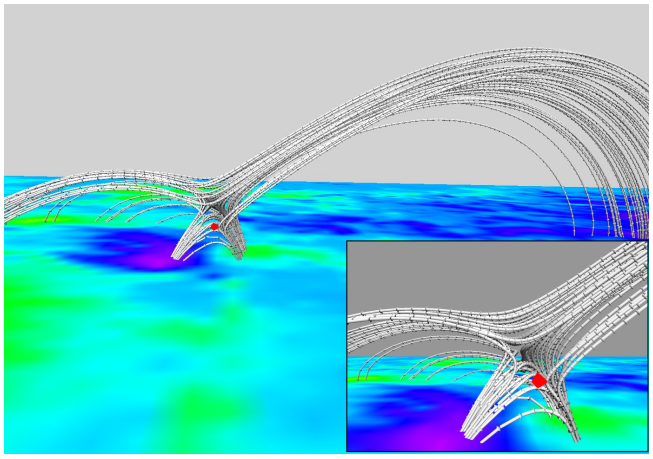

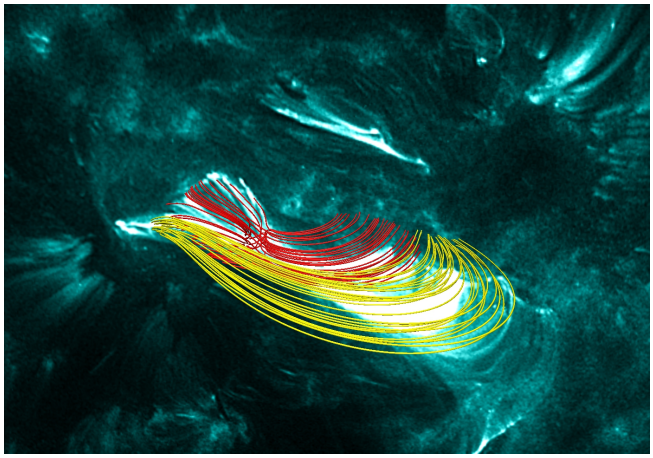

Figure 12.: (a) Extrapolated NFFF showing the 3D null topology for AR 12192. (b) Magnetic field lines showing the correspondence with brightening in the 131 Å channel observed during the flare.

(A. Prasad, R. Bhattacharyya, S. S. Nayak)

Topological and statistical properties of nonlinear force-free fields

The solar corona has a temperature of more than 10^6 K. In order to

maintain this against radiative losses, energy needs to be continuously supplied to the corona. In the high magnetic Reynolds number corona, the magnetic field can be thought as made up of discrete interacting loops/flux-tubes, and the increase of the magnetic energy can be caused by the creation of stresses in the magnetic field lines that are rooted to the photosphere. In particular, the random rotations of the footpoints twist the field lines, while the random walk of the footpoints braid the overlying loop. The coronal field then reorganizes itself through magnetic reconnections to attain relaxed force-free field configuration. Here, we study this reorganization process of a highly braided magnetic field to a force-free geometry.

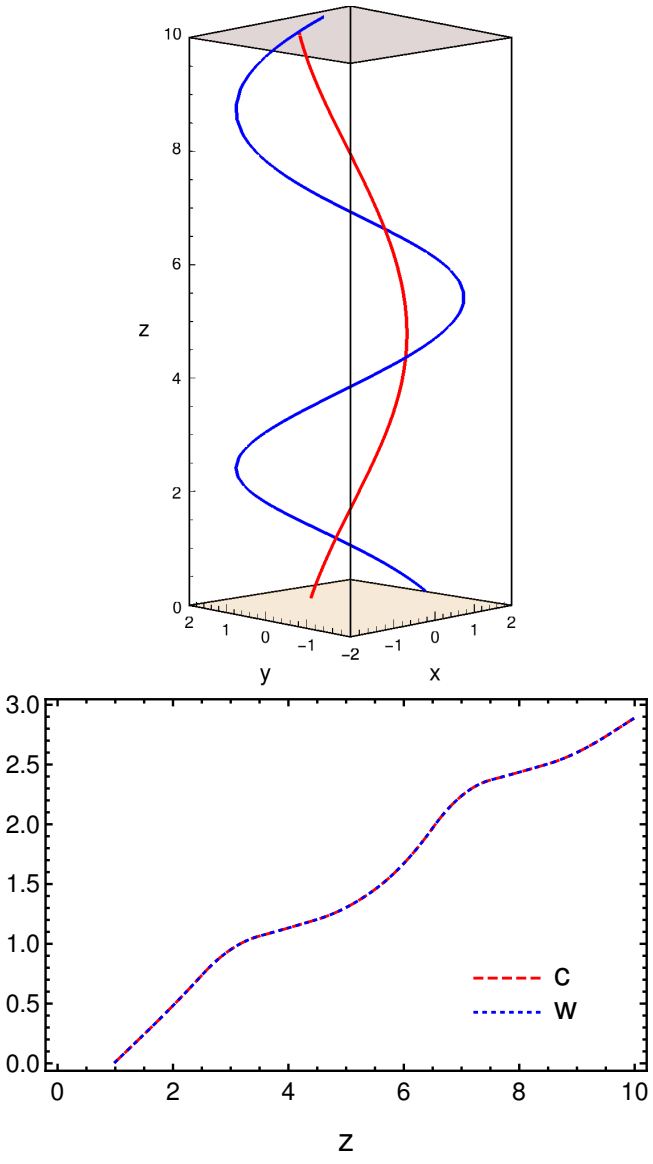

Figure 13.: Panel (a) shows two helical field lines extending between vertical planes. The corresponding variation in the crossing/winding number with height is shown in panel (b).

For this purpose, we use semi-analytic solutions of the nonlinear force-free field equation to construct relevant field topologies and study their statistical properties. In particular, we estimate the degree of braiding exhibited by these field lines by introducing a new formula for calculating the winding number and compare it with the crossing number. The comparison is shown for a toy model of two helices (Figure 13) and for realistic cases of nonlinear force-free fields. We also calculate linkages, which are independent measures of the contribution of magnetic braiding to the total free energy and relative helicity of the field. Finally, we derive new analytical bounds for the free energy and relative helicity for the field configurations in terms of the linking number. These bounds will be of utility in estimating the braided energy available for nano-flares or for eruptions.

This work is done in collaboration with A. Mangalam of Indian Institute of Astrophysics, Bengaluru (India)

(A. Prasad)

Exploring the topological changes in the magnetic field of NOAA AR 11158 from non-force-free extrapolation and its magnetohydrodynamic simulation

The flares and the coronal mass ejections (CMEs) in the solar atmosphere are initiated by a well known process called magnetic reconnection(MR) where the magnetic filed lines (MFLs) rearrange themselves with the liberation of heat and kinetic energy. Hence, it is important to understand and quantify the MFL topology and their evolution which leads to MRs. Contemporary standard is to extrapolate the coronal MFLs using equilibrium models where the Lorentz force on the coronal plasma is zero everywhere, because either there is no current or the current is parallel to the magnetic field. But, here a different approach is attempted to extrapolate the photospheric magnetic field by non-force-free extrapolation (NFFF) technique which is based on the principle of minimum dissipation rate at constant generalised helicity. For the purpose, we select the well documented active region NOAA 11158 and extrapolate MFLs by using magnetogram from HMI/SDO at 01:12 UT on 15th February, 2011, which is roughly half an hour before the peak of an X2.2 class flare (1:45 UT) followed by an earth-directed CME. The coronal MFLs are constructed by NFFF extrapolation technique, resolving a physical domain of extents $\approx 268 \times 134 \times 134$ (in Mm) by a computational domain having $128 \times 64 \times 64$ grids in the x, y and z respectively.

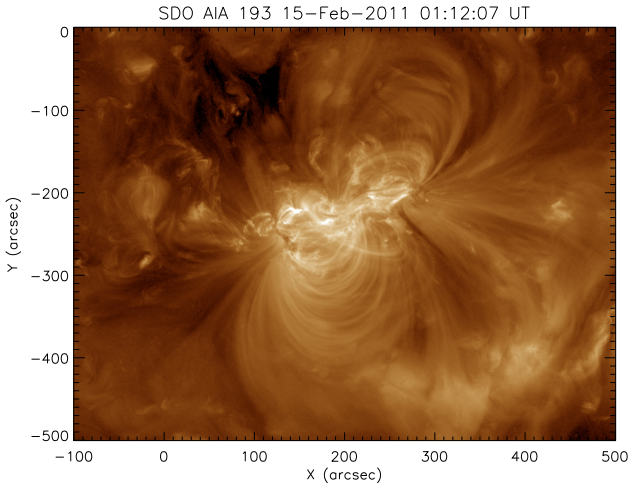

Figure 14.: Image of AR 11158 in 193 Å from AIA/SDO at 01:12 UT.

The normalized deviation of the extrapolated field at the photosphere from its magnetogram value: En=0.227; which renders the extrapolation reasonably accurate. Importantly, there is an overall good match between the extrapolated MFls (Figure 15) with the observed coronal loops (Figure 14).

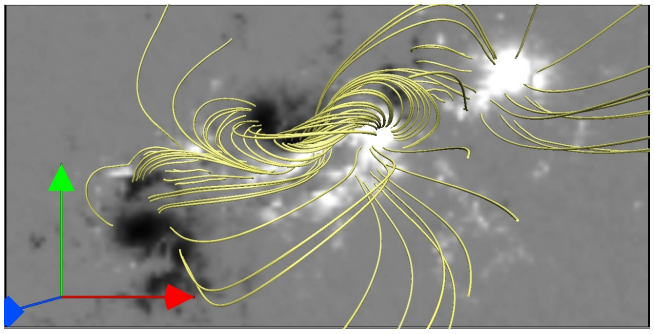

Figure 15.: Extrapolated MFLs at 01:12 UT in a plane(z=0) of dimension (128×64) in x and y directions respectively.

The extrapolated field exhibits interesting magnetic structures like quasi-separatrix layers in a sharp gradient of magnetic field region where current sheets are formed and later lead to reconnection. These QSLs are mathematically expressed as the degree of squashing of MFLs from one foot-point to another. Remarkably, near these QSLs, magnetic field lines appears to be reconnecting continuously in the numerical model. Such type of reconnection is referred as slipping reconnection which are believed to initiate the blowout type jet eruption. To explore such MRs, MHD simulations are performed using the parallelized three dimensional numerical model EULAG-MHD. The computations are carried out on the Vikram-100, the 100TF computational facility at the Physical Research Laboratory. The panel (a) in Figure 16 plots a MFL system having QSLs marked by bifurcating field lines.

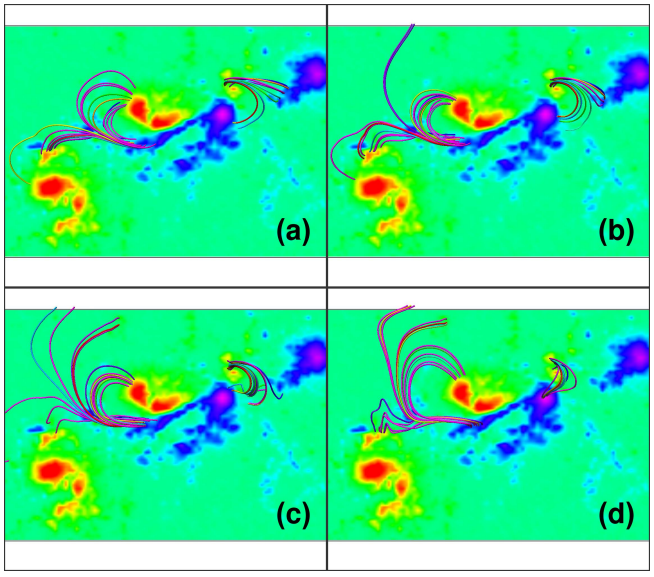

Figure 16.: Flipping of MFLs observed near the qsls at time t= 1, 20, 40, 60.

Subsequent evolution of the MFLs are documented in the panels (a) to (b).The MFLs are readily seen to shift their foot point connectivity from the left of the major bifurcation to its right evident by a temporal increase in number of MFLs on the right. Again, the post-flare CME indicates the possible presence of a flux-rope. After providing a converging flow to the numerical simulated MFLs, a flux rope is generated which is presented in Figure 17. The dynamics in the flux rope is still an ongoing work which will be explained in future with the justification of the eruption of the CME associated with the X-class flare.

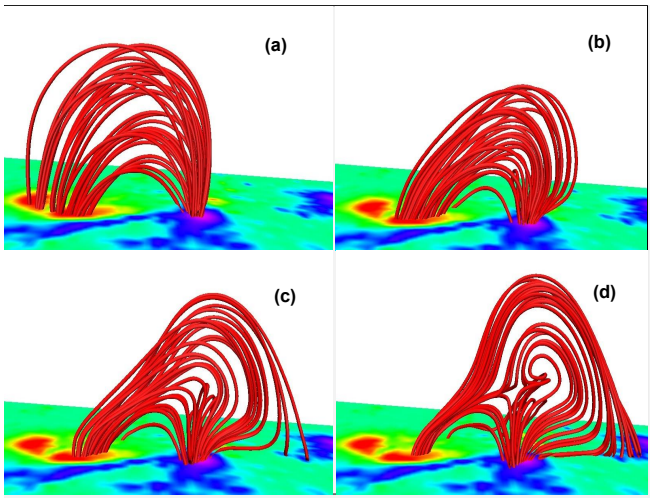

Figure 17.: Evolution of MFLs at t= 60, 1400, 2100, 2800 depicting the formation of flux rope.

(S.S. Nayak, R. Bhattacharyya, A. Prasad)

Chaotically tangled magnetic field lines can heat the solar corona

One of the mysteries in solar physics is the problem of coronal heating. The solar corona-outer “atmosphere” of the Sun-has a temperature of the order of million degrees Kelvin whereas the temperature of the visible surface or photosphere is approximately 6000 K. In comparison to the photosphere, the corona is further away from the core which powers the Sun. Consequently, having a coronal temperature higher than the photosphere is counter-intuitive and seemingly violates the second law of thermodynamics.

A proposed model for the coronal heating relies on nanoflares: solar flares releasing energy in the order of 1024 ergs. The crux of the nanoflare is generation of current ribbons which are near two-dimensional current filaments, called current sheets in contemporary literature. The decay of current sheets and the associated conversion of magnetic energy into heat and energy of mass motion is believed to trigger nanoflares and heat up the corona.

With the whole corona being at million degrees Kelvin and having self-sustained dynamics, the current sheets are required to be distributed throughout the coronal volume and self-generated.

To understand the physics behind generation of current sheets, a set

of original magnetohydrodynamic simulations were performed using Vikram-100, the 100TF High Performance Computing facility at the Physical Research Laboratory. For the simulations, the selected initial magnetic field had chaotically tangled magnetic field lines cf. Panel (a) of Figure 18 showing snapshots of different field evolution. Such spaghetti like convoluted field lines are expected in the solar corona, possibly associated with complex active regions. The simulations, in accordance with the nanoflare model, documented spontaneous appearances of currents sheets which are depicted in panels (e) and (f) , Figure 1. Also, a direct comparison of current sheet distributions in the two panels readily exhibits the distribution becoming more volume filling with time. The temporal increase in current sheet distribution further supports the candidature of chaotically tangled field lines as potential contributors to the coronal heating. Based on additional analyses, the onset of the current sheets were attributed to an autonomous convergence of non-parallel magnetic field lines, depicted in Figure 19.

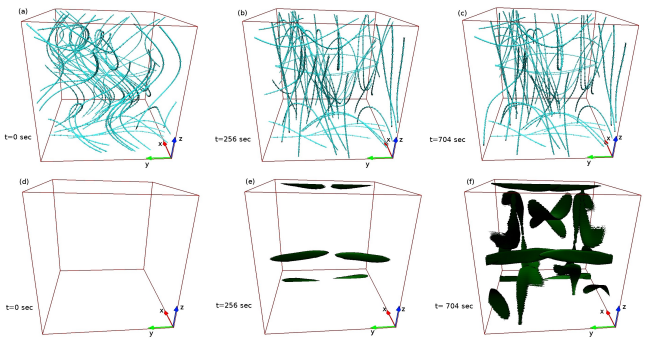

Figure 18.: Figure 1. Panels (a) to (c) depict evolution of magnetic field lines whereas evolution of current sheets are illustrated in panels (d) to (f). Notably, the field lines at t=0s are chaotically tangled and spaghetti like. Initially, the computational volume is devoid of any current sheets. The current sheets start appearing spontaneously at t=256s and become more volume distributed at t=704s.

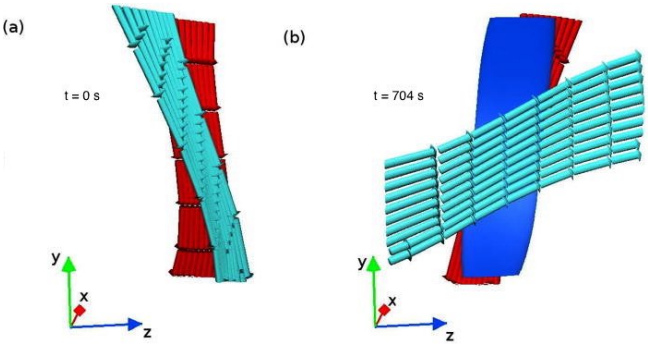

Figure 19.: The arrows represent directions of two sets of representative magnetic field lines depicted in red and indigo. Notably at t=0s, the field lines are almost parallel and no current sheet is present. At t=704s the two sets are more non-parallel and closely spaced, leading to development of the current sheet depicted in blue.

This work is done in collaboration with M. S. Janaki of Saha Institute of nuclear Physics, Kolkata, India and B. Dasgupta of The University of Alabama in Huntsville, USA.

(S. Kumar and R. Bhattacharyya)

Interferometric imaging of Solar features

Efforts are made to demonstrate high-resolution observations of the solar atmosphere using spatial interferometry. Fizeau mask, consist of two apertures separated by a distance known as base-line (BL) is the first step towards interferometric imaging. Two apertures of 7 cm in diameter separated by a distance of 20 cm are placed in the re-imaged pupil of the MAST. Figure 20 shows the image obtained through the mask.

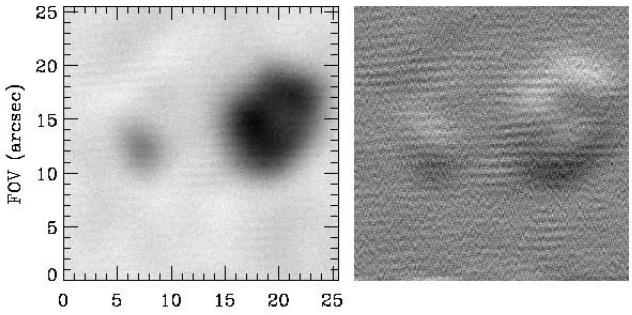

Figure 20.: Image of an active region obtained with Fizeau mask at the re-imaged pupil plane. Left and right side images show the actual image and image after subtracting from a copy of the image shifted by one fringe, respectively. Fringe pattern observed in the image plane signifies the presence of solar structures with sizes smaller than the fringe period of 0.8 arcsec.

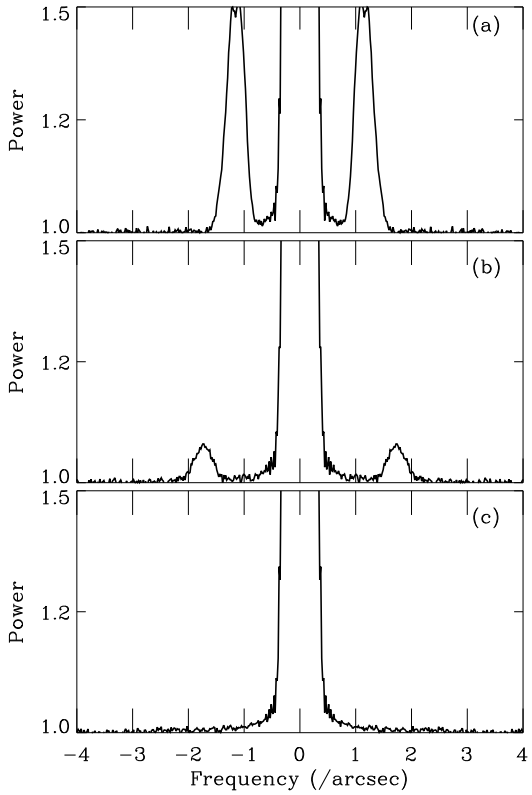

Figure 21.: Spatial power observed from the observations obtained with different base-lines (a) 19 cm, (b) 29 cm and (c) 38 cm, respectively. Power shown here is averaged-over the power obtained from 256 images and it is in arbitrary units.

Fringe pattern observed in the image plane signifies the presence of solar structures with sizes smaller than the fringe period of 0.8 arcsec, which is well known by now from the observations obtained from various high-resolution telescopes. The study is extended by using Fizeau masks with increase in base-line. It is observed that, increase of the base-line causes the reduction in the fringe period and the fringe contrast (c.f. Figure 21). We believe that the reduction in the fringe contrast is due to the low contrast of the solar photospheric features at 820 nm with a bandwidth of 400 nm at longer base-lines. We chose this wavelength to minimize the effect of atmospheric seeing. The study is further extended to reconstruction of the high-resolution observations by sparse aperture imaging employing Golay mask. The data analysis is in progress.

This work is being done in collaboration with Dr. Sridharan and Dr. P. Venkatakrishnan (visiting scientist at USO) from IIAP.

(A. Raja Bayanna and Shibu. K. Mathew)

Science

Planetary Sciences

Modelling of Planetary Atmosphere and Interstellar Medium
Model for Negative Ion Chemistry in Titan's Ionosphere

We have developed a one-dimensional photochemical model for the dayside ionosphere of Titan for calculating the density profiles of negative ions under steady-state photochemical equilibrium condition. We concentrated on the T40 flyby of the Cassini orbiter and used the in situ measurements from instruments on board Cassini as input to the model.

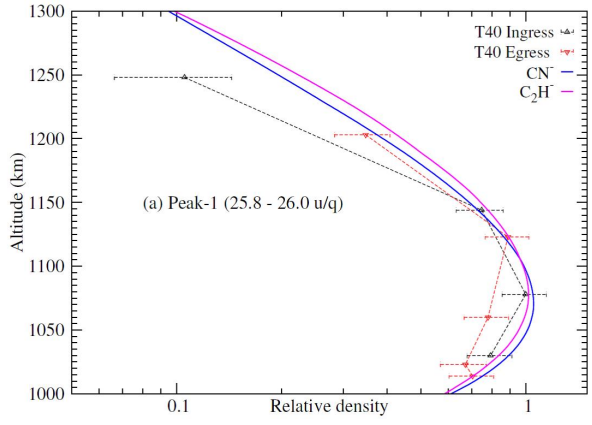

Figure 1: Relative model density profiles of the anions CN^- and C_2H^-, at the mass peaks 25.8-26.0 m/q, compared with the profiles derived from Cassini CAPS/ELS observations during the ingress and egress of the T40 flyby of Cassini spacecraft.

Using the latest available reaction rate coefficients and dissociative electron attachment cross sections, the densities of 10 anions are calculated. Our study shows CN^- as the dominant anion, followed by C_3N^-, which agrees with the results of previous calculations. We suggest that H^- could be an important anion in Titan's ionosphere and is the second most abundant anion at altitudes greater than 1200 km. The main production channel of the major ion CN^- is the reaction of H^- with HCN. The H^- also play a major role in the production of anions C_2H^-, C_6H^-, and OH^-. We found a good agreement between the calculated ion density profiles and the relative density profiles derived using recently reported Cassini CAPS/ELS observations.

(A. Bhardwaj and V. Mukundan)

Modeling of flare and non-flare electron density profiles of Mars' ionosphere

We have developed a model for the calculation of flare and non-flare electron density profiles due to impact of X-rays (0.5-90Å) and Galactic Cosmic Rays (GCR) in the D and E regions of Mars' ionosphere simultaneously. In the non-flare profile D layer is produced at 25 km due to impact of GCR and hard X-rays (0.5-3 Å) with electron densities $1.0 \times 10^2 cm^{-3}$ and $8 \times 10^2 cm^{-3}$ respectively while E layer is produced at 100-110 km due to impact of soft X-rays (3-90 Å) with electron density $\sim 4 - 5 \times 10^4 cm^{-3}$. The D peak density produced by hard X-rays is larger by about an order than that produced by GCR. The D and E flare peaks are produced for a short time at 30 km and 100 km with electron densities $\sim 2 - 4 \times 10^4 cm^{-3}$ and $\sim 1 - 2 \times 10^5 cm^{-3}$ respectively. The predicted flare E-peak density is higher by factor of ~ 2 than the measurements carried out by MGS. The D peak density of flare profile is larger by 1-2 orders of magnitude than that produced for non-flare profiles. These electron densities were modeled for two flares that occurred on 6 April, 2001 and 17 March, 2003. The MGS recorded the effects of these flares in the electron density profiles observed by Radio Occultation (RO) experiment. Figures 2a and 2b show the flare and non-flare electron density profiles that were observed by RO on these two days. Figure 2c represents the modeled electron density profiles produced by GCR and X-ray radiations on

6 April, 2001 and 17 March, 2003 for flare and non-flare period.

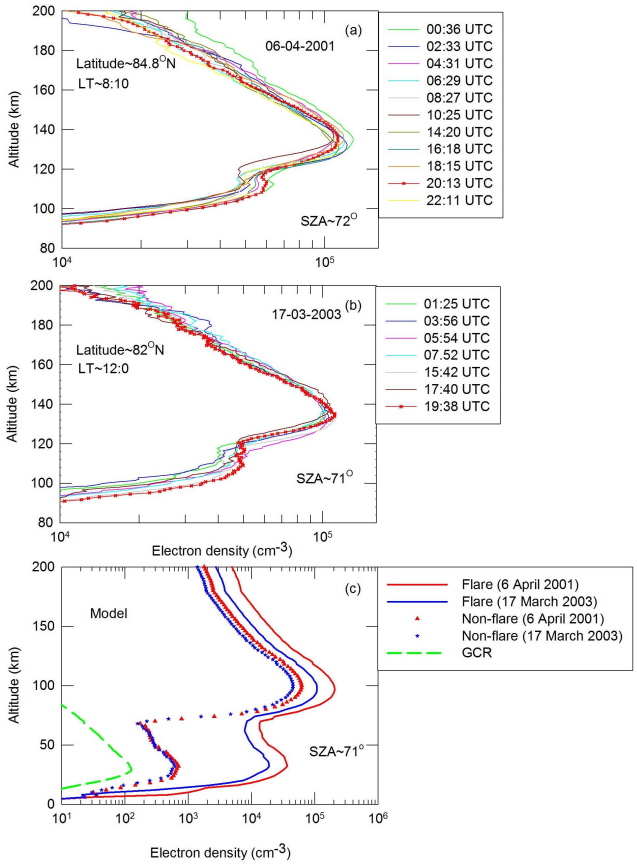

Figure 2: (a) Observed electron density profiles from RO experiment onboard MGS on 6 April, 2006 at latitude 84.8°N, Solar Zenith Angle (SZA) 72°, Local Time (LT) 8:10 for 0:36, 2:33, 4:31, 6:29, 8:27, 10:25, 14:20, 16:18, 18:15, 20:13 and 22:11 UTC, (b) same as figure a but for 17 March, 2003 at latitude 82.0°N, Solar Zenith Angle (SZA) 71°, Local Time (LT) 12:00 for 1:25, 3:56, 5:54, 7:52, 15:42, 17:40 and 19:38 UTC, (c) Modeled electron density profiles on 6 April, 2006 and 17 March, 2003 during flare and non-flare period produced by GCR and X-ray radiations.

(S. Y. Shah and S. A. Haider)

Schumann resonance frequency and conductivity in the nighttime ionosphere of Mars: A source for lightning

Lightning occurs frequently on Earth but it is not detected on Mars. There is a possibility of lightning within the dust devil on Mars. In this work, we have solved Maxwellian equations of electromagnetic waves which oscillate in a cavity formed in the lower ionosphere of Mars between 0 km and 70 km. The electrical conductivity and Schuman Resonance (SR) frequency are calculated in the lower ionosphere of Mars, in presence of major dust storm that occurred in MY 25 at low latitude region $(25-35^{\circ}$S). The atmospheric conductivity is reduced by 1-2 orders of magnitude in the presence of dust storm. It represents a small layer at about 25-30 km in the lower ionosphere of Mars. The SR frequency peaks at about 18 km with values 19.9, 34.5 and 48.8 Hz for modes *l* = 1, 2 and 3 respectively. We suggest that the lightning can occur in the accumulated dust layer at about 20-30 km in the troposphere of Mars. Our calculated results are compared with other model results of *Molina-Cuberos et al.* (2006), *Cardnell et al.* (2016) and *Tolendo-Redondo et al.* (2017) in nearly the same dust storm conditions. We have also developed a prototype Laboratory Experiment for Mars (LEMa) to measure lightning in the lower ionosphere of Mars. Our theoretical work will serve as a diagnostic tool in future to measure the lightning from LEMa instrument onboard Indian Mars mission.

(S. A. Haider, J. P. Pabari, J. Masoom and S. Y. Shah)

Seasonal variability and effect of dust storm on O_3^+ production rate in MY 28 and MY 29: Modeling of SPICAM observations

We have used energy loss model to calculate the zonally averaged production rates of O_3^+ due to impact of Galactic Cosmic Rays (GCR) in the dayside troposphere of Mars between solar longitudes (Ls) 0° and 360° at low, mid and high latitudes in the Martian Year (MY) 28 and MY 29.

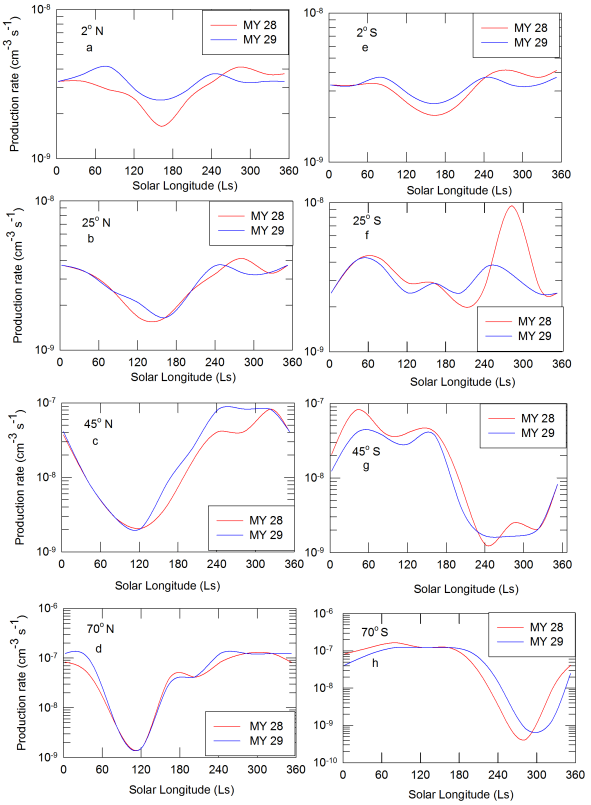

Figure 3: (a-h) Seasonal variability of in MY 28 and MY 29 due to GCR impact ionizations on the surface of Mars at (a) 2°N, (b) 25°N, (c) 45°N, (d) 70°N, (e) 2°S, (f) 25°S, (g) 45°S (h) 70°S.

We also represent the seasonal variability of zonally averaged O_3 column density obtained from Mars Global Climate Model (MGCM) during the daytime. These results are compared with the daytime observations made by Spectroscopy for the Investigation of the Characteristics of the Atmosphere of Mars (SPICAM) instrument onboard Mars Express (MEX). At mid to high latitudes production

rate of O_3^+ are maximum in winter and minimum in summer. It shows a broad peak at about 30-40 km. The peak production rate of O_3^+ increases up to $L_s = 47.5^\circ$ where it stabilized at about $2 \times 10^{-8} cm^{-3} s^{-1}$. At $L_s \geq 47.5^\circ$ the peak production rate of O_3^+ starts decreasing until O_3 layer disappeared after $L_s = 127.5^\circ$. A major dust storm occurred in MY 28 at $L_s = 280^\circ$ in the subtropical region ($25 - 35^\circ$S). It is found that the production rate of O_3^+ increased by a factor of $\sim$ 4 in the dust storm region. Figure 3 a-h shows seasonal variability of ion production rates of O_3^+ at 2°N, 2°S, 25°N, 25°S, 45°N, 45°S, 70°N and 70°S at the surface of Mars between $L_s = 0^\circ$ to 360° in MY 28 and MY 29.

(S. A. Haider, Y. S. Siddhi, J. Masoom and K. D. Prasad)

Competing pathways in oxygen photochemistry of the Martian atmosphere

Though the photochemistry of Mars is comparatively simple, the orbital properties of Mars and its exposure to solar influx lead to pronounced seasonal and latitudinal variations of short lived species (trace gases). However, in previous studies a quantitative comparison between various production and loss processes, with their relative importance in determining the abundance of trace species, has not been performed. Here we use the photochemistry coupled LMD GCM to study in detail the source and sink processes of ozone and oxygen atoms and their contribution in different locations and seasons. This becomes especially important due to the high seasonal variability of water vapor involved in the photochemistry. It is found that for ozone, the near surface loss rates with H, OH and O are higher during summer while the other loss processes are more effective during winter from their daytime values. The study shows few interesting features about the processes. Production rate for ozone are higher during winter, though O production rates are higher during summer. Contrary to expectations, the day time loss rates due to HO_2 do not show a strong seasonal variation. Over southern summer polar region, loss of ozone with H exceeds the photodissociation loss in the upper atmosphere. The season Ls=60°-120°facilitates the ozone production in the altitudes greater than 20 km.

(A. Modak and V. Sheel)

Horizontal winds in the Martian planetary boundary layer

The planetary boundary layer (PBL) mediates interactions between the surface and free atmosphere. In Martian PBL, surface can force convective vortices leading to dust devils. For a turbulent PBL, the horizontal mean wind is found to vary logarithmically with altitude in a Cartesian co-ordinate system. We use the Navier Stokes equation and the continuity equation to determine mean horizontal wind velocity in cylindrical co-ordinate system (within the surface layer of a planetary atmosphere). This yields an additional term that has an inverse square dependency on radial distance from the center of vortex, and quadratic dependence on the altitude. The new form of the wind profile equation provides additional information in context to wind generating vortices, which was not present earlier in the Cartesian coordinate system. For one order increase in the radial distance from vortex center, we observe a decrease of about two orders of magnitude in the mean velocity. We also observe a sharp increase in velocity with increasing altitude in the cylindrical co-ordinate system (due to quadratic dependency on the altitude). As we move far away from the center of a rotating vortex, the velocities in both co-ordinate systems becomes equal. We observe a positive correlation of 0.88 between velocities estimated from our derivation and Burgers vortex solutions.

(S. Uttam, V. Sheel and D. Singh)

Fluorine and Chlorine Chemistry in the Interstellar medium

We have studied the formation of chlorine- and fluorine-bearing species for a variety of interstellar regions using a gas-grain network. Our homogeneous (0D) models are designed for isothermal diffuse, translucent, and dense clouds, as well as warm-up regions. In addition to the regularly observed species, we have added a number of additional halogen-containing molecules and explored their gas-phase and grain surface chemistry. Other molecules include neutral species such as Cl_2, ClO, and CCl, as well as the carbon-halogen species CH_3Cl, and ionic species such as CCl^+, ClO^+ , HF^+, SiF^+, and H_2F+. Predictions are made for the abundances of these species as functions of time and comparisons are made with the observed abundances obtained for halogen species. The peak fractional abundance of the newly detected gas-phase CH_3Cl is predicted to be 10^{-10} - 5.4 $\times$ 10^{-8} in our warm-up simulations depending upon the density and the age of the pre-warm-up phase at which warm-up begins. These values can be compared with the observed abundance of methyl chloride in the hot corino IRAS 16293-2422 if the abundance of methanol is known. Finally, we have shown that the inclusion of halogen-bearing species into our gas-grain network is not likely to affect the destruction rate of existing non-halogen-bearing molecules, but may affect their formation rate through the formation of intermediate radicals, as has already been shown for methyl formate. *This work is done in collaboration with Prof. Eirc Herbst of University of Virginia.*

(K. Acharyya)

Molecular Complexiety in the star forming regions of Magellanic Clouds

We have studied the chemistry of molecules through Complex Organic Molecules (COM's) in complexity in hot molecular cores in the Large and Small Magellanic Clouds using a gas-grain network. Hot molecular cores are characterized by a small source size ($<$ 1 pc), high density (10^6 - 10^7 cm^{-3}) and high gas and grain temperatures ($>$ 100 K), which are considered to represent an early evolutionary phase during star formation. The study of these nearby galaxies can serve to better understand more distant metal- and dust-poor galaxies. We utilized a physical model which consists of three stages. First, the gas collapses isothermally from a low-density cloud of n_H = 3 $\times$ 10^3 cm^{-3} to a final high-density hot core region of 10^7 cm^{-3} in around 10^6 years. In the 2^{nd} stage, collapse is halted, and gas and dust temperatures are increased to 200 K with a power law index of 1 (linearly dependent on time). Finally, we allowed hot

core chemistry until 10^7 years. Since these galaxies might have higher dust temperature in cold regions than observed in the Milky Way, we considered four different temperatures -10, 15, 20 and 25 K for the isothermal collapse phase. We found that for some abundant species such as carbon monoxide and water, hot core abundances are consistent with the reduced elemental abundances of the LMC and SMC. For other less abundant species such as Methane, and hydrogen cyanide, the calculated abundances are larger when compared with elemental abundances whereas for species like ammonia it is lower. Our calculations show that some complex organic molecules (COM's) can also be formed in reasonable quantity for hot cores in the Magellanic clouds when the grain temperature is lower than 25 K. Although when initial dust temperatures are higher, the formation of COM's is severely restricted. Model results are in reasonable agreement with the observed abundances and upper limits.

This work is done in collaboration with Prof. Eirc Herbst of University of Virginia.

(K. Acharyya)

Remote Sensing and Data Analysis

Origin of Lunar Swirls

Lunar swirls are curvilinear albedo markings of tens of kilometers size associated with magnetic anomaly regions. The origin of these astonishing features on the Moon has been much debated. Near-infrared (NIR) spectra of mare swirls have been found to be similar to those of immature mare material therefore prevention of space-weathering due to magnetic shielding has been proposed as a possible formation mechanism. Alternatively, it has been proposed that swirls would have been formed by cometary impacts.

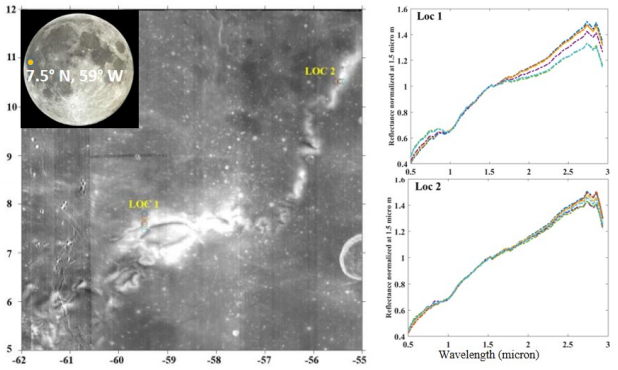

Figure 4: M^3 spectral variability at two locations of Reiner Gamma Formation.

Reiner Gamma (7.5° N, 59° W) is a Type Swirl located in the western Oceanus Procellarum region of the Moon. It is associated with localized magnetic field and is characterized with complex morphology comprising of extensive looping and combination of dark lanes and bright ribbons. In this study, we have examined spectral variability across the Reiner Gamma using Moon Mineralogy Mapper (M^3) data from Chandrayaan-1 mission and compared the observations with commonly observed maturation patterns as well as modeled compaction related spectral behavior. It has been found that two different locations (Fig 4) of the swirl can be ascribed to two different predominant formation mechanisms. Whereas, Loc 1 shows absence of space-weathering, spectral behavior at Loc 2 cannot be accounted for by considering solar wind shielding only. Regolith compaction due to interaction of high-velocity cometary gas with the uppermost regolith layer amicably explains the observed spectral variations at Loc 2.

The work has been carried out in collaboration with SPL, TU Dortmund University, and Moscow State University

(N. Srivastava and A. Bhardwaj)

Terrestrial gullies and debris-flows in Ladakh Himalaya as planetary analogs for Mars

In this study, we compared morphology of gullies within two high-latitude Martian craters (Domoni- 51.38° N; 234.41° E, and Maricourt- 53.34° N; 288.92° E) in the northern hemisphere of Mars with (1) the debris flow gully systems in the Ladakh Himalaya (34° N; 78° E) and (2) Istok Crater (45.11° S; 274.2° E) in the southern mid-latitudes of Mars where water-bearing debris-flow deposits have been previously reported. The study findings led us to suggest that the debris-flow landforms preserved on gully and alluvial fans in the Ladakh Himalaya are potential analogues for the deposits preserved over the equator-facing slopes of Domoni and Maricourt Craters. In addition, we found that the morphological attributes of channels and deposits (including overlapping terminal lobes, levees, tongue-shaped/lobate deposits and broad/small depositional deposits) within both the study craters and Istok Crater are similar. As a result, both the the studied craters emerge as additional sites in which possible evidence of water-bearing debris-flows are preserved on Mars. By comparison to our Earth analogue (in the Ladakh Himalaya), we further propose that episodic melting of snow accumulated within the sheltered alcoves is the most likely source of water for the formation of such gullies. Taken together, our findings suggest that debris-flow may not be a rare process in gully formation on Mars and evidence may be preserved in other unexplored areas.

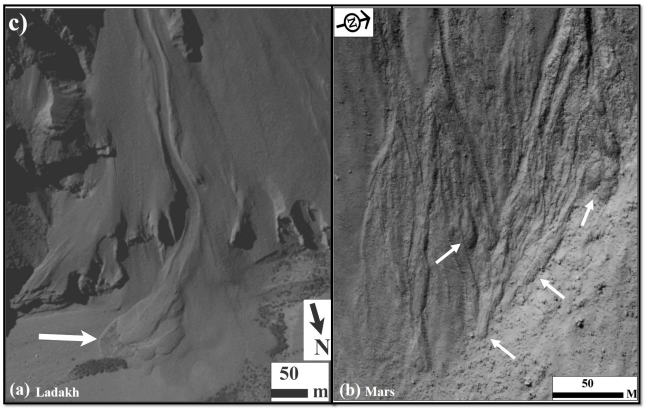

Figure 5: Geomorphic evidence of terminal debris-flow lobes (a) in the Ladakh Himalaya and (b) at the foot of crater rim wall slopes on Mars.

(R. K. Sinha, S. Vijayan, A. D. Shukla, P. Das and F. Bhattacharya)

Study of layered deposits in the East Melas Chasma, Mars using MCC, HiRISE, THEMIS and MOLA data

Mars Orbiter Mission (MOM) Mars Color Camera (MCC) image has been used to study morphology of layered deposits (LDs) and landslide emplaced within the East Melas Chasma region (12.7° S, 69.2° W) on Mars. HiRISE images reveal that the patches of dust and ripples/dunes bind the layers within inferred deposits. These layers are markedly toned in terms of brightness, appears finely layered, show bench-cliff morphology, and consistent with small-large exposures. Topographic profiles derived from MGS-MOLA data reveals that the LDs and landslide are distinctly elevated. Thermal inertia (TI) values derived using Mars Odyssey THEMIS data indicate that the layered materials have TI values ranging from ∼110-690 J m^{-2} K^{-1} $s^{-1/2}$. Further, layered materials with TI values within ∼310-690 J m^{-2} K^{-1} $s^{-1/2}$ show evidence for mafic/basaltic composition at seven locations as inferred from THEMIS DCS images of 8,7,5 band combinations. Taken together, the study provide insights into correlation between morphological, compositional and thermophysical characteristics of LDs and landslide, and influence of aeolian material within this region.

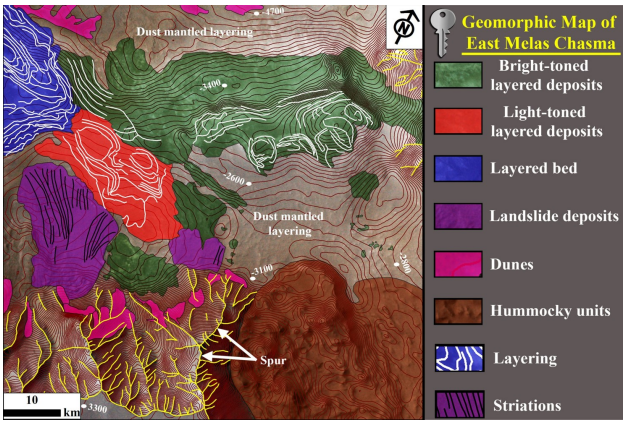

Figure 6: Morphological map of the study region based upon MCC image. The map illustrates the key morphologic units identified within the study region.

(R. K. Sinha and S. Vijayan)

Craters in the vicinity of Valles Marineris, Mars: Implication for geological activities

Valles Marineris (VM), one of the remarkable canyon like feature on Mars probably formed due to the tectonic or magmatic activities. It's the largest canyon like system in the Solar System, whose length, width, depth are ∼2000 km, ∼110 km and ∼4 km respectively. The walls host the largest distribution of landslides on Mars. The relative formation period of this canyon system tend back to older than ∼3.7 Ga. However, over the vicinity of VM region, several impact craters are emplaced and they have undergone modification through formation of pits and graben within or surrounding it. The material collapses in the voids within shear fractures results in the formation of pits. Later, coalescing of adjacent pits results in troughs and they extended over different size over different region. This work intended to decipher the time period of such extension activity underwent throughout the VM region within or adjacent to the craters. We have undertaken a detailed analysis of the distribution of pits and grabens in Valles Marineris region in order to 1) revisit and asses the time-scale of formation of pits and grabens 2) provide more exact age for their relative formation time-scale using associated crater's age as a proxy 3) assess distribution of spatially apart pits and grabens 4) revisit and reassess theories of origin of VM (tectonic or magmatic). For this study, we have dated 30 craters (∼100 Km buffer from VM boundary) associated with Valles Marineris formation activities. Our results suggest there are several craters which was superposed by graben and pits activities. Such craters chronology tends to ∼3.5 Ga suggesting that the VM extensional activity prolonged to Late Hesperian epoch on Mars. This reveals that the VM region was geologically active from Noachian to Hesperian epoch.

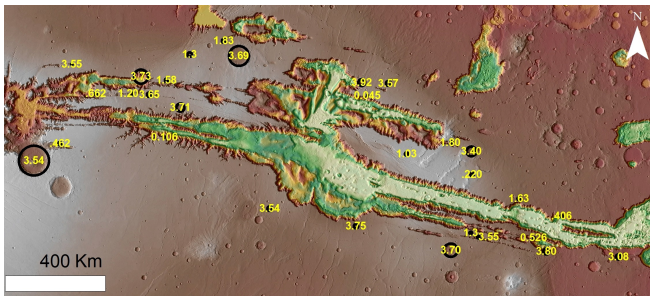

Figure 7: Relative age of craters in the vicinity of Valles Marineris on Mars.

(Harish, S. Vijayan and R K Sinha)

Nernst crater, Moon: Floor fracture and domical uplift

Impact craters are the predominant surface features on Moon, whose floor exposes the deeper crustal material. Most of the lunar crater floors are nearly flat or hummocky. The flat floors are caused due to the materials deposited from the wall or some intrusion of material from beneath the crater floor.

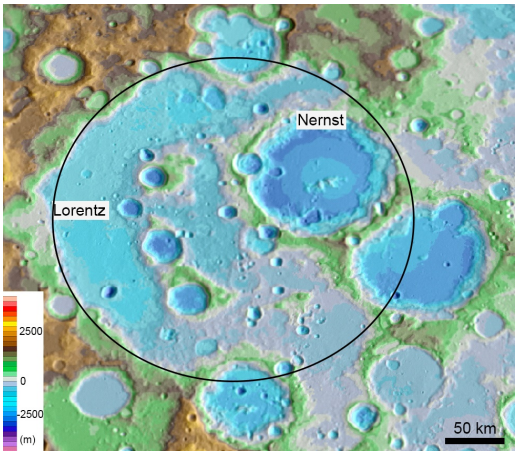

Figure 8: The Nernst crater formed inside the Lorentz basin. The Nernst floor shows topographical uplift.

Apart from flat floored craters, there are very few craters on Moon whose floor are fractured and uplifted. Though the floor fracturing is

related to the impact induced radial and concentric fractures, most of the crater fractures are asymmetric and not all the floor fractured craters are having uplifted floor. This study, carried out to understand such unique craters (floor uplifted and fractured) on moon and their formation hypothesis. Nernst, a ∼116 km diameter crater formed within the Lorentz basin whose diameter is ∼312 km. Nernst crater, located not only on the Near- and Far-side boundary, but also adjacent to the largest mare infilling region of Moon, the Ocenaus Procellarum (OP) basin. The Nernst crater floor got uplifted and formed a dome with fractures over it. The uplift probable caused due to the intrusion of the magma material through the fractures made by impacts (both Lorenz and Nernst) on the surface. The important significance of this domical uplift is rise of magma through the thick OP basin ejecta (∼2-3 km thickness) and the mega regolith on the lunar crust. Such intrusion and infilling are sporadically present over Moon and the mapping revealed that those are mostly adjacent to the biggest infilled basins on Moon. This infilling and uplifting can be probably sourced from such basin filling events. Chronological studies revealed such fracture and uplift occurred around ∼3.8 Ga. To support the intrusion of relative deep crustal material, the presence of low calcium pyroxene confirms that. Similar minerals LCP's are also reported on the OP region, which also exposed the deeper crustal material. This bring the consensus of opinion that the source for the infilling, fracturing and uplift could possibly have relevance to OP basin infilling.

(S. Vijayan, N. Kumari, Harish, I. Varatharajan, R. Anilkumar and R. K Sinha)

Investigating multiple lava flows near Mangala Fossa with SHARAD

Radar evidence suggests that a minimum of two successive infilling events happened in the Mangala crater, separated by sufficient time to allow two rim craters to form and partially bury the first lava infill.

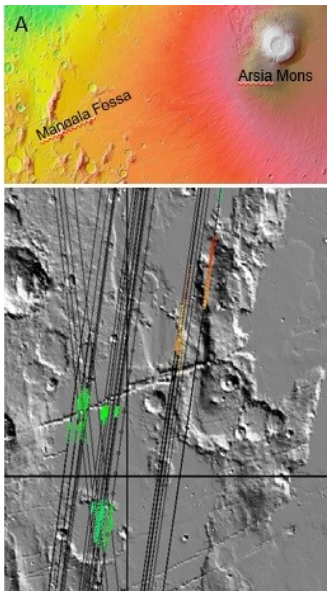

Figure 9: Mangala Fossa and map of radargram subsurface reflection.

The volume of top unit of lava within the crater is ∼81 km^3. A consistent dielectric value between the north and south lava flows do not rule out the possibility that they happened at the same time. Later, the north lava flow was eroded at the formation of the Mangala outflow channel. By comparing the relative ages of Mangala Crater, the successive lava beds, the outflow channel, and the superimposed craters on Mangala Crater, we can begin to put a timeline on the history of events in this region.

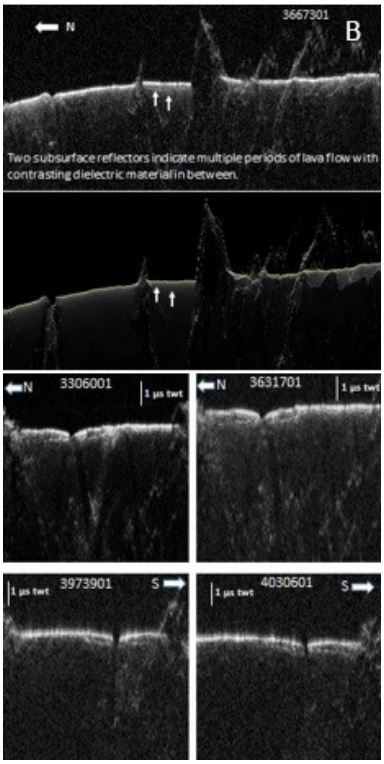

Figure 10: Subsurface reflection in SHARAD.

This work has been carried out in collaboration with Dr. Isaac Smith, Planetary Science Institute, Colorado, USA.

(R. R. Bharti)

Sedimentary responses of surface hydration at gale crater on Mars

This study explores the effect of surface hydration at the present-day aeolian sediment system of Gale crater, Mars. Thus far, study of surface hydration is restricted up to the detection of the soil moisture using bulk soil and spectral geochemistry, transient activity of night time brine, and seasonal frost activity. Detailed sedimentological investigations have been carried out using MSL-Curiosity's Mastcam, Navcam and MAHLI images. Also REMS data has been used to measure the relative humidity of the surface and to assess the extent of the effect of moisture on aeolian sedimentation and climatic control. Penecontemporaneous deformation structures such as disintegration of soil surface, featured by horizontal fractures, break-apart laminae, and brecciated clasts, were identified at multiple places of the regional dune field and inter-dune playa of the Gale crater. Moreover, such

features were observed to be common with the association of fresh grain flow activities, identified with the aid of distinct flow lobes, sharp outlines, and darker tones at the slip-face of large ripples and sand patches. Also cm-scale curve-crested impact ripples over the sand patches were observed. The patches of eroded bedform were recognized by their characteristic flat crests and non-migratory nature. Surface fracturing and grain flow are the associated features observed in few locations. Non-migratory nature of the cm-high impact ripples indicates that the structural stability of three dimensional structures was achieved during sublimation of moisture and re-precipitation of salts along the capillary fringes, typically an early cementation phenomenon. Further the flattening of the ripple crests can be explained by the operation of wind abrasion in subsequent dry phases. Careful observations of sedimentary structures reveal that trapping and binding mechanisms are still active, suggesting the proxy for surface hydration, are restricted up to the topmost layer of the surface. Subsequent dry grain flow processes are manifested by sediment remobilization and differential erosion. Presence of transiently stable capillary moisture retained by inter-particle forces led to the structural stability of the material by early salt cementation during sublimation. However, the absence of hydro-plastic deformational and fluidized features reveals that neither the physical state nor the volume of the fluid was favourable for grain saturation or liquefaction. Therefore, it can be suggested that the inter-grain cohesion bears the testimony of retention of surface moisture even in under-saturated condition at the patches on the Martian surface. Estimated relative humidity of the surface for the studied sols suggests that the formation of the sedimentary structures by hydrous events is predominantly diurnal in nature than so far believed seasonal variability. These observed phenomena at the equatorial driest and warmest region perhaps define the lowest threshold limit of moisture at the surface-atmosphere boundary in the present-day, large-scale climatic model of Mars, and therefore wetting can occur more abundantly and at a greater scale for the rest of the planet.

(P. Das and A. Basu Sarbadhikari)

Meteorite Studies

^{7}Be: The Vanguard of Irradiation

^{7}Be decays to ^{7}Li with half life of 53.06 $\pm$ 0.12 days and is a key short-lived now-extinct radionuclide for deriving information about early solar system event and processes. Lithium-berylium-boron (Li-Be-B) isotope systematics studies in the first forming solar system solids, Ca-Al-rich inclusions (CAIs) provide a unique opportunity of utilising two isotope decay systematics of ^{7}Be-^{7}Li and ^{10}Be-^{10}B, respectively, to understand cosmochemical/astrophysical conditions and plausibly also chronology of the events and processes in the early solar system. A first unambigous detection of ^{7}Be along with fossil records of ^{10}Be corresponding to ^{7}Be/^{9}Be of (1.2$\pm$1.0)$\times10^{-3}$(95% conf.) and ^{10}Be/^{9}Be of (1.6$\pm$0.32)$\times10^{-3}$is being inferred from the regression of the in situ isotopic data obtained using secondary ion mass spectrometer in a pristine type B CAI from Efremovka (CV$\sim$3.1-3.4). Isotopic records of ^{7}Be, ^{10}Be and ^{26}Al in a type B CAI from Efremovka (E40) allow to make following very important inferences: (1) Nascent Sun underwent multiple episodes of enhanced magnetic activity (2) the later episode of enhanced irradiation occuring at the end of “class I” stage of pre-main sequence evolution was more intense (3) Irradiation is the prime source of ^{7}Be and also ^{10}Be. An intense irradiation by a super flare (X-ray luminosity Lx $\approx$ 10^{32}ergs) during the terminal class I stage of a CI (carbonaceous Ivuna $\approx$ solar) composition precursors near the reconnection region for about a year can concurrently explains the isotopic properties (^{7}Be, ^{10}B, ^{26}Al), morphology (texture, modal grain sizes), and petrology (mineral compositions) of CAI, along with preservation of faster diffusing lithium isotope records. *This work has been carried out in collaboration with Mishra R.K, Heidelberg University.*

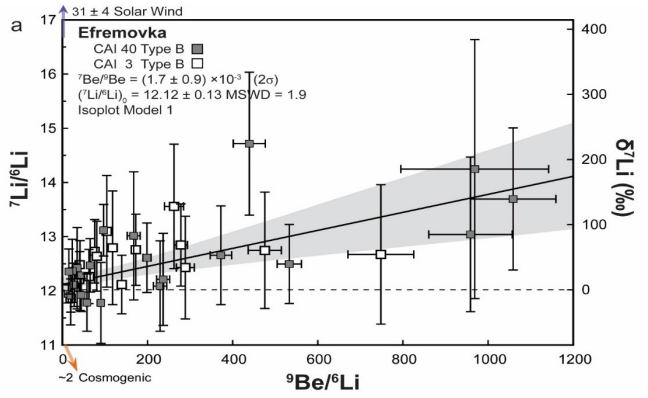

Figure 11: ^{7}Li/^{6}Liratios measured in melilite including cosmogenic correction are plotted against measured ^{9}Be/^{6}Li in two Type B1 CAIs(EF3 and E40)from Efremovka (CV$\sim$3.1-3.4) chondrite. The dotted horizontal line shows the chondritic^{7}Li/^{6}Li ratio.

(K. K. Marhas)

Al-Mg in Bhukka meteorite

Unusual occurrence of corundum (Al_2O_3) in Iron meteorite, Bhuka (IAB low-Ni ungrouped), has been reported earlier. According to the equilibrium thermodynamic condensation calculations for a cooling solar gas, corundum is the first major condensate. Whereas, evidence from Hf–W radiometric dating of iron meteorites shows that most irons come from bodies in which metallic cores formed $<$1 Myr after the growth of the Ca–Al-rich inclusions (CAI). The ‘silicate-bearing iron meteorite’ such as group IAB have poorly defined elemental trends suggesting that the group did not form from a single isolated metallic melt and their formation might be due to impacts mixed molten metal and silicates. The Al-Mg systematics in corundum form the silicate/graphite inclusions of Bhuka meteorite can define the relative formation time of the corundum and throw some light on the formation scenario of this meteorite.

Nano Secondary Ion mass spectrometer measurements on four of these corundum grains provided an initial ratio of (^{26}Al/^{27}Al)$_0$ $\sim$ 5 $\times$ 10^{-5} indicating an early condensates mixing into the iron melt. There could be two possible scenarios: (1) corundum was captured in a silicate or graphite objects for initial few years before getting incorporated into Iron– meteorite as an impactor. In this case, the silicate/ graphite body has to survive the dynamical protoplanetary disk for 1-2 million years. (2) Or, the parent body of the iron meteorite that was disrupted to form iron meteorite had a very primitive chondritic composition component with large number of corundum inclusions.

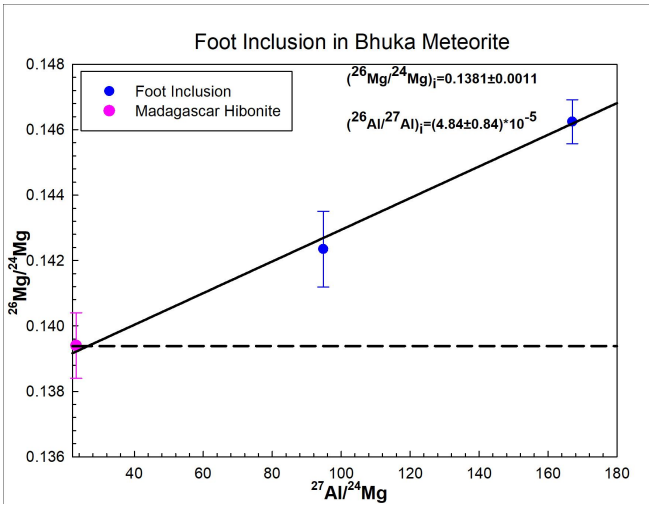

Figure 12: Al-Mg isotopes as measured using NanoSIMS in corundum found within inclusions of Iron meteorite.

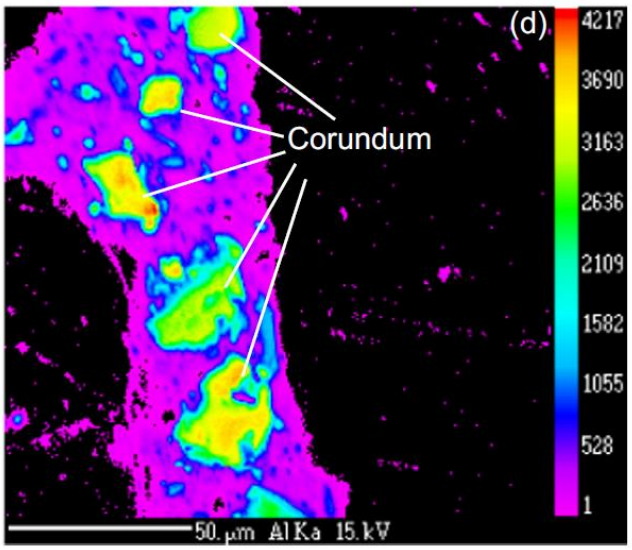

Figure 13: EPMA image of one of the inclusion.

(K. K. Marhas and D. Ray)

Lunar magnetic field anomaly, global distribution, depth of the source bodies and their possible origin

The Earth's Moon is believed to have no global magnetic field at the present day. However, Lunar Prospector and Kaguya missions provided strong global lunar magnetic field anomalies at different regions of the Lunar crust such as the Reiner-Gamma, South Pole Aitken Basin etc. We have made an attempt to map the global magnetic anomalous regions using the data available from the Selene-Kaguya mission.

Eight regions have been demarcated with higher crustal total magnetic field than the background values. The highly magnetic anomalous regions are: northern rim of South Pole Aitken Basin (SPAB), eastern extended arm of SPAB, Reiner-Gamma, Airy, and three other selected regions. Significant variations of the total and horizontal magnetic fields were observed. The Northern rim of the SPAB shows total magnetic field intensity in the range 50-300 nT. The Reiner-Gamma region shows higher total magnetic field intensity between 100-500 nT, while Airy region shows less magnetic field value between 10-70 nT. We attempted to determine the depth of the source bodies in the different magnetically anomalous regions. We have used the second, third and fourth order horizontal derivatives obtained from observed magnetic anomalies to calculate the depth of the magnetic sources. The computed higher-order horizontal derivative datasets are used to solve nonlinear equations for depth determination. We have created different profiles at the magnetic anomalous regions like Reiner Gamma, South Pole Aitken basin, Airy etc., and using the magnetic dataset from the Selene Kaguya mission, we have estimated the depths for each profile. Depth analysis of the Reiner Gamma region has been shown in Fig. 14. The depth for the source body from the surface to the top of the body at the centre along the profile A-B is found to be 8.3-8.4 km. Similar analysis has been done for the other regions also.

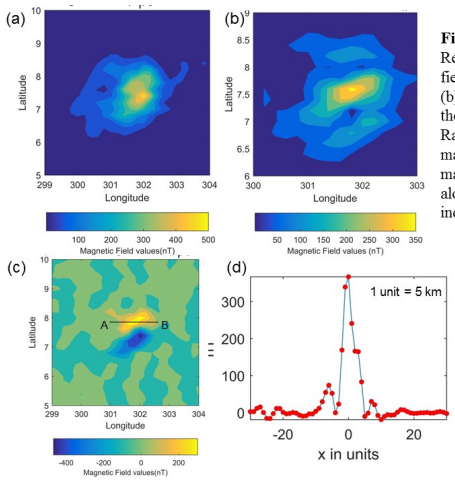

Figure 1: Reiner-Gamma Region. (a) Total magnetic field anomaly (B_T) contour; (b) Horizontal component of the magnetic field (B_H); (c) Radial component of the magnetic field (B_r); (d) The magnetic field anomaly along a profile A-B is indicated in (c).

Figure 14: Reiner-Gamma Region. (a) Total magnetic field anomaly (BT) contour; (b) Horizontal component of the magnetic field (BH); (c) Radial component of the magnetic field (Br); (d) The magnetic field anomaly along a profile A-B is indicated in (c).

We suggest that the different range of anomalous magnetic values is because of the magnetic bodies, plausibly emplaced at different depths, which has resulted in variable attenuation of the magnetic field at the surface. The horizontal component of the magnetic field intensity has some global pattern or orientation for almost all the magnetic anomalous regions. This alignment of horizontal component gives an idea about the geometry of the source magnetized body and suggests possibility of a paleopole. In case of Airy the source body is mainly vertical and is pointing downward at the centre, and for Reiner-Gamma the source magnetization is mainly horizontal. These regions might have been strongly magnetised by a source that acquired its long lasting magnetic field under the influence of the lunar dynamo.

(G. Arora, J. Ghosh and A. Basu Sarbadhikari)

Implications for formations of alkali-rich rocks of the Moon

Study of the lunar highland crust yields the record of oldest crust formation history of the terrestrial planets. High abundance of Na are observed by LCROSS impact at the Cabeus crater of the southern highland and Chandrayaan-1's X-ray Spectrometer (C1XS) near Tycho crater at the nearside of the southern highland has detected Na-rich domains (3-7 wt% Na_2O). The modal mineralogy and the bulk composition indicate that the rock type is alkaline and was classified as nepheline troctolite. Calculated parent melt (PM) composition was considered based on i) the field relations and the compositional trends of the highland rocks to define the syn-crystallization assemblages, ii) equilibrium relation with co-existing olivine, and iii) comparison of elemental oxides with different highland rocks.

The calculated LMO composition (LMO_n) has following characteristics. The silica content is lower in LMO_n than that earlier estimations (by 1.3-2.9 wt% SiO_2; alkali (Na_2O+K_2O) content in LMO_n is 0.3 wt% more. Perhaps the major difference in LMO compositions are in TiO_2 content, which is 3.5 – 7.0 times higher in LMO_n (1.12 wt%). Crystallization calculation from the LMO_n has successfully yielded the early to intermediate stage of crystal settlement at the bottom of the LMO. The nepheline troctolites of Tycho and the associated rocks are not the result of late stage magmatism, rather are crystallized from the LMO in a maximum time span of $\sim$ 500 Ma. It can also be concluded that the Moon has formed much cooler than that by the giant impact and with high volatile content similar to the earth. Much of the volatiles are retained in deep inside of the Moon.

(A. Basu Sarbadhikari)

The Mukundpura meteorite: A new fall of carbonaceous chondrite

Mukundpura is a new CM chondrite which fell in Mukundpura village near Jaipur, Rajasthan, India on June 6, 2017 at 5:15 IST. According to eyewitnesses, the stony object was fragmented into several pieces once it hit the ground. Based on petrography, mineralogy and bulk composition, Mukundpura is classified as CM2 chondrite. This rare type of specimen is the fifth carbonaceous meteorite fall in India since 1890.

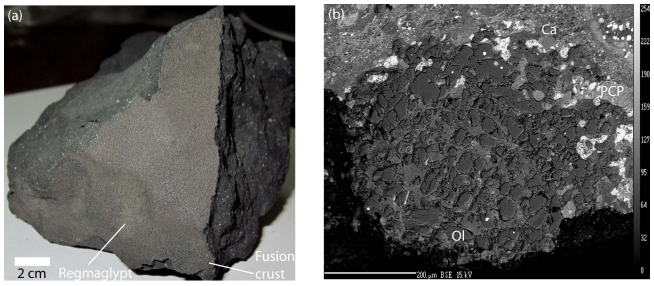

Figure 15: (a) Fragment of Mukundpura chondrite (Fall, 2017) (b) Porphyritic Olivine (Ol) Chondrule. Calcite (Ca) and Poorly Crystallised phases (PCP) are also shown.

The specimens appear as encrusted with thin fusion crust (Fig. 15b). The chondrules are forsteritic olivine in composition and commonly rimmed by fine-grained accretionary dust mantles (Fig. 15b). Phyllosilicates (serpentine and Fe- cronsteidite) are the most common secondary mineral in matrix and largely occur as poorly characterised phases (PCPs). Other mineral phases in matrix include calcite (pure $CaCO_3$), Fe-Ni metal and sulphides. The bulk chemical composition of Mukundpura is largely similar to other well known CM type chondrite (e.g. Paris CM). The role of substantial aqueous alteration activities were suggested to explain the variegated matrix mineralogy, while the effect of thermal metamorphism was found negligible.

(D. Ray and A. D. Shukla)

Formation of high pressure polymorphs in the shocked ordinary chondrite, Katol L6-7

High Pressure polymorphs are expected to form in the deep of the Earth or any planetary interior. With increasing temperature and pressures, common rock forming minerals (olivine, pyroxene, feldspar) generally dissociates under solid-state condition and therefore provides the specific clues for a shock excursion. The natural dissociation process of minerals is still least understood. As the samples from planetary interior remains elusive, the shock-induced planetary materials are, therefore, important and rich inventories to study the natural dissociation processes under higher P-T regime. Planetesimal collisions are common event and produced multifaceted shock-melt veins and melt pockets within the chondritic, lunar and Martian meteorite samples. In this study, we examined the microstructures developed due to high shock pressure in one of the recent chondrite falls Katol L6-7 (2012) to constrain precise shock gauge. The unique chondrite hosts an unusual piece of troilite-metal nodule (TMN). The abundant shock melt veins and quenched sulphide melt vein textures suggestive of high shock metamorphism and likely the preservation of multitude of high pressure polymorphs and glasses within a single meteorite.

The presence of thin ringwoodite lamellae within olivine suggests a shock pressure 45 GPa or higher (further confirmed by Raman peaks 798 cm^{-1} and 844 cm^{-1} respectively). Newly identified high pressure polymorphs include majorite (928 cm^{-1}), akimotoite (796 cm^{-1}) and lingunite (768 cm^{-1}). Other high pressure microstructures include pyroxene glass. Identification of new high pressure phases using FE-SEM and laser micro Raman is further in progress. The dissociation mechanism producing high pressure polymorph minerals is not only important for Planetary science but also can be used to constrain corresponding the deep Earth science models. *This work is done in collaboration with Dr. Sujoy K Ghosh, IIT Kharagpur.*

(D. Ray)

Mineralogy and Spectroscopic study of spinel group of minerals: implications for future planetary exploration

The mineralogy and spectroscopy (Visible-Near Infrared and micro Raman) of chromite (and or chrome-spinel) from Nidar ophiolite complex, Leh-Ladakh, J&K, India was studied. Ladakh is benefitted

by cold, arid climate with minimum annual rainfall, therefore expected to manifest the least weathering effect of the rock exposures. Chromite, a common rock forming mineral, is found to occur as bands (up to several feet wide) or disseminated grains within the dunite and peridotite of the ophiolite suite. The Cr_2O_3 content is generally high (>60 wt%) and chemically homogeneous across the grains. The X-ray Diffraction (XRD) analyses show highest peak intensity at $\sim 36^{\circ}$ 2θ, followed by other diagnostic peaks for chromite. Micro-Raman yields very strong diagnostic peak band for chromite at 685 cm^{-1}(A_{1g}), followed by 520 cm^{-1} ($F_{2g(2)}$). The other peaks, viz. 446 cm^{-1} and 610 cm^{-1} are rather weak and correspond to E_g and F_{2g}, respectively. VNIR (0.4μm to 2.4μm) reflectance spectroscopy of chromite suggested strong absorption feature near 2 μm and could be useful to quantify the chemical composition (especially Cr_2O_3, $Al_2O_3$and Cr#). Our study reveals a very good match between raman band, VNIR absorption and chemical composition of chromite. This study, therefore, implies a significant understanding in characterisation of minerals (especially chromites) and could be a useful tool for the future planetary exploration. *This work was done in collaboration with SAC team*

(Naveen, T. N. Kumar, D. Ray and A. D. Shukla)

Noble gas and mineralogy of Beni M'hira chondrite

Beni M'hira, fell on Jan. 8, 2001 in Tunisia is classified as L6 chondrite. Noble gases and nitrogen were studied in this meteorite with the objective of finding cosmic ray exposure age, as well as to look for pre-atmospheric size.

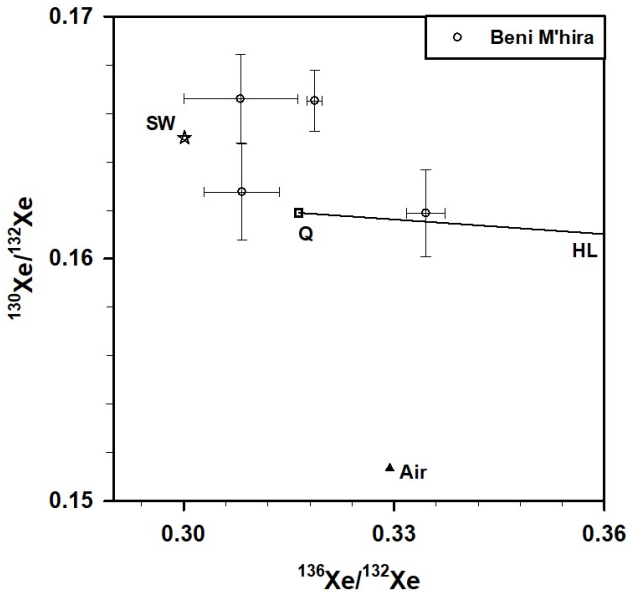

Figure 16: Xenon three-isotope plot for Beni M'hira chondrite.

The sample was analysed by stepwise pyrolysis in order to better recognise and decouple trapped and in situ produced components. Isotopic measurements were done in 'Noblesse' multi-collector noble gas mass spectrometer facility at Thaltej campus. The trapped ratios $(^{36}Ar/^{132}Xe)_t$ and $(^{84}Kr/^{132}Xe)_t$ are 382 and 1.19 respectively, falls between the primordial component Q and solar, therefore suggest that the gas is mixture of Q and solar gas. The presence of solar gas is indicated from xenon three isotope diagram (Fig. 16) of $^{130}Xe/^{132}Xe$ versus $^{136}Xe/^{132}Xe$. Therefore Beni M'hira has trapped gases of type primordial and solar. The solar type gas could be implanted either in at the time of formation in early solar system duration or during exposure at regolith. The trapped $^{14}N/^{36}Ar$ in this meteorite is 1.01×10^5 and clearly distinct from other solar system reservoirs. Trapped nitrogen from another reservoir could be present in this meteorite. Helium and neon components are mainly of cosmogenic origin. The radiogenic age 485 $\pm$ 64 Ma from ^4He implies that this meteorite is part of Ordovician impact event. The cosmic ray exposure age of this meteorite is 15.6 Ma, and falls at the peak in ordinary chondrite histogram. Therefore this meteorite belongs to the group of meteorites ejected at this time. Chondrules with disticnct outlines are typically absent due to extensive re-crystallization resulting chondrule-matrix textural integration. Olivine is the most dominant mineral irrespective of chondrule and matrix. Mineral composition of olivine suggests that Beni M'hira chondrite is highly equilibrated. Feldspar appeared to be transformed into either maskelynite or shocked glass. Presence of opaque melt veins, polycrystalline troilite and immiscible droplets fonfirms a shock stage up to S5 for Beni M'hira.

This work was carried out in international collaboration with Dr. L. O. Nejia of University of El Manar, Tunisia.

(R. R. Mahajan, S. Naik and D. Ray)

Paleoclimatic history of Red (Teri) sediments along Vagai region of Southern Tamil Nadu

Studies of coastal processes and evolution have frequently encountered problems in obtaining reliable chnologies for depositional events. The Vagai River is one of the major rivers in the southernmost part of the Peninsular India originating from the Western Ghats, flowing in a south-easterly direction, and confluencing into the Bay of Bengal in the east. Based on this condition the Vaigai river deposited their sediments and developed the delta delta with six series of beach ridges in south and three series of beach ridges in the north, parallel to the present day coast from land towards sea. Our work aims at post-infrared infrared stimulated luminescence dating to reconstruct the Palaeo-sea level changes and past depositional environments for quaternary sediments in Vaigai during Quaternary periods. We have tested the applicability of the post-infrared infrared stimulated luminescence dating of 90-150 m feldspar-rich grains in 5 sediment samples collected from upto $\sim$3.5 m depths near Ramanathapuram. The single aliquot regenerative dose procedure was used in the determination of equivalent doses. The natural, regenerative dose and test-dose OSL signals were measured after a 60 s, 320°C preheat procedure. The equivalent dose measurements were determined using both 60°C and 200°C IR stimulation temperatures. The second IR stimulation temperature was chosen to be 290°C. U, Th and K measurements were performed using high resolution (Ge) gamma spectrometry. The post-IR IR_{290} age from depths 0.45 and 1.0 m were estimated to be $\sim$3.3 ka and $\sim$6.5 ka respectively. The post-IR IR_{290} ages from the lower horizons (depth = 1.5 m, 2.3 m and 3.3 m) in the core were estimated to be $\sim$12 ka, 27 ka and 57 ka respectively. These ages are stratigraphically consistent and

suggest deposition of sands during high sea levels in south-eastern Indian coastal areas at ∼6 ka and at ∼60 ka. Future work will address the question whether breaks in deposition occurred or not as additional luminescence ages are required at closer depth intervals. *This work is done in collaboration with D. Ramesh and S.Sathiyaseelan of Bharathidasan University.*

(D. K. Panda, D. Banerjee and A.D.Shukla)

Development of Payloads for Planetary Mission
Development of a Cerium bromide gamma ray spectrometer for space applications

Elemental composition of a planetary surface can be deduced from in-situ measurements, remote sensing techniques, and by laboratory analysis of returned samples. Gamma ray and neutron spectroscopy comprise some of the basic tools for mapping of planetary surfaces. We are developing a gamma ray spectrometer (GRS) for future planetary orbiter missions for global mapping of U, Th, K, Fe and other major elements on moon and Mars, and the feasibility of using a CeBr3 detector for measuring individual concentrations of ^{40}K, ^{238}Uand ^{232}Th in laboratory samples using gamma ray spectra. Since $LaBr_3$:Ce crystal has a large intrinsic activity which inhibits estimation of the concentrations of Th and K, we next attempted the development of a $CeBr_3$ gamma ray spectrometer.

Linearity and Source-to-Detector distance dependence Measurement of the channel to energy conversion requires analysis of gamma ray spectra collected and fitting with Gaussian distribution functions for estimation of peak centroid and FWHM. The calibration and photo-peak identification has been done using several radioactive sources. The radioactive sources were kept in front of the detector at a distance of ∼55 mm. Figure 3 shows the response of the $CeBr_3$ detector using various radioactive sources. The linearity curve for the $CeBr_3$gamma ray spectrometer is shown in Figure 4. In this figure, the ADC channel vs energy data has been fitted with a straight line having a slope (gain) of ∼0.36 and an intercept (offset) of ∼4.8. We have also evaluated the FWHM energy resolution at various energies for the $CeBr_3$ gamma ray spectrometer. The energy resolution at 662 and 1274 keV, measured using ^{137}Cs and ^{22}Na radioactive source, are ∼4.0% and 2.8% respectively. (Quarati et al., 2013) measured the energy resolution of ∼4% at 662 keV for a 2 2 $CeBr_3$ gamma ray spectrometer. The energy resolution obtained from $CeBr_3$ were compared with that obtained from a $2'' \times 2''$ NaI(Tl) detector from Saint Gobain. Using NaI(Tl), the energy resolution obtained at 662 and 1274 keV are determined to be 6.8% and 5.2% respectively.

The next set of experiments involved testing the performance of $CeBr_3$ detector for various source to detector distances. The source to detector has been varied from 1 to 30 cm within the lead shield while it has been varied from 1 to 100 cm when kept outside the lead shield chamber. The photo-peak counts of the 511 keV peak at different source heights has been plotted as a function of the source to detector distance in Figure 6. It has been observed that with increase in source to detector distance, the variation in the energy resolution estimate is 10%. As expected, the photo-peak count rate decreases as distance of the source is increased.

Estimation of U and K concentrations from samples The minimum detection limit (LD) for the K and U windows have been estimated using an equation provided in Gilmore et al., 1995). For the K window, the minimum detection limit is estimated to be ∼0.0049 counts per second, whereas for the U window the value is ∼0.0048 counts per second. Furthermore, we attempted to investigate the feasibility of using CeBr3 for determining the elemental concentrations of K, U and Th in a granite from Godhra (3A), Gujarat, India. For this purpose, we have used GHRF#2, a soil samples from Uttarkhand, India, as a standard. The K, U, Th for GHRF#2 were earlier estimated using HPGe gamma ray spectrometer using a standard (STD #107) with the concentrations of U, Th and K being 5.7 ppm, 14.5 ppm and 2.6% respectively. Using unprocessed (raw) data from the CeBr3 gamma ray spectrometer, we could estimate the K concentration of sample 3A to be 4.2%; this estimate is ∼13% higher than the HPGe based value of ∼3.7%. Smoothing the spectra improved the K estimation, and the K concentration of sample 3A was determined to be 3.8%. The concentration of U in our sample was estimated using the 1764 keV (^{214}Bi) gamma line. Using processed spectra, we could estimate a U concentration of 2.1 ppm for the sample (3A), which agrees very well with a HPGe based U concentration of 2.04 ppm. Estimation of Th using the CeBr3 could not be performed using 2615 keV line due to low efficiency of the $1'' \times 1''$ detector at this energy. Other low energy gamma lines from Th could also not be utilized due to low energy resolution, and since there are interferences due to gamma lines from other elements (e.g., U).

(D. K. Panda, D. Banerjee and A. D. Shukla)

Mars Orbit Dust Experiment (MODEX)

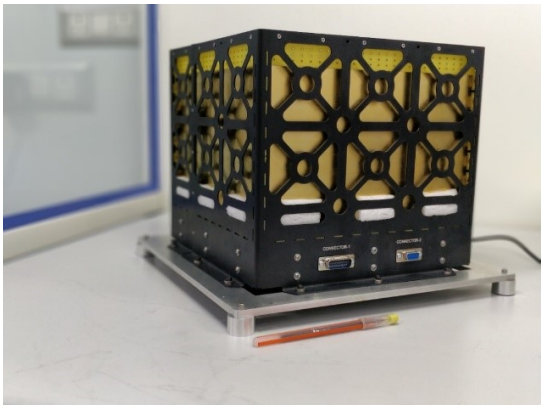

Figure 17: Snapshot of MODEX.

To study origin, abundance, flux, distribution and possible seasonal variation of high altitude dust at Mars, a Mars Orbit Dust Experiment (MODEX) is proposed for future Mars orbiter. The additional objective is to measure interplanetary dust particle (IDP) during cruise phase of orbiter for understanding the dynamical evolution. Earlier, a prototype of impact ionization dust detector and its electronics were developed and tested using a pulse laser. Further model of the dust detector with space compliance has been made from scratch, whose photograph is depicted in Figure 17. The detection scheme of the detector has been finalized using signal coincidence technique to identify the dust impact from the noise due to solar wind. A block diagram of the MODEX is shown in Figure 18 and PCB of the electronics is depicted in Figure 19. In addition, a vacuum chamber and test set up was made for

testing the dust detector as shown in Figure 20. The dust detector of cross-section 25 cm $\times$ 25 cm has been tested using a pulse laser and both channel, viz., electron channel and ion channel have been separated by electrostatic field inside the detector. The results are shown in Figure 21. Further work in this direction is underway.

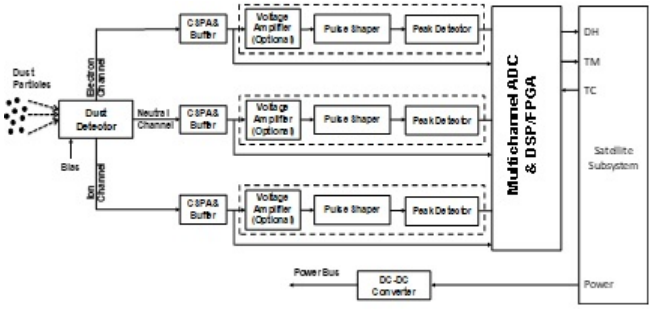

Figure 18: Block diagram of MODEX.

Figure 19: MODEX electronics PCB mounted on back side of detector.

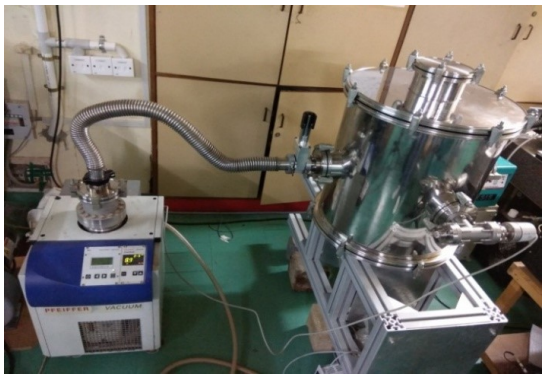

Figure 20: Photograph of vacuum chamber and MODEX testing set up.

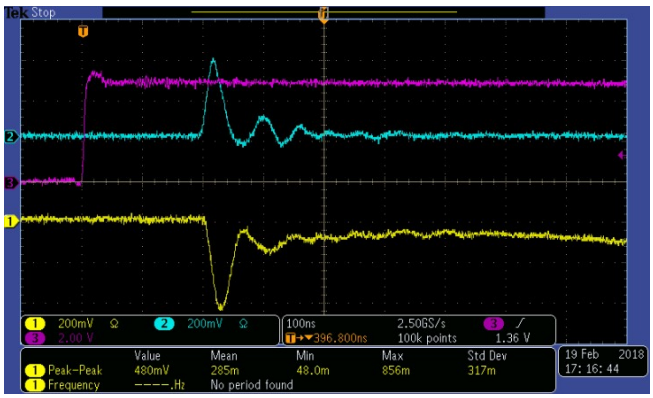

Figure 21: MODEX testing results, showing simultaneous extraction of electron channel (negative pulse, yellow) and ion channel (positive pulse, cyan) signals.

(J. P. Pabari, D. Patel, S. Nambiar, S. Jitarwal, K. Acharyya, S. A. Haider, A. Bhardwaj, V. Sheel, B. M. Pandya, R. Mahajan, A. Kumar, R. Singh and Team)

Lightning Instrument for VEnus (LIVE)

Lightning is a large electrical discharge of short duration that occurs in planetary atmosphere. It generates optical signal, electromagnetic waves in ELF and VLF range as well as acoustic waves. In Earth's atmosphere, the lightning is an outcome of convective motion of atmospheric ions and the electrification of colliding precipitation. In addition, the lightning can also be produced in volcanic clouds, dust storms and snow storms. On Venus, the clouds occur from about 47 to 65 km.

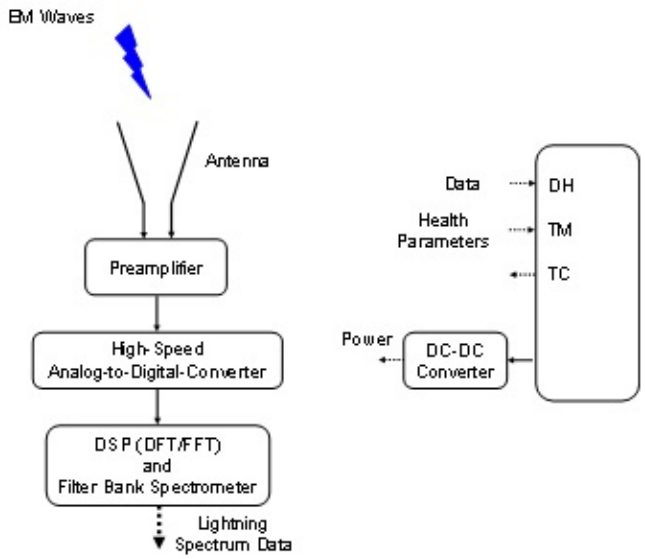

Figure 22: Block diagram of LIVE.

The sulfuric acid, the major constituent of Venus cloud, has a dielectric constant of 110 (higher than that of the water, 80) at

room temperature, which can change with the temperature. It also freezes at similar temperature (melting point 10 $^{\circ}$C) as water. Thus, sulphuric acid could be reasonably good candidate in the context of lightning. Few spacecraft experiments have provided evidence, suggesting the occurrence of lightning activity on night side hemisphere of the Venusian atmosphere. However, the lightning on Venus has been in discussion and its rate, strength, cloud model etc are not known. To understand the lightning on Venus in detail, we have proposed a Lightning Instrument for Venus (LIVE) for future orbiter, with the objective to detect the lightning in low frequency to radio frequency range, to determine its frequency of occurrence and to obtain its variability over a time period. The block diagram of LIVE is shown in Figure 22. A LIVE model is under development at PRL and its testing set up is depicted in Figure 23.

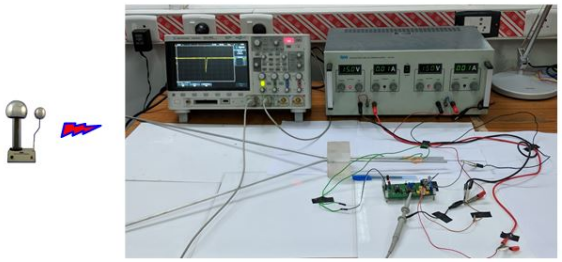

Figure 23: LIVE testing in laboratory.

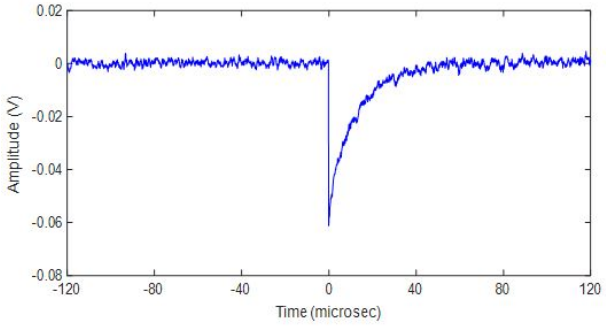

Figure 24: Electrostatic discharge pulse captured by LIVE model.

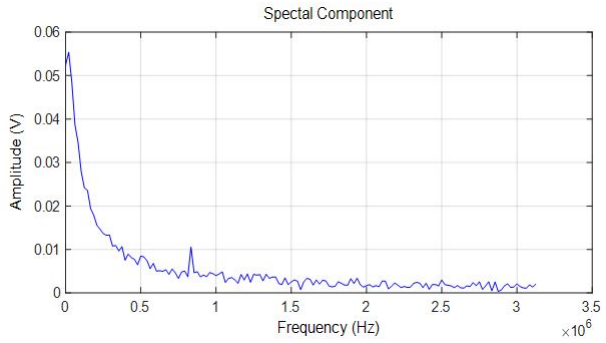

Figure 25: Frequency spectrum of discharge pulse using Fourier analysis.

It was tested using an electrostatic discharge pulse from a Van-de-graaff generator and result is shown in Figure 24. Further, Fourier analysis of the discharge pulse was carried out as depicted in Figure 25. The frequency spectrum shows the lightning signal strength at a given frequency and help deciding the filter for component separation. It has been observed that the peak occurs in kHz range where maximum lightning energy is concentrated. Further work is underway.

(J. P. Pabari, D. Patel, S. Nambiar, S. Jitarwal, K. Acharyya, S. A. Haider, A. Bhardwaj, V. Sheel, B. M. Pandya and Team)

Venus Orbit Dust Experiment (VODEX)

The Interplanetary Dust Particles (IDPs) are expected to be coming from asteroid belt and bigger ($>$ 0.5 μm) particles travel inward, toward the Sun. The flux of IDP is known at Earth, however, it has not been measured from 0.7 AU to 1 AU, i.e., between Earth and Venus. Also, there are no IDP measurements at Venus, expect a few spot measurements at larger distances from Venus. The study of IDP enables to understand dynamical evolution of the particle in inner solar system and further, how they react in the vicinity of a planet due to gravitational resonance. Moreover, such particles when encounter the atmosphere of a planet, they are ablated and leave metallic ion layer behind. This contributes the atmospheric species and can further explain nature of the atmosphere. To study flux and distribution of high altitude dust at Venus, a Venus Orbit Dust Experiment (VODEX) is proposed for future Venus orbiter. The additional objective is to measure interplanetary dust particle (IDP) during cruise phase of orbiter for understanding the dynamical evolution. Earlier, a prototype of impact ionization dust detector and its electronics were developed and tested using a pulse laser. The VODEX detector is an impact ionization dust detector which has been made and tested in a similar way as that of MODEX.

(J. P. Pabari, D. Patel, S. Nambiar, S. Jitarwal, K. Acharyya, S. A. Haider, A. Bhardwaj, V. Sheel, B. M. Pandya, R. Mahajan, A. Kumar, R. Singh and Team)

LUnar Micrometeorite EXperiment (LUMEX)

The Moon receives micrometeorites on its surface due to continuous bombardment of dust particles from interplanetary space. Since, Moon does not have atmosphere, all particles reach the surface without ablation in the atmosphere. This causes ejecta dust to come out from the lunar surface and creates dusty environment near the surface. It is expected that water ice (volatile) is preserved in Permanently Shadowed Region (PSR) near the poles. When incoming dust particles come to the PSR, they remove ejecta having regolith and also some portion of volatile (water ice). From the information of incoming dust particles and also the impact model, the mass, velocity and flux of ejecta can be obtained. This enables to study the volatile escape from Moon over a period of time. To study the volatile escape from the lunar surface and also to understand the lunar dust environment, we have proposed a LUnar Micrometeorite EXperiment (LUMEX) for future mission. The objectives of LUMEX are to measure the mass, velocity and flux of incoming dust particles to derive the

volatile escape from the lunar surface. The LUMEX detector is an impact ionization dust detector which has been made and tested in a similar way as that of MODEX. In addition, we have also initiated the modelling work for understanding the ejecta parameters. Further work in this direction is underway.

(J. P. Pabari, V. Shah, D. Patel, S. Nambiar, S. Jitarwal, K. Acharyya, S. A. Haider, A. Bhardwaj, V. Sheel, B. M. Pandya, R. Mahajan, A. Kumar, R. Singh and Team)

Langmuir Probe and Electric Field Experiment (LPEX) for MOM-2

Due to the lack of intrinsic magnetic field, solar wind interacts directly with the upper atmosphere of Mars resulting in a complex plasma environment. The distribution, dynamics and behaviour of this plasma environment is not fully understood. The upper atmosphere of Mars is characterised by different regimes such as bow shock, ion tail, magnetosheath, magnetic pileup boundary, ionopause boundary etc. The boundaries and physical mechanisms for the formation of these regions is not well understood. Plasma dynamics and variability at Mars is expected to be manifested as a variability in plasma densities and electric field in various regimes of the upper atmosphere of Mars and needs to be studied. Knowledge of electron number density (N_e), electron temperature (T_e), electric field waves and their variation will not only help us to understand the plasma environment but also help us constrain ionospheric, photochemical, and solar-wind-related processes. Electric field detection of plasma waves serves as an indicator for understanding the bow shock processes, magnetosheath and meagnetotail boundaries. For this purpose, a Langmuir Probe and Electric Field Experiment (LPEX) as a part of MAPS payload for mars Orbiter Mission-2 (MOM-2) mission was proposed from PRL. The proposal was reviewed by a shortlisting committee and later by ADCOS and the experiment is now selected to be flown on MOM-2 mission. This experiment aims at in situ investigation of electron density, electron temperature and electric field in the vicinity along the spacecraft path at different layers of upper atmosphere of Mars. LPEX consists of two independent instruments, a Langmuir probe (LP) and Electric field (EF) experiment. There will be one Langmuir probe and two Electric field sensors each followed by independent front-end electronics. However, both the instruments share a common processing electronics, power etc. The Langmuir probe and electric field sensors, each mounted on a $\sim$1.5m boom at appropriate locations on the orbiter, will be deployed once the spacecraft is in Mars orbit. Capabilities such as variable and programmable Gain, sweep, sampling are provided to cater the needs of measurements to be carried out during various regimes of the spacecraft path. While the Langmuir Probe front-end (FE) consists of sensor, a low current measuring electrometer and other electronics, the Electric field consists of dual probe setup, sensitive potential difference measurement front-end and filter circuits. Prototype sensors and design verification model of LP and EF electronics have been developed and currently under testing. Figure 26 shows the prototype LP and EF sensors along with their DVM electronics and their evaluation.

Figure 26: Prototype designs of (a) Langmuir Probe and (b) Electric field sensors (c) Electric Field FE characterisation (d) Langmuir Probe Electrometer Characterisation

(K. Durga Prasad, C. Kumar, S. Mishra, P. K. S. Reddy, J. Kumar, V. Sheel, S. A. Haider and A. Bhardwaj)

Retarding Potential Analyser (RPA) experiment for MOM-2 and Venus missions

The understanding of Martian ionosphere is critical for evaluating the importance of atmospheric escape for the evolution of the planet's climate. The wide spread variations in upper atmosphere and its solar interactions along with magnetic field results in different chemistry, dynamics and energetics at different positions and times in Martian ionosphere. Many atmospheric loss processes, including sputtering by pickup ions, photochemical escape, and ion outflow, involve the ionosphere. The major data for the densities of ions in ionosphere is available through either remote sensing data or through the Viking 1 and Viking 2 lander experiment data during its one time pass. The ionosphere structure during the night-time is still unknown. On the other hand, the ionosphere of Venus exhibits a complex dynamics due to its structure, variation and its interaction with solar wind. The dayside ionosphere is primarily produced by photoionisation of thermospheric neutrals by solar EUV radiation. The major source of ionisation in Venus is Solar EUV. The ionospheric electrons are heated from within by photoelectrons and from above by solar wind interactions at the ionopause, with the latter apparently becoming more important. Therefore, there is a need for in-situ ionospheric investigations for a proper understanding of the ion densities and the plasma temperature of the upper atmospheres of Mars and Venus. A Retarding potential Analyser (RPA) is one of the most conventional and powerful techniques to make in-situ measurements of these ionosphere parameters. Therefore, an RPA experiment has been proposed for MOM-2 and Venus missions which has now been selected as a joint payload of PRL, Ahmedabad and IIST, Trivandrum. PRL is a lead team in Science while IIST will develop the instrument. In parallel, we are also developing an RPA as a backup which can also be flown on any future mission. The RPA instrument being developed uses multi-layer grids which are biased at different Potentials. The outermost grid is either biased at negative potential for acquiring ions or positive for acquiring electrons. The plasma particles pass through

the different grids based on their charge and fall on a collector plate. The particles hitting the collector results in generation of current. This current with respect to the applied bias results in a characteristic curve. CAD design of RPA sensor has been developed and the sensor is currently under fabrication. Prototype electronics for RPA front-end is under test and evaluation.

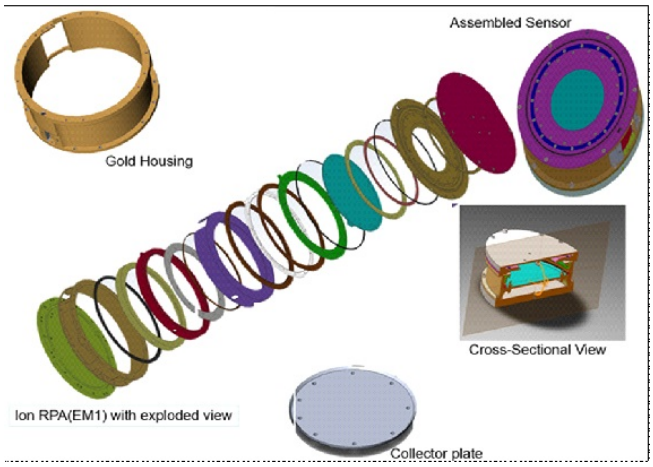

Figure 27: CAD design of RPA sensor currently under fabrication

(C. Kumar, K. Durga Prasad, S. Mishra, P. K. S. Reddy, J. Kumar, V. Sheel, S.A. Haider and A. Bhardwaj)

Realisation and delivery of ChaSTE Front-end Flight (FM) Package

A payload called “Chandra’s Surface Thermophysical Experiment (ChaSTE)” for Chandrayaan-2 Lander is being developed jointly by PRL, Ahmedabad and SPL/VSSC, Trivandrum. In addition to the other responsibilities, the front-end electronics card of the payload is designed, developed and the flight model of the same has been realised at PRL. The Engineering model of ChaSTE front-end electronics developed and tested was further modified according to the mission requirements and the Qualification Model (QM) and Flight Model (FM) realisation was initiated. The QM activities were followed by FM activities with the help of SAC QA/QC and other facilities. A series of of activities were carried out for realisation QM and FM cards. Some of those activities include - final schematic design as per QA/QC guidelines, schematic design verification by SAC Electronic QA/QC and generation of Gerber, fabrication of Flight grade PCB, preparation and approval of fabrication flowchart, wiring of cards etc. Since it was an inter-centre effort, all these activities were closely monitored and coordinated with scientists/engineers of different entities at PRL, SAC and SPL/VSSC for smooth functioning. Functional tests were carried out on the QM and FM cards at different stages as per the fabrication sequence. Once the QM and FM cards of the ChaSTE FE electronics have been completely realized, QA/QC clearances were taken for further activity and the cards were finally delivered for further integration/testing at SPL/VSSC and onward transit of the payload to the mission. After QC clearance for further activity by SAC, the flight package of ChaSTE Front-End (FE) Electronics was flushed with Nitrogen, sealed in an ESD safe cover & container and packed for transportation. After a formal flag-off, the sealed package to SPL/VSSC, Trivandrum where it was opened in the presence of QA of VSSC and thoroughly inspected for integrity and functionality. After successful functional verification test at SPL/VSSC and their acceptance, the flight package was handed-over to SPL/VSSC team. Test setup for functional testing of ChaSTE FE QM is shown in figure 28. The flight package of ChaSTE FE FM and its flag-off are shown in figure 29. Test and Evaluation activity is currently underway at VSSC faciltiy, Trivandrum.

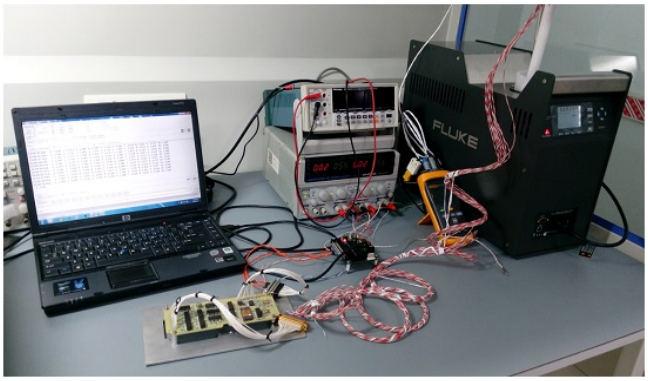

Figure 28: QM functional Test Setup at SAC

Figure 29: ChaSTE FM flight Package and Flag-off

(K. Durga Prasad, C. Kumar, S. Mishra, P. K. S. Reddy, A. Patel, T. Ladiya, M. Shanmugam, V. K. Rai, S.V.S. Murty, C. S. Raju and ChaSTE Team, SPL/VSSC)

Calibration and Characterisation facility for ChaSTE Payload

A calibration and characterization facility for ChaSTE has been setup in SIMPEX (Simulations for Planetary Exploration) Lab of Physical Research Laboratory (PRL). This activity will cater to the needs of ChaSTE calibration and characterization aspects right from sensor

level upto the overall integrated system. Since there is no provision for onboard calibration, in-depth calibration on ground is planned to be done. Calibration data will be properly analysed and documented for post-flight use. Based on the landing site constraints, the expected measurements from ChaSTE on the Moon are expected to be in the range from $\sim$ -200°C to 100°C. The temperature sensor employed in ChaSTE are Pt1000 RTD sensors. In order to calibrate and characterize the full ChaSTE system (Sensor + Probe + Front End Electronics), a dry block calibration facility with custom inserts has been setup at PRL that can facilitate calibration from -95° C to 140°C with an accuracy of better than 0.1° C both for sensor as well as the integrated system. To achieve an extreme lower temperature point, a Liquid Nitrogen (-196.7° C) bath is used. Characterisation will be done both under laboratory and simulated lunar conditions. Calibration and characterization setups and procedure detailed in the previous annual report has been now upgraded to cater the needs of the complete ChaSTE payload including post-flight data processing and interpretation. The setup for measuring thermal conductivity and thermal diffusivity is already in place. Peak Decay Method was utilized to estimate the thermal diffusivity from the temperature data of the samples. This method is preferred when the observation duration is smaller than the period of heat wave. In this technique, we measure the temperature (T) from two or more sensors that are placed in the sample and are separated by a known distance (z).

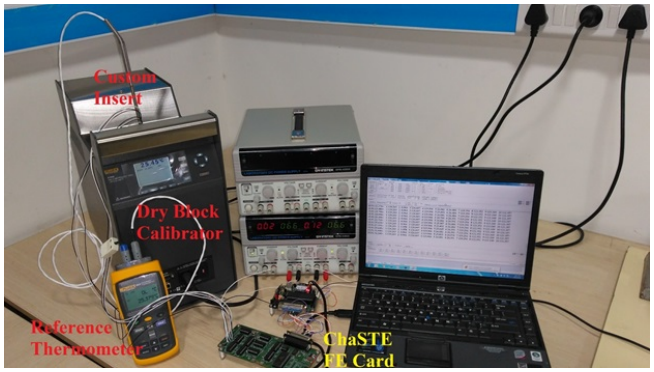

Figure 30: Typical Calibration Setup for ChaSTE under Lab environment

The samples we use are lunar Analogous samples prepared in our lab. As the operational period of ChaSTE is expected to be around 14 days, this method is most suitable. The repeatability of measurements was also ascertained. Once the repeatability is established, the measured value is verified with that of a certified dual needle probe. All the characterisation experiments are first carried out in terrestrial environment followed by experiments under simulated lunar environment. Appropriate modifications have been made in earlier designed lunar environment simulation chamber to accommodate the full ChaSTE setup. For thermal conductivity measurement, a controlled heat source gives a known amount of heat to the sample. Utmost care is taken to ensure the flow of heat radially outwards from a Linear Heat Source. The temperature variation with time is logged and the obtained data is processed to arrive upon the estimated thermal conductivity. To verify this estimation, we use a certified standard Thermal Conductivity Measurement System. The relative error for all types of measurements is documented and accepted if found within limits. Finally, a random test is carried out with different samples and the observed (ChaSTE) values are cross verified with the measured values. The calibration and charactersiation setup for ChaSTE payload is shown in figures 30 and 31 respectively.

Figure 31: Characterisation setup for ChaSTE at SIMPEX lab, PRL

(K. Durga Prasad, S. Mishra, C. Kumar and P. K. S. Reddy)

Validation of 3D lunar surface thermophysical model using Laboratory Experiment

To augment laboratory experiments and also to have a global perspective, a comprehensive three-dimensional multi-layer finite element model has been developed and implemented for the first time to understand the lunar surface and subsurface thermophysical behaviour. Details of this model have been reported in the last annual report. One of the important aspects of any numerical model is to test its output with a ground truth so that the model becomes credible.

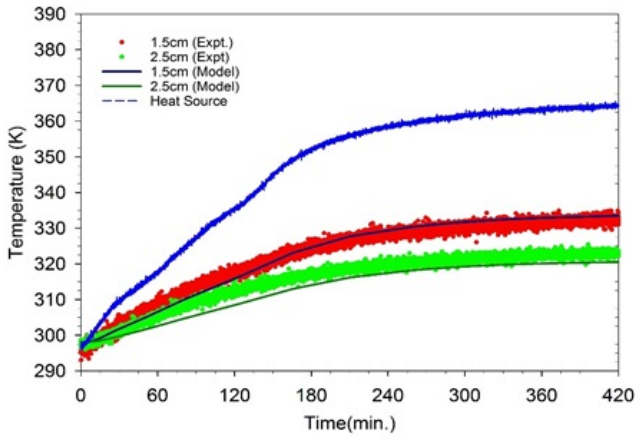

Figure 32: Comparison of model derived output with experimental result for model validation

The developed 3D model results have been verified through a laboratory experiment and results are compared to verify the credibility and performance of the model. Using our experimental setup (described in earlier annual report), we have conducted an experiment to measure thermal profile within 10 cm column of soil under simulated lunar environment is compared with the model-derived results. The model parameters and boundary conditions have been considered to match the experimental conditions and parameters. The model simulations were carried out for the same length of time (nearly 7

hours) for which the experiment was considered. Temporal evolution of temperatures during the experiment as well as calculated by the model for two depths 1.5 cm and 2.5 cm is shown in figure 32.

The source temperature profile used in both model and experiment can also be seen. A comparison of the experiment results and model-derived results are in good agreement within the experimental/model uncertainties. Therefore, this validates the credibility of the model for carrying such complex simulations.

(K. Durga Prasad and V. K. Rai)

Diurnal and Latitudinal Variability of surface and subsurface temperatures from 3D thermophysical

The diurnal variability of lunar surface and subsurface temperatures for equator were calculated from the developed 3D thermophysical model. Details of the model were reported in the last annual report.

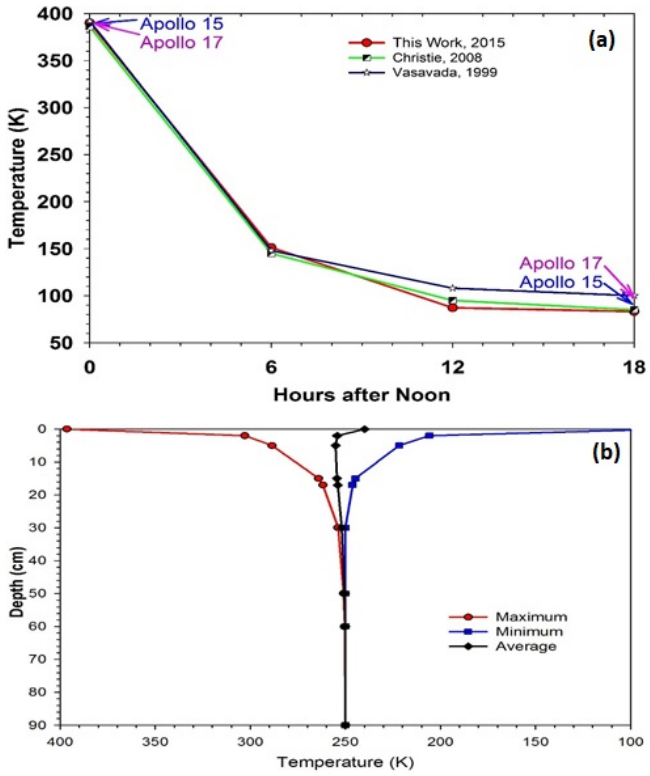

Figure 33: (a) Model derived diurnal evolution of temperature - Comparison with Apollo data and earlier Models (b) Plot showing diurnal variation of subsurface temperatures for 2-layer case

A 2-layer model has been used and the input parameters have been assumed based on the available literature and ground truth. Since, the calculations are done for equatorial latitudes, the initial value of temperature was considered to be 250K throughout based on Apollo in situ measurements.

Although, the diurnal variation of surface and subsurface temperatures were obtained from the model for all possible cases (1 and 2 layers), results for a 2-layer case is shown in figure 33(a). The surface temperatures for equatorial latitude for one diurnal cycle were derived from the model and the variation has been plotted in figure 33(b). The profile obtained was then compared with Apollo in situ data and earlier models.

(K. Durga Prasad and V. K. Rai)

Identification and Characterisation of Lunar analogous samples with India

Because of the scarcity of lunar soils and simulants, terrestrial analogue rocks within India for Lunar Basalt and Anorthosites were identified and collected from Dhinodhar and Sittampundi areas. It was identified through analysis that basalt rocks from Dhinodhar have the potential of using them as analogues of lunar basalts, particularly for the study of thermophysical properties.

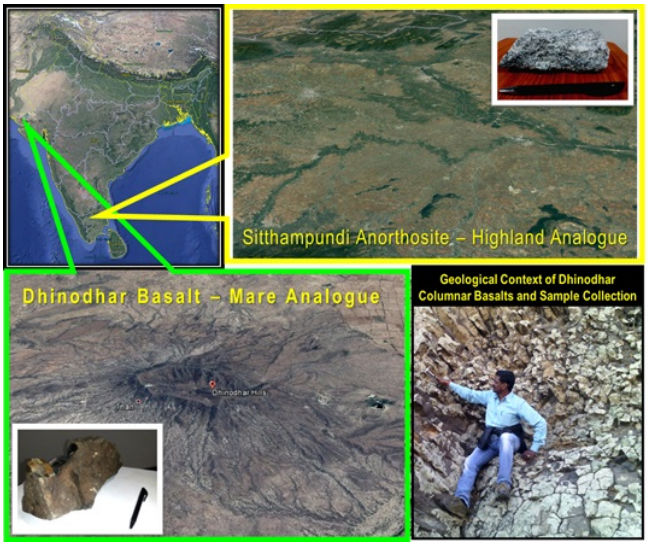

Figure 34: Geological context of sites and sample collection

Figure 34 shows the geological context of the sites and sample collection for the mentioned work. Powdered samples of different grain sizes were prepared from the rock sample by following a specific sample preparation procedure involving cleaning, cutting, grinding and powdering. A specific method has been followed to make sample sizes similar to that of the lunar soils and reported. Validation of the samples as lunar analogues for carrying out thermophysical studies has been done by measuring the compositions of the collected samples using XRF and comparing them with that of the lunar soils and other analogues.

The plots given in figures 35(a) and 35(b) respectively show the comparison of the selected analogous with respect to lunar soil samples. It can be clearly seen that the chemical composition of the selected samples are similar to that of the respective lunar soils thus making them suitable for lunar analogous studies.

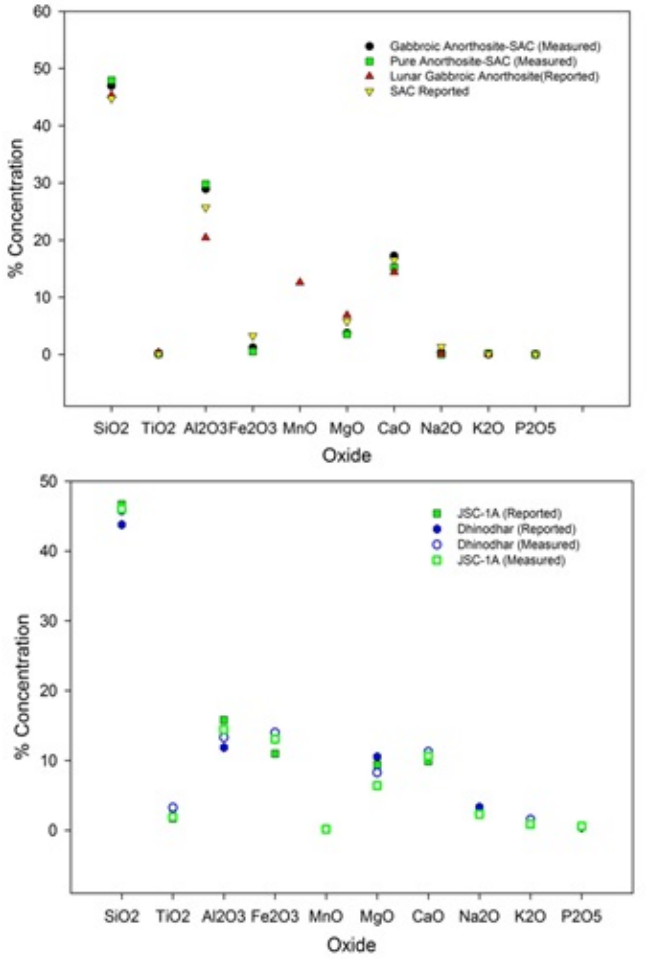

Figure 35: Comparison of (a) Anorthosite and (b) Basalt analogous soil samples with lunar soils and other terrestrial analogues

(K. Durga Prasad, D. Ray and V. K. Rai)

Supra Thermal & Energetic Particle Spectrometer (STEPS) - Subsystem of ASPEX payload

Aditya Solar wind Particle EXperiment (ASPEX) is one of the seven scientific experiments onboard the Aditya - L1 mission (the forthcoming Indian solar mission), to be placed in a halo orbit around the L1 Lagrangian point of the Sun-Earth system, at a distance of 1.5 million km from the Earth, along the Sun-Earth line. ASPEX will carry out the in-situ, multi-directional measurements of the slow and fast solar wind, supra-thermal particles and solar energetic particles in the energy range of 100 eV to 20 MeV/n with its two sub-systems namely Solar Wind Ion Spectrometer (SWIS) and Supra Thermal & Energetic Particle Spectrometer (STEPS). SWIS measures the angular and energy distribution of solar wind ions in the energy range of 100 eV to 20 keV and STEPS measures the energy spectrum of high energetic particles from six directions covering the energy range of 20 keV/n to 20 MeV/n. The scientific objective of the STEPS is to investigate the origin of the suprathermal particles and their relationship with the primary solar wind constituents.

The STEPS subsystem has been configured into two packages: STEPS-1 and STEPS-2. STEPS1 has four detector units for four different directional measurements (1) Sun Radial, (2) Intermediate to Sun radial and Parker Spiral, (3) Parker Spiral and (4) Northward direction.

STEPS2 has two detector units for two directional measurements (1) Earthward direction and (2) Southward direction.

Figure 36 shows one of the detector units consisting of single window Si-PIN detector, magnetic assembly, collimators and PCB for charge sensitive preamplifier (CSPA). Figure 37 is the stack of two PCBs (110 mm $\times$ 100 mm) for the STEPS2 package. Power card (bottom PCB) houses the circuits for biasing voltages for the two detector units, voltage regulator and high voltage monitors. FEE PCB (top PCB) houses the circuits for the analog chain of the shaping amplifiers, event triggers, DACs for the variable threshold and voltage multiplexers.

The engineering model design is under progress. Thermal & structural analysis of the STEPS packages is going on. SAC, Ahmedabad is also involved in the development of certain aspects of the payload.

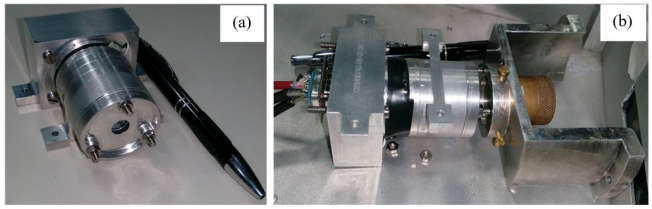

Figure 36: (a) Single window Si-PIN detector unit, (b) Testing with ^{241}Am radioactive source.

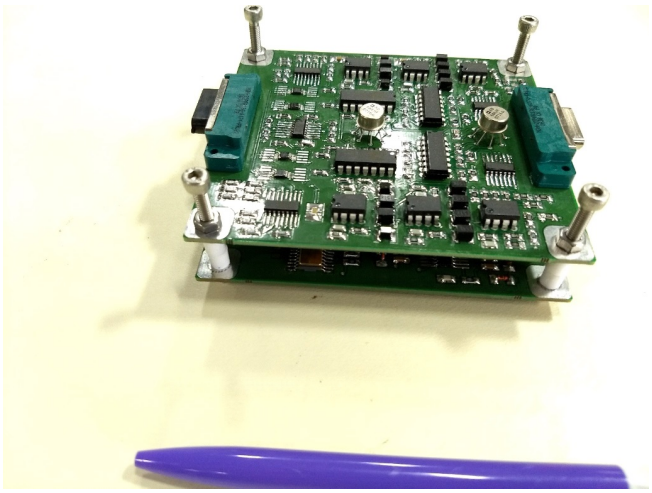

Figure 37: Stack of two PCBs for STEPS2 package.

(S. K. Goyal, M. Shanmugam, A. R. Patel, N. K. Tiwari, T. Ladiya, S. V. Vadawale, P. Janardhan, D. Chakrabarty, A. Sarkar and Team)

Design & development of position sensitive Hard X - ray detector using Scintillator and SiPM

Silicon Photomultiplier (SiPM) is a new development in the field of photon detection and can be described as 2D array of small (hundreds of μm^2) avalanche photodiodes. The gain of each APD is $\sim 10^5$ to 10^6 electrons. The current flow through the parallel combination of APDs is linearly proportional to the number of incoming photons. SiPM is a linear amplifier device, where the amount of output charge is linearly proportional to the number of incoming photons, as long as these numbers of incoming photons does not exceed the total number of APDs in detection area.

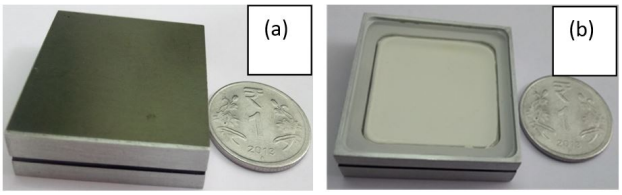

Figure 38: $CeBr_3$ crystal. (a) Top view, (b) Rear view.

In our experiment, we are carrying out the development of the position sensitive detector (2D) using new generation scintillator and SiPM. Figure 38 shows the $CeBr_3$ scintillation crystal packed in an aluminum housing. The quartz window is provided on the readout side. The total size of the hybrid packaging is 33 mm $\times$ 33 mm $\times$ 9 mm with weight of 30 gm. The surface area of the crystal is 25 mm $\times$ 25 mm with thickness of 5 mm. The $CeBr_3$ crystals have been procured from M/s Scionix, Netherlands.

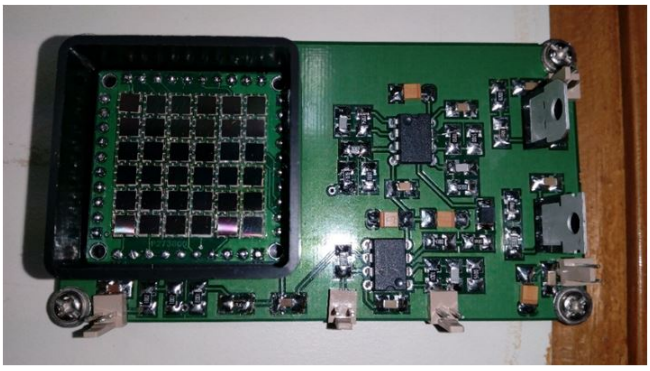

Figure 39: SiPM array (6x6) with the CSPA and shaping.

Figure 39 shows the experiment for the $CeBr_3$ scintillation crystal, readout by the 6$\times$6 SiPM array along with the FEE board consisting of CSPA, shaping amplifier and voltage regulator circuit. The experiment is carried out in a light tight black delrin box. The cathode terminals of all the SiPMs (total 36 nos.) are biased with the voltage ($>V_{br}$) using a biasing resistor. The common cathode terminal is AC coupled and connected to the CSPA.

This detector module consisting of $CeBr_3$ scintillator and SiPM array has been tested at the room temperature with different X-ray sources: ^{241}Am (13.9 keV, 17.8 keV and 59.5 keV), ^{109}Cd (22 keV and 88 keV) and ^{57}Co (122 keV). The energy spectrum shown in Figure 40 is for the biasing voltage of 26.5 V_{dc}. The pulse peaking time of the shaping amplifier is 0.3 μs. The lower energy threshold obtained is $\sim$10 keV and full width at half maximum (FWHM) for 59.5 keV is $\sim$13 keV.

The project "position sensitive hard X-ray detector using scintillator and silicon photomultiplier (SiPM)" is under development as part of Technology Development Program (TDP) of PRL.

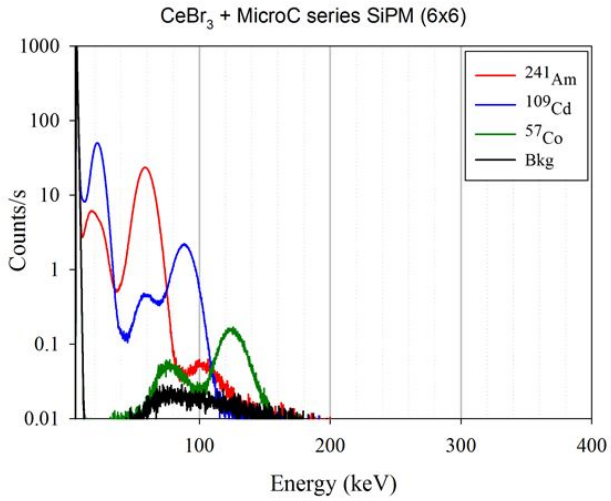

Figure 40: Energy spectrum using $CeBr_3$ scintillator and SiPM array

(S. K. Goyal, S. Vadawale, Mithun N. P. S., N. K. Tiwari, A. R. Patel and T. Ladiya)

Energetic Ion Spectrometer (EIS) for Mars Orbiter Mission (MOM-2)

Energetic particles of the solar and interplanetary origin continuously bombard the Martian ionosphere and can play an important role in the atmospheric loss processes at a shorter time scale. These particles can change the state of the Martian ionosphere significantly. In order to evaluate and quantify the changes in the Martian ionosphere due to the arrival of energetic particles generated close to the Sun during flare or due to the passage of interplanetary coronal mass ejection (ICME) and co-rotating interaction region (CIR), it is important to identify the arrival of these energetic particles at the Martian orbit relatively accurately. By measuring the alpha (H^{++}) - proton (He^{++}) ratio in the Solar Energetic Particles (SEP), the precise time of arrival of these particles at the Martian orbit will be known. Further, measurements of the proton and alpha fluxes at the Martian orbit will also help to understand the energetic particle environment around the Martian orbit.

Keeping these objectives in mind, the Energetic Ion Spectrometer (EIS) is planned for future Indian Mars Orbiter Mission. The prime objective of the EIS is to make the in-situ measurements of the high-energy charged particles (H^+ and He^{++}) in the energy range of 20 keV/n to 20 MeV/n from the Martian orbit. EIS uses customized Si-PIN detectors in the E-E configuration mode for the energy

measurement and identification of the H^+ and He^{++} particles. It uses a stack of 20μm thick and 1.5 mm thick Si-PIN detectors (Figure 41) to cover the entire energy range. Third detector is placed behind the 1.5 mm Si-PIN detector to work in the flag mode. This detector and the Anti-Coincidence Shield (ACS) are designed using plastic scintillator and Silicon Photomultiplier (SiPM) readout. Electrons measurements up to the energy of 400 keV are avoided by using the permanent magnetic assembly designed using SmCo magnets and Mu metal shielding. Figure 42 shows the CAD model design of the EIS payload. SAC, Ahmedabad is also involved in the development of certain aspects of the payload.

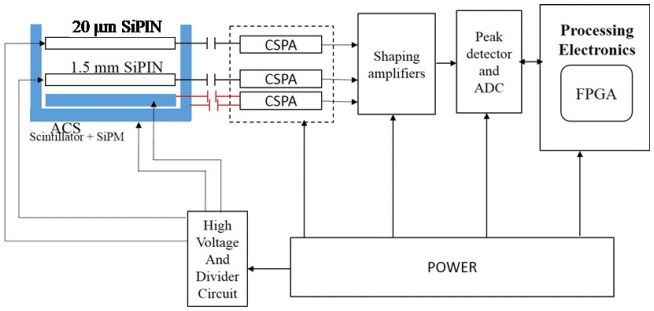

Figure 41: Block schematic of the EIS payload.

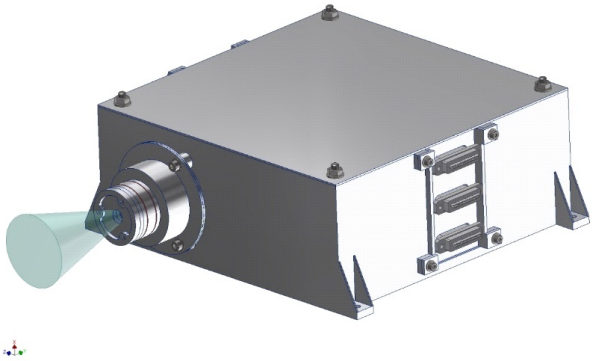

Figure 42: CAD model design of the EIS payload.

(S. K. Goyal, D. Chakrabarty, S. V. Vadawale, N. K. Tiwari, A. Sarda, A. Auknoor, Piyush Sharma, T. Ladiya and S. A. Haider)

Neutral & Ion Mass Spectrometer (NIMS)

Neutral and ion mass spectrometer is being developed as a new initiate for the in-situ measurements of neutral and ion species for future planetary missions. This has been proposed for the Venus Orbiter, the first Indian mission to Venus. The scientific objective of the instrument is to measure the composition, structure, variability and thermal state of the Venus atmosphere and its dynamics. The mass spectrometer will operate in the dual mode, separately for both neutrals and ions. The instrument will be operated from helium to mass 200 amu. Isotopic ratios will also be determined with high mass resolution. The basic instrument consists of a quadruple filter, which separates the ions as per the quadrupole filtering voltage for specific m/q ratio. Figure 43 shows the quadrupole mass analyzer and ionizer. This unit is under use for the development and testing of the electronics. An experimental setup consisting of residual gas analyzer (RGA), UHV components and dry pump is shown in Figure 44. This setup consists of several ports for mounting the mass spectrometer in multiple combination of units consists of ion source, gauges and gas inlet system for introduction of external gases.

Figure 43: Quadrupole mass filter and ionizer.

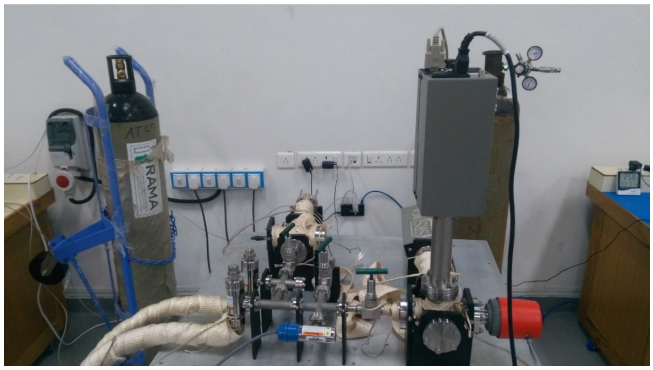

Figure 44: Test setup for the testing and calibration of the mass spectrometer.

(S. K. Goyal, R. R. Mahajan, D. K. Panda, M. S. Shah, A. Auknoor, P. Sharma, N. K. Tiwari, T. Ladiya, S. A. Haider and A. Bhardwaj)

Alpha Particle X-ray Spectrometer onboard Chandrayaan-2 rover

Alpha Particle X-ray Spectrometer (APXS) is a well proven instrument for quantitative elemental analysis of the planetary surfaces through in-situ measurements. This technique involves measurement of X-ray fluorescence by irradiating the lunar surface with Alpha particles and X-rays using radioactive alpha source. The objective of APXS instrument is to acquire the spectral response of several soil/rock samples along the rover track in the high latitude south polar region for the major elements giving fluorescent X-rays in the energy region 1 to 25 keV. APXS uses ^{244}Cm radioactive alpha source which emits both Alphas and X-rays. The energy of alpha particle is ∼5.8 MeV and the energy of X-rays are 14.3 keV and 18.4 keV. It is well known that the PIXE is dominant for low Z elements while XRF is for high Z elements, allowing the determination of elements from Na to Br, spanning the energy range of 0.9 to 25 keV, for the Kα X-rays. We use six alpha sources, each with activity of ∼5 mCi (total activity of ∼ 30 mCi).

The development of the Qualification Model (QM) and Flight Model (FM) of the APXS instrument has been completed. The photographic view of the FM version of the APXS payload is shown in figure 45. The developed instrument provides energy resolution of ∼140 eV at 5.9 keV with low energy cut-off of about 0.8 keV. The QM and FM version of the APXS has been tested for various environmental conditions and successfully passed all the tests with desired performance. The detailed scientific calibration of the these instruments were completed. The X-ray fluorescence spectrum obtained from Deccan Basalt rock sample from the APXS instrument is shown in figure 46. It can be clearly seen from the spectrum that all the elements present in the rock sample can be clearly identified. The flag-off ceremony to deliver the FM version of the APXS payload to ISRO satellite centre was held on 6th December, 2017. Subsequently, some of the interface tests of QM version of the payload with rover subsystems has been carried out and some more tests are under progress. The detailed scientific calibration to quantify the elemental abundance is being carried out on the FM Spare version of the APXS payload.

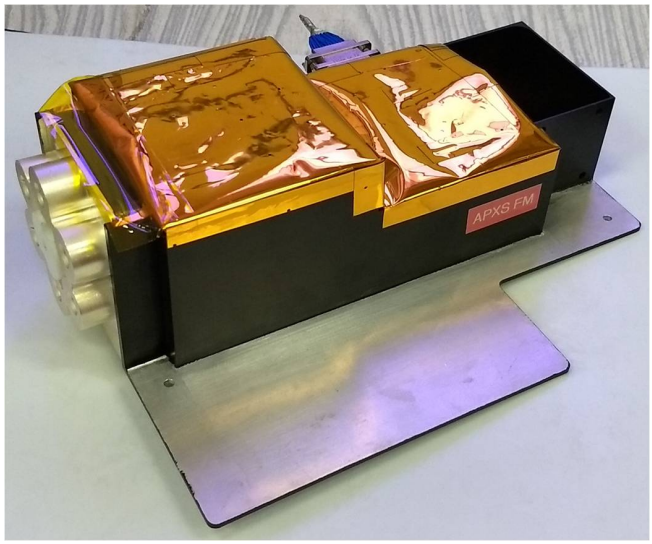

Figure 45: Photographic view of Flight Model of the APXS payload.

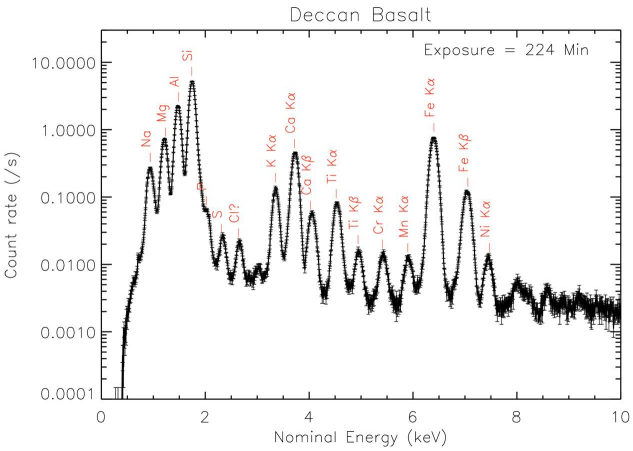

Figure 46: The X-ray fluorescence spectrum obtained from the FM version of the APXS instrument for Deccan Basalt rock sample.

(M. Shanmugam, S. V. Vadawale, A. Patel, N. P. S. Mithun, H. Kumar, S. K. Goyal, T. Ladiya, N. K. Tiwari and N. Singh)

Solar X-ray Monitor (XSM) onboard Chandrayaan-2 Orbiter

The primary scientific objective of Solar X-ray Monitor (XSM) onboard Chandrayaan-2 Orbiter is to provide the real time solar X-ray spectrum for quantitative interpretation of lunar X-ray fluorescence spectra measured by a companion instrument Chandra's Large Area Soft X-ray Spectrometer (CLASS). The simultaneous observation of X-ray fluorescence from the lunar surface and the Solar X-rays are essential for quantitative estimation of elemental composition of the Moon. The XSM instrument is being developed at Physical Research Laboratory (PRL), Ahmedabad and the CLASS instrument is being developed at ISRO Satellite Centre (ISAC), Bangalore. XSM will accurately measure the Solar X-ray spectrum in the energy range of 1-15keV with high energy resolution of ∼180eV @ 5.89keV. This is achieved by using state-of-the-art Silicon Drift Detector (SDD) with precision readout electronics and the combined system having the capability of maintaining high energy resolution at very high incident X-ray rates expected from the Sun. This instrument also provide high temporal resolution of ∼1s.

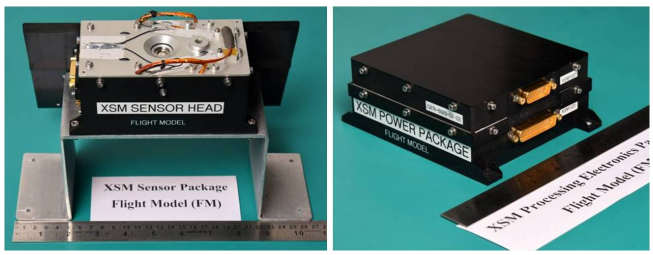

Figure 47: Photographic view of Flight Model of the XSM payload packages.

The development of the Qualification Model (QM) and Flight Model (FM) of the XSM instrument has been completed. XSM

instrument is designed with two packages namely XSM sensor package containing SDD and the front-end electronics and the XSM processing electronics package consisting of digital control & readout and the satellite interfaces. The photographic view of the FM version of the XSM payload is shown in figure 47. The developed instrument provides the energy resolution of ∼180 eV at 5.9 keV with low energy cut-off of about 0.8 keV. The QM and FM version of the XSM has been tested for various environmental conditions and successfully passed all the tests with desired performance. The performance of the XSM instrument during various phases of the environmental tests is shown in figure 48.

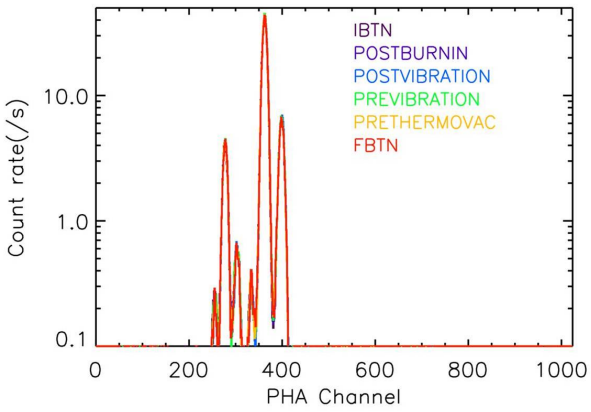

Figure 48: Performance of the XSM instrument during the environmental tests.

The detailed scientific calibration of the these instruments were completed. The high count rate performance measurement shows that XSM instrument provides the stable energy resolution and the peak energy position for count rates up to 80 kcts/s, as shown in figure 49. The XSM instrument is also calibrated for the field of view coverage (FOV) and the instrument response for various solar X-ray incident angles as shown in figure 50. This has been carried out by developing an parallel X-ray beam setup using X-ray gun. The flag-off ceremony to deliver the FM version of the XSM payload to ISRO satellite centre was held on 6^{th} December, 2017. Subsequently, the interface tests of FM version of the payload with Orbiter subsystems has been completed. The XSM payload also undergone the thermo-vacuum tests along with the Chandrayaan-2 Orbiter with the performance as expected.

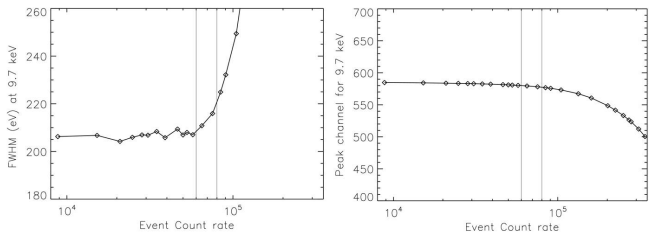

Figure 49: High count rate performance measurements of the XSM payload.

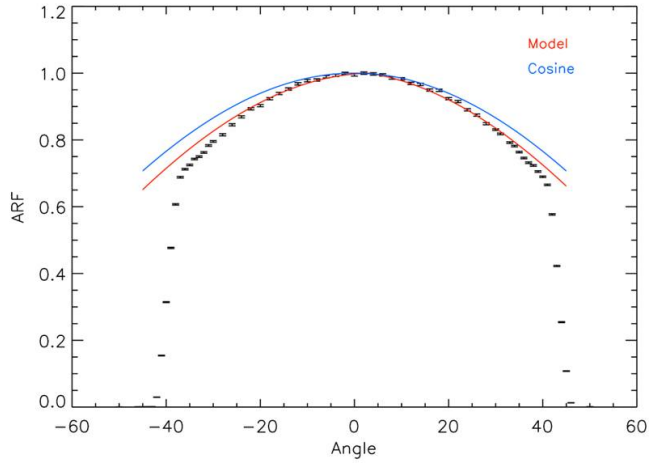

Figure 50: Field of View coverage calibration for the XSM payload.

(M. Shanmugam, S. V. Vadawale, A. Patel, N. P. S. Mithun, H. Kumar, S. K. Goyal, T. Ladiya, N. K. Tiwari and N. Singh)

Science

Space and Atmospheric Sciences

Atmospheric boundary influence on black carbon aerosols

Influence of atmospheric boundary layer (ABL) on black carbon (BC) aerosols is investigated over tropical India, for the first time, over a source (Ahmedabad, urban) and background (Gurushikhar, high-altitude) region. BC mass in Ahmedabad is significantly higher (2 to 5 times) than Gurushikhar. BC mass concentrations in Ahmedabad are in the 2-12 μg m^{-3} range (Figure 1), while in Gurushikhar BC mass concentrations are in the $<$0.5-2 μg m^{-3} range during the year. Diurnal pattern of BC mass concentration is governed by ABL evolution and anthropogenic emissions (Figure 1).

BC mass concentrations in Ahmedabad peak during morning and evening hours when ABL is shallow and anthropogenic (domestic and vehicular) emissions are high. In contrast over Gurushikhar BC emissions are higher in afternoon due to a fully evolved ABL, and upward transport of pollutants from the valley/foothills (Figure 1).

Nighttime BC contributes 60% to total over an urban region, while day-night contributions are almost equal over a background site. BC$_{max}$ over Gurushikhar is close to BC$_{min}$ in Ahmedabad, and this occurs during the afternoon hours when ABL is fully evolved and anthropogenic sources are almost nil in Ahmedabad while over Gurushikhar BC is transported from the foothills surrounding the measurement site. During monsoon peak ABL heights are relatively lower.

In addition, aerosol concentrations are less because of wet removal (Figure 1). Measurements-model comparison revealed that model significantly underestimates BC mass over an urban source region, while over a background region the agreement is good. Such quantitative evaluation of BC aerosols over a source and a background region due to the influence of ABL are hitherto unavailable, and can serve as valuable inputs in representation of aerosols in models.

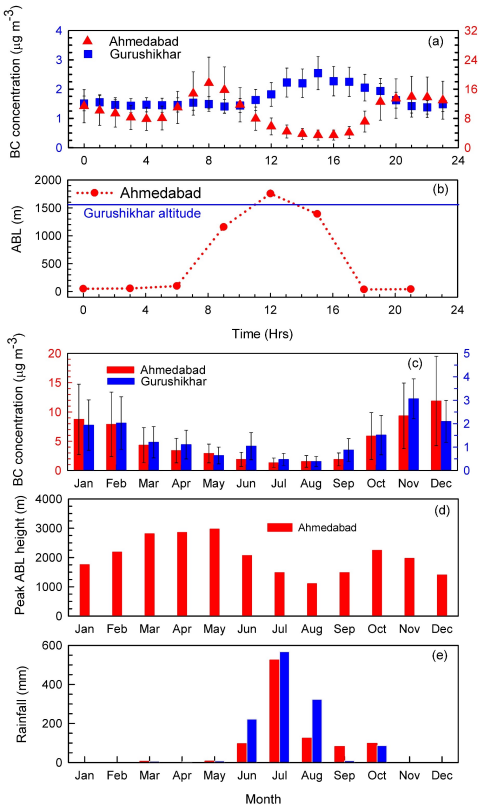

Figure no.1: (a) Diurnal variation of black carbon (BC) mass concentration over Ahmedabad and Gurushikhar during January. (b) Diurnal evolution of atmospheric boundary layer over Ahmedabad in January. The altitude of Gurushikhar is mentioned in the figure. (c) Monthly mean variation of BC mass over Ahmedabad and Gurushikhar during 2015-16. (d) Peak atmospheric boundary layer height over Ahmedabad during the year. (e) Rainfall (mm) over Ahmedabad and Gurushikhar. Vertical bars indicate $\pm 1\sigma$ variation from the mean.

(S. Ramachandran and T. A. Rajesh)

Radiative Implications of black carbon aerosols over urban and high altitude remote regions

Black carbon aerosols are the single largest absorbers of shortwave and longwave radiation. The radiative impact of BC aerosols on the Earth-atmosphere radiation budget is deduced from aerosol radiative forcing (ARF) estimated for composite and BC aerosols over Ahmedabad (urban) and Gurushikhar (high-altitude location). Maximum atmospheric forcing due to BC aerosols is observed during December ($\sim$15Wm^{-2}) and November ($\sim$8Wm^{-2}) over Ahmedabad and Gurushikhar respectively, as BC mass concentrations are highest in those months. Surface composite forcing is observed highest during postmonsoon ($\sim$-27Wm^{-2}) and premonsoon ($\sim$-16Wm^{-2}) over Ahmedabad and Gurushikhar respectively due to the maximum aerosol optical depth values (Figure 2). The top of the atmosphere (TOA) forcing changes its sign when only BC aerosols are present in the atmosphere. BC aerosol was found to contribute >60% to the shortwave atmospheric forcing over an urban as well as a remote location in the same region, which can play a significant role in modulating the tropospheric temperature, atmospheric stability and cloud formation.

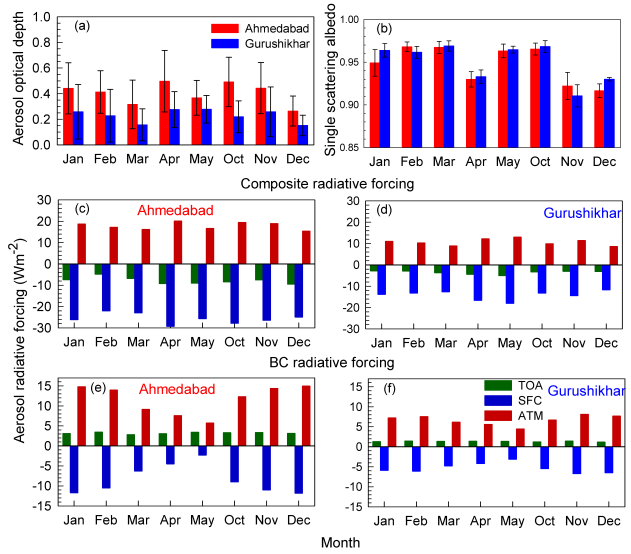

Figure no.2: Monthly mean variation of (a) aerosol optical depth (550 nm), (b) single scattering albedo (500 nm), composite aerosol radiative forcing at the top of the atmosphere (TOA), surface (SFC) and in the atmosphere (ATM) for (c) Ahmedabad and (d) Gurushikhar, and radiative forcing due to black carbon aerosols only for (e) Ahmedabad and (f) Gurushikhar during 2015-2016. Vertical bars represent $\pm 1\sigma$ variation from the mean.

(T. A. Rajesh and S. Ramachandran)

Size resolved aerosol black carbon content and its influence on the hygroscopic growth of aerosols

Atmospheric aerosols are chemically diverse which limit our understanding of the process of aerosol activation to cloud droplets. Additionally, the hygroscopicity of aerosol particles play a crucial role in determining the thermodynamic barrier between aerosol and cloud droplet, highlighting the need for reliable hygroscopicity data for aerosol components at different relative humidity (RH) conditions. Hygroscopicity of atmospheric aerosols depends on its size and chemical composition, mostly influenced by the presence of hydrophobic component known as black carbon (BC) due to its mixing state, and hence may influence the cloud condensing nuclei (CCN) formation. In this study, size selective aerosol hygroscopic growth factor (HGF) and refractory black carbon (rBC) content measured using hygroscopic tandem differential mobility analyzer (HTDMA) and single particle soot photometer (SP2) respectively in Ahmadabad during February 2018. HGF is lower (1.39$\pm$0.13) for Aitken mode ($\leq$ 100 nm) particles whereas higher (1.60$\pm$0.02) for accumulation mode ($\geq$ 100 nm) particles (Figure 3). In our observations, particles in higher size range are more externally mixed whereas particles in lower size ranges are more internally mixed and presence of rBC suppresses the HGF of the particles when RH is higher (Figure 3). The hygroscopicity parameter (κ), which represents the chemical composition of particles, is lower (0.26$\pm$0.08) for Aitken range particles and higher (0.39 $\pm$0.03) for accumulation range particles. κ value suggests that Aitken mode particles possibly may be composed of glutamic acid, glutaric acid and levoglucosan (from biomass burning), whereas accumulation range particles may be composed of ammonium sulfate, ammonium bisulfate and malonic acid (from secondary aerosol formation sources).

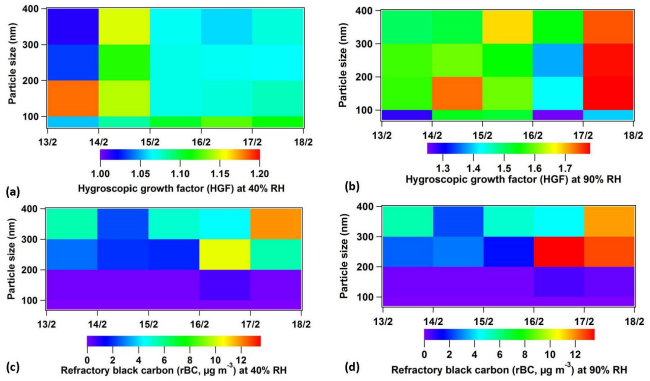

Figure no.3: Hygroscopic growth factors corresponding to (a) 40% relative humidity (RH) and (b) 90% RH as a function of particle size during February 2018 over Ahmedabad. Refractory black carbon (rBC) mass concentrations measured corresponding to (c) 40% and (d) 90% RH.

(Bighnaraj Sarangi, S. Ramachandran, T. A. Rajesh and Vishnu Kumar Dhaker)

Relative humidity effect on aerosol optical properties: Experiment vs Model

Hygroscopic aerosols can exhibit changes in their physical (size), optical (aerosol scattering (β_{sca}) and extinction coefficients) properties and chemical composition as a function of relative humidity (RH), which has significant implications to aerosol radiative properties. Understanding the effect of RH on the optical properties of aerosol is important to better estimate the aerosol radiative forcing. Generally, the optical properties of aerosols are corrected for the ambient variation in RH using model derived scaling factors. In the present

study, an aerosol sampling system (based on diffusion dryer) has been developed in house to study the real-time effect of RH on optical and radiative properties of aerosols. The study utilizes the simultaneous measurements of aerosol scattering coefficients from two nephelometers through the sampling system at ambient and dry (<40%) RH conditions during the monsoon season (July-September). The study reveals that aerosol scattering is strongly dependent on RH. The measured dry β_{sca} decreases by 40% when compared to the β_{sca} values measured at ambient RH, whereas the model corrected β_{sca} shows the decrease by only 20%, hence the model is underestimating the influence of RH on aerosol scattering (Figure 4). The estimated Ångström exponent in ambient condition shows lower values than dry by 30% confirming the particle growth due to the water uptake of aerosols (Figure 4). The hygroscopic growth factor shows a strong linear dependence on RH; it decreases from 1.9 to 1.6 when RH decreases from 82% to 66%. Single scattering albedo (SSA) for the dry condition is found to decrease by 10% than the ambient. These results will be important to reduce the uncertainty in aerosol radiative forcing as the relation between the SSA and aerosol forcing is non-linear.

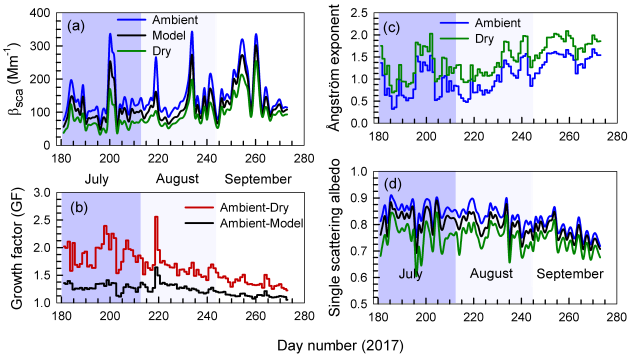

Figure no.: Daily averaged (a) aerosol scattering coefficients (b) growth factor (c) Ångström exponent (d) single scattering albedo at 550 nm for ambient and dry sampling conditions along with model estimated values in Ahmedabad during July-September 2017.

(T. A. Rajesh, S. Ramachandran and Vishnu K. Dhaker)

Spatial distribution of aerosol characteristics: Road campaign experiment

A scientific road campaign experiment has been conceived to study the spatial distribution of aerosol characteristics in the Aravalli range of mountains in western India. An instrumented vehicle fitted with aethalometer (for black carbon mass concentration and absorption coefficient measurements), nephelometer (for scattering coefficient measurement), aerosol spectrometer (for aerosol number concentration measurement) and meteorological data logging system is being used in the campaign. The scientific road campaign spans from the foothills of Mt. Abu (Abu road, 290 m above mean sea level (AMSL)) to one of the peaks of Mt. Abu (Gurushikhar, 1680 m AMSL), which provides an opportunity to investigate the vertical distribution of aerosol characteristics. The preliminary result shows the decrease in ambient temperature with altitude at an adiabatic lapse rate of 5° C/km during March (Figure 5). The pressure compensated black carbon mass concentration also reveals the decrease with altitude but with enhancements in the intermittent altitudes due to vehicular traffic and domestic emissions (Figure 5).

An year-round measurements are envisaged to understand the relative influence of manmade emissions and transport effects on a variety of aerosol characteristics, and apportion these as a function of lower troposphere and seasons.

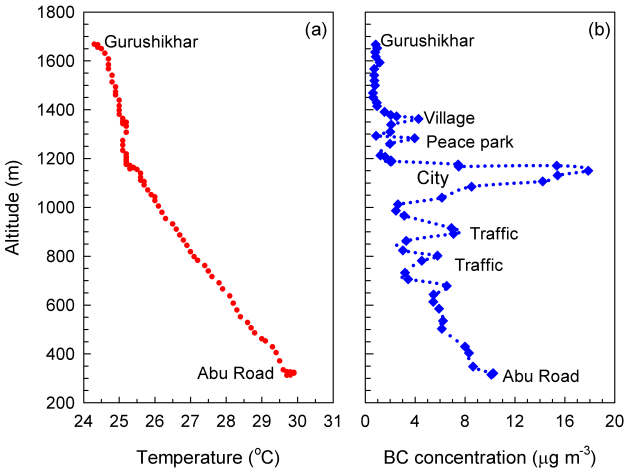

Figure no.5: Altitude profiles of (a) temperature and (b) black carbon mass concentration measured during a road campaign from Abu Road (290 m AMSL) to up to Gurushikhar (1680 m AMSL) during March 2018.

(T. A. Rajesh, Vishnu K. Dhaker, Malaidevan P., Mitesh B.Bhavasar and S. Ramachandran)

Meteorological data logging system (MetDLS)

We have designed and developed a meteorological data logging system (MetDLS) for the real time measurement of position (latitude, longitude and altitude), time, temperature, humidity, pressure and total solar radiation. MetDLS has been developed exclusively for a mobile platform. The heart of the MetDLS is an 8-bit ATmega 2560 microcontroller which is integrated with real time clock (DS1307), temperature-humidity sensor (HYT-939), and pressure sensor through I2C interface, memory SD card via serial peripheral interface, GPS - GSM module and computer through UART interface, total solar radiation via on board ADC, and display (LCD) and keypad through DIO interface. The system acquires the data and will store the data onto memory card along with time stamping at every second. A front-end graphical user interface software has been developed to acquire, visualize and log the MetDLS data. MetDLS has been successfully implemented and integrated with various ongoing scientific road campaign in western India.

(T. A. Rajesh, Vishnu K. Dhaker, Mitesh B. Bhavasar and Malaidevan P.)

Role of biomass burning in Earth's climate.

Biomass burning activity releases varieties of gaseous and particulate species in the atmosphere. Most notably the black carbon (BC) particles and organic compounds. In general BC particles cause warming of the atmosphere but their role is obscured when produced from biomass burning since the biomass burning activity releases many other compounds in the atmosphere which as bulk may or may not have warming effect and also the co-emitted organic compounds can change properties of individual black carbon particles. Hence the effect of biomass burning activity on climate is not known with high confidence. Biomass burning activity is also a component of Earth System science which has both natural and anthropogenic factors and they change with changing climate as well as change in living standard of people and economic policies of countries. We have carried out numerical simulations to estimate source-receptor relationship for black carbon particles with Ahmedabad and Gadanki as receptor site. It is used to rank individual days for level of biomass burning activity using MODIS fire hotspots. These simulations coupled with observations of black carbon concentrations and other aerosol properties will be used to delineate effect of biomass burning on these properties.

(Harish Gadhavi, S. Ramachandran, T. A. Rajesh, K. Renuka)

Light non-methane hydrocarbon at Ooty

Non-methane hydrocarbons are the precursors of ozone with a higher ozone producing potential. They all have natural as well as anthropogenic sources. They play a major role in the tropospheric chemistry. Fossil fuel burning is a major anthropogenic source of NMHCs in the urban region. Over a longer period of time, these emissions from various sources invariably alter the regional background concentrations of many of these trace gases involved in ozone chemistry. Background measurements are important to study their levels, variability and their impact on ozone chemistry. South Indian region is less affected due to the absence of regional pollutant sources and is also flushed by the monsoon winds. Realizing the absence of the regionally representative trace gases observations in Southern Indian region, an environmental laboratory was set-up at Ooty (11.4°N; 76.7°E; 2520 m amsl), a hill station in Tamil Nadu, in collaboration with Tamil Nadu Agricultural University (TNAU), Coimbatore under the Atmospheric Trace Gases and Modelling (ATCTM) project of ISRO-GBP. Air samples are being collected from this site and are analysed for light NMHCs (C2-C5) at PRL using a gas chromatograph equipped with a flame ionisation detector. Figure 6 shows variation of ethane (averaged over two/three days with measurements at the interval of every 2/3 hours) at Ooty during different months. Ethane value is highest in the winter (December) and low value is observed during summer/monsoon (August) season indicating the effect of regional emissions, transport and sink. Ethane concentration is the highest among C2-C5 hydrocarbons over this site and has the longest lifetime in NMHCs. Its major sources are fossil fuel emission especially venting and flaring, bio-mass burning and oceanic and biogenic emission constitute a minor source. As methane and ethane share the common anthropogenic sources with a longer and shorter lifetime respectively, ethane measurements can help constrain the studies of methane which is a major greenhouse gas. In addition, systematic ethane measurements will provide valuable information about its variability and its growth rate. The correlation study of ethane with other hydrocarbons, CO etc helps to study photochemical processing of the air parcel, source appropriation, transport processes etc.
This work is done in collaboration with Prof. C. Udayasooriyan of TNAU, Coimbatore.

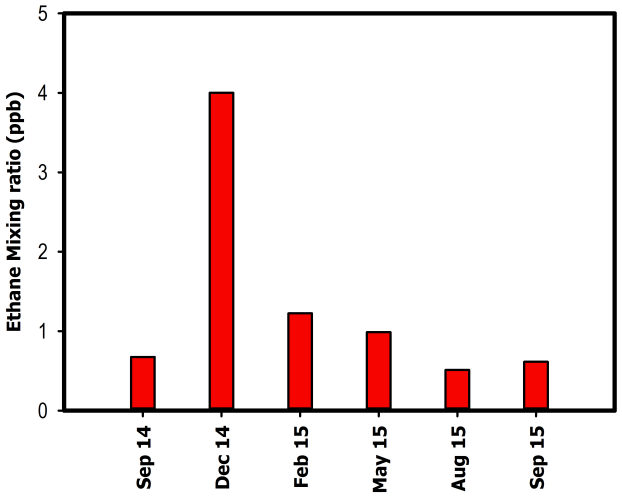

Figure no.6: Monthly average ethane concentration at Ooty, Tamil Nadu

(S. Venkataramani, S. Lal and T. K. Sunil)

Trends of biomass burning and photochemical oxidation sources during winter to summer transition at urban site of India

Biomass burning plumes are identified by using acetonitrile (CH_3CN) as a tracer. Frequency distributions of acetonitrile and toluene/benzene (T/B) ratio using 5-min interval data measured using proton transfer reaction-time of flight-mass spectrometer (PTR-TOF-MS) during February-March 2014 are presented in Figure 7. The histograms show peaks between 0.4-0.7 ppbv during both the months but the overall patterns differ significantly. In February, the percentage frequency distribution gradually declined with the increase of the acetonitrile mixing ratio. During this month, about 24-31% of data were measured with the mixing ratios of acetonitrile exceeding 1.0 ppbv level but in March the frequency declined rapidly with the increase of acetonitrile mixing ratio and only about 12-19% of the data was measured at higher values. This result clearly indicates the decreasing contribution of biomass burning sources from February to March. However, except sporadic cases, activities of biomass burning in Ahmedabad city are negligible during both the months. Therefore, the transport from biomass burning sources in upwind regions could contribute to ambient levels of VOCs. The ambient T/B ratio is related to the photochemical age of the air, assuming that the emission ratio at source is fairly constant. The histograms of T/B ratio also show distinct distribution patterns for February and March. In February, T/B ratio and declined gradually and about 50-55% of data were measured at higher ratios ($>$2.0 ppbv ppbv^{-1}). In March, the frequency declined more rapidly with the increase of

T/B ratio from and about 45% of data were measured with higher T/B ratios. This trend also implies increasing fractions of biogenic and photochemical sources to the trends of oxygenated-VOCs and BVOCs. However, the reduction of about 10% seems rather small considering higher ambient temperature and solar intensity hence faster photochemical aging compared to February. On the other hand, the higher evaporation rates of fossil-fuels under summer conditions could compensate the faster aging processes as deduced using T/B ratio. The overall analysis indicates the increasing influence of photo-chemically aged air masses from February to March. However, the quantitative estimation of biomass burning and photo-oxidation sources of ambient VOCs in urban regions is ambiguous mainly due to the coexistence of a variety of emission sources.

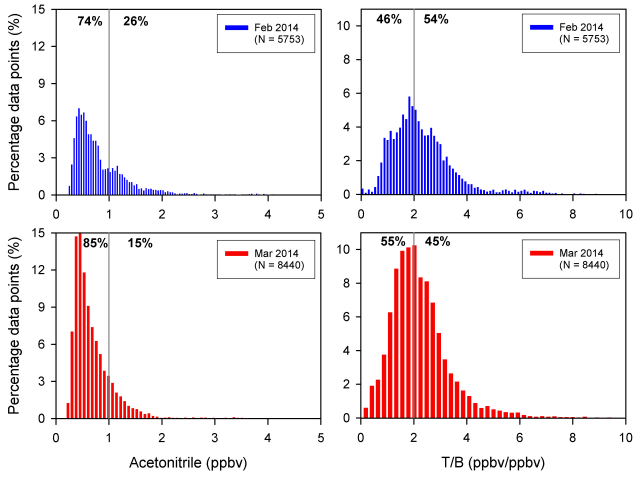

Figure no.7: Frequency distributions of acetonitrile mixing ratio and toluene/benzene (T/B) ratio using 5-min interval data measured using proton transfer reaction-time of flight-mass spectrometer (PTR-TOF-MS) at Ahmedabad during February-March 2014.

(L. K. Sahu, Nidhi Tripathi, R. Yadav)

Emission and ambient air concentrations of aromatic VOCs at a semi-urban site in western India

This is the first study to characterize emission and ambient concentrations of aromatic volatile organic compounds (VOCs) in a semi-urban site of Udaipur in western India. Air samples were collected on the rooftop of computer center building in the campus (24.58°N, 73.68°E) of Mohanlal Sukhadia University (MLSU). In this region, the major contribution to ambient air pollutants shifts from vehicular emissions in winter to biomass burning (agricultural waste burning) in the early pre-monsoon. Air samples were analyzed using a thermal desorption-gas chromatography-flame ionization detector (TD-GC-FID) instrument in which "Ozone Precursor" was used as cryotrap to pre-concentrate NMVOCs. Based on the analysis of measurements during February-December 2015 we have investigated the role of local emission, meteorology, photochemical aging and long-range transport. Both the aromatic VOCs namely benzene and toluene exhibit clear diurnal dependence with prominent features in winter but weaker in the monsoon season. Mixing ratios of aromatic VOCs exhibit elevated values from night to morning and lower values during the daytime. The seasonal trends of both benzene and toluene exhibit higher values during winter to pre-monsoon period while the lowest in the monsoon season. Monthly average mixing ratios of benzene and toluene vary in the ranges of 0.58-1.18 ppbv and 0.62-1.48 ppbv, respectively. The highest values of benzene, toluene and the toluene/benzene (T/B) ratio in winter season were due to shallow boundary layer, limited photochemical loss and transport from the polluted Indo-Gangetic Plain (IGP). While, their lowest values in monsoon season were due to transport of cleaner air from the Arabian Sea.

(L. K. Sahu, Ravi Yadav, Nidhi Tripathi)

Impact of the tropical cyclone "Nilam" on the vertical distribution of carbon monoxide over Chennai on the Indian peninsula

In this study we have investigates the impact of tropical cyclone (TC) Nilam on the vertical distribution of CO over Chennai in southern India. Measurements of OZone and water vapor by Airbus In-service airCraft (MOZAIC) profiles of CO measured during October-November 2012 were analysed. The vertical profiles of CO on October 15^{th} and November 2^{nd} were influenced by convective motions with a significant decrease in outgoing longwave radiation (OLR) compared to that on normal days of observations. The near-surface mixing ratios of CO (185$\pm$24 ppbv) in convectively influenced conditions were much lower than those measured during normal days (>210 ppbv).

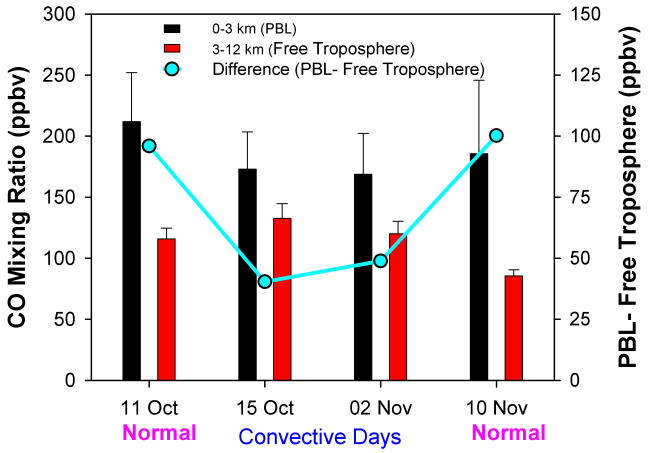

Figure no.8: Comparison of mean values of CO mixing ratio (MOZAIC Aircraft observation) in the PBL (0-3 km) and free troposphere (3-12 km) for different days of post-monsoon season 2012 over Chennai.

The occurrence of minimum CO values at altitudes of 4-6 km coincided with the lowest lapse rate (LR) value of 4-5°C km^{-1}. The uplift of surface air masses led to a large increase in the CO mixing ratio in the free troposphere. The differences in CO between the lower and free troposphere were relatively small (40-50 ppbv) and large (90-100 ppbv) during convective and normal days, respectively (Figure 8). In the lower troposphere, elevated values of CO (>250 ppbv) were measured for lighter wind speeds from the north, while lower values (<150 ppbv) were measured for

strong winds from the western sectors. The Model for OZone And Related chemical Tracers (MOZART-4) and Chemistry Climate Model 2 (CCM2) simulations did not capture the detailed features of the CO profiles. For cyclone-influenced measurements in the lower troposphere, MOZART-4 underestimated the CO values by approximately 13%, but CCM2 overestimated the CO values by 70%. In the upper troposphere, MOZART-4 and CCM2 underestimated the observations by 6-8% and 12-22%, respectively. The mixing scheme of the model and simulated concentrations seem to be the key causes of disagreements. However, the performance of both the MOZART-4 and CCM2 simulations was better for convection-free normal days.

(L. K. Sahu, Nidhi Tripathi, and Varun Sheel)

First PTR-TOF-MS based measurement of VOCs at New Delhi: Role of emissions and atmospheric processes

Atmospheric volatile organic compounds (VOCs) are short lived trace gases which play indirect but very important role in climate change as precursors of tropospheric ozone (O_3) and secondary organic aerosols (SOA). Atmospheric VOCs are oxidized by reactions with hydroxyl radical (OH) and lead to the formation of peroxy radical which play a crucial role in the tropospheric chemistry. The VOCs and peroxy radicals control the oxidizing capacity of the global atmosphere which have major impact on the concentration and life time of greenhouse gases. This study is based on the measurements of many VOCs using a Proton Transfer Reaction-Time of Flight-Mass Spectrometer (PTR-TOF-MS) at Delhi, India during January-March 2018. The main objective of this study is to estimate the contribution of different emission sources, atmospheric processes and meteorological conditions (fog, cloud, clear–sky, etc.). Delhi is one of the most polluted regions in the Indo-Gangetic Plain (IGP) where measurements of VOCs composition are rarely reported. The change in the contribution of different sources to oxygenated-VOCs (OVOCs, e.g. methanol, acetone and acetaldehyde), biogenic-VOCs (BVOCs, e.g., isoprene and monoterpenes) and aromatic-VOCs (benzene, toluene and xylene) has been estimated during the winter to summer transition period. The change in relative compositions of VOCs was analyzed in the view of the day-to-day variation in the local weather condition. To identify the major sources of VOCs we used tracers viz. isoprene, benzene and acetonitrile for the biogenic, vehicular and biomass burning emissions, respectively. As inferred from the trends of aromatic VOCs, the site is predominantly influenced by vehicular and industrial emissions throughout the study period. The slope of toluene to benzene ($\Delta T/\Delta B$) is used as an indicator to identify major anthropogenic sources in fresh plumes. The slopes estimated during the daytime provide information of the rate of photo-chemical transformation hence used as a measure of photochemical aging. A $\Delta T/\Delta B$ slope value of 2.5 ppbv/ppbv suggests the vehicular exhaust is the dominant source of aromatic VOCs. The episodic enhancements of acetonitrile were due to the transport from crop residue burning activities in the surrounding areas of Delhi. During these episodes, the concentration of methanol shows good correlation with acetonitrile (r^2 =0.84) indicating major contributions from biomass burning sources. While, a strong correlation (r^2 =0.83) between acetone and isoprene indicate major contributions from biogenic sources. But acetaldehyde does not show significant relations with any of the primary emission tracers revealing the contribution of photochemical formation. Overall, BVOCs and parts of OVOCs show significant contributions from local biogenic emissions. This result suggests the need of emission inventory of chemically speciated VOCs assess their contributions to regional ozone and SOA formation.

(Nidhi Tripathi and L. K. Sahu)

Signature of the quasi-27-day oscillation in the MLT and its relation with solar flux and convection

Intermittent occurrence of the quasi-27-day oscillation is observed in the mesosphere and lower thermosphere (MLT) zonal wind in the long term database over three southern hemispheric Brazilian locations, i.e. Sao Joao do Cariri (7.4°S, 36.5°W), Cachoeira Paulista (22.7°S, 45°W) and Santa Maria (29.7°S, 53.7°W).

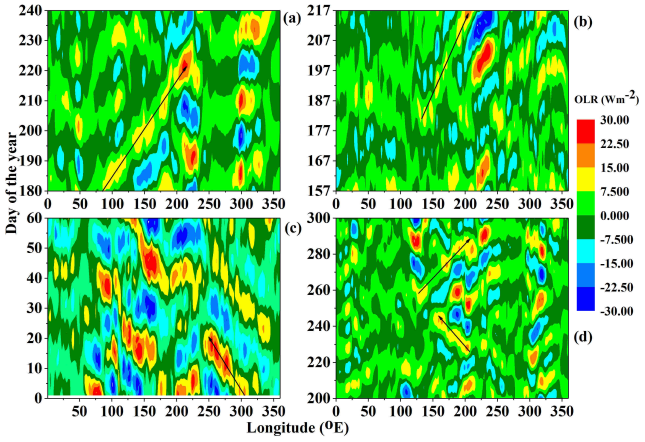

Figure no.9: Filtered (pass band $\sim$ 20-34 days) OLR profiles with respect to longitudes showing the zonal propagation behavior for (a) Cachoeira Paulista in 2000, (b) Santa Maria in 2006, (c) Sao Joao do Cariri in 2007, (d) Cachoeira Paulista in 2012. Arrows in the plots denote the zonal direction of the propagation.

The oscillation shows a peak amplitude of $\sim$15 m/s in the lower MLT. To determine the plausible sources of the quasi-27-day oscillation, the variation of the solar Ly-α flux and outgoing longwave radiation (proxy for convection) have been looked into. The oscillation shows considerable consistency with the solar UV flux implying potential solar influence on excitation. The oscillation in the MLT also exhibits good correlation with the outgoing longwave radiation (OLR-a proxy of convection) at Cachoeira Paulista indicating plausible influence of lower atmospheric convective activity. Non-concurrent occurrence of the oscillation among the observational stations indicates potential role of local geophysical conditions. The zonal background wind in the MLT might cause dissipation of the upward propagating waves (modulated by 27-day oscillation) and hence imprint the lower atmospheric 27-day signature in the MLT.

This work was done in collaboration with

1. P. P. Batista, National Institute for Space Research, São José dos Campos, São Paulo, Brazil,
2. R. A. Buriti, Federal University of Campina Grande, Campina Grande, Paraiba, Brazil and

3. N. J. Schuch, Southern Regional Space Research Center, Santa Maria, Rio Grande do Sul, Brazil.

(A. Guharay)

Zonal wave characteristics in the daytime thermosphere

In one of our earlier works it was shown that asymmetric diurnal behaviour in the low-latitude dayglow emission intensities is due to intensification of the strength of the equatorial electrodynamics. Further investigations have been carried out to understand the large scale features of the thermosphere on the days with symmetric and asymmetric diurnal behaviour in the dayglow emission intensities. Zonal scale sizes of the gravity waves (GWs) at three different altitudes (∼130, 230, and 300 km) have been obtained from the spatial variation of the dayglow emissions at 557.7, 630.0, and 777.4 nm. Diurnal distribution of the GW zonal scale sizes are obtained for two days with a common (either symmetric (30 Dec 2013) or asymmetric (6 Feb 2014)) behaviour of dayglow emission intensities at these wavelengths and are shown in the bottom, middle, and upper panel of the Fig 10 (a-c) and Fig 10 (d-f), respectively. Notable contrast exists in the values of zonal scale sizes and their diurnal behaviour between these two days at all the three dayglow emission altitudes. The contrast is not just for these two days but is true for all the other days that showed symmetric/asymmetric diurnal behaviour (Fig 10 (g-i) / Fig 10 (j-l)), respectively. It is striking that the pattern of the diurnal distribution of the zonal scale sizes is: (i) remarkably similar within the days with symmetric or asymmetric diurnal behaviour, and (ii) distinctly different when compared with one type to another in zenith emission intensity, even though these days belong to different months spread over the duration from Dec 2013 to Mar 2014. This indicates that the neutral wave dynamics is mainly influenced by the strength of the equatorial electrodynamics and follows a broad order in the upper atmosphere.

To further investigate the behaviour of the wave dynamics, information on the propagation characteristics of the waves at each altitude has been obtained and are shown as keograms on two days in Fig. 11. To follow the propagation of waves, black/violet lines have been drawn (to aid the eye) that join the crests/troughs with respect to time. Dotted lines show the most probable movement of the GWs with time when the power of the scale sizes are found to be below the FAL. On 30 December 2013 (symmetric diurnal behaviour), a westward movement of the zonal component of GWs is seen at the altitude of 777.4 nm dayglow emission (Fig. 11a). At 230 and 130 km, no significant movements of the crests and troughs are noticed. They seem to follow a standing wave type of pattern throughout the day (Fig. 11b, c). A uniform pattern of waves without any significant zonal movement of the wave-fronts on the days with symmetric diurnal behaviour indicate to a systematic and uniform behaviour in the dynamic processes over a large spatial extent and thus the absence of zonal differences within the given spatial coverage. On 6 February 2014 (asymmetric diurnal behaviour), thermospheric neutral waves at 777.4 nm emission altitude show a westward propagation (Fig. 11d) similar to the days with symmetric diurnal pattern. At 230 km altitude, the crests/troughs towards east of zenith move eastwards and those towards the west move westwards (Fig. 11e). The waves at 130 km altitude show an eastward propagation (Fig. 11f). Moreover, at different longitudinal regions the gradient of the change in propagation direction of the waves are also different. This type of spatially varying direction of propagation of waves in forenoon and afternoon clearly indicates to the different nature of the processes and dynamics that are prevalent at the respective longitudes.

Thus, the thermospheric neutral wave dynamics in terms of their scale sizes and propagation directions show different behaviour on the days with symmetric/asymmetric diurnal pattern in the optical dayglow emission intensities. These new results hold a lot of promise on various aspects of the coupling of atmosphere that vary as a function of time.

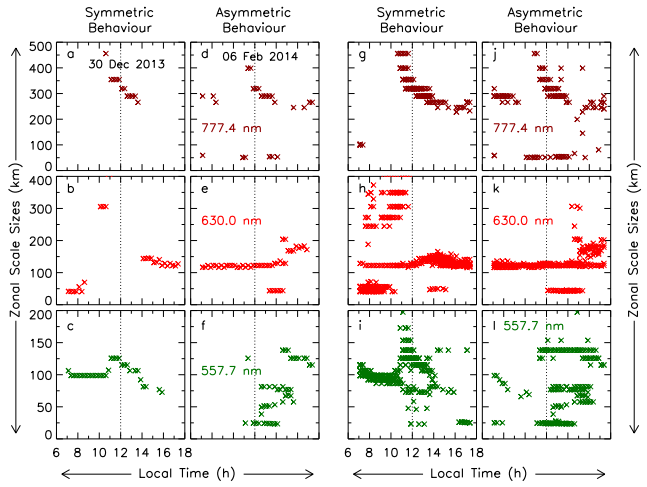

Figure no.10: shows the diurnal distribution of the zonal scale sizes on two sample days with symmetric (a-c)/asymmetric (d-f) behaviour of the dayglow emission intensities at all the three wavelengths. Diurnal distribution of the zonal scale sizes are collated for all the days with symmetric (g-i)/asymmetric (j-l) behaviour of the dayglow emission intensities at all the three wavelengths. The diurnal distribution patterns are found to be significantly different on these two types of days.

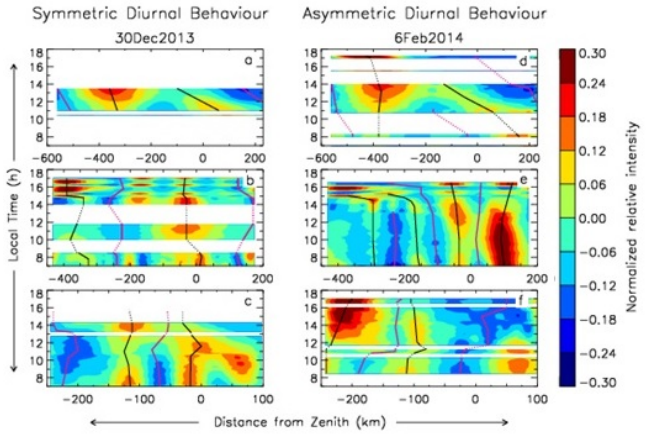

Figure no.11: Keograms of the normalized relative dayglow intensity variations on two sample days (a-c; symmetric/ d-f; asymmetric) are shown. The x- and y-axes show the zonal distance from zenith in km and local time in hours, respectively. Positive/negative values of the distance correspond to the eastern/western direction with respect to the zenith.The values of the normalized relative intensity are shown in the bar on the right hand side. Contrasting characteristics in the zonal propagation of waves can be seen in the days with symmetric/asymmetric diurnal pattern.

(Deepak K. Karan and Duggirala Pallamraju)

Zonal waves in daytime thermosphere during geomagnetic quiet and disturbed times

Diurnal distribution of the zonal scale sizes are compared between geomagnetically quiet (18 Feb 2014) and disturbed days (19 Feb 2014) in Fig. 12. The diurnal distribution of the zonal scale sizes over low-latitudes show distinctly different pattern on the days with symmetric and asymmetric diurnal pattern of the zenith dayglow emission intensities as shown in the Fig 10. The diurnal pattern of the three dayglow emission intensities on the two days considered in Fig 12 are asymmetric in nature. The diurnal distribution pattern of the zonal scale sizes for all the dayglow emissions on 18 Feb (Figs. 12a, b, c) show similar pattern as seen for the days with asymmetric diurnal behaviour in Fig. 10g-i. Contrary to this, the distribution pattern on 19 Feb 2014 shows altogether different. Even though both these days showed asymmetric diurnal pattern in their zenith dayglow intensities, the contrast seen in the diurnal pattern of the gravity wave zonal scale sizes between these two days is attributed to the effect of geomagnetic disturbances on the thermospheric neutral wave dynamics. The scale sizes and propagation directions of the GWs depend on the thermospheric ambient neutral winds which are modified due to the traveling atmospheric /ionospheric disturbances that propagate from higher-latitudes. The equatorial electric field can and does change because of both prompt penetration and disturbance dynamo electric fields. These electric fields redistribute the ion densities over equatorial- and low-latitude regions through phenomenon such as the equatorial fountain effect and equatorial temperature and wind anomaly. Due to such effects changes are brought in the wave dynamics during geomagnetic storms. Such observations on the effect of geomagnetic disturbances on the low-latitude thermospheric wave dynamics as inferred from the neutral optical dayglow emission measurements have brought new information on the daytime thermospheric neutral wave dynamics.

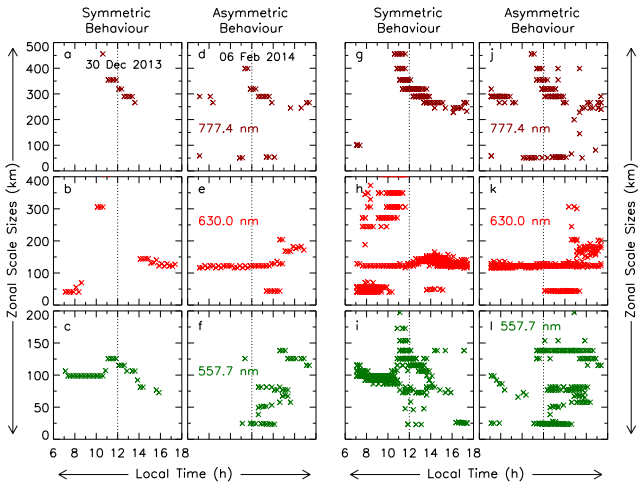

Figure no.12: Diurnal distribution of the zonal scale sizes at the emission altitudes of 777.4 (upper panels, a, d), 630.0 (middle panels b, e), and 557.7 nm (bottom panels c, f) dayglow emissions on 18 Feb 2014 (left column) and 19 Feb are shown. The vertical dashed line is drawn at local noon. It may be noted that the diurnal distribution of the zonal scale sizes is different on the geomagnetic quiet and disturbed days.

(Deepak K. Karan and Duggirala Pallamraju)

Effect of geomagnetic storms on the daytime low-latitude thermospheric dynamics

The equatorial- and low-latitude thermospheric dynamics is affected by both equatorial electrodynamics and neutral wave dynamics, the relative variation of which is dependent on the prevalent background conditions, which in turn has a seasonal dependence. Depending on the ambient thermospheric conditions, varying effects of geomagnetic disturbances on the equatorial- and low-latitude thermosphere are observed. To investigate the seasonal variations of the effect of the geomagnetic disturbances the thermospheric wave dynamics at these latitudes, daytime airglow emission intensities at OI 557.7 nm, OI 630.0 nm, and OI 777.4 nm wavelengths are compared with the thermospheric O/N2 values and equatorial electrojet (EEJ) strength in different seasons. Variations of the dayglow emission intensities are investigated during three events of geomagnetic disturbances that occurred in different seasons. It is seen that the neutral dayglow emission intensities at all the three wavelengths showed different type of variations with the disturbance storm time (Dst) index in different seasons. Even though the dayglow emission intensities are sensitive to the variation in the equatorial electric fields, during the periods of geomagnetic disturbances, especially in solstices, these are dependent on the thermospheric O/N2 values. If a geomagnetic disturbance occurs traveling atmospheric /ionospheric disturbances are set up at high-latitudes. Due to the high- to low-latitude wind circulation, the relative atomic to molecular nitrogen contribution (O/N2) varies at low-latitudes. This seems to govern the oxygen dayglow emission intensities and hence, during this period, the dayglow emission intensities show similar type of variation with O/N2 instead of that with EEJ. This shows the dominance of storm influenced neutral dynamics over the electrodynamics in the low-latitude upper atmosphere during geomagnetic disturbances. However, based on the measurements during equinoxes, it seems that the low-latitude variations of dayglow emission intensities are influenced to a greater extent by equatorial electrodynamics than the effects of neutral dynamics of high-latitude origin.

(Deepak K. Karan and Duggirala Pallamraju)

Gravity waves and their relative dependence on solar flux and or geomagnetic activity: Intial results

A new approach of deriving gravity wave propagation in vertical direction has been arrived at using the data from digisonde located at PRL, Ahmedabad, (23.0°N, 72.5° E). A special mode of analyses was adopted wherein iso-electron contours are obtained at several fixed frequencies. Iso-electron density contours at different levels are plotted as a function of time. On some days (and nights) these show a constant phase shift in their undulations. If the periodograms at these levels also show similar periodicities, then the time difference between the undulations at different iso-electron densities yield information on the propagation speeds of gravity waves in the vertical direction. Using these two information vertical scale sizes of the gravity waves have been derived. The magnitudes of the vertical scale sizes vary from day-to-day and range between 50-400 km for the analyses carried out for a whole year 2013. As the wave energy changes due to incident solar flux energy on a given day and geomagnetic activity, a comparison has been made for this data with solar F10.7 cm flux and Ap values. From initial results it is seen that the vertical scale sizes are

smaller during periods of magnetic quiet and low solar flux. They seem to be more sensitive to geomagnetic variations as compared to that of solar flux. Detailed analysis of the relative strengths between these two parameters on the magnitudes of vertical scale sizes of gravity waves is underway.

(Subir Mandal, Duggirala Pallamraju, and Pradip Suryawanshi)

Results on mesospheric temperature inversions obtained from Gurushikhar, Mount Abu – Statistical perspective

Mesospheric temperature inversions (MTIs) or Mesospheric inversion layers are the narrow thermal layers showing an inversion of the vertical temperature gradient from negative to positive and are formed in the middle atmosphere. In general, there are two type of MTIs, namely, lower MTI that is formed near 70 km and upper MTI that are generally found at altitudes between 85-100 km. For the formation of these MTIs various possible mechanisms have been proposed that include, GW breaking, nonlinear gravity wave-tidal interactions, and chemical heating due to exothermic chemical reactions. It can be seen that as both dynamics and chemistry play a major role for maintaining the thermal balance of the MLT region, it is difficult to assess the relative contribution of these mechanisms for the occurrence of the MTIs, let alone their seasonal/geographical dependencies.

Detailed investigation of the upper MTIs has been carried out by using around five years of simultaneous measurement of O_2(0-1) and OH(6-2) nightglow emission intensities (I(O_2) and I(OH)) and temperatures (T(O_2) and T(OH)) from Gurushikhar, Mount Abu. These measurements were carried out by using an in house built instrument namely, Near Infrared Imaging Spectrograph (NIRIS). The results obtained in this work are based on the NIRIS measurements of 745 nights of observations. It is found that the mean of T(O_2) and T(OH) are 199.6 K and 203.0 K indicating that, in general, the mesopause region is close to or above 94 km altitude over Mount Abu. However, there are nights which showed T(O_2) greater than T(OH) for substantial duration ($>$ 2 hrs) which is different on different nights.

It was found that maximum number of nights showed this temperature enhancement for a duration of around 4 hrs followed by 3, 2, 5, and 6 hrs. Among these nights, it is found that around 28% (209 out of 745) show MTIs. Investigation of the time intervals over which these MTIs occurred show that 75% of MTIs occurred during pre-midnight hours as compared to 25% that occurred during post-midnight hours. The causative mechanism for these upper MTIs have been investigated and it is found that both wave dynamics and chemical heating by the exothermic reactions works in tandem. The current statistical results suggest that chemical heating of atmosphere due to the exothermic reactions seems to be a more probable cause as compared to the dynamical processes for the occurrence of the upper MTIs observed over Mount Abu. So far, such detailed statistics on MTIs does not exist in the published literature, and thus this information provides a gateway for a greater understanding of the atmospheric temperature structure through modelling and simulation studies.

(Ravindra P. Singh and Duggirala Pallamraju)

An Infrared Spectrograph for OH temperature measurements

Spectroscopic technique is one of the most accurate methods for the determination of the rotational temperatures by recording OH emission rotational line spectra. Traditionally, certain OH band emissions (such as OH(8-3) around 730 nm and OH(6-2) around 860 nm) are preferred for the ground based observations of nightglow emission intensities and temperatures. However, intensities of these bands are around 70 times lower than those of OH(3-1) and OH(4-2) bands which have emissions at wavelengths of around 1.5 microns. Working with longer wavelengths is advantageous as this spectral region is less affected by water vapour absorption and scattering. Thus, it is expected to work even during full moon phase as well (of course, except for the duration when the moon is directly above the slit of the spectrograph). For the observation of these bright OH emissions, a medium resolution grating spectrograph has been arrived at which is sensitive enough to record the atmospheric OH rotational line spectra in the wavelength region of 1.5 to 1.6 microns with a high data cadence of around 30 seconds. This spectrograph uses InGaAs photodiode array of 1x512 pixels (with a pixel size of 25x500 microns). Simulation and data analysis scheme is being developed to derive the mesospheric temperatures using the spectra obtained from this spectrograph.

(Ravindra P. Singh and Duggirala Pallamraju)

Geo-effectiveness of Co-rotation Interaction Region: role of solar wind azimuthal flow angle

It is not clear why some CIRs are geo-effective and others are not. In order to address this problem, the geo-effectiveness of CIR is parameterized, for the first time, based on prompt penetration electric field perturbations that reach equatorial ionosphere. The CIR events under consideration are those that occurred during the minimum phase of solar cycle 23.

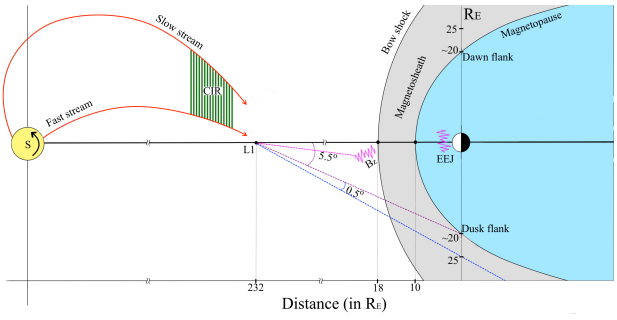

Figure no.13: Schematic (not to the scale; viewed from above the ecliptic plane) depicts the Co-rotation Interaction Region (CIR) caused by the different velocity outflows from the Sun. The investigation shows that the geo-effectiveness of CIRs can be gauged by the azimuthal flow angle at L1 point.

Based on Superposed Epoch Analysis, 43 CIR events are identified wherein characteristic changes in the solar wind magnetic field, density, temperature, azimuthal flow angle etc. are noted. Out of 43 events, 22 events are selected when EEJ variations (based on ground based magnetometer measurements) were available from the Jicamarca sector. The periodicities associated with the prompt penetration electric field perturbations are identified based on the

detailed harmonic analyses of the EEJ variations. It is found that when the solar wind azimuthal flow angle is less than 6 degrees at the L1 point of the Sun-Earth system, the EEJ variations, on most of the occasions, show coherent fluctuations with the fluctuations in IMF Bz in CIR indicating that CIRs are geo-effective. This does not generally happen when the solar wind azimuthal flow angle exceeds 6 degrees at the L1 point. Interestingly, it can be seen that if the azimuthal flow angle exceeds 6 degrees at the L1 point, the CIRs will miss the flanks of the magnetopause and hence will no longer remain geo-effective.

(Diptiranjan Rout, D. Chakrabarty, P. Janardhan, R. Sekar, Vrunda Maniya, and Kuldeep Pandey)

On the occurrence of the Equatorial counter electrojet during June solstice in Solar minimum years

Whether the reversal of daytime eastward equatorial electrojet (EEJ) during magnetically quiet period is a local phenomenon or manifestation of global changes in the E region current, remained a longstanding, unresolved scientific enigma. Observations reveal that quiet time westward electrojet (Counter electrojet or CEJ) occurs frequently (80% of days) over Indian sector during June solstice in solar minimum years. In order to understand the frequent occurrence of westward electrojet during June solstice in solar minimum years, the first principle Equatorial Electrojet (EEJ) model developed by Anandarao et al. (GRL, 1976) is used. The inputs to the electrojet model are zonal Sq electric field, altitude profiles of E region electron density, neutral atmospheric density, and temperature, in addition to the three-dimensional geomagnetic field. The zonal Sq electric fields at different local times are obtained based on climatological vertical drifts of Fejer et al. (2008) model. The representative noon time electron density profile is constructed based on the measured profiles from Thumba during 1000-1400 LT under similar solar epoch. It is found that the strength, duration, peak value, and the occurrence time of CEJ computed by the model match well with the observation, suggesting the explicit role of westward Sq electric field in the generation of these CEJ events. Therefore, the present investigation suggests that afternoon CEJ events over the Indian sector during June solstice in solar minimum periods are part of the global current system.

(Kuldeep Pandey, R. Sekar, B. G. Anandarao, S. P. Gupta and D. Chakrabarty)

Investigation on the effects of the step-I of the main phase of 17 March 2015 geomagnetic storm on the low latitude ionosphere

Based on TEC observations by India's GPS Aided GEO Augmented Navigation (GAGAN) network, the response of the dayside low latitude ionosphere over the Indian region during the moderate main phase step-I of the 17 March 2015 geomagnetic storm is studied. In addition, the efficacy of GPS inferred TEC maps by International GNSS service (IGS) in capturing large scale diurnal features of equatorial ionization anomaly (EIA) over the Indian region during this period is also investigated. The anomalies between the GAGAN TEC and IGS TEC maps are discussed in terms of the possible limitations of the IGS TEC maps in capturing storm time EIA variability over the Indian region.

This work is done in collaboration with the scientists from Indian Institute of Geomagnetism, Navi Mumbai and Space Applications Center, Ahmedabad.

(D.Chakrabarty)

An unusual electric field perturbation over equatorial ionosphere - New magnetospheric driver?

During a space weather event, Jicamarca Radar observed quasi-periodic variations in vertical plasma drifts in the pre-noon hours. These variations occurred in the absence of any prompt penetration of interplanetary electric field (IEF) or magnetospheric substorms. Synchronous variations in magnetometer measurements during this time across large latitudinal extent point towards global origin of the drift fluctuations. Detailed investigation reveals a possible new magnetospheric driver for the periodic fluctuations observed in equatorial vertical drifts.

This work is done in collaboration with a scientist from the Los Alamos National Laboratory, USA.

(Debrup Hui, D. Chakrabarty, and R. Sekar)

Response of equatorial ionosphere corresponding to solar flares and Interplanetary Coronal Mass Ejection

Based on a space weather event in 2017 in which Interplanetary Coronal Mass Ejection hit the terrestrial magnetosphere-ionosphere system, the impacts of the sheath and magnetic cloud regions in the ICME on the equatorial ionosphere have been evaluated. In addition, the impact of the solar flares that occurred during this event were also investigated. This investigation shows the complex interplay of flare and ICME related effects on the equatorial ionosphere.

(Diptiranjan Rout, Kuldeep Pandey, D. Chakrabarty, R. Sekar)

On the origin of extremely non-radial solar wind outflows

The solar wind is primarily radial in nature with the azimuthal component of the flow typically being between 10-30 km/sec. However, non-radial flows (azimuthal flow angle $>6^{\circ}$) are observed on many occasions. Although the non-radial flow associated with “solar wind disappearance event” was noticed earlier, the causes for the non-radial flow was not addressed. The degree of deviation from the radial direction also has consequences on geo-effectiveness and space weather. A large number of such cases in cycles 23-24, covering the period 1995-2017, have been investigated. This investigation reveals that these non-radial solar wind events originate closer to the sun under special circumstances.

This work is done in collaboration with a scientist from the Institute for Space-Earth Environmental Research (ISEE), Nagoya University, Japan.

(Diptiranjan Rout, P. Janardhan and D. Chakrabarty)

Variations in OI 630.0 nm airglow intensity over Mt. Abu in response to prompt penetration electric field

Two narrow spectral band, narrow field of view (FOV) photometers were operated to measure the changes in the OI 630.0 nm thermospheric airglow intensity from zenith and southward elevation from Mt. Abu, a station under the crest of equatorial ionization anomaly, during 21-25 December, 2014. These observations show that the post-sunset and post-midnight variations in the OI 630.0 nm airglow intensity under the influence of prompt penetration electric field are different. The causes for these differences are investigated to understand the local time dependence of the effects of prompt penetration electric field on low latitude ionospheric electrdynamics.

This work is done in collaboration with scientists from the Space Environment Laboratory National Institute of Information and Communications Technology, Japan and Los Alamos National Laboratory, USA.

(D. Chakrabarty, Avik Paul, Diptiranjan Rout, Kuldeep Pandey, Anil Yadav and R. Sekar)

Rayleigh Lidar observed atmospheric temperature characteristics over a western Indian location: Intercomparison with satellite observations and models

General characteristics of sub-tropical middle atmospheric temperature structure over a high altitude station, Mt. Abu (24.5° N, 72.7° E) are studied using Rayleigh Lidar. The monthly mean temperature contour plot shows two distinct maxima in the stratopause region ($\sim$45–55 km), occurring during February-March and September-October, a seasonal dependence similar to that reported for mid- and high-latitudes respectively. Semi-Annual Oscillation (SAO) are stronger at an altitude $\sim$60 km in the mesospheric temperature in comparison to stratospheric region. A comparison with the satellite (Halogen Occultation Experiment, (HALOE)) data shows qualitative agreement, but quantitatively a significant difference is found between the observation and satellite. The derived temperatures from Lidar observations are warmer $\sim$2–3 K in the stratospheric region and $\sim$5-10 K in the mesospheric region than temperatures observed from the satellite. A comparison with the models, COSPAR International Reference Atmosphere (CIRA)-86 and Mass Spectrometer Incoherent Scatter Extended (MSISE)-90, showed differences of $\sim$3 K in the stratosphere and $\sim$5–10 K in the mesosphere, with deviations somewhat larger for CIRA-86. In most of the months and in all altitude regions model temperatures were lower than the Lidar observed temperature except in the altitude range of 40–50 km. MSISE-90 Model temperature overestimates as compared to Lidar temperature during December-February in the altitude region of 50-60 km. In the altitude region of 55-70 km both models deviate significantly, with differences exceeding 10-12 K, particularly during equinoctial periods. An average heating rate of $\sim$2.5 K/month during equinoxes and cooling rate of $\sim$4 K/month during November-December are found in altitude region of 50-70 km, relatively less heating and cooling rates are found in the altitude range of 30-50 km. The stratospheric temperature derived from the Lidar and columnar ozone observed by the Total Ozone Mapping Spectrometer (TOMS) over Mt. Abu shows good correlation and indicates the association of ozone with the temperature.

(S. Sharma, S. Lal, H. Chandra and Y. B. Acharya)

Fog/low clouds detection over the Delhi Earth Station using the Ceilometer and the INSAT-3D/3DR satellite data

Fog is a meteorological phenomenon in which cloud has its base near to the surface which disrupts public health and transportation due to decrease in visibility. In the present study, a collective method has been implemented for detection of fog/low clouds over the Delhi Earth Station during fog season for the years 2016 and 2017. A detailed comparison has been performed with the use of ground-based cloud-base height measurements from the Ceilometer and the Indian National Satellites (INSAT-3D/3DR)- retrieved fog product. Fog/low clouds have been effectively detected by both the Ceilometer and the INSAT-3D/3DR during single-layer cloud in the range of 0–200 m in most of the cases. Since the INSAT-3D/3DR fog product is derived under clear sky condition, fog detection during multilayer clouds is a challenging task. Results indicate that the Ceilometer can capture fog/low clouds effectively even in presence of single- and multilayer clouds. Remote-sensing technology can provide better opportunity by providing complete temporal and spatial coverage of fog. The present technique which incorporates both ground-based Ceilometer and space-based INSAT-3D/3DR measurements is observed to be more promising than other conventional methods for an improved detection and monitoring of fog/low clouds.

This work has been done in collaboration with Space Applications Centre (ISRO), Ahmedabad, India

(Som Sharma)

Science

Geosciences

Provenance of Harappan potteries and Ghaggar sediments

The ephemeral Ghaggar-Hakra River of northwestern India has always been considered to be the remnant of an ancient perennial glacier-fed river (Vedic Saraswati). The exact reason and timing of major hydrological change of this river remains speculative. The river's purported association with the zenith of the Harappan civilisation remains a conjecture because the timings of its fluvial past are still being debated. In this study we have made an attempt to resolve this issue using geochemical provenance of sediments from some dated horizons in the Ghaggar flood plain and that of the material used in the potteries from the Mature Harappan period (4600 to 3900 yr BP) at Kalibangan. Sampled sedimentary horizons were dated by radiocarbon and optically stimulated luminescence (OSL) methods. Results of our study from the Ghaggar alluvium indicate that the river did have glacial sources during the early Holocene. However, the data from the potteries suggest that during the Mature Harappan period, the sediments in the Ghaggar as used by the potters did not have a higher Himalayan provenance and hence, were not derived from glaciated Himalayas. These findings imply that during the time of the Mature Harappans the Ghaggar had already become a foothill-fed river.

(A. Chatterjee and J.S. Ray)

Role of fractionation correction in accurate determination of ^{142}Nd/^{144}Nd by TIMS

The short-lived isotopic systematics of ^{146}Sm-^{142}Nd is a tracer of early silicate Earth differentiation events. Evidence for these events comes from anomalous ^{142}Nd/^{144}Nd, defined in terms of μ^{142}Nd (μ^{142}Nd= [{(^{142}Nd/^{144}Nd)$_{sample}$ / (^{142}Nd/^{144}Nd)$_{standard}$}-1]$\times 10^6$) with respect to a terrestrial standard representing the modern accessible mantle. This requires measurement of accurate and highly precise ^{142}Nd/^{144}Nd, which is carried out by Thermal Ionization Mass Spectrometry (TIMS). Since multiple factors affect the accuracy of the final results, we carried out a detailed investigation on the effect of various data acquisition, fractionation correction and normalization methods on the accuracy of ^{142}Nd/^{144}Nd determinations. Based on the analyses of Ames Nd standard using various combinations of the most commonly employed methods we observed that for a multi-dynamic mode of data acquisition, the power-normalized exponential law is the most appropriate method for mass fractionation correction. The time delays between successive sequences in a multi-dynamic mode had little effect on the final value of ^{142}Nd/^{144}Nd. The different standards have different ^{142}Nd/^{144}Nd ratios and therefore, their uses yield different μ^{142}Nd values for the same sample. We extended this information to understand the two contradicting results from 1.48 Ga alkaline rocks from Khariar, India, carried out on the same sample aliquots by earlier workers. A confirmation of ^{142}Nd anomalies in such younger rocks is important because it could establish the longevity of early silicate differentiation signatures beyond Archean. Our experiment on freshly collected samples from the same outcrops, using identical analytical procedures, could not reproduce the earlier results. We did, however, observe slightly negative μ^{142}Nd values with respect to Ames Nd, which became normal with respect to JNdi^{-1}.

(I. Gautam and J.S. Ray)

Carbon isotope stratigraphy of Marwar Supergroup,Rajasthan

The Neoproterozoic Era had witnessed some of the remarkable events in the Earth's history, such as the first appearance of animal life, oxygenation of the oceans, break-up of the supercontinent Rodinia and three major global glaciations. Evidences for these global events generally come from contemporary marine carbonate deposits.In search of evidence for Neoproterozoic glaciations in Indian subcontinent, we studied the geochemical signals in the carbonate formations of the Marwar Supergroup of western India, which is believed to have been deposited during the terminal Neoproterozoic. Using the principles of Sr isotope stratigraphy (observed ^{87}Sr/^{86}Sr = 0.7081) we determined an age of $\sim$570 Ma for the deposition of the

Bilara Group, the middle Marwars. The δ^{13}C of the Bilara carbonates varies from -5.8 to +2.1 ‰and δ^{18}O from -11.3 to +7.4‰.Carbon isotope stratigraphy reveals a negative δ^{13}C excursion in the Gotan Formation, Bilara Group, where the δ^{13}C values plunge to near mantle values of $\sim$ -5‰.This excursion can be correlated throughout the basin and represents a temporal change in the ocean chemistry during the Ediacaran Period and can be correlated to the globally synchronous Gaskiers glaciation.

(B.G. George and J.S. Ray)

Hydrometeorological processes in the NE India: significance of recycled moisture from wetlands

Understanding hydro-meteorological processes in the northeast India is important because it concerns the water availability for large-scale wetland irrigation and also sustains the wetland ecosystems in the region affecting over 45 million people. The total wetland area in the seven NE Indian states (Assam, Meghalaya, Tripura, Mizoram, Manipur, Nagaland, and Arunachal Pradesh) is estimated to be 1065658 ha, of which about 764372 ha (71.7%) is located in the state of Assam alone. In view of the presence of such a large areal extent of wetlands providing inland surface water bodies, a significant contribution of continentally derived vapour from wetlands to the rainfall is expected in this region. With Brahmaputra River draining a large volume of precipitation from NE India back into the Bay of Bengal, passing through wetland repository, a regional hydrological circulation in the NE India can also be envisaged, involving admixture of moisture derived from wetlands with moisture advected from the Bay of Bengal to generate precipitation in NE India and its transportation back to the Bay of Bengal by Brahmaputra river passing through wetlands. There is also a possibility of transportation of moisture from adjoining region during Kal Baisakhi or western disturbances. With a view to study these unexplored but important hydro-meteorological aspects, isotope data of daily precipitation collected for two years at Jorhat under the IWIN National Programme, have been examined (Fig. 1). Based on the time series of δ^{18}O (Fig. 1), three major time-periods can be distinguished, namely, January to May (δ^{18}O: -1$\pm$2‰), June to mid-September (δ^{18}O:decreasing from -6 to -14‰), and mid-September to December (δ^{18}O: increasing from -17 to 1‰), superimposed on significant daily variation. From January onwards δ^{18}O of precipitation slowly decreases from 1‰up to -4‰. With onset of monsoon, the δ^{18}O of precipitation suddenly decreases from $>$-4‰to $<$-6‰and continues to decrease (up to -17‰) until mid-September. From mid-September onwards the δ^{18}O of precipitation increases up to 1‰until January.

During January to May when monsoon circulation has not set in, rain is derived from local convective cells. From March, the land surface is progressively heated and the temperature rises. Local depressions are formed over the Brahmaputra plain where strong convection develops specially in the afternoon lifting the vapour derived from the wetlands and resulting into rain. This is manifested in a hump in the d-excess time series during March-April (Fig.1). Sudden decrease in d^{18}O of precipitation in June can be ascribed to: (1) change in temperature; (2) change in amount of rainfall; and/or (3) change in vapour source. However, the observed isotopic variation is found to be unrelated to temperature and amount of rainfall suggesting change in vapour source as the responsible factor. The change in the vapour source could be from terrestrial to marine (Bay of Bengal) and/or from isotopically enriched wetlands to depleted wetlands as source.

The observed decrease in δ^{18}O from -6 to -14‰during latter part of the monsoon suggests that the vapour source (wetland) itself is getting depleted because in Assam River/Stream account for 84% percent of the wetlands. The rivers carry water derived from isotopically depleted high altitude rainfall and snow melt. A hump in the d-excess time series during August suggest enhanced contribution of vapour derived from wetlands. There is a progressively increasing trend in δ^{18}O of precipitation from September to January (-17 to 1‰) which suggests that on cessation of monsoonal rainfall and snow melt contribution from high altitude to riverine influx, the wetlands undergo progressive evaporative isotopic enrichment which is also manifested in corresponding enrichment in δ^{18}O of rainfall from the vapour with significant contribution from.

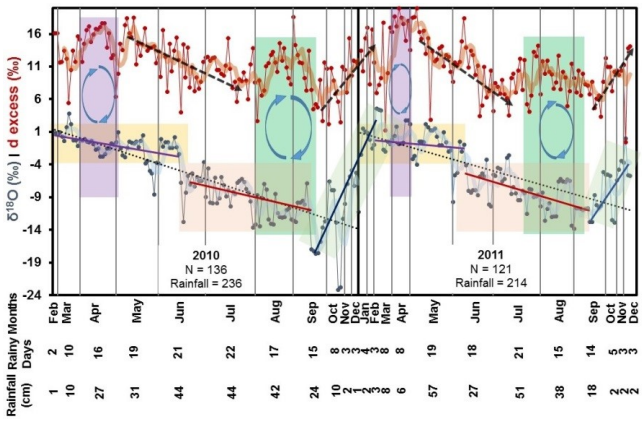

Figure no. 1: Time series of δ^{18}O and d-excess (= δD-8* δ^{18}O) of daily precipitation at Jorhat for two years, along with monthly rainfall and rainy days.

(H. Oza, V.R. Padhya & R.D. Deshpande)

Influence of southwest monsoon in the Kashmir Valley, Western Himalayas

The regional climate of the Himalayas is pre-dominated by the southwest monsoon and the western disturbances. The uplift of the Pir Panjal mountain range to its present height is believed to restrict the southwest monsoons from entering into the Kashmir Valley in the western Himalayas.

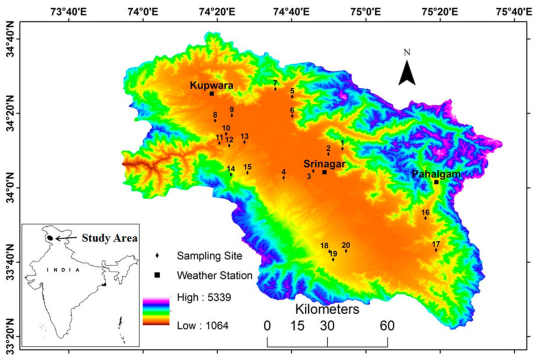

Figure no. 2: Map of the study depicting orography and the precipitation sampling locations across the Kashmir valley. Precipitation location No. 1–4 are located near Srinagar weather station; No. 5–15 near Kupwara weather station; and No. 16–20 near Pahalgam weather station.

With a view to isotopically fingerprint the influence of western disturbances and the southwest monsoon in the Kashmir valley (Fig. 2), vis-à-vis the role of Pir Panjal range as an effective orographic barrier, monthly composite precipitation samples were collected for two years from 20 stations across the Kashmir Valley for analysing their oxygen and hydrogen isotopic composition (δ^{18}O and δ^{2}H).

Except in August, the precipitation is enriched in ^{18}O and ^{2}H from June to September and depleted from October to May. The sharp depletion of ^{18}O in precipitation along with the decrease in d-excess in August confirms the maximum intrusion of southwest monsoons into the valley. A significant temperature – δ^{18}O relationship was found during October and May (westerlies period) to decrease during June and September (southwest monsoon period).

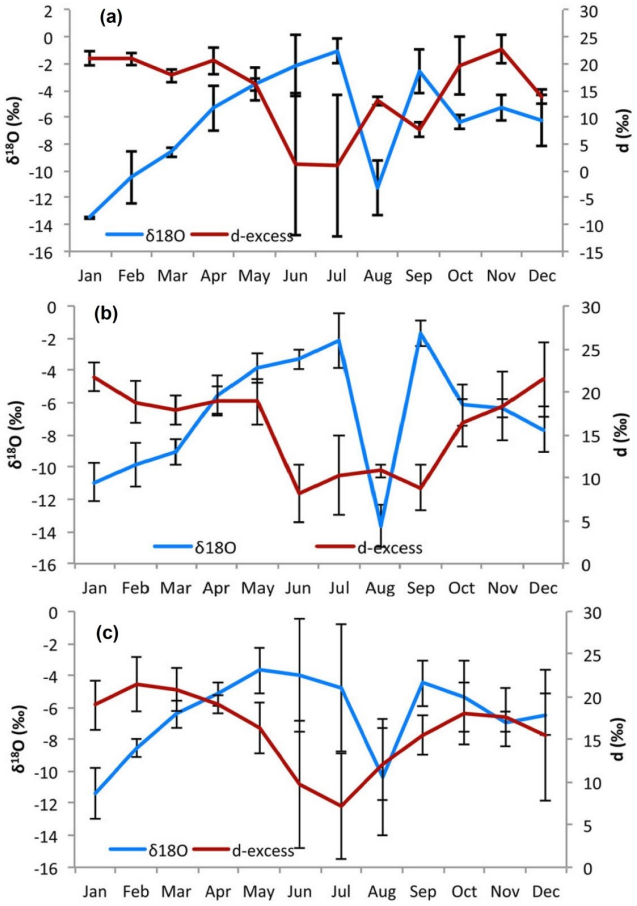

Figure no. 3: Variation in average monthly δ^{18}O and d-excess (d = δ D-8* δ^{18}O) at (a) four locations around Sringar weather station; (b) 11 locations around Kupwara weather station; and (c) 5 locations around Pahalgam weather station.

The local meteoric water line for the whole Kashmir Valley based on the precipitation-weighted monthly samples is δ^{2}H = 7.97(+0.3)$\times$ δ^{18}O+16.3(+2.5) (n=229,R^2=0.97, p$\leq$0.05). Higher intercept of the regression equation suggested dominant contribution of precipitation from western disturbances. The average d-excess was higher (16–21.8‰) from October to May and lower (5–11‰) from June to September indicating influence of western disturbances up to May and beginning of change in vapour source from June. A sudden lowering of δ^{18}O ($<$-10‰) is observed at all the stations across the Kashmir valley in the month of August. This confirms that the southwest monsoon prominently enter the Kashmir Valley from southwest, crossing over the Pir Panjal Mountain which does not seem to be an effective orographic barrier for monsoon winds.

This study was carried out in collaboration with Dr.Gh. Jeelani and his team from Kashmir University.

(R.D. Deshpande and V.R. Padhya)

Isotope fingerprinting of precipitation associated with western disturbances and Indian summer monsoons across the Himalayas

With a view to understand the imprints of the two dominant weather systems affecting precipitation in Himalayas, namely, western disturbances (WDs) and Indian summer monsoon (ISM), oxygen and hydrogen isotopic data (δ^{18}O and δD) of monthly composite precipitation samples collected across the Himalayas from Kashmir (western Himalaya) to Assam (eastern Himalaya) under the IWIN National Programme were examined together with data from new samples collected by Kashmir University and the published data.

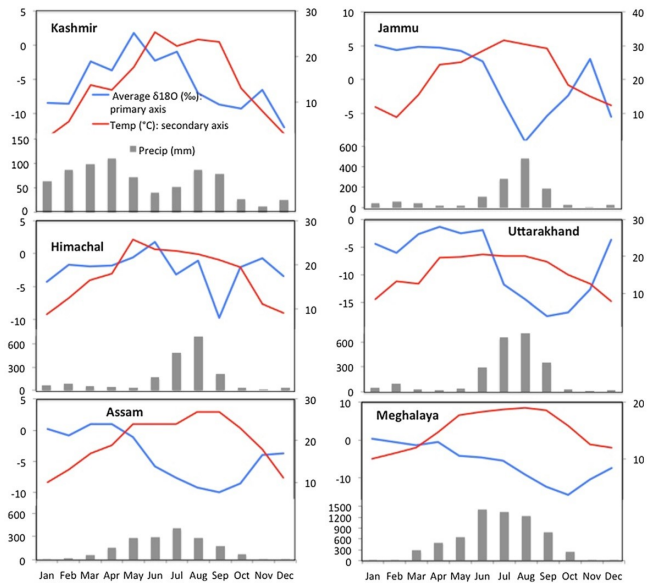

Figure no. 4: Average monthly δ^{18}O and its relationship with average ambient temperature and precipitation in different regions of the Himalayas.

Using distinct isotopic signatures, the regions receiving precipitation from two different weather systems have been identified. Large spatial and temporal variations in isotopic values were noted with δ^{18}O and δD values ranging from $-$30.3 to +9.3‰and $-$228 to +59‰, respectively. The d-excess values also exhibit a large range of variation from $-$30 to +40‰. In general, higherr isotopic values are observed in most of the samples in Jammu, whereas lower values are observed in majority of the samples in Uttarakhand. Precipitation at Jammu seems to have undergone intense evaporation while that from Uttarakhand suggest normal Rayleigh fractionation/distillation of the air mass as it moves from the source region to the precipitation site and/or orographic lifting. The d-excess of rainfall in Kashmir has a

distinctly higher median value of 18‰compared to other precipitation sites with a median of 9−12‰, indicating influence of western disturbances.

Isotopic composition of precipitation at a particular location may be related to the temperature, amount of precipitation, altitude, latitude, longitude and distance of sampling location from the sea, possible vapour source and typical rainout history of the air parcel.

Average monthly δ^{18}O and its relationship with average ambient temperature and precipitation in different regions of the Himalayas are shown in (Fig.4). Except Jammu and Meghalaya, average δ^{18}O of the precipitation of all regions showed a good relationship with the average ambient temperature from December-January to May-June. However, the precipitation of all the regions showed decrease in δ^{18}O from June/July to September/October despite higher ambient temperatures. The apparent decrease in δ^{18}O of precipitation, although coincides with higher precipitation amount, may be attributed to the change in the source of precipitation, as the correlation between the precipitation amount and the δ^{18}O of precipitation is statistically insignificant.

This study suggests that up to Uttarakhand in central Himalayas, the moisture regime is dominated by the primary marine source, most likely the Bay of Bengal. Further west of Uttarakhand, there seems to be significant admixture of evapotranspired vapour. However, at stations west of Uttarakhand, the d-excess is not very high. This suggests that vapour admixture is due to transpiration and not the evaporation, which would have manifested in high d-excess as well.

This study was carried out in collaboration with Dr. Gh. Jeelani of Kashmir University.

(R.D. Deshpande and V.R. Padhya)

Distinguishing and estimating recharge to karst springs in snow and glacier dominated mountainous basins of the western Himalaya, India

Recharge assessment is a challenge in snow and glacier dominated Himalayan basins. Quantification of recharge to karst springs in these complex geological environments is important both for hydrologic understanding and for effective water resource management. In order to distinguish and estimate the sources of spring water and to identify the flow paths of the recharging waters in three mountainous basins (Bringi, Liddar and Kuthar) of the western Himalaya spring hydrographs and environmental tracer technique (isotopes and solutes) were employed. The karst springs are perennial with high discharge amplitudes. The results indicate that ambient temperature has a strong influence on the hydrological behavior of the springs. Although the spring flow is dominantly controlled by the melting of snow and/or glaciers, rain events produce sharp spikes in spring hydrographs. The facies patterns in springs within the Bringi basin (Ca-HCO_3) and the Liddar basin(Ca-HCO_3 and Ca-Mg-HCO_3) suggest dominant flow through limestone and dolomite. Higher concentrations of $SO_4{}^{-2}$and Na^+ in warm springs of the Kuthar basin indicate flow through carbonate, silicate and other rocks. The isotopic composition (δ^{18}O, δ^2H) of precipitation, snowpacks, glacier melt and karst springs exhibits a wide variation both in space and time, and is strongly influenced by the basin relief and meteorology. The tracer-based two- and three-component mixing models suggest that the snowmelt dominantly contributes to the spring flow (55–96%), followed by glacier melt (5–36%) and rain (4–34%). Based on tracer tests with good recovery rates, springs are dominantly recharged through point sources rather than by diffuse infiltration. Changes in the timing, form, and amount of winter precipitation substantially affect the timing and magnitude of spring discharge during the rest of the year. *This study was carried out in collaboration with Dr. Abhijit Mukherjee of IIT, Kharagpur and Dr. Gh. Jeelani of Kashmir University.*

(R.D. Deshpande)

Evaluating the sensitivity of glaciers in Liddar and Suru basins in Kashmir to regional weather using stable water isotopes and remote sensing

Glaciers in the Himalayan Mountain system are undergoing rapid retreat, and the global climate change has a significant impact on it. In order to understand the impact of climate on melting behaviour of some high altitude glaciers in two glacier-fed basins of western Himalaya, India stable water isotope (δ^{18}O and δ^2H) and remote sensing data have been used. Glacier samples were collected from four major glaciers (Kolahoi, Hoksar, Sheshram, and Sonsar) of Liddar basin (Kashmir region) and two major glaciers (Parachik and Drung-Durung) in Suru basin (Ladakh region) during melting season from May to November for isotopic analyses.

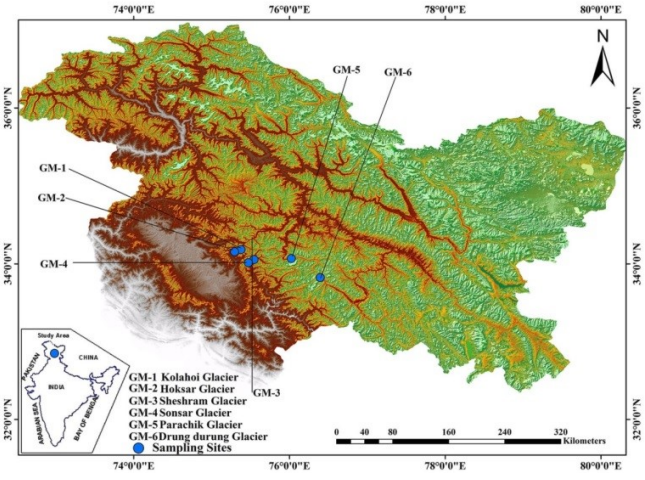

Figure no. 5: Map showing the location of the glaciers in Jammu and Kashmir.

It was observed that the glacier samples from Suru basin were more depleted in ^{18}O and ^{2}H (-10.9 to -16.2% and -73 to -128%) than the glaciers of Liddar basin (-8.2 to -14.9% and -52 to -102%). However, the d-excess of the glacier samples in Suru basin was lower (13.5–21.6%) than the glaciers of Liddar basin (17–28%). It was observed that the temporal changes in weather pattern strongly influence the isotopic composition of the glaciers with progressive decrease and increase in δ^{18}O (or δ^2H) with the increase in ambient temperature and rainfall, respectively. The results suggest that during the sunny days of August and September, the glaciers are melting at higher altitudes (3900–4172 m) in the accumulation zone, reflecting

that the glaciers of Liddar basin are not the ideal sites for the ice coring for paleoclimatological studies. The study also revealed that approximately 11-29 % of glacierized area has been lost in <35 years in Liddar basin, which is quite higher than that of Suru basin (2%).

The glacial melt is seen to display marked diurnal isotopic variation the magnitude of which fluctuates as per weather condition. Overall, the isotopic values of glacier melt samples collected at snout tend to become more depleted(lighter) in the afternoon or evening depending upon the ambient temperature of the day and rainfall. Highly depleted/lighter isotopic values (-14.9%), a characteristic isotopic signature of precipitation representing an altitude of more than 4000 m amsl were observed at the snout of the glacier during sunny days of September when the winter-accumulated snow cover is reduced to <7%.

This study was carried out in collaboration with Dr. Gh. Jeelani of Kashmir University.

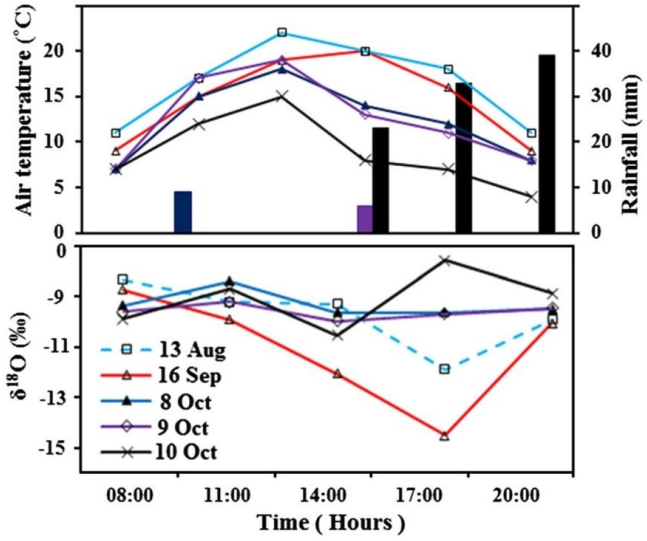

Figure no. 6: Diurnal variation in isotopic composition of glacial melt water from 8:00 hr to 20:00 hr during August, September and October with corresponding variation in temperature and rainfall.

(R.D. Deshpande and V.R. Padhya)

Northern Indian Ocean warming recorded in Lakhshadweep corals

Corals, growing in shallow marine environment, provide an important archive for past sea surface condition proxies. Corals are sensitive to temperature and salinity changes in seawater and growth rate of the coral is thus indicative of past sea surface conditions. The coral samples from Kadmat and Agatti islands of Lakhshadweep were investigated for annual growth rate variations. The x-radiograph of the coral shows alternate dark and white bands representing high and low density bands in the skeleton. The thickness of bands represents coral growth which depends on the surrounding environment and sea surface conditions. The counting of these bands provides chronology of the coral sample. The growth rate (cm/yr) estimates of two corals, from Kadmat (KD1) and Agatti islands (AG3) were 1.4 $\pm$ 0.4 cm/yr and 1.3 $\pm$ 0.3 cm/yr, respectively. The growth rate of both corals from Lakshadweep during 1996-2012 is significantly lower than that during 1981-1995 (Fig.7). This time period coincides with warmer average annual sea surface temperature in the region. This suggests stressed condition for coral growth after 1995 is due to increased sea surface temperature.

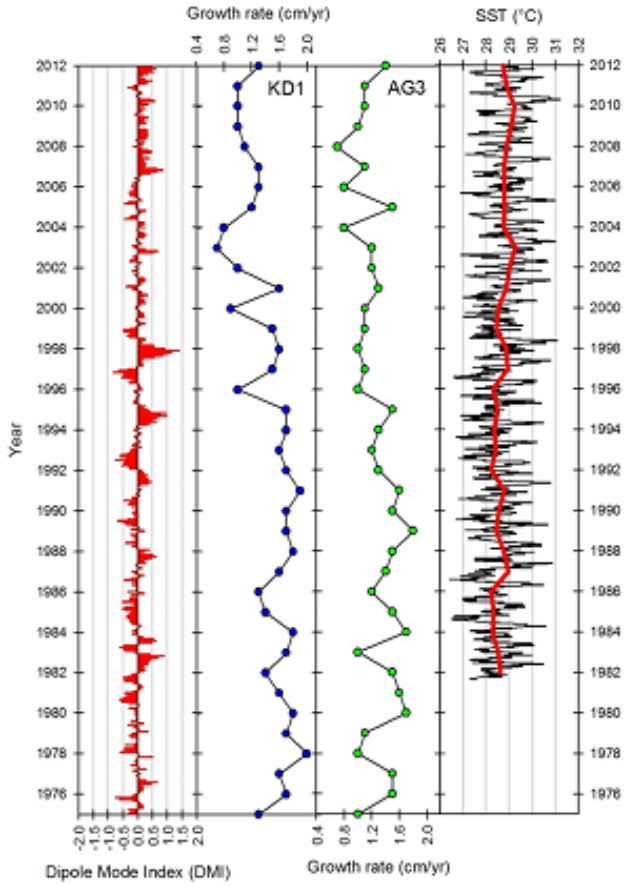

Figure no.7: Growth rate comparison of corals from Kadmat and Agatti Islands from Lakshadweep along with SST (*www.oceanmotion.org*) and Dipole mode Index (*www.jamstec.go.jp*).

(H. Raj, U.S. Banerji, C.S. Shah & R. Bhushan)

Results from PRL Accelerator Mass Spectrometer: Sedimentation rate in the Andaman Basin

The 1MV Accelerator Mass Spectrometer (AMS) facility has been established for measurement of radiocarbon and has been acronymed AURiS (Accelerator Unit for RadioIsotope Studies). The chronology of the northern Andaman sea sediment core SK/304B-18 has been established based on radiocarbon dates of select planktonic foraminifer species using AURiS. The sedimentation rate was determined using Clam software which employs linear interpolation age-depth model using the radiocarbon dates. The sedimentation rate

varied between 10.7 to 39.0 cm kyr^{-1} with minimum sedimentation rate during 2994-4769 cal yr BP and maximum sedimentation rate during 5800-6744 cal yr BP (Fig.8). Low sedimentation rate are attributed to reduced detrital influence as a function of reduced monsoonal activity, while high sedimentation rates is ascribed to enhanced monsoonal activity. A gradual shift in climate from wetter to drier conditions from 10000 to 4000 yr in the Bay of Bengal is due to gradual weakening of summer monsoon. Drier conditions with increased aridity between 4000 to 1700 cal yr BP pertains to reduced summer monsoon as a function of which low sedimentation rates between 2994-4769 cal yr BP has been identified for the Northern Andaman sea sediment core.

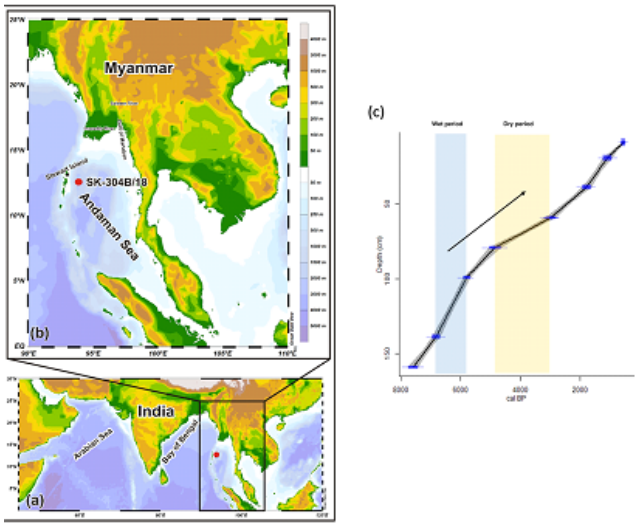

Figure no.8: Age-depth plot using linear interpolation model showing wet and dry period.

(R. Bhushan, M.G. Yadava, M.S. Shah, U.S. Banerji, H. Raj, C.S. Shah & A.J. Dabhi)

Performance of 1MV Accelerator Mass Spectrometer facility (AURiS)

To ascertain system performance of 1MV AMS facility, various samples provided as part of an international inter-comparison exercise for radiocarbon intecalibration were measured. The precision of measurement for radiocarbon using AURiS was found to be 2.21‰with background values of 3.89E-16. The statistical uncertainty for $^{14}C/^{12}C$ was found to be below 0.5% with relative standard deviation below 0.6%. The standard deviations for $^{13}C/^{12}C$ ratios for corresponding runs were below 0.2%. In order to check the accuracy of the AURiS data, four different radiocarbon reference standards (IAEA C-1, IAEA C-2, FIRI-E and VIRI-U) were analysed. The consensus and the measured values by AURiS are mentioned in Table. Fig.9 shows the comparison between multiple measurements of reference standards with consensus values. The AURiS values for reference standards are well within the acceptable limits of $<$2 % of the consensus values. These results suggest that AURiS is capable of making routine radiocarbon measurements with high precision.

Table : Radiocarbon measured and reference standard values

Reference	Material	Unit	Consensus ^{14}C value	PRL-AURiS ^{14}C Value*
IAEA-C1	Marble	pMC	0.00 $\pm$ 0.02	0.14 $\pm$ 0.04
IAEA-C2	Travertine	pMC	41.14 $\pm$ 0.03	41.89 $\pm$ 0.36
FIRI-E	Humic acid	years (BP)	11780 $\pm$ 7	11797 $\pm$ 164
VIRI-U	Humic acid	pMC	23.079 $\pm$ 0.0155	23.013 $\pm$ 0.245

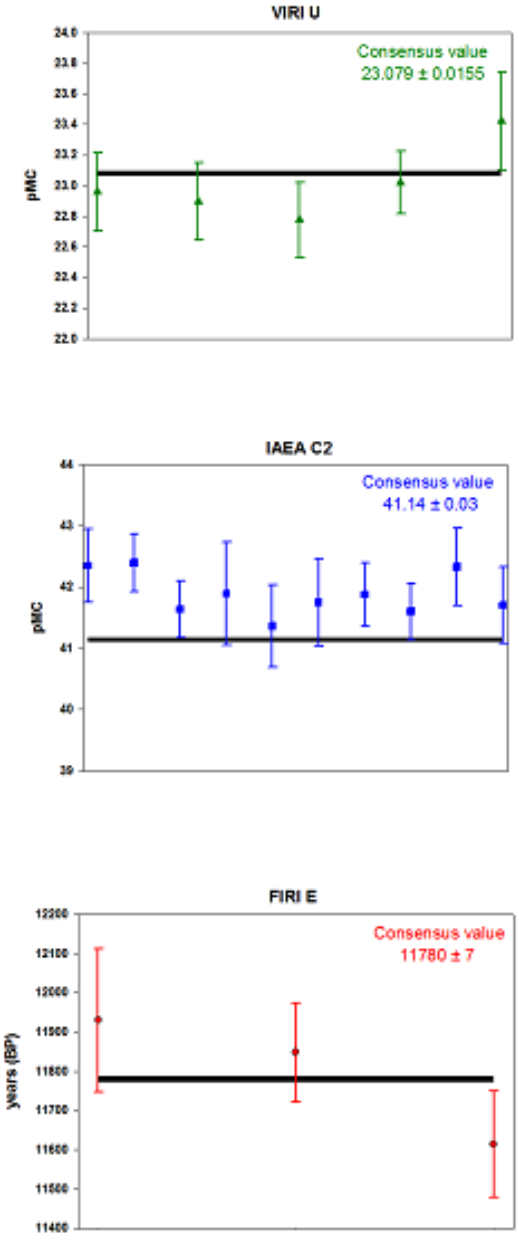

Figure no.9: Plot of multiple runs of radiocarbon reference standards and its deviation from the consensus values.

(R. Bhushan, M.G. Yadava, H. Raj, M.S. Shah & A.J. Dabhi)

Dissolved aluminium in the southern Bay of Bengal, southern Andaman Sea and the equatorial Indian Ocean

Aluminium is sparingly soluble in the modern oxidised ocean water and shows minimal recycling with marine biology, and is largely insensitive to the redox changes in the ocean water column. Comprehensive study on dAl would provide better constrains to the extent of sources supplying Al and other important bioessential trace metals (Fe, Mn, etc.) to the marine system. This study aims to decouple the controls of different sources and processes on the dAl distribution in these regions. In the BoB and Andaman Sea, dAl profiles show maxima at the surface (<50m), followed by steep decrease in sub-surface (50-300m) waters (Fig.10). Significant dAl inputs with large freshwater influx has been observed from Himalayan rivers (Ganga and Brahmaputra), Indian peninsular rivers (Mahanadi, Godavari, Krishna) and Irrawaddy river in the BoB and Andaman Sea. Al leaching from suspended and/or settling particulate matter derived from continental margins, near the coastal regions has been noticed. The dAl concentrations (2.70 – 15.35 nM) in the equatorial waters were low compared to the northern BoB and Andaman Sea (7.32 – 48.35 nM) waters and steadily decreased towards the western equatorial region (Fig.10). Rapid decline of dAl below surface results from its removal from the water column by passive scavenging (physical adsorption on particles surfaces) and by active uptake (biological removal) in the surface waters. Sparsely placed increments near sediment-water interface towards the seafloor suggests prominent dAl input from partial dissolution (or desorption) of sedimentary Al via resuspension of sediments from the continental margins and the seafloor, to the intermediate and deep waters.

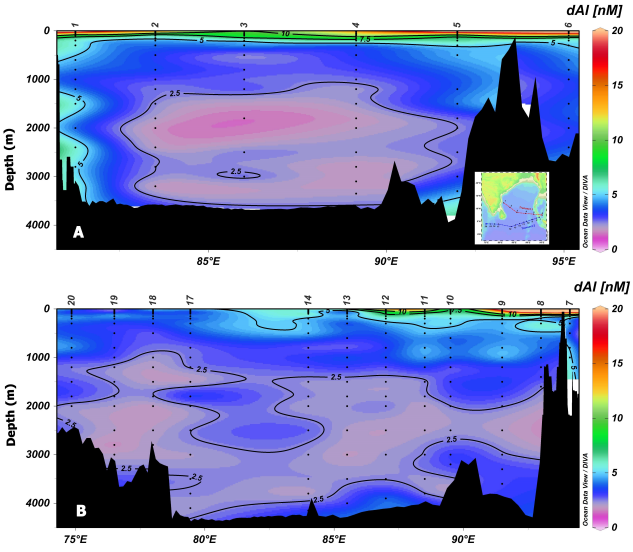

Figure no.10: Distribution of dissolved aluminium along A) transect 1 and B) transect 2 (see inset in Figure A) in the southern BoB, southern Andaman Sea and equatorial Indian Ocean

(Naman Deep Singh, S.K. Singh & R. Bhushan)

Paleoproductivity and evidences of ITCZ migration along the equatorial Indian Ocean

The northern Indian Ocean is unique due to its topographical setting and noticeable behavioural pattern with changes in the strong monsoonal winds over the ocean. The equatorial Indian Ocean region experiences distinct signature of both the monsoon and provides an ideal platform to reconstruct the intensities of both the monsoons (SW and NE). In view of this, a sediment core raised off Sri Lanka (∼60 km from the coast) during onboard SK 304A in 2013 was investigated for various geochemical parameters. Sri Lanka is uniquely located within the equatorial belt of the northern Indian Ocean and experiences seasonal reversal of wind and is exposed to both monsoon periods. In the present study, high productivity observed during LGM corroborates well with the globally known low summer insolation in the Northern Hemisphere. The latitudinal migration of ITCZ in response to the alteration in solar insolation has led to weakening of SW monsoon winds and intensification of NE monsoon winds (trade winds). Strong NE trade winds or monsoon winds caused divergence of the surface waters near the SW coast of Sri Lanka resulting in upwelling of nutrient rich deep waters triggering high surface productivity in this region. High productivity is observed during LGM along SW coast of Sri Lanka. After 11 ka, enhanced values associated with increase in terrestrial flux compared with high summer solar insolation indicates strengthened SW monsoon associated with high sediment accumulation rate during 11-9 ka, attesting better preservation of productivity proxies.

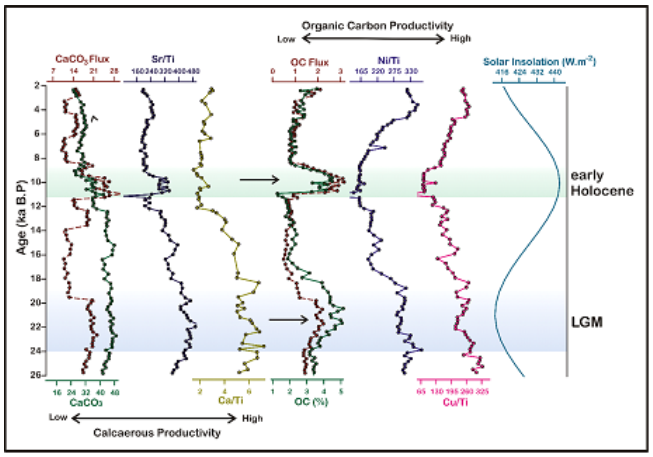

Figure no. 11: (a)Climatic zones (Wet and Dry zones) and shadow areas of Sri Lanka produced by Central Highlands during the monsoons with the location of the core SK-304A/05.(b) (b)Comparison of productivity indices (OC, $CaCO_3$, Ni/Ti, Cu/Ti, Ca/Ti and Sr/Ti ratios) of core SK-304A/05 with mid-summer solar insolation. The red discontinuous line is the flux values. The light blue bar indicates the LGM and light green bar indicate the early Holocene.

(Chandana K.R. and R. Bhushan)

Growth rate variation of Indian corals: An abrupt response to climate change

In past few decades, coral and coral reefs have been found to be most vulnerable due to continuous rise in sea surface temperatures (SST) triggered by natural and anthropogenic activities. Corals thriving near the surface ocean have emerged as potential marine proxy from tropics to study the climate perturbation. Changing intensity of Indian Summer Monsoon (ISM) has significantly influenced the climate and

socio-economic growth of the Indian subcontinent. The anomalies in the ISM have been linked with El Nino Southern Oscillation (ENSO) and Indian Ocean Dipole (IOD) events. Severe impacts of El Nino registered in corals from tropical oceans are in the form of Mass Coral Bleaching Events. Such bleaching events led to reduced growth rates or death of coral colonies. The coral bleaching is a generalized stress, and mass bleaching has been linked with the global SST increase. To identify the influence of ocean atmospheric processes (ENSO and IOD) and global SST rise on ISM, two *Porites* sp. colonies from Kavaratti and Amini Islands of Lakshadweep were investigated. This study demonstrates abrupt reduction in growth rates corresponding to the rise in global SST since 1970. The global known Mass bleaching events (MBE) recorded during 1987, 1998, 2010 has been registered in the form of low growth rates in both the corals. The rainfall too played role in controlling the GR of Amini coral, i.e., high rainfall triggered the enhanced detrital contribution that inhibited the coral growth. On comparing the Growth Rate with climate indices such as ENSO and IOD, it can be underscored that IOD signatures are more prominent and its co-occurrence with ENSO diminished the impacts of ENSO. Further, geochemical and isotopic investigation would provide important clues to comprehend the interconnectivity of ISM-SST-ENSO-IOD relationship.

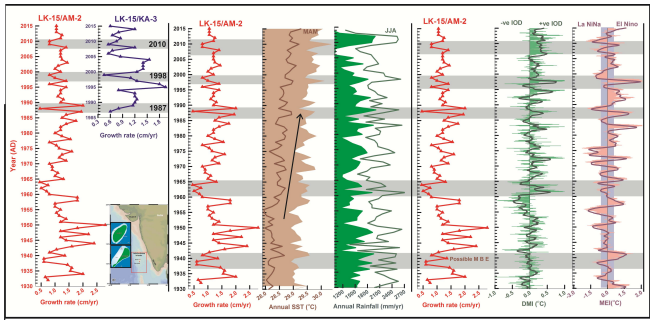

Figure no.12: The growth rate variations for LK-15/AM-2 and LK-15/KA-3 raised from Amini and Kavaratti Island, Lakshadweep. Inset shows the core collection area for both the locations. GR of LK-15/AM-2 has been compared by SST, Rainfall, ENSO and IOD.

(U.S. Banerji, C. Shah & R. Bhushan)

Carbon export flux vs Aeolian flux in the western Arabian Sea during the last 19 ka

Carbon export flux (CEF) or downward transport of particulate organic carbon in ocean is intimately related with the global climate through the modulation of CO_2 in the atmosphere and its influence on the heat budget. Increase in CEF has been suggested as a reason for the reduction in atmospheric CO_2 during Last Glacial Maximum (LGM). In addition, Aeolian flux was assumed as the nutrient supplier for the increased CEF during LGM. The relation between CEF and Aeolian flux has been studied mostly in high nutrient and low chlorophyll (HNLC) regions. Recent studies show that the western Arabian Sea mimics High Nutrient Low Chlorophyll (HNLC) conditions during the peak monsoon season (Naqvi etal., 2010). A sediment core from the western Arabian Sea demonstrates that the CEF was low during 19 to 16 ka BP, indicating low surface productivity. The low productivity in the study area during LGM, as compared to modern, suggests its insignificant role in the biological pump for the reduction of CO_2 during LGM. The CEF increased almost six times from 5 $gC.m^{-2}.y^{-1}$ at 11.7 ka BP to 30 $gC.m^{-2}.y^{-1}$ at 10 ka BP, at the beginning of Holocene suggesting high nutrient conditions in the western Arabian sea due to strengthened upwelling. The aeolian flux and CEF shows a negative correlation from 19 to 11.7 ka BP indicating increase in aeolian flux tends to decrease the surface productivity. This is in contradiction to the conventional understanding that increase in aeolian flux increases micro-nutrient (Iron, Zinc, etc) availability leading to increased productivity. However, the positive relation between aeolian flux and productivity is valid in the presence of excess macronutrients (like Nitrogen, Phosphorous, etc). The availability of macro-nutrients was thus limited in the western Arabian sea during 19 to 11.7 ka BP. The present study suggests that the modern observation of HNLC like condition during southwest monsoon in Arabian Sea was started at the beginning of Holocene. Also, the northern Arabian sea in general and north-western in particular is not a part of the last glacial biological pump that reduced atmospheric CO_2 to LGM levels. *(This work was done in collaboration with Mr. D. Balaji from M.S. University of Baroda, Vadodara)*

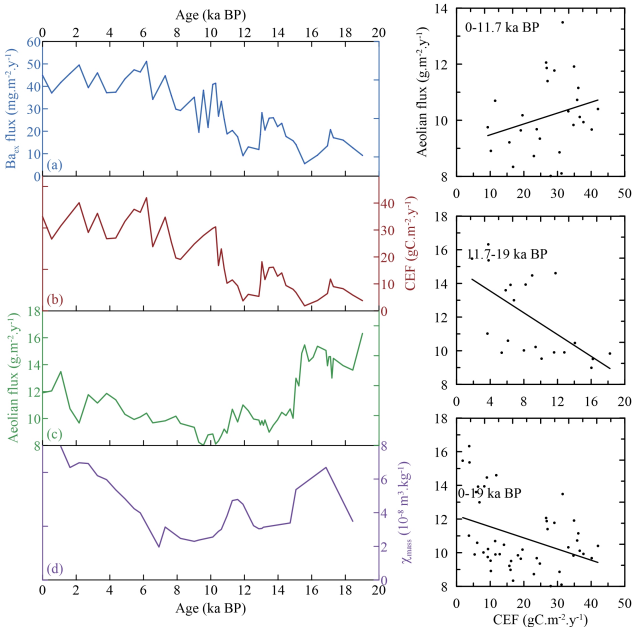

Figure no.13: Temporal variation of productivity and Aeolian flux in the western Arabian sea during the last 18.5ka BP. (a)flux of excess barium, (b)carbon export flux, (c)Aeolian flux and (d)low frequency magnetic susceptibility. Scatter plots on the right side shows the linear relation between carbon export flux and aeolian flux at different time gaps (inset text).

(R. Bhushan)

Fluoride contamination in the Jaisalmer groundwater

Major groundwater resources in the Jaisalmer district of Rajasthan contamination have been assessed for fluoride. All samples have fluoride content above the required limit (1 mg/l) and 62% of the samples were severely contaminated (>1.5 mg/l) (Fig.14). Alarming level of fluoride (up to 7.8 mg/l) has been observed at the major

distributary well in Jaisalmer town. The groundwater samples have been categorised in four categories based on their safety aspects for domestic use (Fig.14): Category-***I*** groundwater being the safest with fluoride and calcium content within permissible limit (F=1-1.5mg/l; Ca=75-200mg/l), Category-***II*** groundwater are calcium deficient but satisfactory as per fluoride concentration, Category-***III*** groundwaters have sufficient calcium and high fluoride and Category-IV groundwater being the worst with high fluoride and low calcium. Only three groundwater samples were safe among the 21 samples. Five groundwater samples each fall in category-***II***and***III***. In category-III, except one other groundwater were found safe. The residence time of groundwater and aquifer lithology are the major controlling factors for the fluoride contamination in the Jaisalmer area. The excess groundwater drawdown at the populated areas also contributes to the high fluoride concentration. Defluorination process should be practiced prior to use of Jaisalmer groundwater. Supporting studies on fluorosis and hypertension in the Jaisalmer district may provide additional information for efficient management of groundwater resources. *This study was done in collaboration with Mr. D. Balaji from M.S. University of Baroda, Vadodara and Prof. J.S. Rathore from Department of Chemistry, J.N.V University, Jodhpur.*

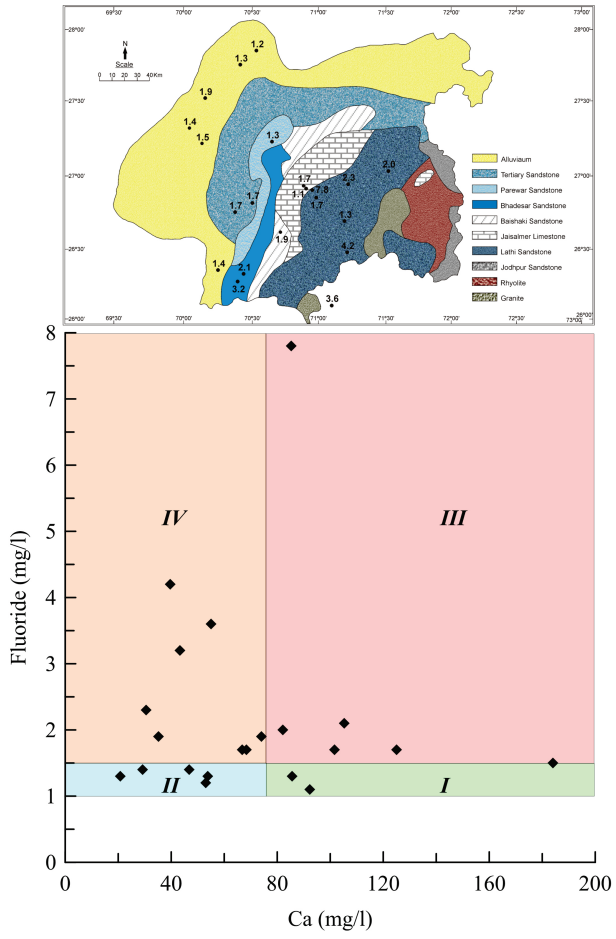

Figure no.14: The hydrogeological map of Jaisalmer district showing sampling sites and their fluoride concentration in mg/l. Categorisation of Jaisalmer groundwater samples based on Fluoride and Calcium concentration.

(R. Bhushan and A.K. Sudheer)

High-resolution mid-Holocene Indian Summer Monsoon (from Central India)

Pproxy based climate reconstruction suggests that magnitude and occurrence of past climate change was not uniform at different locations on the Earth's surface, suggesting inhomogeneity in the forcing mechanisms at regional scales. During the last 10 kyr, climate of the mid-latitude observed rapid change, believed to have been triggered by the internal climate feedback mechanisms, yet to be fully understood. Indian sub-continent, primarily affected by monsoon system needs to be looked for signatures of the rapid variations and the causative mechanism using past records which are rather sparse. A stalagmite that grew in the deep interior part of the Kotumsar cave, Chhattisgarh was used for high resolution δ^{18}O (a proxy of monsoon intensity, more negative values indicate strong monsoon) measurements. The $\sim$3000 year long Mid-Holocene variability record, spanning 8.5 to 5.6 ka, allows us to understand structure of prolonged weak monsoon events at sub-annual to decadal scale (Fig. 15). Most of the significant shifts in monsoon activity are observed to have occurred within few decades followed by multi-centennial prolonged droughts. Ages (U-Th) were obtained from National Taiwan University, Taiwan.

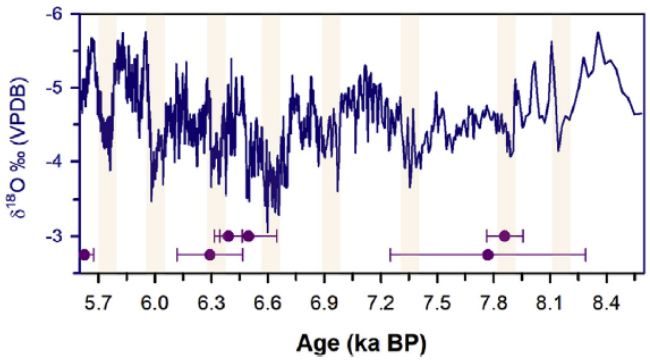

Figure no.15: δ ^{18}O (dark blue) time series of the stalagmite. Ages (purple filled circles) with 2σ error used for developing age model. Shaded orange regions demarcate abrupt decrease in monsoon corresponding to North Atlantic Climate changes.

(S. Band, R. Ramesh & M.G. Yadava)

Composition and characteristics of NR-PM$_1$ using HR-TOF-AMS

Poor understanding on the characteristics and composition of non-refractory PM$_1$(mainly secondary aerosol) leads to large uncertainty in the assessment of their effects on air quality and climate. Towards this, it is important to study and understand their composition, characteristics and temporal evolution in different regions. Present study reports real-time characteristics of non-refractory submicron aerosol (NR-PM$_1$ namely organic aerosol, sulfate, nitrate, ammonium and chloride) using newly procured high-resolution time-of-flight aerosol mass spectrometer (HR-ToF-AMS) during post-monsoon (September, 2017 to October, 2017) season over Ahmedabad (23.0^{o}N, 72.6^{o}E, 49m amsl). In HR-ToF-AMS, ambient air is sampled through a critical orifice into an aerodynamic lens, which focuses particles into a narrow beam. A supersonic expansion at the exit of

the lens accelerates the particles into the sizing region (10^{-5} Torr), where particle size is determined by measuring flight time across a fixed distance. Time zero of particle flight is defined by a rotating mechanical chopper, and the end of particle flight is defined as the time of mass spectrometric detection. Particles are vaporized by impaction on a resistively heated surface ($\sim$600°C) and ionized by electron ionization (70 eV). Only NR species are vaporized, and detected with multichannel plate (MCP) detector. The HR-ToF-AMS includes ion optics for two modes of operation, referred to as V- and W-modes. Here, V-mode is a standard reflectron-ToF-MS configuration in which ions follow a trajectory from the extraction region into the reflectron and back to the multichannel plate (MCP) detector (effective ion path length *L*=1.3 m). In W-mode, ions exiting the reflectron are directed into a hard mirror, which focuses them back into the reflectron for a second pass before travelling to the MCP detector (*L*=2.9 m). All the species of NR-PM_1 showed increasing trends in their mass concentrations over Ahmedabad with higher slope for organic aerosol(OA). These changes in concentrations of species reflect the role of local/regional sources and atmospheric processes in loading of aerosol in the atmosphere. OA was observed to be dominant contributor to NR-PM_1 with the contribution of more than 50% during the study period. Evolution and composition of bulk OA was also studied. Scatter plot (also known as triangle plot) between f44 (signal at m/z 44 to total organic signal) and f43 (signal at m/z 43 to total organic signal) is often used to study the evolution of oxygenated organic aerosol over a given site. Triangle plot of the data collected over Ahmedabad is shown in Fig.16. All the data obtained during the present study fall within the triangular space marked with dashed line, which is characteristics of ambient measurements. The m/z 44 is mostly due to acids or acid derived species whereas, m/z 43 is predominantly referred to non-acid oxygenates. Higher f44 and lower f43 associated with more oxidized and aged aerosol whereas lower f44 and higher f43 values referred to less oxidized and fresh secondary/organics. Fig.16 suggests that the OA over Ahmedabad is a mixture of fresh and aged OA.

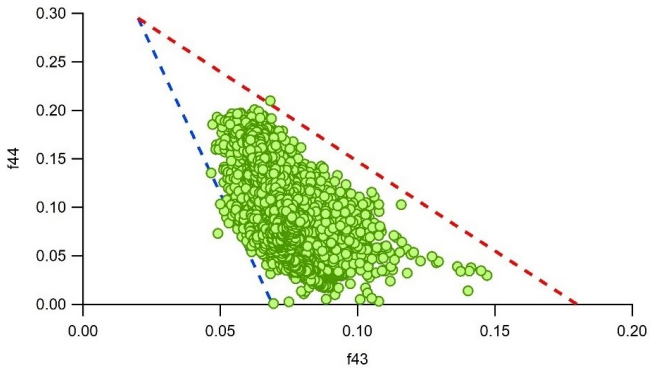

Figure no.16: Triangle plot depicting oxygenated and non-oxygenated OA

(Atinderpal Singh, R.V. Satish & N. Rastogi)

Change in Brown Carbon Spectral Characteristics during Paddy-Residue Burning over the Indo-Gangetic Plain

$PM_{2.5}$ samples were collected using high volume air sampler before, during and after a large-scale paddy-residue burning period over Patiala (30.2 $^{\circ}$N,76.3°E, 250m amsl), a site located in the Indo-Gangetic Plain (IGP). Subsequently, brown carbon (BrC) absorption spectra of water- and methanol-soluble particles were measured using liquid waveguide capillary cell and a portable UV-visible spectrophotometer. In addition, levoglucosan, major cations and anions, total organic carbon (OC), water-soluble OC (WSOC), and elemental carbon (EC) were also measured using standard techniques. $PM_{2.5}$ concentration ranged from $\sim$90 to 500μg m^{-3} (avg$\pm$sd230$\pm$114) during the study period with the average values of 154$\pm$57, 271$\pm$122, 156$\pm$18μg m^{-3} during pre-burning, burning and post-burning periods, respectively. Levoglucosan and K^+ (tracers of biomass burning, BB) showed a strong correlation with each other with a slope different than those reported for domestic wood burning, savanna fires, and bio-fuel in literature. It is suggested that the observed ratio (slope, close to 1) can be used as a fingerprint of emissions from the paddy-residue burning over the IGP. Further, the absorption coefficient of BrC at 365 nm (b_{abs_365}), was assessed from absorption spectra of water-soluble ($b_{abs\_365\_water}$) and methanol-soluble ($b_{abs\_365\_methanol}$) OC. Subsequently, mass absorption efficiencies (MAE) of light absorbing water-soluble (MAE_{BrC_water}) and methanol-soluble ($MAE_{BrC\_methanol}$) fraction of organic carbon were estimated. Observed $MAE_{BrC\_methanol}$ was about 1.5, 1.9 and 1.9 times higher than MAE_{BrC_water} during pre-burning, burning, and post-burning periods, respectively. It suggests that there is a significant and variable fraction of water-insoluble BrC over the IGP. Further, water- and methanol-soluble BrC during burning period exhibited different spectral behavior compared to that during pre- and post-burning period, reflecting different characteristics of BB derived BrC. Such studies have important implications in assessing the effect of BrC on climate. *Logistic support for the sample collection was provided by Dr. Atinderpal Singh and Prof. Darshan Singh (Punjabi University, Patiala).*

(R.V. Satish and N. Rastogi)

Oxidative potential of ambient particulate matter over Mount Abu

Role of particulate matter (PM) has been well documented in causing cardiopulmonary diseases because of their redox active nature that can generate reactive oxygen species (ROS) *in situ* in human body. Capacity of PM to catalyze *in situ* formation of ROS is known as their oxidative potential (OP). However, studies on OP of PM over different regions are scarce. Towards this, PM_{10} samples were collected over Mount Abu (24.6°N, 72.7°E, 1680m asl) during 10^{th} March 2014 to 25^{th} May 2016. These samples were analyzed for carbonaceous aerosol, major ions and dithiothreitol (DTT)-based OP. All the data were classified into four seasons based on prevailing meteorological conditionswinter (December–January), spring (February–April), pre-monsoon (May–June) and post-monsoon (October-November). PM_{10} mass concentration varied from 29 to 273μg m^{-3} during the study period. Seasonally averaged ($\pm 1\sigma$) volume normalized OP (OP_v) were 0.76$\pm$0.52, 1.44$\pm$0.48 , 1.04$\pm$0.57, and 1.69$\pm$0.80 nmol DTT min^{-1} m^{-3}, and mass normalized OP (OP_m) were 14$\pm$8, 14$\pm$7, 10$\pm$7, and 23$\pm$9 pmol DTT min^{-1} µg^{-1}during winter, spring, pre-monsoon and post-monsoon, respectively. The OP_v values found in this study (range0.09-3.04 nmol DTT min^{-1} m^{-3}) are somewhat higher than those documented over Los Angeles and Beijing, and similar to those reported over

Orinda and Patiala. Highest $OP_m$and OP_v values were found during post-monsoon (October-November), which is attributable to long-range transport of anthropogenically emitted pollutants brought by the NE air masses. It was observed that source(s) emitting elemental carbon also emit other species which are several times more DTT active than those emitted along with anthropogenically derived inorganics.

(A. Patel and N. Rastogi)

Effect of a tidal cycle on biogeochemistry of a mangrove dominated tropical estuary (Sundarbans, India)

Based on a 24-hour observation at a fixed location, a study was carried out to investigate the effect of a tidal cycle on nitrogen and carbon biogeochemistry of a mangrove dominated tropical estuary (Sundarbans) located in the eastern part of India. Salinity, dissolved oxygen and pH showed clear variability with tidal fluctuations with respective maximum during flood tide. On diurnal scale, dissolved silicate and inorganic nitrogen showed effects of marine and freshwaters mixing, which was missing for dissolved inorganic phosphate. Dissolved inorganic carbon (DIC) concentrations varied over a narrow range (1.92-2.19 mM) with relatively higher values during ebb-tide; reverse trend, however, was noticed for $\delta^{13}C_{DIC}$ with significant variability (–4.27 to –2.21‰).

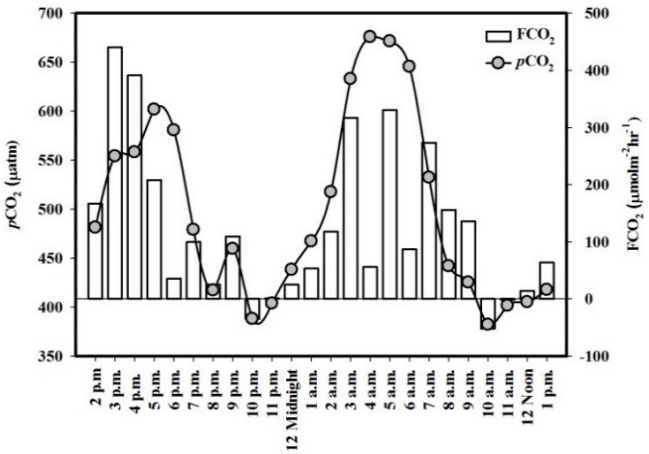

Figure no. 17: Variation in pCO_2 and FCO_2 during a tidal cycle in Sundarbans.

Evidences for significant effects of ground or pore water discharge and organic carbon mineralization on estuarine DIC pool was observed throughout. Dissolved organic carbon, being mostly biogeochemically controlled, showed no significant variability with tidal fluctuations; however, possibility of photo-oxidation was noticed. Both particulate organic carbon and nitrogen concentrations reached maximum during ebb-tide with stable isotopic compositions showing predominantly marine signature along with possibility of biogeochemical modifications within the estuary. Being largely regulated by marine and freshwater mixing as well as organic carbon mineralization throughout, significantly higher pCO_2 was found during ebb tide phase (Fig. 17). Integrating the mean diurnal emission flux of CO_2over entire surface area of the estuaries of Sundarbans (1800 km^2) results into emission of 87.2Gg CO_2 (≈23.8 GgC) annually to the regional atmosphere, which is ∼0.003% to global C emission via humid tropical forest annually.

(M.K. Dutta and S. Kumar)

Laser fluorination technique to measure oxygen isotopes in silicates

In early 90s, Zachary Sharp developed laser fluorination technique to extract oxygen from silicates (rock, minerals, and biogenic silica) where IR laser (CO_2 laser) was used as a heat source. Later, this technique was modified by Kusakabe (2004). Our system at PRL is similar to modified version of Kusakabe (2004) system, which consists of stainless steel reaction chamber and tube lines along with two small glass tubes with zeolite for purification of oxygen. The reaction chamber is covered with BaF_2 glass window for vacuum sealing. In the reaction chamber, BrF_5 gas is used for reaction with silicate samples placed on nickel sample holder. Initially, the chamber is filled with BrF_5 gas (∼100 torr) and left for the · -1 hour for pre-fluorination to remove atmospheric moisture adsorbed on BaF_2 glass window surface and samples. Residual gas is pumped out. Again, about 100 torr BrF_5 gas is filled into the chamber and sample is ablazed with laser by increasing its power. After the laser fluorination, except oxygen, other condensable gases (BrF_5, BrF_3, SiF_4) are trapped into the line at liquid nitrogen temperature. Only oxygen and minute amount of F_2remains in the line where F_2 is removed by the fluorine getter containing coarse-grained Salt kept at 150°. The purified O_2 is finally trapped into the molecular sieve 13X cold finger at liquid nitrogen temperature, which is finally released to the mass spectrometer by heating the molecular sieve with heat gun. This system at PRL is on test mode. So far, after a lot of effort, we have analysed NBS quartz 28 with $\delta^{18}O$ = 9.54±0.2‰(n=7), whose IAEA reported value is 9.57±0.1‰. Efforts are being carried out to obtain more precise values for both $\delta^{18}O$ and $\delta^{17}O$.

(A. Rahman and S. Kumar)

Anthropogenic perturbations to carbon fluxes in Asian river systems

Human activities are drastically altering water and material flows in river systems across Asia. These anthropogenic perturbations have rarely been linked to the carbon(C) fluxes of Asian rivers that may account for up to 40–50% of the global fluxes. As part of multi-country project funded by Asia Pacific Network for Global Change (APN), a review was conducted to provide a conceptual framework for assessing human impacts on Asian river C fluxes, along with an update on anthropogenic alterations of riverine C fluxes. Drawing on case studies conducted in three selected rivers (the Ganges, Mekong, and Yellow River) and other major Asian rivers, the review focused on the impacts of river impoundment and pollution on CO_2 outgassing from the rivers draining South, Southeast, and East Asian regions that account for the largest fraction of river discharge and C exports from Asia and Oceania. Although the municipal wastewater constitutes only 1% of the renewable surface water, it can disproportionately

affect the receiving river water, particularly downstream of rapidly 40 expanding metropolitan areas, resulting in eutrophication, increases in the amount and lability of organic C, and pulse emissions of CO_2 and other GHGs. In rivers draining highly populated urban centers, lower reaches and tributaries tended to exhibit higher levels of organic C and the partial pressure of CO_2 (*p*CO2) than less impacted upstream reaches and eutrophic impounded reaches, often plagued by frequent algal blooms and pulsatile CO_2 emissions from urban tributaries delivering high loads of wastewater. More field measurements of pCO_2, together with accurate flux calculations based on river-specific 45 model parameters, are required to provide more accurate estimates of GHG emissions from the Asian rivers that are now under represented in the global C budgets.

This Study was carried out as an International collaborative program funded by Asia Pacific Network for Global Change.

(S. Kumar)

Gross nitrogen transformation rates in forest soils of the Western Ghats, India

Primary productivity on land and ocean collectively acts as a major sink for anthropogenic CO_2 present in the atmosphere. Tropical forests behave as a net carbon sink and contribute to approximately 25% of the global and 55% of the terrestrial C sequestration. The productivity of the plant species present in a forest is controlled by the availability of nutrients in the system. The availability of nutrient in any ecosystem is dependent on many factors including the climate, micro fauna, temperature and rainfall conditions of the region.Nitrogen behaves as a limiting nutrient for the primary productivity in many of the ecosystems because its availability is solely controlled by microbial processes. An experiment was conducted in the hot and humid tropical forest soils of the Western Ghats, India for determination of gross nitrogen transformations by using ^{15}N isotope dilution technique. The study provides an insight into the nutrient profile and nutrient exchange in the forest soils of the Western Ghats. The sampling was carried out at five different locations and from two depths (0-20 cm and 20-40 cm) to understand the nutrient dynamics in and among the depth profiles. The soils showed low gross mineralization (2.4$\pm$1.0 mg N kg^{-1} d^{-1}) and gross nitrification (1.6 $\pm$1.0 mg N kg^{-1} d^{-1}) rates in the top soil layers which further decreased with depth. The results indicated a very high concentration of $NH_4{}^+$ (up to 33 $mgkg^{-1}$ $NH_4{}^+$-N) and a few hotspots of available $NO_3{}^-$ in the surface layer of these forest soils, which suggests the presence of additional sources of mineral nitrogen other than the internal nutrient recycling in the forest soils. Similar to the mineralization pattern, the gross nitrification rates also showed very distinct values for top and bottom layers of the soil. The overall consumption of both $NH_4{}^+$ and $NO_3{}^-$ exceeded the production rates in these soils, even with the presence of high ambient nutrient concentrations. This indicates the presence of a nutrient conservation mechanism, especially for $NH_4{}^+$, adapted by the microbes present in these systems.

(N. Sharma and S. Kumar)

Dissolved inorganic carbon (DIC) dynamics in Asia's largest brackish water lagoon

Identifying the mechanisms controlling DIC variability in estuarine environments is important to understand C biogeochemistry. Isotopic composition of C in DIC ($\delta\ ^{13}C_{DIC}$) is particularly important for distinguishing and tracing sources, sinks and transformations of C in the water column and for identifying benthic-pelagic coupling. During the present study, samples were collected during three different seasons to understand the DIC dynamics in the Chilika lagoon. The Chilika lagoon in the east coast of India is in the transition zone of Bay of Bengal and tributaries of Mahanadi River. Previous studies suggested various sectors of the lagoon to be heterotrophic during monsoon season pointing towards the existence of hotspots for CO_2 emission. The results of this study pointed towards existence of different processes during different seasons in the Chilika. Calcite dissolution was found to be an active process throughout the year, whereas degradation of organic matter appeared to play a limited role. Primary production during postmonsoon was the dominant process modulating DIC dynamics and outgassing played a significant role during premonsoon.

(R. Mukherjee and S. Kumar)

Integrated Scanning Electron Microscopy and Micro Raman Spectrometry (SEM-μ Raman

An integrated Scanning Electron Microscope integrated with Micro-Raman Spectrometer (SEM-Raman) to identify and characterize the rock forming mineral was installed at Physical Research Laboratory, Ahmedabad, India (Fig.18).

Figure no.18: Laboratory for SEM-μ Raman Spectrometer

The Raman spectroscopy is a molecular spectroscopy, where interaction of electromagnetic radiation with the atoms or molecules is observed. This is a non-destructive technique where the characteristic Raman shifts (wave numbers) enable us acquiring the structural information and chemical fingerprint for any rock forming mineral. For the micron size samples the unique SEM-Raman system can provide information about material's the degree of crystallinity, unit cell information as well as the structural and compositional variations.

The complete system a Scanning Electron Microscope (SEM) (model JEOL IT300) integrated with a HybriScan Molecular Microscope (HSCMM_21) from HybriScan Technologies B.V. The HSCMM_21 is a dispersive Raman micro spectrometer based on a 785 nm diode laser and back-thinned CCD detector. A scan stage with a fast 25 nm step resolution enables Raman imaging of user-defined areas. The optical microscope objective in the HSCMM_21 is designed for a vacuum environment and optimized for Raman light scattering. The light collection strength or numerical aperture is 0.65 and the spatial resolution of the confocal Raman micro-spectrometer is 1 µm in the lateral direction and 6 μm in the axial direction (for transparent materials). The Raman spectral signals are collected within the range 280 cm^{-1} to 2400 cm^{-1} with a spectral resolution better than 5 cm^{-1} Raman shift. The Raman hyper-spectral images are generated with 30 mW, 785 nm excitation, 1s exposure time.

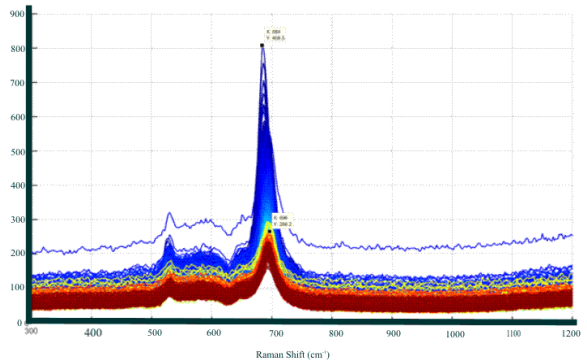

Figure no. 19: Spectra generated using 30mW 785nm excitation for chromite mineral. One can see the Raman shift in the band around 685cm^{-1}.

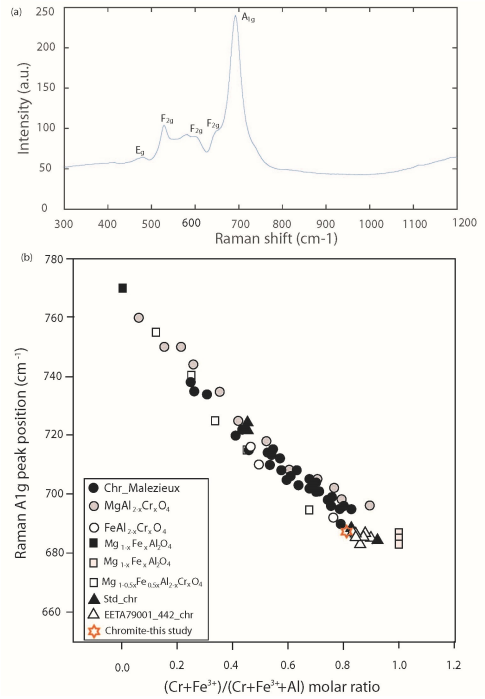

Figure no. 20: Identification of Raman bands with proper band assignment.

In order to check the functionality of this analytical instrument a pre-studied chromite mineral from a spinel group was analysed. A total number of 5508 spectra were acquired for Raman analyses and finally yield the single average spectra using on a 1μm grid. The typical Raman spectra is shown in Fig.19. Further characterization of material in terms of specific mineral is carried out by identifying the characteristic various Raman shifts.

In the present study we observed the most prominent the 685cm^{-1} peak, which is produced by the bonds of (Cr^{3+}, Fe^{3+}, Al^{3+})O6 octahedra. The other bands around 200-300 cm^{-1}, 480-520 cm^{-1} and 600 cm^{-1} are diagnostic for first, second and third symmetry of species.

(A.D. Shukla)

Palaeocene-Eocene Thermal Maximum (PETM) in shallow-marine successions of the Jaisalmer carbonate platform, Rajasthan, Western India.

The Paleocene–Eocene Thermal Maximum (PETM; 55 Ma), representing the extreme warming event in the Cenozoic Era, is of particular interest to the Geoscientists as it is considered as an analog to the present climate change. The Khuiala Formation of the Jaisalmer basin represents shallow marine Paleocene-Eocene sequences on the basis of index fossil and other evidences. This sedimentary succession offer a rare opportunity to learn about the PETM and its impact on the shallow-water ecosystems. Geochemical analysis of selected elements were analysed in the carbonate samples along with USGS rock standard BHVO-2 following standard HF-HNO_3 dissolution technique in Savillex Teflon vials. Carbon and oxygen isotopic analysis in carbonate samples were performed using continuous flow isotope ratio mass spectrometer (MAT 253) attached to a Gas-Bench system where samples were treated with 100% orthophosphoric acid. For Sr isotope analysis the silicate fraction of the samples, together with known amount of ^{84}Sr spike was digested completely using HF-HNO_3 −HCl acids. Pure fractions of Sr were separated from the solution using conventional column chromatography. Measurements of Sr isotopes were carried out using Thermo Neptune MC-ICP-MS in static multi collection mode.

In the studied carbonate samples, the Mn and Sr concentrations and low Mn/Sr ratio ($<$1) together with the stable and radiogenic isotope data suggest that they are pristine with little diagenetic alterations and have retained their primary isotopic signatures. The occurrence of *Numulites burdigalensis*and the values of ^{87}Sr/^{86}Sr minimum 0.70833) indicate a Paleogene interval for the studied stratigraphic succession. Here, we use carbon and oxygen isotope data to determine a high-resolution paleoclimatic record for the PETM.A prominent negative excursion inδ ^{13}C curves of bulk-rock (-3‰) is interpreted as the carbon isotope excursion during the PETM. Also, the δ ^{18}O (-6.4 to -9.3‰), values are very similar to PETM carbonate values in the studied samples. All these evidences indicate that the Khuiala Formation of the Jaisalmer basin, India preserves shallow marine PETM signatures those are very limited throughout the world. The detailed work is under progress in order to understand the larger benthic foraminiferal biostratigraphy and stable isotope systematics, in interpreting effects of PETM on the biota of the Jaisalmer basin, India.

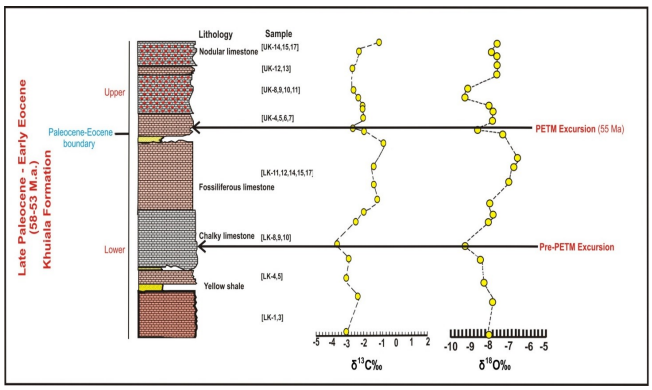

Figure no. 21: Profile of C and O across the PETM sequences in Khuiala Formation, Jaislmer Basin, Rajasthan.

(A.Patra, S. Kumar & A.D. Shukla)

Mukundpura Meteorite: a new carbonaceous Chondrite fall in India

Mukundpura is a new CM chondrite fell near Jaipur, Rajasthan, India on June 6, 2017 at 5:15 IST (Fig. 22).

Figure no. 22: The Mukundpura Meteorite

The fall was observed by local villager. According to eyewitnesses, the meteorite was fragmented into several pieces once the object hit the ground. Once the meteorite hit and penetrated a few cm into ground, the single object broke in to several fragments of different sizes and shapes. Due to the landing of this meteorite a pit of $\sim$15 cm in diameter and 10 cm in depth was formed on the agricultural field. The macroscopic examination suggests that this is black colour, covered with dull, black fusion crust. Thickness of the fusion crust is $\sim$2 mm and highly friable. One can observe the interior is imbedded with white/grey minerals. Megascopically, the meteorite is fine grained, coherent and studded with grey white silicate minerals. Chondrules are often discernible and easy to delineate. Texture occasionally appears as clast-rich. Petrographic characters of Mukundpura invoke a clast-rich, CM carbonaceous chondrite and petrologic type 2. Majority of chondrules are similar to chemically type I chondrule, i.e. high MgO olivine (Fa $<$ 1 mol%). Chondrules are surrounded by compact, fine grained accretionary rim which may be attributed towards its formation in the dusty region of solar nebula. Iron rich olivine generally occurs as barred olivine type and also as isolated grains within the matrix. Spinel is the dominant refractory inclusion. Abundance of secondary minerals (phyllosilicates), a clast and carbonates in matrix suggest Mukundpura has undergone modest aqueous alteration. However, locally matrix of Mukundpura appears to be experienced extensive but not pervasive alteration. Evidences of thermal metamorphism are apparently absent. The metals and silicates within the chondrule are largely pristine and likely to escape from any alteration effect. Comparing the bulk elemental composition especially the REE abundances of Mukundpura shows good agreement with the CM carbonaceous chondrite (type 2).

(A.D. Shukla and D. Ray)

Niche construction by non-diazotrophic cyanobacteria for dinitrogen fixation

Diazotrophic cyanobacteria, a source of bioavailabile nitrogen by definition, flourish in warm oceans when phosphate and iron nutrients are available. However, some of the phosphate depleted warm waters of the Atlantic Ocean are mysteriously known for their existence of diazotrophs. Upwelling fluxes, atmospheric deposition and river inputs are depleted in phosphate compared to nitrate in this region. Hence, the reasons behind the source of sustained phosphate supply for dizotrophy in this region are not known. We have discovered that non-diazotrphic cyanobacteria create an environment of excess phosphate for their diazotrophic phylum group members. In an environment of sustained phosphate supply in the oligotrophic waters, iron inputs seem to determine the magnitude of nitrogen fixing rates. *This work was done in collaboration with co-workers from GEOMAR, Germany.*

(A. Singh)

Secondary organic aerosol formation over coastal ocean:Inferences from atmospheric water-soluble low molecular weight organic compounds

Lack of consensus on the distributions and formation pathways of secondary organic aerosols (SOA) over oceanic regions, downwind of pollution sources, limits our ability to assess their climate impact on a global scale. As a case study, we studied water-soluble SOA components such as dicarboxylic acids, oxocarboxylic acids and α-dicarbonyls in the continental outflows from the Indo-Gangetic Plain (IGP) and Southeast Asia (SEA) to the Bay of Bengal. Oxalic acid (C_2) is the dominant species followed by succinic (C_4) and glyoxylic acids (ωC_2) in the outflow. Non-sea-salt SO_4^{2-} dominates ($\sim$70%) total water-soluble inorganic constituents and correlates well with aerosol liquid water content (LWC) and C_2, indicating their production through aqueous phase photochemical reactions. Furthermore, mass ratios of dicarboxylic acids (C_2/C_4, $C_2/\omega C_2$), and their relative abundances in water soluble organic carbon (WSOC) and total organic carbon

(OC) are quite similar between the two continental outflows (IGP and SEA), indicating the formation of SOA through aqueous phase photochemical reactions in LWC-enriched aerosols, largely controlled by anthropogenic SO_4^{2-}. The high abundance of oxalic acid over the open ocean could influence the CCN activity, affecting cloud albedo and lifetime and have implications to aerosol-cloud interactions and SOA formation over coastal ocean. noindent *This study was done in collaboration with Prof K. Kawamura, Hokkaido University, Sapporo, Japan.*

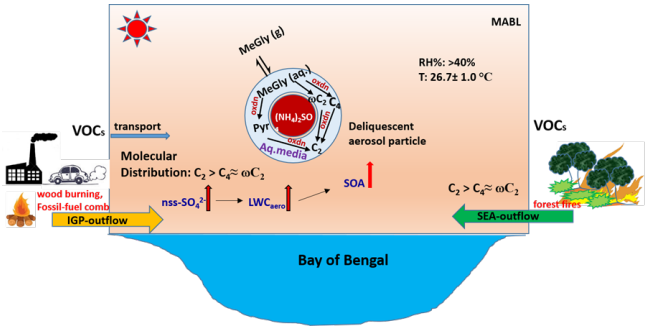

Figure no. 23A conceptual perspective of formation of dicarboxylic acids over Bay of Bengal is shown. /noindent **C_2=oxalic acid**; **C_3=Malonic acid; C_4Succinic acid; ωC_2glyoxylic acid; PyrPyruvic acid; MeGly = methylglyoxal.**

(B. Srinivas and M.M. Sarin)

Nitrogen dry-deposition to the Ocean

Anthropogenic nitrogen(N) emissions to the atmosphere have significantly increased the deposition of nitrate(NO_3^{--}) and ammonium (NH_4^+) to the surface waters of the open ocean, with potential impacts on marine productivity and the global carbon cycle. Global-scale understanding of the impacts of N deposition to the oceans is reliant on our ability to produce and validate models of nitrogen emission, atmospheric chemistry,transport and deposition. Assessment of the impacts of atmospheric N deposition on the ocean requires atmospheric chemical transport models to assess deposition fluxes.In this study, designed by participants of GESAMP Working Group Workshop, a unique dataset of particulate NO_3^{--} and NH_4^+ concentrations in the marine atmosphere was compiled based on about 2900 samples from the eastern tropical North Atlantic, the northern Indian Ocean and northwest Pacific. In these three ocean regions, the density and distribution of observational data were considered sufficient to provide effective comparison to model products. All these regions are affected by transport and deposition of mineral dust, which alters the deposition of N, due to uptake of nitrogen oxides (NOx) on mineral surfaces.

The data were mapped to 5^0 x 5^0 grid cells and annual average concentrations were calculated for each cell. Dry deposition fluxes for each cell were calculated from these average concentrations. The gridded concentrations and calculated dry deposition fluxes were compared with two different model products: the ACCMIP (Atmospheric Chemistry and Climate Model Inter-comparison Project) multi-model mean products of NOy and NHx dry deposition, and the TM4 (Tracer Model 4 of the Environmental Chemical Processes Laboratory) model of NOy and NHx deposition fluxes and NO_3^{--} and NH_4^+ aerosol concentrations and deposition fluxes.

Comparisons of deposition fluxes of oxidized N (NOy) and reduced N (NHx) from the ACCMIP-MMM product and from TM4 with observation-derived fluxes (CalDep) show similar performances for both products, with significant over estimation of the lower levels of observed NH_4^+ deposition fluxes. Mod-Dep of NO_3^{--} and NH_4^+ from TM4 show much better agreement with CalDep than NOy and NHx, which is consistent with significant contributions of gaseous deposition to NOy and NHx deposition fluxes. Recommendations are made for improvements in N deposition estimation through changes in observations, modelling and model–observation comparison procedures. *This joint work was carried out as part of GESAMP-WG Workshop held at UEA, Norwich(UK).*

(M.M. Sarin & A. Singh)

Changing Atmospheric Acidity and the oceanic solubility of nutrients

The atmosphere has already been through a major phase of anthropogenic acidification due to the emissions of SO_2 and NOx to the atmosphere from combustion sources. This acidification has been offset to some extent by neutralisation associated with ammonia emissions which come mainly from agriculture. Vigorous regulatory efforts over the last few decades have greatly decreased SO_2 emissions, and the impact of NOx control measures on cars have meant that NOx emissions from these have been stabilising. However, continuing intensification of agriculture has increased ammonia emissions. The combined effect of these changes in emissions is a steady reduction in atmospheric acidification. This process has reduced acidity in many areas of the world and may even lead to alkaline rain in long term. The solubility of several key ocean nutrients (particularly Fe and P) which are mineral aerosol bound is very sensitive to pH, and hence changing atmospheric acidity has the potential to change the inputs of bioavailable soluble nutrients in the future. GESAMP-Working Group Workshop held at University of East Anglia, Norwich, UK (Feb 27-Mar 2, 2017), with my participation as Co-Chair, considered this issue and its effects on ocean biogeochemistry, utilising a wide range of approaches from fundamental chemistry, through modelling, to field work. As a specific approach, impacts of changes in atmospheric acidity on Fe solubility in aerosols was reviewed to synthesize the current scientific information.

Aerosol Fe solubility can be affected by acidic species. The production of sulphate (SO_4) may be promoted via catalytic oxidation of SO_2 by minerals in cloud water or on the surface of fine particles with NO_x. Nitric acid (HNO_3) is formed in the atmosphere by the reaction of nitrogen dioxide (NO_2) with hydroxyl radical (OH), which is enhanced under high temperature and solar radiation via photochemical reactions. Mineral dust contains ferrihydrite on the surface (about 1% of Fe solubility) and delivers insignificant labile Fe fluxes to the oceans in present days. An increase in Fe solubility has been observed up to about 2% in the vicinity of dust sources, suggesting the variability of labile Fe content in soils and the effects of atmospheric processes on dust properties. Further away from the source regions,Fe solubility for dust-dominated aerosols is enhanced up to about 10%, which is much larger than the variability of labile Fe content in soils. Significant correlations have been

observed between bulk Fe solubility and concentration of acidic species over the Indo-Gangetic Plain suggesting acid processing of Fe-containing mineral aerosols (Srinivas et al 2014). At the same time, elevated levels of Fe solubility more than 10% have been observed in aerosols dominated by combustion sources (Srinivas et al., 2012). Aerosols from combustion sources are dominated by fine-mode particles that usually have high Fe fractional solubility and low loading. It has been inferred that Fe-containing aerosols from fossil fuel combustion are highly acidic and thus supply labile Fe. However, it is somewhat uncertain as to how important the changes in atmospheric acidity can influence Fe solubility from aluminosilicate mineral lattices to labile Fe. Furthermore, there are large uncertainties associated with Fe solubility for fly ash at initial rapid release of Fe sulfate and nanoparticles as well as subsequent dissolution rates of aluminosilicate glass. The knowledge of the specific mineral properties (e.g., chemical composition, specific Fe content, and its dissolution rate) is a key factor in reducing uncertainties in the prediction of Fe solubility changes due to atmospheric processing. A conceptual scenario (past, present and future) of the influence of changing source strengths on atmospheric acidity, aerosol chemical processing and deposition of labile nutrients to the ocean and their impacts is shown in Fig.24.

This work was carried out as Member of UN/GESAMP-Working Group #38 on "Atmospheric input of chemicals to the ocean".

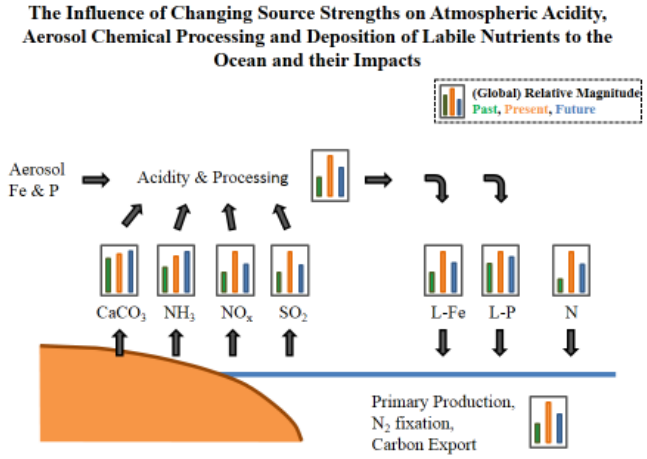

Figure no. 24It shows of changing Source Strengths on Atmospheric Acidity, Aerosol Chemical Processing and Deposition of Labile Nutrients to the Ocean and their Impacts.

(M.M. Sarin)

ˇRole of Aerosol pH on NH_3 partitioning to particulate phase

It was hypothesized recently that gaseous ammonia plays a major role in nearly quantitative neutralizing the aerosol acidity, caused by SO_4^{2-} and NO_3^- species. This significantly increases the aqueous phase SO_2 oxidation mediated via NO_2.

$$2NO_{2(aq)} + HSO_3^-{}_{(aq)} + H_2O_{(aq)}\ 3H^+{}_{(aq)} + 2NO_2^-{}_{(aq)} + SO_4^{2-}{}_{(aq)}$$

This process can substantially contribute to the incorporation of gaseous NH_3 as well as NO_2 to particulate phase, thereby influence the net deposition fluxes of N-species if the same is applicable globally. Hence, it is important to evaluate the possibility for such pathways in different environmental conditions with varying aerosol composition. The key parameters that control the NO_2 mediated aqueous phase oxidation of SO_2 is aerosol liquid water content and aerosol pH. Cation to anion ratio, NH_4^+/SO_4^{2-} ratio or $NH_4^+/(SO_4^{2-}+NO_3^-)$ ratio are generally used as index for aerosol pH or aerosol acidity in the ambient atmosphere. H^+ ion concentrations are also calculated from the pH of the deionized water extract of aerosol sample and used for the quantitative representation of aerosol pH. But, all these parameters either do not consider the chemical equilibrium of these ionic constituents or modulated by large dilution, compared to actual pH of deliquescent droplet particle in the air. Hence, we explored the possibility of elevated pH due to high concentrations of ambient NH_3, using thermodynamic equilibrium model ISORROPIA II and aerosol ionic composition and ambient NH_3 data from Kochi. The model output of H^+ ion concentration in air ($H^+{}_{air}$) and aerosol liquid water content is used for calculating aerosol pH.

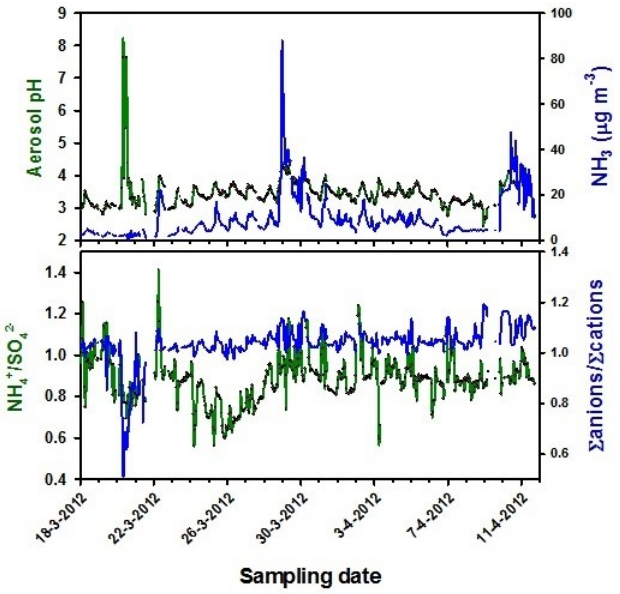

Figure no. 25: Temporal variation in (a)Aerosol pH and NH_3 (b)Nh_4^+/SO_4^{2-} ratio and anion to cation ratio.

Except for a few hours of 20 March (Fig. 25), the pH was varying between 3 and 4. The elevated pH above 7 was observed on 20 March only during high levels of crustal elements like Ca^{2+} or Na^+ concentration (only 4 data points) which is not a general trend. The temporal trend of both NH_3 and aerosol pH suggest the variability in ambient NH_3 can influence the pH. But, it may be noted that when concentration of NH_3 is highest, more than 80 μg m^{-3}, but the total ionic balance is not an absolute indicator of aerosol neutral pH. NH_4^+/SO_4^{2-} ratio indicate overall deficiency of ammonia, but it also provides misleading trend with respect to aerosol pH. Hence, the neutral or alkaline pH does not prevail in deliquescent particle over the study region and SO_2 oxidation mechanisms proposed by earlier studies based on laboratory experiments at pH $\sim$7 may not be a significant process for nitrogen incorporation in the particle phase.

(A. K. Sudheer)

An Automated Instrument For Separation Of Rare Earth Elements&Strontium By Ion Exchange Chromatography

Rubidium(Rb), Strontium(Sr) and Rare Earth Elements(REE) along with their isotopic composition have a wide range of application in studies of Earth surface and Oceanographic processes. REEs are also useful to constrain high temperature fractionation and redox conditions during planetary evolution. Similarly, the decay of long-lived radionuclide ^{87}Rb to stable ^{87}Sr has also been applied to the radiometric age determinations of rocks and minerals. However, these elements do not exist in pure form naturally and must be separated to their pure form from matrices before accurate measurements using mass spectrometric techniques because of mass interference. Although separation protocol by ion chromatography is well established, it requires significant manual efforts and time. Here, we have designed an automated equipment (Fig.26) to carry out such a separation procedure for Sr and REE fractions from aqueous samples. The equipment follows the separation protocol and provision of three simultaneous column separation units to increase the sample throughput. It comprises of syringe pumps, multi position valves, fraction collectors, appropriate column and integrated controlled software (Fig.27). All the components have been tested independently and integration and calibration of all components as complete unit is currently being performed. Once the equipment is calibrated, it can carry out sequence of samples with minimal user intervention.

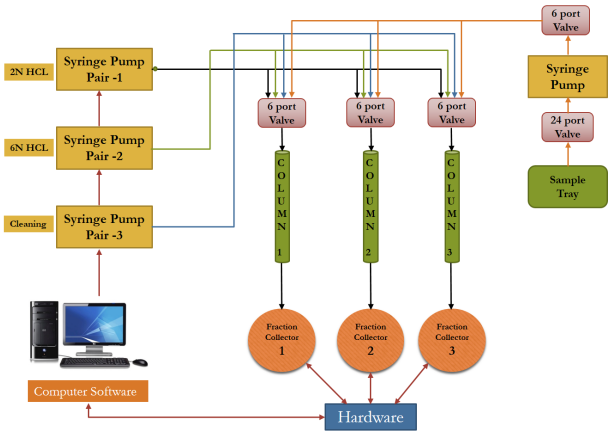

Figure no. 26: Block diagram of instrument

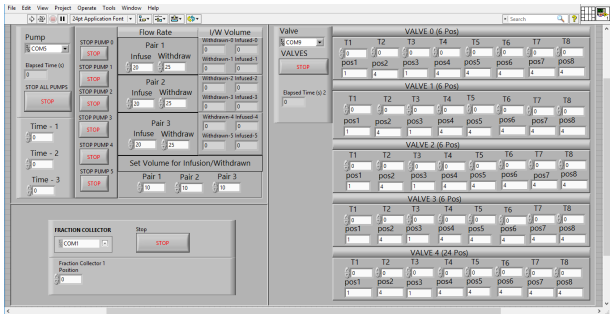

Figure no. 27: Control Software for calibration

(M. Shah, A.K. Sudheer, S.K. Singh & H. Vaghela)

^{234}Th/^{238}U and ^{210}Po/^{210}Pb activity ratios in a hydrothermal vent region along the Southwest Indian Ridge System

Vertical profiles of naturally occurring particle-reactive radionuclides (^{234}Th, ^{210}Po and ^{210}Pb) in seawater were measured at two stations in submarine hydrothermal vent region along the southwest Indian ridge (SWIR) system, during November 2015, as a part of the Indian GEOTRACES program to estimate the POC export flux from the euphotic zone and the particle dynamic characteristics within the hydrothermal plume over the SWIR (Fig. 28).

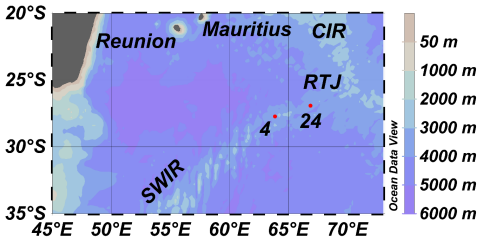

Figure no. 28: Location map of two stations (Sta. 4 and 24) sampled for particle-reactive radionuclides in the Southwest Indian Ridge (SWIR) system. The Rodriguez triple junction (RTJ) and the southern extent of the Central Indian Ridge (CIR) are also shown.

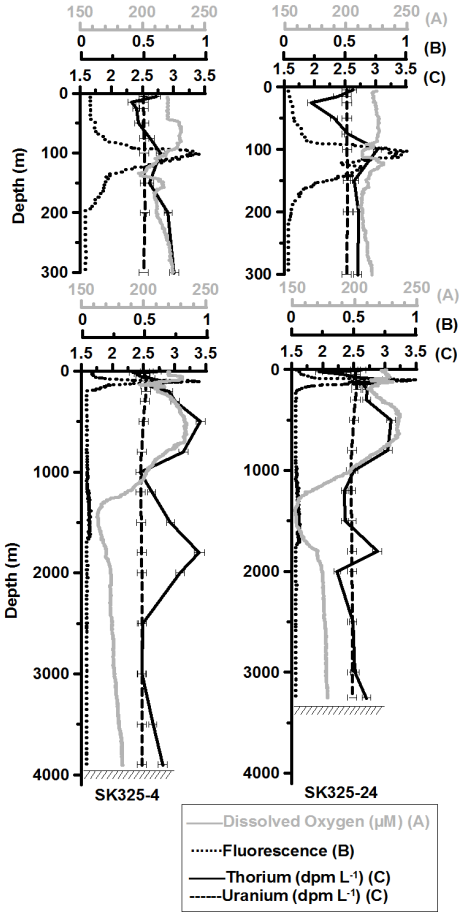

Figure no.29: Vertical seawater profiles of ^{234}Th, ^{238}U, Fluorescence and Dissolved Oxygen from two stations (Sta. 4 and 24) in the SWIR system. The upper figure shows data only for the top 300 m.

The ^{234}Th activity varied from 1.94±0.05 to 3.41±0.07 dpm L^{-1} (Fig. 29). The modest ^{234}Th deficit found in the upper ocean was followed by ^{234}Th excess from 75 to 800 m, 1200 to 2000 m and 3000 m to bottom of the water column. The POC/^{234}Th ratio on particulates was 1.14±0.07 and 1.80±0.11 μmol dpm^{-1}, the depth integrated ^{234}Th deficit flux was negligible and 271±91 dpm m^{-2} d^{-1} and the ^{234}Th based POC export flux was negligible and 0.5±0.2 mmol m^{-2} d^{-1}, for Sta. 4 and 24, respectively. On the other hand, continuous deficit of ^{210}Po with respect to ^{210}Pb was observed from surface to bottom of the water column. However, an increase in ^{210}Po and ^{210}Pb activity was recorded in the intermediate depths (1200 m to 2000 m). The POC/^{210}Po ratio was 280±30 and 292±24 μmol dpm^{-1},the depth integrated ^{210}Po deficit flux was 20±1.2 and 31±1.2 dpm m^{-2} d^{-1} and the ^{210}Po based POC export flux was 5.5±0.6 and 9.1±0.7 mmol m^{-2} d^{-1}, for Sta. 4 and 24, respectively. Organic matter remineralization, hydrothermal plume intrusion and suspension of solids from seamounts and seawater-sediment interface are possible causes in regulating the ^{234}Th/^{238}U and ^{210}Po/^{210}Pb activity ratios in the water column.

(R. Rengarajan and S. Anand)

Science

Theoretical Physics

A Novel Effect of Electron Spin Resonance on Electrical Resistivity

We extend the well known phenomenon of magnetoresistance (extra resistivity of materials in transverse magnetic field) to a new and unexplored regime where in addition to a transverse mag- netic field, a transverse AC field of resonant frequency is also applied. In a magnetic field, electron spin levels are Zeeman split. In a resonant AC field, we uncover a new channel of momentum re- laxation in which electrons in upper Zeeman level can deexcite to lower Zeeman level by generating spin fluctuation excitation in the lattice (similar to what happens in Electron Spin Resonance (ESR) spectroscopy). An additional resistivity due to this novel mechanism is predicted in which momentum randomization of Zeeman split electrons happen via bosonic excitations (spin fluctuations). An order of magnitude of this additional resistivity is calculated. The whole work is based upon an extension of Einstein's derivation of equilibrium Planckian formula to near equilibrium systems.

(L. Rani and N. Singh)

The Memory Function Formalism: A Review

An introduction to the Zwanzig-Mori-Gotze-Wolfle memory function formalism (or generalized Drude formalism) is presented. This formalism is used extensively in analyzing the experimentally obtained optical conductivity of strongly correlated systems like cuprates and Iron based super- conductors etc. For a broader perspective both the generalised Langevin equation approach and the projection operator approach for the memory function formalism are given. The GW perturbative expansion of memory function is presented and its application to the computation of the dynamical conductivity of metals is also reviewd. This review of the formalism contains all the mathematical details for pedagogical purposes.

(K. Kumari and N. Singh)

Probing Effect of Nonstandard interactions in determining CP sensitvity of future experiments

We studied the effect of non-standard interactions (NSI) on the propagation ofneutrinos through matter and how it affects the CP sensitivity of the proposed DUNE experiment. We consider the special case when the diagonal NSI parameter $\epsilon_{ee} = -1$ and cancels the standard matter effect. If in addition there is maximal CP violation, as suggested by data, then this gives rise to an exact intrinsic hierarchy degeneracy, in the appearance channel, irrespective of thebaseline and energy. I Overall, given the current model independent limitson NSI parameters, no hierarchy sensitivity can be observed in the DUNE experiment if NSIs exist in nature. How this degeneracy affects the CP snesitivity is studied in detail.

(S. Goswami, K. N. Deepthi and N. Nath)

Spotlighting the sensitivities of future neutrino oscillation experiments DUNE, T2HK, T2HKK and ESS

Neutrino oscillation physics has entered the precision era and the potential forthcoming experiments Hyper-Kamiokande, Deep Under-ground Neutrino Experiment (DUNE) and European Spalllation Sorurce procject (ESSνSB) are expected to lead this endeavor. We performed a comprehensive comparative study of the octant, mass hierarchy and CP discovery sensitivities of DUNE, T2HK & T2HKK and ESSνSB in their individual capacity and investigated the synergies of the aforementioned experiments. We present a comparative account of the probabilities at the three baselines and explore in detail the physics issues which can cause the differences in the sensitivities among the various experiments. We also find out the optimal exposure required by these experiments for achieving 5σ hierarchy and octant sensitivity and to discover CP violation at 5σ for 60% values of $\delta_{\rm CP}$. In addition we vary the neutrino-antineutrino runtime ratios for T2HK & T2HKK and check if the sensitivities are affected significantly due to this.

(S. Goswami, K. Chakraborty and K. N. Deepthi)

Probing partial $\mu - \tau$ symmetry in future neutrino oscillation experiments

We study origin, consequences and testability of a hypothesis of 'partial $\mu - \tau$' reflection symmetry. This symmetry predicts $|\mathrm{U}_{\mu_i}| = |\mathrm{U}\tau_i| (i = 1,2,3)$ for a single column of the leptonic mixing matrix U. Depending on whether this symmetry holds for the first or second column of U different correlations between θ_{23} and δ_{CP} can be obtained. This symmetry can be obtained using discrete flavour symmetries. In particular, all the subgroups of SU(3) with 3-dimensional irreducible representation which are classified as class C or D can lead to partial $\mu - \tau$ reflection symmetry. We show how the predictions of this symmetry compare with the allowed area in the $\sin^2\theta_{23} - \delta_{cp}$ plane as obtained from the global analysis of neutrino oscillation data. Furthermore, we study the possibility of testing these symmetries at the proposed DUNE and Hyper-Kamiokande (HK) experiments (T2HK, T2HKK), by incorporating the correlations between θ_{23} and δ_{CP} predicted by the symmetries. We find that when simulated data of DUNE and HyperKamiokande is fitted with the symmetry predictions, the $\theta_{23} - \delta_{cp}$ parameter space gets largely restricted near the CP conserving values of δ_{CP} . Finally, we illustrate the capability of these experiments to distinguish between the two cases leading to partial $\mu - \tau$ symmetry.

(S. Goswami, K. Chakravorty, K. N. Deepthi, A. Joshipura and N. Nath)

U(1) extended inverse seesaw Model for Neutrino Mass, Dark matter and Vacuum Stability

We consider Standard Model extended by an U(1) gauge group and outline a model which can give neutrino masses by the Inverse seesaw mechanism. The model contains additions fermion and scalar singlets. We study the effect on the stability of the electroweak vacuum and consider the possibiity of a fermionic Dark matter. In this case the neutrino mass is generated through the minimal inverse seesaw scenario. The parameter space consistent with all experimental observations is being explored.

(This work is done in collaboration with A. Das and T. Nomura of Korea Institute of Advanced Study).

(S. Goswami and K. N. Visnhudath)

Scrutinizing R-parity violating interactions in light of $\mathrm{R}_{\mathrm{K}^{(*)}}$ data

LHCb collaboration's observation of lepton flavour non-universality (expected to be universal within the standard model) in the $\mathrm{B} \to \mathrm{K}^*\ell^+\ell^-$ ($\ell = e, \mu$) modes strengthens the similar observation earlier obtained in $\mathrm{B} \to \mathrm{K}\ell^+\ell^-$ decays. Whether it is due to new physics is not immediately clear. Within the context of R-parity violating supersymmetric standard model, these modes are systematically studied, including the one loop generated Wilson coefficients, usually ignored. It is shown that, consistent with other constraints, there is a region in parameter space that allows for a simultaneous explanation of these anomalies.

(D. Das, C. Hati, G. Kumar and N. Mahajan)

Decaying atmospheric neutrinos at INO

Neutrino oscillation solution to atmospheric neutirno problem is well established now and the focus has shifted to probe if subdominat solution to oscillations can be probed by future experiments. We explore how the hierarchy and octant sensitvity are affected in presence of neutrino decay and oscillations.

This work is done in collaboration with Sandhya Choubey from Harish-Chandra Research Institute and Tarak Thakore from Louisianna State University, US.

(S. Goswami, C. Gupta and L. S. Mohan)

A_4 flavour symmetry in the context of Left-Right Symmetric models

Understanding of pattern of neutrino masses and mixing is still an open challenge in particle physics. In this regard, the minimal left-right symmetry is one such scenario which naturally embeds various seesaw mechanism to explain tiny neutrino mass. On the other hand, discrete flavour symmetries (for example A_4, S_4) are widely used to explain observed neutrino mixing. Hence we are working on a model based on left-right symmetry embedded in A_4 discrete symmetry to simultaneously explain observed neutrino mixing and tiny neutrino mass. We are also studying role such flavour symmetry in CP violation (Dirac CP phase δ) in neutrino sector as well as in neutrinoless double beta decay. Furthermore, we are also exploring the possibility of extending flavour symmetry for sterile neutrinos too.

(S. Goswami, B. Karmakar and K.N. Vishnudath)

A Leptoquark explanation for $(g-2)_\mu$, R_{K}, $\mathrm{R}_{\mathrm{K}^*}$ and, IceCube PeV events

In a concrete and consistent leptoquark model, an attempt is made to seek a simultaneous solution to various anomalous observations, which taken on the face value seem totally unrelated. The muon anomalous magnetic moment and B-decay anomalies have been addressed earlier in the literature. However, combining them with the PeV energy events seen at the IceCube experiment was not attempted earlier. It is found that all these can be simultaneously addressed. However, the conclusions change drastically once the leptoquark searches at LHC are included. This seems to be a general feature, not restricted to the leptoquark model adopted here.

(B. Chauhan, B. Kindra and A. Narang)

Determining form factors and Wilson coefficients using $\mathrm{B} \to \mathrm{K}^*\mu^+\mu^-$ data

The recent anomalies in the $b \to s\mu^+\mu^-$ mediated decay modes is taken as a serious hint of physics beyond the standard model.

However, it is also known that there are unaccounted non-perturbative QCD contributions, whose size is not easy to even estimate. The question that is asked and studied is whether there can be a data driven method to carefully evaluate the extent to which the hadronic form factors are reliable. Using the data, expected to be collected and analysed in detail in near future, the form factors and their ratios are extracted in the low energy transfer region. This is the region that is theoretically cleanest. The same data is utilised to extract combinations of Wilson coefficients. The advantage of such a method is that it does not rely on any particular model dependent assumptions.

(B. Kindra and N. Mahajan)

Invoking Chiral Vector Leptoquark to explain LFU violation in B Decays

The flavour anomalies, as observed by various experiments, could possibly be addressed by leptoquarks. The LHCb observation of lepton flavour non-universality in $\mathrm{B}_c \to \mathrm{J}/\psi\tau\nu_\tau$ mode compared to the e or μ mode is studied. Though the errors at quite large at this moment, within 2σ, there is a consistent explanation of this discrepancy and also $\mathrm{R}_{\mathrm{D}^{(*)}}$, as well as $\mathrm{R}_{\mathrm{K}^{(*)}}$ data.

(B. Chauhan and B. Kindra)

Predictions of Angular Observables for $\mathrm{B} \to \rho\ell\ell$ and $\mathrm{B}_s \to \mathrm{K}^*\ell\ell$ in Standard Model

In recent years, quark level $b \to s\ell\ell$ transitions have shown discrepancies in some of the angular observables, which are strong hints of new physics. However, the analogous $b \to d\ell\ell$ modes have received little attention. The advantage of the latter modes is the large CP violation within the standard model itself. The first detailed predictions of the angular observables are provided for the two relevant modes: $\mathrm{B} \to \rho\ell\ell$ and $\mathrm{B}_s \to \mathrm{K}^*\ell\ell$. The branching ratio of $\mathrm{B}_s \to \mathrm{K}^*\ell\ell$ is in good agreement with the recent preliminary result presented by LHCb collaboration

(B. Kindra and N. Mahajan)

Electromagnetic charge radius of the pion at high precision

A determination of the pion charge radius from high precision data on the pion vector form factor from both timelike and spacelike regions, using a novel formalism based on analyticity and unitarity is presented. The phase shifts, via the Roy equations, in $\pi\pi$ scattering are used as inputs and the experimental uncertainties are implemented by Monte-Carlo simulations. The results, which do not rely on a specific parametrization, are optimal for the given input information and do not depend on the unknown phase of the form factor above the first inelastic threshold. The prediction for the charge radius of the pion is $r_\pi = (0.657pm0.003)fm$, which amounts to an increase in precision by a factor of about 2.7 compared to the PDG average.

(D. Das, B. Ananthanarayan and I. Caprini)

Heavy quark complex potential in a strongly magnetized hot QGP medium

We study the effect of strong constant magnetic field, generated in relativistic heavy ion collisions, on the heavy quark complex potential. We work in the strong magnetic field limit with lowest Landau level approximation. We find that the screening of the real part of the potential increases with the increase in the magnetic field. Therefore, we expect less binding of heavy quark antiquark pair in the presence of strong magnetic field. The imaginary part of the potential increases in magnitude with the increase in magnetic field, leading to a increase of the width of the quarkonium state with the magnetic field. All of these effects results in the early dissociation of quarkonia states in a magnetized hot quark-gluon plasma medium.

(B. Singh, L. Thakur and H. Mishra)

Chiral symmetry breaking , color superconductivity and gapless modes in charge neutral magnetised quark matter

We discuss chiral symmetry breaking and color superconductivity in dense quark matter using an explicit varitional costruct for the ground state with quark antiquark as well as quark quark pairs. The asatz function are detrmined through a minimisation of the thermodynamic potential. The effect of magnetic field is also taken into account. The equation of state of such magnetised charge netral matter is calculated. Imposing the charge neutrality condition leads to gapless modes where the superconducting gap is non zero but the excitation energy can vanish. The equation of state so calculated can be used for neutron star structure. The gapless modes can be very important for the transport properties of such matter.

(A. Abhishek and H. Mishra)

Thermoelectric effect of hot and dense hadronic matter

It is known that a temperature gradient in a conducting medium can generate electric field which is known as thermoelectric effect. Seeback coefficient is a measure of this relation between thermal and electrical conductivity. This effect can be important for heavy ion collision particularly at finite baryon density. We have estimated the seeback cofficient for hadronic matter within hadron resonannce gas model which increases with chemical potential demonstrating the importance of such effect in generating electromagnetic field in heavy ion collisions like FAIR or at NICA.

(J.R. Bhatt, A. Das and H. Mishra)

Perfect fluid nature in weakly-interacting magnetized quark matter

We have investigated shear viscosity of quark matter in presence of a strong uniform magnetic field background where

Nambu-Jona-Lasinio model has been considered to describe the magneto-thermodynamical properties of the medium. In presence of magnetic field, shear viscosity coefficient gets splitted into different components because of anisotropy in tangential stress of the fluid. Those splitted components normalized by entropy density in fact measure the fluidity of magnetized quark matter. A nearly perfect fluid nature is found even in weakly interacting quark matter at high temperature and high magnetic field zone which is not possible in the case of vanishing magnetic field. Our results indicate that the magnetic field may be regarded as one of the possible sources that can increase the fluidity of quark matter.

(S. Ghosh, B. Chatterjee, P. Mohanty, A. Mukharjee and H. Mishra)

Finite temperature expansion dynamics of Bose–Einstein condensates in ring traps

We explore the effects of finite temperature on the dynamics of Bose-Einstein condensates (BECs) after it is released from the confining potential. In addition, we examine the variation in the expansion dynamics of the BECs as the confining potential is transformed from a multiply to a simply connected geometry. To include the effects of finite temperatures we use the frozen thermal cloud approximation, and observe unique features of the condensate density distribution when released from the confining potential. We find that at $\mathrm{T} \neq 0$, during the initial stages of expansion, the multiply connected condensate has more pronounced interference rings compared to the case of zero temperature. Such difference in the dynamical evolution is also evident for simply connected condensates.

(A. Roy and D. Angom)

Bifurcations, stability and mode evolution in segregated quasi-2D condensate mixtures

We present new features of low energy Bogoliubov quasiparticle excitations of a two component Bose-Einstein condensate (TBEC) in quasi-2D geometry at zero temperature using Hartree-Fock-Bogoliubov (HFB) formalism. We, in particular, consider the TBECs of ^{133}Cs -^{87}Rb and ^{85}Rb -^{87}Rb, and show specific features in the low energy excitation spectrum as a function of the interaction strength. For ^{85}Rb -^{87}Rb TBEC, the appearance of a new zero energy mode is observed. Whereas for ^{133}Cs -^{87}Rb TBEC we report a bifurcation of the slosh mode at the point of transition from miscible to immiscible domain. The lower energy mode, after the bifurcation, goes soft and becomes a new Nambu-Goldstone mode of the system.

(S. Pal, A. Roy and D. Angom)

Dynamics of phase separation in two-species Bose-Einstein condensates with vortices

We examine the dynamics associated with the miscibility-immiscibility transition of trapped two-species Bose-Einstein condensates (TBECs) of dilute atomic gases in presence of vortices. In particular, we consider TBECs of Rb hyperfine states, and Rb-Cs mixture. In the case of a singly charged vortex in only one of the condensates, there is enhancement when the vortex is present in the species which occupies the edges at phase-separation. But, suppression occurs when the vortex is in the species which occupies the core region. To examine the role of the vortex, we quench the inter-species interactions to drive the TBECs from miscible to immiscible phase, and use the time dependent Gross-Pitaevskii equation to probe the phenomenon of phase-separation. We also examine the effects of higher charged vortex to phase-separation.

Work done in collaboration with Dr. Arko Roy from Max-Planck-Institut für Physik komplexer Systeme, Dresden, Germany.

(S. Bandyopadhyay and D. Angom)

Ramifications of topology and thermal fluctuations in quasi-2D condensates

We explore the topological transformation of quasi-two-dimensional Bose-Einstein condensates of dilute atomic gases, and changes in the collective modes as the confining potential is modified from rotationally-symmetric multiply connected to multiply connected with broken rotational symmetry and ultimately to a simply connected geometry. In particular, we show that the condensate density, and the non-condensate density arising from the quantum fluctuations follow the transition in the geometry of the confining potential. The non-condensate density arising from the thermal fluctuations, in contrast, remain multiply connected when the thermal energy exceeds the maximum value in the basin of the confining potential. Otherwise, both the condensate and non-condensate densities become simply connected. The topology of the non-condensate densities are determined by the thermal energy, the repulsive interaction energy between atoms, and the trapping potential energy. In particular, the origin of the difference lies in the structure of the low-energy collective modes, which we examine using the Hartree-Fock-Bogoliubov formalism. We, then use the Hartree-Fock-Bogoliubov theory with the Popov approximation to investigate the density, and the momentum distribution associated with the thermal fluctuations.

(A. Roy and D. Angom)

Collective modes in multicomponent condensates with anisotropy

We report the effects of anisotropy in the confining potential on two component Bose-Einstein condensates (TBECs) through the properties of the low energy quasiparticle excitations. Starting from generalized Gross Pitaevskii equation, we obtain the Bogoliubov de-Gennes (BdG) equation for TBECs using the Hartree-Fock-Bogoliubov (HFB) theory. Based on this theory, we present the influence of radial anisotropy on TBECs in the immiscible or the phase-separated domain. In particular, the TBECs of ^{85}Rb -^{87}Rb and ^{133}Cs -^{87}Rb TBECs are chosen as specific examples of the two possible interface geometries, shell-structured and side by side, in the immiscible domain. We also show that the dispersion relation for the TBEC shell-structured interface has two

branches, and anisotropy modifies the energy scale and structure of the two branches.

Work done in collaboration with Dr. Arko Roy from Max-Planck-Institut für Physik komplexer Systeme, Dresden, Germany.

(S. Pal and D. Angom)

Demystifying the compressed top squark region with kinematic variables

The ongoing perplexing scenario with no hints of new physics at the Large Hadron Collider can be elucidated amicably if the exotic particle spectrum in many of the well-motivated theoretical models possesses degenerate mass. We investigate the usefulness of different kinematic variables sensitive to the compressed mass region, and propose a search strategy considering a phenomenological supersymmetric scenario where the top squark undergoes a four-body decay due to its extremely narrow mass difference with the lightest supersymmetric particle. Considering a challenging but relatively clean dileptonic decay channel, we demonstrate that one can effectively restrain the significant background from the top quark, which provides a complementary approach to the present CMS analysis. With the new strategic approach the current limit can be extended to a phase-space region that was not explored before.

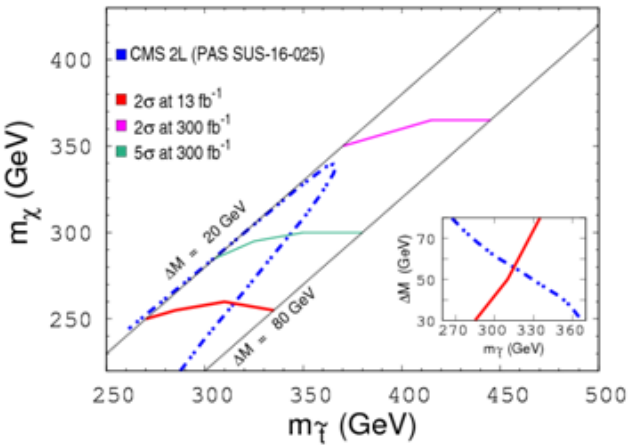

Figure 1: Exclusion limit in terms of top squark and lightest neutralino masses with 13 and 300 fb^{-1} data and discovery plot for 300 fb^{-1} data are demonstrated . Efficiency of newly constructed variables such as M_{bl}, $\mathrm{R}_{b\mathrm{E}}$. $\mathrm{R}_{l\mathrm{E}}$ and $\mathrm{M}_{\mathrm{T2}}(bll)$ are demonstrated showing significant improvements in exploring compressed scenario where traditional detections are difficult and less efficient.

(P. Konar, T. Mondal, A.K. Swain)

Search for a compressed supersymmetric spectrum with a light Gravitino

Presence of the light gravitino as dark matter candidate in a supersymmetric (SUSY) model opens up interesting collider signatures consisting of one or more hard photons together with multiple jets and missing transverse energy from the cascade decay. We investigate such signals at the 13 TeV LHC in presence of compressed SUSY spectra, consistent with the Higgs mass as well as collider and dark matter constraints. We analyse and compare the discovery potential in different benchmark scenarios consisting of both compressed and uncompressed SUSY spectra, considering different levels of compression and intermediate decay modes. Our conclusion is that compressed spectra upto 2.5 TeV are likely to be probed even before the high luminosity run of LHC. Kinematic variables are also suggested, which offer distinction between compressed and uncompressed spectra yielding similar event rates for photons + multi-jets + Missing ET.

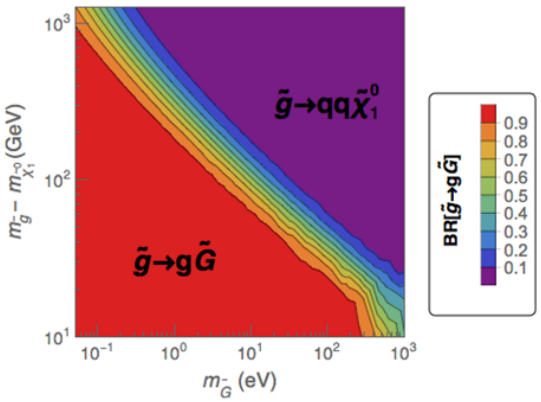

Figure 2: Variation of different modes of Branching Ratios and the fraction shown colour coded in a plane consist of gluino and lightest neutralino mass difference and the gravitino mass.

This work was done in collaboration with Dutta, J., Mondal, S., Mukhopadhyaya, B. and Rai, S.K from HRI, Allahabad.

(P. Konar)

Jet substructure shedding light on heavy Majorana neutrinos at the LHC

The existence of tiny neutrino masses and flavor mixings can be explained naturally in various seesaw models, many of which typically having additional Majorana type SM gauge singlet right handed neutrinos (N). If they are at around the electroweak scale and furnished with sizeable mixings with light active neutrinos, they can be produced at high energy colliders, such as the Large Hadron Collider (LHC). A characteristic signature would be same sign lepton pairs, violating lepton number, together with light jets – $pp \to \mathrm{N}\ell^{\pm}, \mathrm{N} \to \ell^{\pm}\mathrm{W}^{\mp}, \mathrm{W}^{\mp} \to jj$. We propose a new search strategy utilising jet substructure techniques, observing that for a heavy right handed neutrino mass M_{N} much above $\mathrm{M}_{\mathrm{W}^{\pm}}$, the two jets coming out of the boosted $\mathrm{W}^{\pm}$ may be interpreted as a single fat-jet (J). Hence, the distinguishing signal topology will be $\ell^{\pm}\ell^{\pm}\mathrm{J}$. Performing a comprehensive study of the different signal regions along with complete background analysis, in tandem with detector level simulations, we compute statistical significance limits. We find that heavy neutrinos can be explored effectively for mass ranges 300 GeV $\leq \mathrm{M}_{\mathrm{N}} \leq 800$ GeV and different light-heavy neutrino mixing $|\mathrm{V}_{\mu\mathrm{N}}|^2$. At the 13 TeV LHC with 3000 fb^{-1} integrated luminosity

one can competently explore mixing angles much below present LHC limits, and moreover exceed bounds from electroweak precision data.

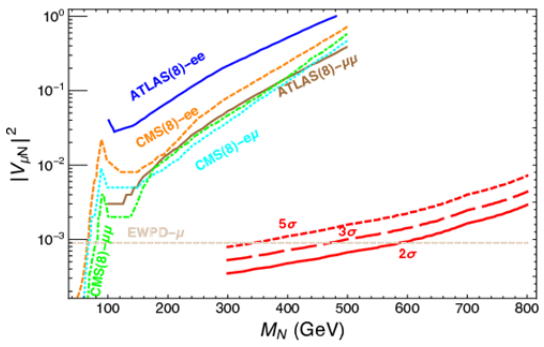

Figure 3: Exclusion limit in terms of heavy neutrino mass M_N and the mixing $|V_{\mu N}|^2$ at the 13 TeV LHC with other available limits.

This work was done in collaboration with A. Das from KIAS, Seoul, Korea and A. Thalapillil of IISER, Pune.

(P. Konar)

Revisiting CMB constraints on warm inflation

We revisit the constraints that Planck 2015 temperature, polarization and lensing data impose on the parameters of warm inflation. To this end, we study warm inflation driven by a single scalar field with a quartic self interaction potential in the weak dissipative regime. We analyse the effect of the parameters of warm inflation, namely, the inflaton self coupling λ and the inflaton dissipation parameter QP on the CMB angular power spectrum. We constrain λ and QP for 50 and 60 number of e-foldings with the full Planck 2015 data (TT, TE, EE + lowP and lensing) by performing a Markov-Chain Monte Carlo analysis using the publicly available code CosmoMC and obtain the joint as well as marginalized distributions of those parameters. We present our results in the form of mean and 68 % confidence limits on the parameters and also highlight the degeneracy between λ and QP in our analysis. From this analysis we show how warm inflation parameters can be well constrained using the Planck 2015 data.

This work was carried out in collaboration with G. Goswami of Ahmedabad University and J. Prasad IUCAA, Pune.

(R. Arya, A. Dasgupta, and R. Rangarajan)

Science

Atomic, Molecular and Optical Physics

High power, higher order ultrafast hollow Gaussian beams

We report on linear and nonlinear generation of ultrafast hollow Gaussian beams (HGB_s). Using only two spiral phase plates (SPP_s) having phase variation corresponding to vortex orders, l=1 and 2, and an experimental scheme, we have generated high power, ultrafast HGB_s of orders up to 3 at 1064 nm. Based on single-pass, frequency doubling of the HGB_s in a 5 mm long, MgO doped, periodically poled $\mathrm{L}i\mathrm{N}b\mathrm{O}_3$ (MgO:PPLN) crystal, we have produced HGB_s of average output power in excess of 250 mW at 532 nm and order as high as 6. Experimentally, we verified that the frequency doubled HGB_s have orders twice those of the pump HGB_s. Like the Gaussian beams, the HGB_s of all orders have an optimum focusing condition for the highest conversion efficiency. On the contrary to previous reports, we observed that the propagation of the vortex beam of order, l, through a SPP corresponding to the vortex order of, -l, results in HGB_s of the same order, $|l|$.

(Apurv Chaitanya N., Amrit Chaitanya, J. Banerjii, and G. K. Samanta)

High power, high repetition rate, tunable broadband mid-IR source based on single-pass optical parametric generation of a femtosecond laser

We report on single-pass optical parametric generation for high power, high repetition rate (RR), ultrafast broadband optical radiation in the mid-IR. Taking advantage of broad phase-matching bandwidth (BW) of the crystals for the interacting waves having zero group velocity mismatch, we have used a 50 mm long MgO-doped periodically poled $\mathrm{L}i\mathrm{N}b\mathrm{O}_3$ crystal to develop a single-pass, parametric source producing femtosecond output pulses at a RR of 78 MHz. Pumping with a femtosecond Yb-fiber laser at 1064 nm, the source produces signal and idler radiation tunable across 1422-1561 nm and 4229-3342 nm, respectively. The signal radiation has a pulse and spectral BW of 296 fs and 9.2 nm centered at 1492 nm, respectively, with a time-BW product ~ 0.37, close to the transform limit. The idler radiation has spectral BW as high as 123 nm centered at 3709 nm. The source produces a signal (idler) beam of power of 2.07 W (0.54 W) at 1492 nm (3709 nm) in a Gaussian spatial profile with peak-to-peak passive power fluctuation better than 5% (4%) over 4 h at a single-pass conversion efficiency as high as $\sim 55\%$.

(A. Aadhi, and G. K. Samanta)

Direct transfer of classical nonseparable states into hybrid entangled two photon states

Hybrid entangled states, having entanglement between different degrees-of-freedom (DoF) of a particle pair, are of great interest for quantum information science and communication protocols. Among different DoFs, the hybrid entangled states encoded with polarization and orbital angular momentum (OAM) allow the generation of qubit-qudit entangled states, macroscopic entanglement with very high quanta of OAM and improvement in angular resolution in remote sensing. Till date, such hybrid entangled states are generated by using a high-fidelity polarization entangled states and subsequent imprinting of chosen amount of OAM using suitable mode converters such as spatial light modulator in complicated experimental schemes. Given that the entangled sources have feeble number of photons, loss of photons during imprinting of OAM using diffractive optical elements limits the use of such hybrid states for practical applications. Here we report, on a simple generic experimental scheme to generate hybrid entangled states in polarization and OAM through direct transfer of classical nonseparable states of the pump beam in parametric down conversion process. As a proof of principle, using local non-separable pump states of OAM mode $l = 3$, we have produced quantum hybrid entangled states with entanglement witness parameter of $\sim 1.25 \pm 0.03$ violating by 8 standard deviation.

(M. V. Jabir, Apurv Chaitanya N., Manoj Mathew, and G. K. Samanta)

Continuous-wave, singly resonant parametric oscillator-based mid-infrared optical vortex source

We report on a high-power, continuous-wave source of optical vortices tunable in the mid-infrared (mid-IR) wavelength range. Using the orbital angular momentum (OAM) conservation of the parametric processes and the threshold conditions of the cavity modes of the singly resonant optical parametric oscillator (SRO), we have transferred the OAM of the pump beam at the near-infrared wavelength to the idler beam tunable in the mid-IR. Pumped with a vortex beam of order $l_p = 1$ at 1064 nm, the SRO, configured in a four curved mirror-based ring cavity with a 50 mm long MgO-doped periodically poled $LiNbO_3$ crystal, produces an idler beam with an output power in excess of 2 W in a vortex spatial profile with the order $l_i = 1$, tunable across 2217–3574 nm and corresponding signal beam in Gaussian intensity distribution across 1515–2046 nm. For pump vortices of the order $l_p = 1$ and 2, and a power of 22 W, the SRO produces idler vortices of the same order as that of the pump beam with a maximum power of 5.23 and 2.3 W, corresponding to near-IR to mid-IR vortex conversion efficiency of 23.8% and 10.4% respectively. The idler vortex beam has a spectral width, and a passive rms power stability of 101 MHz and 4.9% over 2 h, respectively.

(A. Aadhi, Varun Sharma, R. P. Singh, and G. K. Samanta)

Robust, high brightness, degenerate entangled photon source at room temperature

We report on a compact, simple and robust high brightness entangled photon source at room temperature. Based on a 30-mm-long periodically-poled potassium titanyl phosphate crystal, the source produces non-collinear, type-0, phase-matched, degenerate photons at 810 nm with spectral brightness as high as $\sim 0.41 \pm 0.02 (\sim 0.025 \pm 0.02)$ MHz/mW/nm for multi (single) mode fiber coupling. So far, this is the highest number of degenerate photons generated using a continuous-wave laser pumped bulk crystal and detected using multimode fiber. We have studied the dependence of pump focusing on the brightness of the generated photons collected using both multimode, and single mode fibers. For a fixed pump power and crystal parameters, the SPDC source has an optimum pump waist radius producing maximum number of paired photons. Combining the crystal in a novel system architecture comprised with Sagnac interferometer and polarizing optical elements, the source produces polarization entangled photon states with high spectral brightness. Even in the absence of any phase compensation, the entangled photon states detected using single mode fiber have a Bell's parameter, $S = 2.63 \pm 0.02$, violating the Bell's inequality by nearly 32 standard deviations and fidelity of 0.975. The compact footprint, robust design, and room temperature operation, make our source ideal for various quantum communication experiments.

(M. V. Jabir, and G. K. Samanta)

High-power, high repetition rate, tunable, ultrafast vortex beam in the near-infrared

We report on experimental demonstration of high power, ultrafast, high repetition rate (RR) vortex beam source tunable in the near-IR wavelength range. Based on single-pass optical parametric generation of Yb-fiber laser of vortex order $l_p = 1$ in a 50 mm long MgO doped periodically poled $LiNbO_3$ crystal, the source produces signal beam in vortex profile of order $l_s = 1$ across 1433-1553 nm. Additionally, the source produces broadband idler radiation tunable across 3379–4132 nm in the Gaussian beam profile. We observed that the vortex profile of the pump beam is always transferred to the signal beam due to the highest overlapping integral among the interacting beams and the idler maintains a Gaussian spatial profile owing to the conservation of orbital angular momentum in optical parametric processes. For a pump power of 4.72 W, the signal and idler beams have a maximum power of 1.7W at 1509 nm and 0.48W at 3625 nm respectively. The signal vortex beam has output pulses of width ~ 637 fs at a RR of 78 MHz. The signal (idler) has a spectral width of 4.3 nm (129.5 nm) and a passive peak-to-peak power fluctuation better than $3\%(1.1\%)$ over 30 min, respectively.

(A. Aadhi, and G. K. Samanta)

Comparative study to increase the dating rage of geological samples probing different luminescence signal.

Due to constrains like saturation of signal growth with radiation dose, and fading of signal on storage, luminescence dating applicability has been in the range of few hundred ka for quartz and $\sim Ma$ for feldspar. Though the fading correction methods have been developed, the ages do tend to be underestimated towards the extremum upper bound. A systematic study to examine the range of dating in identical samples using blue light stimulated (BLSL), infra-red stimulated (IRSL) and post infra-red infra-red stimulated (pIR-IRSL) luminescence signals from samples of known ages from recently deposited sediments to sediment deposited far beyond the luminescence dating range and from various depositional environment.

By inter-comparison of ages from these luminescence signals, a first estimation of the extent of underestimation is deduced and a correction factor is obtained. The results offer some hope to date samples up to 1 – 1.2 Ma ages compared to present limit of 700 ka using violet stimulated luminescence (VSL) or re-distributed infra-red luminescence (RD-IRSL) signals.

This work was done in collaboration with Dr. Rohtash Kumar of Wadia Institute of Himalayan Geology, Dehradun and Prof. P.N. Gajjar of the Department of Physics, Gujarat University.

(H. Rajapara, N. Chauhan and Rohtash Kumar and A.K. Singhvi)

Bleaching of Luminescence of Quartz by Moonlight

Studies so far have assumed that the bleaching of luminescence occurs by exposure to daylight. Under the surmise that the moon light is also a reflected sun light, it should also bleach. To estimate the bleaching of luminescence signal by moon light on earth surface the effect of full moon light exposure on quartz grain for various duration in the range 15 min to 6h was studied. The luminescence signal after 15 min exposure to moon light was reduced by 7% dose, 26% after 4 hours and it remained $\sim 27\%$ after 6 hours. Beyond this there is no appreciable change was seen. In contrast, the day light exposure reduces the signal to $> 99\%$ level in a matter of a second. This is

being examined keeping in mind that Moonlight has a spectral peak around 650nm and that the sun peaks at around 550nm and flux of moonlight is about 0.5 Million times lower than that of sunlight but it is clear that the moon light can bleach the signals by a significant amount.

This work was done in collaboration with Prof. P.N. Gajjar of Gujarat University, Ahmedabad.

(H. Rajapara, N. Chauhan and A.K. Singhvi)

Optically stimulated luminescence ages from the Lake Agassiz basin in Manitoba

During the final glacial retreat from the Northern Great Plains of Canada and the U.S., lakes formed along the margin of the Laurentide Ice Sheet (LIS), as runoff was dammed on the north-sloping landscape. The newly deglaciated topography controlled the extent of these lakes, the routing of meltwater, and the late-glacial flow patterns of the retreating LIS.

Lake Agassiz was the largest ice-marginal lake, occupying in total, an area of $\sim 1.5\ million\ km^2$, although only a part of that area was covered by water at any one time. The lake expanded and contracted, and deepened and shallowed, as the LIS fluctuated and outlets from the lake changed. The life of Lake Agassiz spanned nearly 6000 cal years, forming first in the southernmost end before 14 cal ka BP and finally draining into Hudson Bay 8.2-8.4 cal ka BP.

The floor of the Lake Agassiz basin is generally flat and covered by lacustrine clay and silt; it is rimmed by numerous sandy and gravelly beaches of varying size. These today inform of the lake levels in the past. Geomorphic analysis and optically stimulated luminescence (OSL) ages from undated Lake Agassiz beaches and fluvial sediments on adjacent Riding Mountain in Manitoba provided insight into their early history of this lake and a detailed chronicle of the lake levels was created. OSL ages ranged from 14.5 ± 2.4 ka and 13.4 ± 0.7 ka on the oldest beaches of Lake Agassiz indicated that the Laurentide Ice Sheet (LIS) retreated from that part of the Agassiz basin by ~ 14.5 ka. This in turn will inform the timing of melt water input to the thermohaline circulation.

This work was done in collaboration with Prof. J. T. Teller, University of Manitoba, Prof. R.A. McGinn, Brandon University, Brandon.

(H. Rajapara, A.D. Shukla and A.K. Singhvi)

Luminescence dating of Early Middle Palaeolithic culture in India

Post infrared-inferred stimulated Luminescence(pIRIRSL) dating of Paleolithic tool bearing sediments from the prehistoric site of Attirampakkam, India suggest that the end of Acheulian culture and the emergence of a Middle Paleolithic culture occurred at $385 \pm\ 64$ thousand years ago (ka). This is much earlier than conventionally presumed for South Asia and nearly simultaneous those in Africa and Europe. These imply that the arrival of Human in the region was earlier that 140ka, assumed so far. These dates open new debates on, a) the origins and early evolution of these cultures, b) their association with modern Humans or archaic Hominins, c) their links with preceding Acheulian cultures and, d) the spread of Levallois lithic technologies.

Methodologically these pIRIRSL ages demanded considerable effort as these were at the extemum limits of the dating range. However stratigraphic order of ages, concordance of OSL ages on quartz and other consideration suggest that the ages were reliable.

Archeologically, in the strata with Middle Paleolithic tools, the gradual disuse of bifaces, the predominance of small tools, the appearance of distinctive and diverse Levallois flake and point strategies, and the blade component suggested a shift away from the preceding Acheulian large-flake technologies.

These findings document a process of substantial behavioral change that occurred in India at 385 ± 64 ka and establish its contemporaneity with similar processes recorded in Africa and Europe and call for a re-evaluation of models that restrict the origins of Indian Middle Paleolithic culture to the incidence of modern human dispersals after approximately 125 ka.

This work was done in collaboration with Prof. S. Pappu and K. Akhilesh of the Sharma Centre for Archeological Research and Prof. Y. Gunnel of the Univ. of Lyon, France.

(Haresh M. Rajapara, A.D. Shukla and Ashok K. Singhvi)

Study of luminescence response of amorphous glasses for very high radiation doses (100Gy to 50kGy)

One of the limitation of luminescence dosimetry phosphors is related to saturation of luminescence signal at high doses (~ 500 Gy). Some of the phosphors signal saturate even at much less than the specified dose. This limits their application to only low dose environments and cannot be used for applications which involves very high radiation doses (> 1000 Gy). It has been observed that the amorphous solids normally have very low dose response and the response of amorphous solids starts at doses ~ 200 Gy. So this work tried to investigate the possibility of using amorphous glasses to high radiation dose environments. In this artificial amorphous europium doped zinc bismuth borate glass phosphor is prepared. The interaction of $10\mathrm{Zn O} - 5\mathrm{Na_2O} - 10\mathrm{Bi_2O_3} - (75-x)\mathrm{B_2O_3} - x\mathrm{Eu_2O_3} (where x = 0.7 mol\%)$ glasses exposed to high gamma doses (0.25 kGy-50kGy) were investigated experimentally using XRD, FTIR, absorption photoluminescence, thermally and optically stimulated luminescence studies. XRD confirmed the amorphous nature of the pristine and exposed glasses. Changes in the FTIR spectra revealed the structural deformation of borate groups after high dose gamma irradiation. As the gamma dose was increased, total glass absorbance was enhanced and absorption edge shifted towards longer wavelength side in the UV-Visible absorption spectra (which is confirmed by UV-Visible absorption spectra). Estimation of optical bandgap and urbach energy of irradiated samples confirmed the photo induced traps/color centers in the forbidden energy gap of the glass matrix. Photoluminescence (PL) studies have shown luminescence intensity quenching at high gamma doses. Lifetime of $^5\mathrm{D}_0$ state of Eu^{3+} ions was estimated by the decay curves and color purity calculated using 1931 CIE chromaticity coordinates (x,y) of the ZNBBE-4 glasses did not show any variations after gamma irradiation. Thermally stimulated

luminescence (TL) and optically stimulated luminescence (OSL) techniques were used to study trap centers induced by irradiation. Each TL glow curve has shown two broad emission peaks with peak temperatures at 490K and 625K.The number of peaks and their trapping parameters (E, S, T and b) have been determined using the computerized glow curve deconvolution (CGCD). The dose response of $0.7mol\%\mathrm{Eu}^{3+}$ doped zinc sodium bismuth borate glasses has shown linear behavior within the dose range of 250-3kGy proving their suitability for dosimeter in this radiation zone.

This work is done in collaboration with Vinod Hegde from MIT, Manipal, Karnataka

(N. Chauhan)

Establishing chronology of Toba ash deposits in Purna basin.

The ash samples (YTT) from the Narmada, Son, Kukadi, and Jurreru valley etc. is already dated by the earlier workers which proposed its absolute age as ~ 74 ka. Similar ash layers are also found in nearby Hudki and Sukli areas. However, the ingenuity of ash layer deposits in Hudki and sulki is not established and its questionable whether the ash deposits in these areas are the original Toba ash deposits or they are reworked deposits. In case they are reworked then what is the possible time duration of the their redeposition and mechanism of reworking. Further it is interesting to have an idea of the depositional ages which will help us in establishing precise stratigraphy of the Quaternary succession of Purna Alluvial basin, will will help in establishing climate impact in Indian subcontinent. The samples were collected from the Quaternary areno-argillaceous sediments of Purna river. The samples include the ash layer and samples from layers below and above the ash layer. The samples were processed for luminescence dating, however due to lack of sufficient quartz in sediment matrix, the feldspar was used for luminescence measurements. In order to circumvent the problem of anomalous fading the Post IR IR protocol of measurements was used, which is expected to give stable signal from feldspar. The fading rate of the sample was found to be less than 1%, which also suggest no fading in the signal. The ages for ash layers in Hudki area was found to be between ~ 57 ka while that of sukli area was ~ 59 ka. The estimated ages suggest that the present deposits in Sukli and Hudki areas are the reworked deposits and not the pristine toba ash. Now we are trying to predict the mechanism of reworking and its relation with paleoclimate in this basin.

This work is done in collaboration with Dr. Ashok Srivastava of Amravati university, Maharashtra.

(N. Chauhan)

New protocols for extending dating range using Quartz and Feldspar

The prospects of extending the range of luminescence ages were explored using the residual signal after a fixed daylight bleaching. The residual signal in both quartz and feldspar samples, demonstrated a good dose dependence, did not saturate at the conventional doses of 200-300Gy and indicated the prospect of obtaining reliable doses of 1000 Gy or more. These is being investigated further and relevant protocols for measurement have been developed.

This work was done in collaboration with Prof. Z. P. Lai, Univ. of Wuhan, China and Prof. P.N. Gajjar, Gujarat University.

(H.M. Rajapara, N. Chauhan and A.K. Singhvi)

Solar Wind Ion Spectrometer (SWIS) payload: Development of Front End Electronics (FEE) & High Voltage Power Supply (HVPS)

SWIS is a sub-system of Aditya Solar Wind Particle Experiment (ASPEX) payload onboard Aditya-L1 mission and is primarily meant to measure ions in the energy range of 100 eV - 20 keV. SWIS subsystem is mainly configured with two electrostatic analyzers called Top Hat Analyzer - 1 (THA-1) and Top Hat Analyzer - 2 (THA-2). The first analyser (THA-1) will scan ions coming in the ecliptic plane and has the capability to measure angular, energy and mass distributions simultaneously in the required energy range. The second analyser (THA-2) has the acceptance plane perpendicular to the ecliptic. Both THA-1 and THA-2 uses Micro Channel Plate (MCP) as a detector followed by in-house developed Resistive Anode Encoder (RAE) for position detection. Development of HVPS and FEE for both analyzers are currently in progress with the aim to measure the four important parameters of the solar wind particles in conjunction with processing electronics (PE). These parameters are, (i) energy (ii) mass (iii) flux (iv) direction.

High Voltage Power Supply : HVPS are required to provide energy scanning to analyzer, biasing of detectors (MCP) and focusing of the ions. THA-1 requires three and THA-2 requires two programmable HV power supplies respectively.

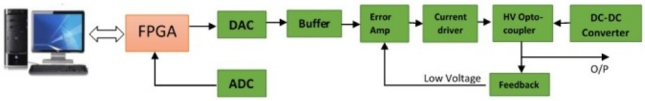

Figure 1: Block Diagram – HVPS Design

The energy scan and MCP bias power supplies can be programmed from 0 to -3 kV with ~ 1.2 V resolution and Focus power supply is ranged from 0 to -7 kV with ~ 2.4 V resolution. These power supplies provide fast settling time (¡50 ms) for quick energy scan. HVPS design block diagram is shown in fig. 1. The design configuration is based on driving HV opto-coupler connected to HV DC-DC modules with closed loop feedback mechanism. All HV power supplies are designed to provide read back to monitor current applied values. In addition, detector power supplies have current read back and over current protection. The High Voltage power supply circuit boards are interfaced with FPGA to perform full functionality test (Fig.2) which includes high speed (min. 50ms) energy scan for analyzer and ramping MCP supply.

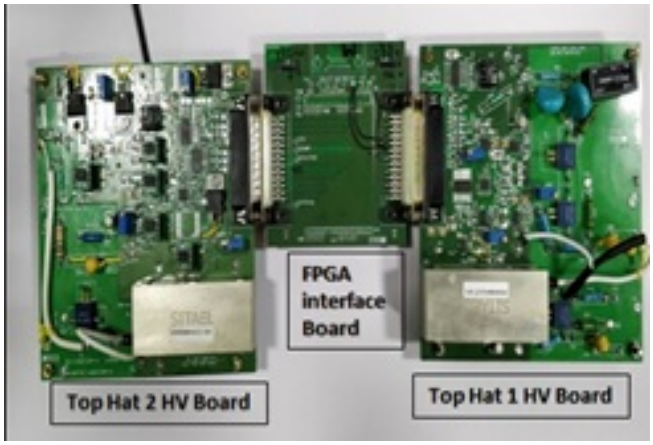

Figure 2: HVPS for THA 1 & THA 2 interfaced with FPGA

In addition, LabVIEW based software is developed to control and monitor all the necessary parameters of HV supplies (Fig.3). The functional testing of these supplies are successfully completed. The vacuum compatibility test is in progress.

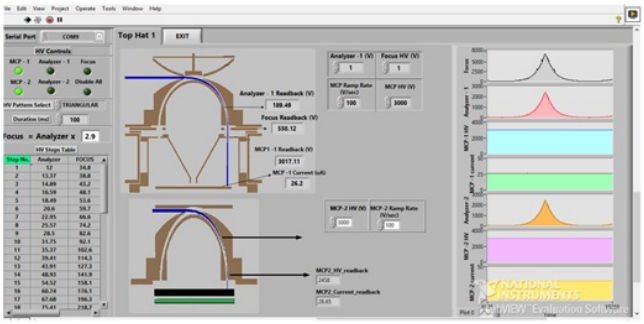

Figure 3: HVPS Test Software

Front End Electronics : The FEE consists of resistive anode encoder (RAE), charge sensitive preamplifier (CSPA) and shaping amplifier (SA) as shown in the block diagram (fig.5). For the charge division process, a printed circuit board (PCB) based RAE (fig.6) is developed which consists of a set of four resistive channels with specific geometric pattern and resistance. Each resistive channel is formed by a set of small smd resistors (case code 0402) connected in series. To collect and integrate charges from RAE, a JFET based fast and low noise CSPA is developed which outputs voltage pulse. To increase the signal-to-noise ratio (SNR) of CSPA output and to make it compatible to PE, a three stage shaping amplifier is developed. FEE consists of total ten identical channels of CSPA and SA. Eight of them are used in Top-Hat Analyzer (THA) (fig.7) which is analyzing particles from ecliptic plane and providing 2π viewing angle with angular resolution of 22.5° and radial resolution of 1.2 mm for mass separation. The rest two channels are used in THA which is analyzing the plane perpendicular to ecliptic with 2π viewing angle and angular resolution of 11.25°. The FPGA based ground check-out system and data acquisition software (fig .8) have been developed to verify the functionality of the FEE and performance analysis of the complete experiment. The functional and vacuum testing of FEE is completed successfully and it is being optimized to handle high count rate (up to 100 kcps) with desired position accuracy and resolution. To meet the space instrumentation standards, both HVPSU and FEE are developed using electronic components whose space qualified versions are available. The space qualification process for MCP detector is also been initiated recently.

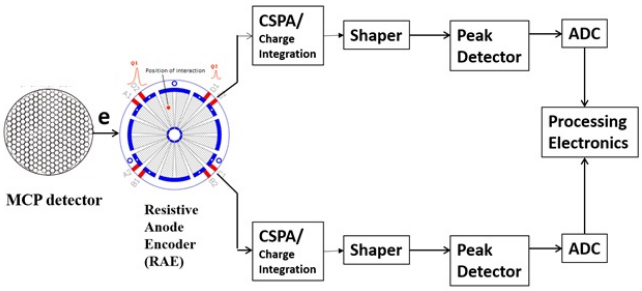

Figure 4: Block Diagram FEE & PE (Single Channel)

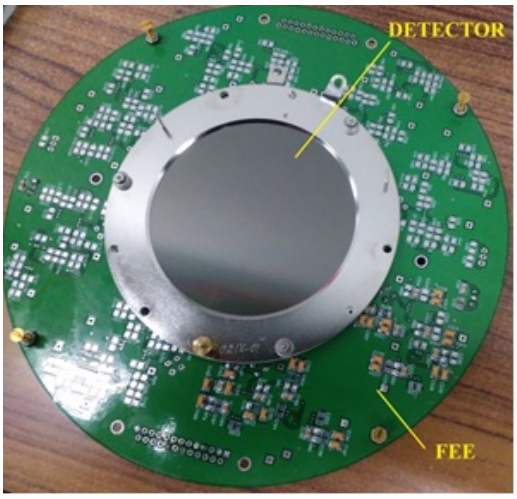

Figure 5: MCP detector, RAE & FEE

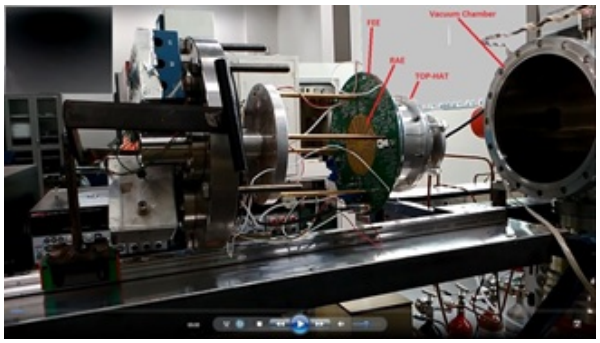

Figure 6: Top-Hat Analyzer, RAE & FEE with mounting

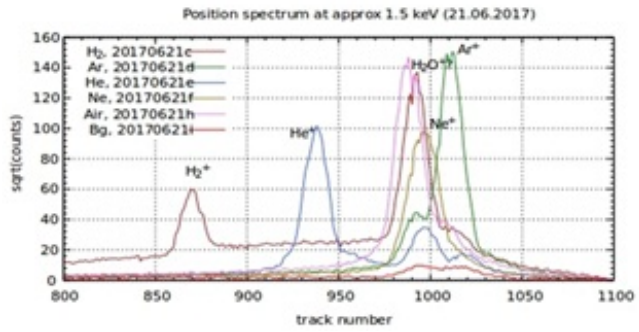

Figure 7: Experiment result with different gas injection

Figure 8: GCS for FEE, histogram for calibration

This work was carried out in collaboration with Dr. Bhas Bapat of IISER, Pune.

(Swaroop B Banerjee, Pranav Adhyaru, Manan Shah, Prashant Kumar, K P Subramanian and M B Dadhania)

Quantitative estimation using synthetic LIBS spectrum generation

Optical emission spectroscopic studies on some standard as well as rock samples were performed with the installed LIBS system. Concentration estimation of metal alloys was demonstrated using a algorithm which employs synthetic generated spectra. Estimation of stark widths along with the degree of self absorption of the emission lines for optically thick plasma was demonstrated. A provision to manipulate the sample inside vacuum chamber was made via translation stages. Control software for the same was developed in Labview software. A double pulse set up comprising of a short wavelength source (Excimer laser) and a long wavelength source (Nd:YAG) is currently being developed to enhance the emission intensities for spectroscopic determination of concentration of trace elements.

(Prashant Kumar, Nageswara Rao Epuru, Swetapuspa Soumyashree, Rajesh K Kushawaha, Manan Shah, K P Subramanian, and S B Banerjee)

Studying Molecular Structure and Dynamics via Coulomb Explosion Imaging

The fragmentation dynamics of $C_2H_2Br_2$, $C_2H_2CL_2$, and difluoroiodobenzene induced both strong-field and inner-shell photoionization have been investigated using Coincidence momentum imaging technique. The goal of the studies is to experimentally identify and separate cis and trans isomers using the Coulomb Explosion Imaging (CEI) method. Our results show that the geometric structure of the isomers can be distinguished by triply ionizing the molecule into the $C_2H_2^+ + Br^+/Cl^+ + Br^+/Cl^+$ fragmentation channels via inner-shell photoionization using X-ray synchrotron beams or via strong-field ionization with ultrafast femtosecond laser pulses.

This work is done in research collaboration with Prof. Daniel Rolles, Prof. V. Kumarappan and team of KSU, USA

(R. K. Kushawaha)

Direct transfer of pump amplitude to parametric down-converted photons

In general, the spatial distribution of individual photons (signal or idler) generated by spontaneous parametric down-conversion (SPDC) does not evidently show any particular spatial mode structure because of their randomness in generation and the incoherent nature. Here, we numerically showed that all individual photons generated by the SPDC process carry the transverse amplitude as that of the pump and then confirmed it experimentally. The pump amplitude is revealed in SPDC when individual photons are spatially filtered from the total SPDC distribution. This is observed simply by imaging the photons that are filtered using a minimum-sized aperture. The phase measurements showed that the observed mode distribution does not possess the transverse phase distribution as that of the pump.

(Ali Anwar, P. Chithrabhanu, P. Vaity, and R. P. Singh)

Quantum information with even and odd states of orbital angular momentum of light

We address the possibility of using even/odd states of orbital angular momentum (OAM) of photons for the quantum information tasks. Single photon qubit states and two photon entangled states in even/odd basis of OAM are considered. We present a method for the tomography and general projective measurement in even/odd basis. With the general projective measurement, we show the Bell violation and quantum cryptography with Bell's inequality. We also describe hyper and hybrid entanglement of even/odd OAM states along with polarization, which can be applied in the implementation of quantum protocols like super dense coding.

(P. Chithrabhanu, N. Lal, Ali Anwar, S. G. Reddy, and R. P. Singh)

Structuring Stokes correlation functions using vector-vortex beam structures

Higher order statistical correlations of the optical vector speckle field, formed due to scattering of a vector-vortex beam, are explored. Here, we report on the experimental construction of the Stokes parameters covariance matrix, consisting of all possible spatial Stokes parameters correlation functions. We also propose and experimentally realize a new Stokes correlation functions called Stokes field auto correlation functions. It is observed that the Stokes correlation functions of the vector-vortex beam will be reflected in the respective Stokes correlation functions of the corresponding vector speckle field. The major advantage of proposing Stokes correlation functions is that the Stokes correlation function can be easily tuned by manipulating the polarization of vector-vortex beam used to generate vector speckle field and to get the phase information directly from the intensity measurements. Moreover, this approach can be used for a complete experimental Stokes characterization of a broad range of random fields.

(Vijay Kumar, Ali Anwar, and R. P. Singh)

Scattering of Poincaré beams: polarization speckles

Polarization speckle is a fine granular light pattern having spatially varying random polarization profile. We generate these speckle patterns by using the scattering of Poincaré beams, a special class of vector vortex beams, through a ground glass plate. Here, the Poincaré beams are generated using a polarization sensitive spatial light modulator displaying an on-axis hologram corresponding to an optical vortex phase profile. The different inhomogeneities of the rough surface experience different polarizations, which control the ability for scattered waves to interfere at the detection plane and causes a spatially varying polarization profile. We experimentally determined the spatial variation of local degree of polarization and orientation of the polarization ellipse for these speckle patterns from the Stokes analysis. We also determined the size of scalar speckles using the auto-correlation function of Stokes parameter S_0 and the size of polarization speckles using the sum of auto-correlation functions of remaining three Stokes parameters. We found that the change in scalar speckle size with the index of the vector beam is very small and of the order of 1pixel size of the camera but the size of polarization speckles decreases with the increase in index of the vector beam.

This work was done in collaboration with Yoko Miyamoto of The University of Electro-Communications, Chofugaoka, Chofu, Tokyo 1828585, Japan.

(S. G. Reddy, Vijay Kumar, Yoko Miyamoto, and R. P. Singh)

First detection of some complex molecules in the hot molecular core G31.41+0.31

We report a detail observational analysis of a hot molecular core (HMC) in the high-mass star-forming region G31.41+0.31. Using ALMA data , here we are reporting some complex organic molecules (COMs) in the source. For the first time, we are reporting a pre-biotic species among the COMs in the source G31.41+0.31, outside the Galactic center. Beside the species, we also report HCN, $H^{13}CO^+$ SiO in absorption, and formyl radical (HCO), formaldehyde (H_2CO), thioformaldehyde (H_2CS), methanol (CH_3OH), methanethiol(CH_3SH), and methyl formate (CH_3OCHO) in emission. Using all these line together, we have described possible condition under which the complex molecule may form in the source.

(D Sahu)

This work was done in collaboration with Indian Center for Space Physics.

Infrared and vacuum ultraviolet spectra of nano-blocks of benzonitrile frozen on cold dust grains

Benzonitrile, was recently discovered to be a component of the complex chemical structure in the interstellar medium.

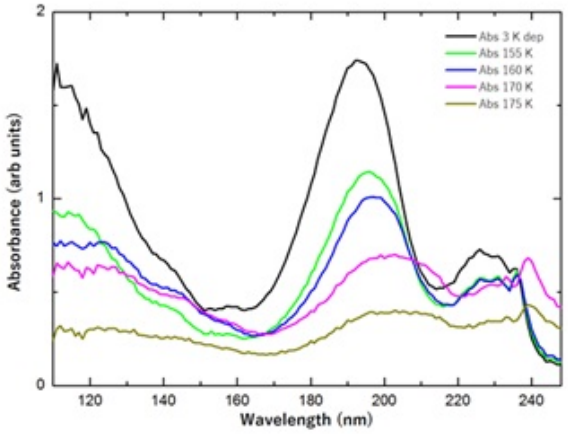

Figure 9: Shows the vacuum ultraviolet photoabsorption spectra

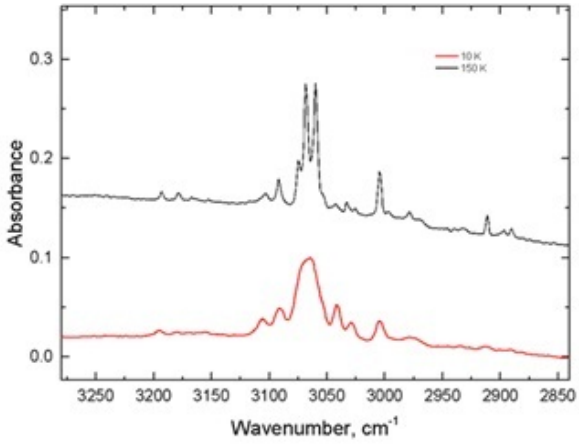

Figure 10: Shows the vacuum ultraviolet infrared spectra

The cold molecular cloud TMC-1, where benzonitrile was observed

is of particular interest because of the presence of multiple cyano-containing species. Since, benzonitrile can be formed via the reaction of CN with a molecule of benzene, the estimation of benzonitrile's abundance can shed light on the abundance of benzene. Further laboratory-based experiments will help in exploring the various pathways of formation and help improve the theoretical models. This will also be a step in helping us understand the formation of other suspected polycyclic aromatic hydrocarbon molecules. In order to understand the physico-chemical nature, the spectroscopic details of benzonitrile are imperative at astrochemical icy conditions. Here, we present the first VUV and IR spectra of nano-blocks of benzonitrile formed in astrochemical icy conditions.

(B Sivaraman)

This work was done in collaboration with National Synchrotron Radiation Research Center, Taiwan.

Mukundpura Meteorite Fall: Implications from impact fragmentation

On 6 June 2017, around 5 AM a meteorite fell in Mukundpura village, near Jaipur. The meteorite impacted on an agricultural field before ploughing, therefore the soil was porous and dry. The meteorite impact on the porous target surface lead to its multiple fragmentation. The fragmented meteorite samples were collected up to a distance of ~ 1 m from the main impact crater by sieving the soils around the impact site. We collected ~ 1300fragmented samples around the impact size, which comprised of different size, shape and weight. The fragments were collected from all sides of the crater. The fragment length ranges from ~ 1 to 9.5 mm, whereas the fragment weight ranges from ~ 4 to 106 mg. The fragment collected weigh about ~ 12 grams.

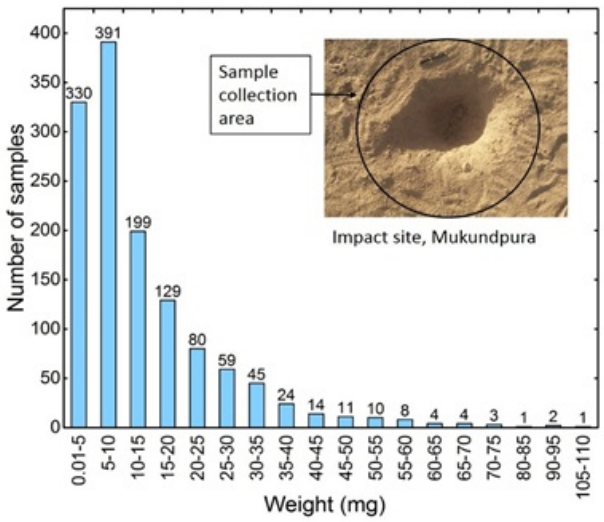

Figure 11: Shows the sample collection area

The mixing of the impactor within the target body depends on the efficiencies of fragmentation, penetration and ejection of impactor materials. The major implication that stems out from the fragmentation analysis is that, the possibility of meteorite samples around the impact crater (even small size ~ 1 m) is high on any planetary bodies. The Mars and Moon are the best analogous for such porous soils and holds fresh craters, whose ejecta may still preserve such small meteorite sample. In-situ / high resolution remote sensing analysis over such fresh craters may not only lead in understanding the planetary bodies, but also will lead us to explore the extra-terrestrial materials if not buried or eroded. Impact crater of ~ 1 m on an atmospheric body like Earth hold the fragmented meteorite and suggests that predominant meteorite samples could be possibly present within other planetary bodies. This adds as another evidence for the projectile survival from impact events.

(J K Meka, K K Rahul, S Vijayan and B Sivaraman)

Ethanethiol – Water layered ices: Evidence for reversible phase change even in layered ices

In an experiment, after the first report of reversible phase change observed in astrochemical pure ethanethiol ices, ethanethiol – water layered ices were deposited on cold dust analogue kept at 10 K. According to the sublimation temperature of the molecular ices known from previous experiments, ethanethiol ice was formed first and then water ice was deposited on top of the ethanethiol ice at 10 K. The layered ices, ethanethiol below water ice was then gradually warmed to higher temperatures. At temperatures between 110 K to 115 K, the first phase change temperature of ethanethiol ice, amorphous to crystalline phase change was observed. Then further warming the ice to 125 K, the second phase change from crystalline to amorphous phase change was also observed. It must be noted that the reversible phase change was occurring even below an icy layer of amorphous water ice whose phase change temperature from amorphous to crystalline is around 150 K. While subjecting the sample to more temperature cycles the reversible phase change was found to repeat. This experiment proves the reversible phase change is not due to the liquefaction of crystalline ice at lower temperatures / ultrahigh vacuum conditions.

(B Sivaraman)

Discovery of hot-corino and complex-molecule in IRAS 4A1, an ALMA observation

The NGC 1333 IRAS 4A, a protostellar binary, host a well known hot-corino A2 and abundant of complex organic molecules (COMs). The other core A1, well separated by 1.8 arc-second from A2 core and no COMs have been reported in this source. Hot-corinos are rich in COMs, and depending on the nature of the object COMs may trace the presence of hot-corino. In this letter, we report the first presence of COMs in the A1 core of the protobinary IRAS 4A. We detect these molecules in absorption, and compared it with same molecular line emission from A2 core. Our observation suggests that the A1 core hosts a hot-corino too like the A2 core and surrounded by optically thick dust emission. Also, we find a low $\sim 10^{-2}$ D/H ratio of methanol which may imply typical hot-gas condition in the observed objects.

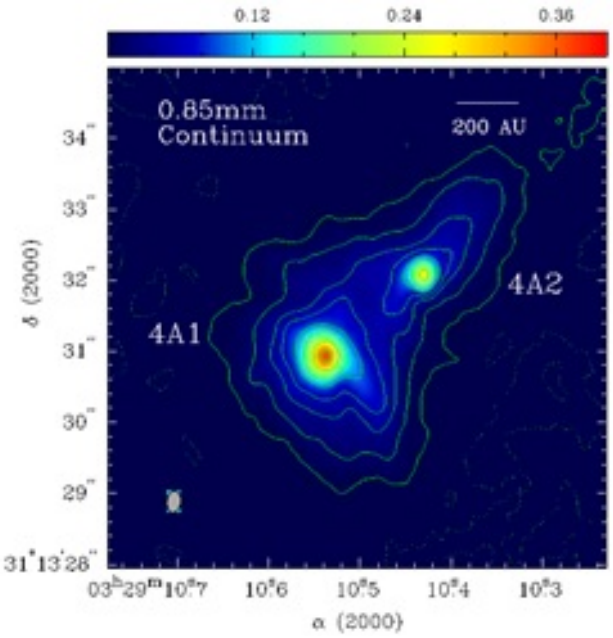

Figure 12: Shows the two core A1 and A2 of the IRAS

(D Sahu)

This work was done in collaboration with Tohoku University, Japan.

Estimation of Thermal history of North Almora Thrust Fault using newly established thermochronology technique.

Very recent dynamical evolution of the Himalayas is poorly understood.

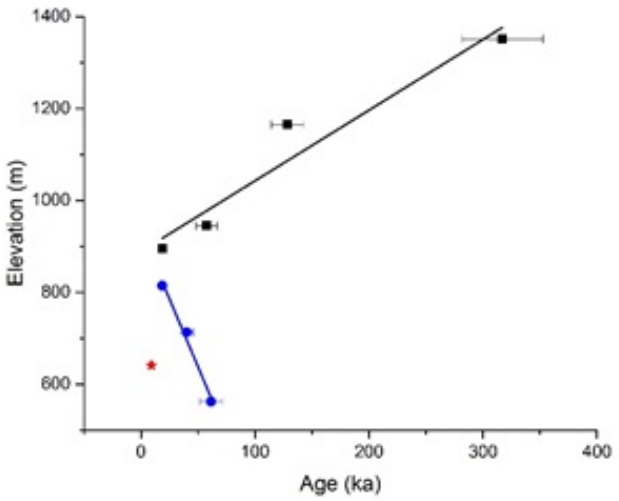

Figure 13: Age-elevation plot for samples collected from hanging wall of NAT

Various temperature dependent dating techniques based on changes in the signal/signatures of the system as it moves up through the earth's varying temperature field across its crust are employed to study the exhumation history of an orogeny. Most of these techniques, however, are incapable of resolving very recent geological history (10 ka to 100 ka) of crustal deformation. Also, their applicability is limited in the region below 2 km of the earth's crust because of a higher Closure Temperature (temperature below which a thermally decaying system becomes close). OSL methods, on the other hand, have a low closure temperature which has been demonstrated in recent studies. Towards this, we have undertaken a preliminary study in the Central Himalayan region of Uttrakhand, India, which is traversed by regionally extensive terrain boundary thrusts viz. the Main Boundary Thrust (MBT), the Main Central Thrust (MCT) and the South Tibetan Detachment System (STDS) along with the out of sequence thrusts such as the North Almora Thrust (NAT).

Optical Luminescence (OSL) dating is based on the fundamental concept that a buried sample, not exposed to light and heat, keeps on accumulating latent energy due to the continuous bombardment of irradiation from surrounding radioactive materials and cosmic rays. This latent energy, which is proportional to the burial time for which the sample was buried, is released when stimulated by light or heat. The amount of emitted light gives an approximate of sample's burial age. The entire process occurs at molecular scale and its kinetic is temperature dependent. This temperature dependency of accumulation of latent OSL signals is exploited to use OSL-dating as a thermo-chronometer.

OSL thermos-chronology is also dependent on a critical parameter called the Closure Temperature - maximum temperature below which a system becomes close and stops losing signal due to thermal decay (Herman et al 2010). It is a function of the activation energy (E_a) and the frequency factor (s) of the traps responsible for the stimulated signal, and of the rate at which the rock sample cooled (T°). Thermal gradient (dT/dz) present in the Earth's top most crust implies that this critical temperature will sit at a specific depth below the surface of the Earth. All the points at this depth can be assumed to be at same temperature, the Closure Temperature, and can be viewed as a surface of constant temperature or an isotherm. OSL, being a low-temperature thermo-chronometer, has a shallower closer temperature isotherm. This depth is of critical importance because only the samples collected above this depth will have any OSL signal which can be interpreted. Closure Temperature for 125°C OSL was determined by isothermal decay method and was found to be $\sim 50^\circ$C.

Presently, 9 samples from Srinagar area were dated. Samples were collected from the hanging wall of North Almora Thrust (NAT), dated and plotted against elevation. The slope of age-elevation plot distinctively shows a break at $\sim 20ka$ marking two different rates of exhumation post and pre 20ka. The exhumation rate for the period 20-320ka comes to be around 2.01 ± 0.38 mm/a for samples presently located at elevation range of 900 to 1350m. Samples sitting below $\sim 900m$ show a negative exhumation rate of 2.52 ± 2.72 mm/a. The inferred exhumation rates were also corrected for perturbation caused in underlying thermal structure due to finite amplitude topography. The degree of perturbation of an isotherm from its flat geometry was found by solving a 2D diffusion-advection model.

The abrupt break in age-elevation and negative exhumation at roughly around 20 ka could be due to a moving thrust fault at NAT. Thrust fault motion can markedly change the underlying thermal structure causing the isotherms (including the closer-temperature isotherm) to become

almost vertical or even inverted causing samples at higher elevation to exhibit younger age. The model for the effect of thrust fault motion on acquisition of OSL age is being developed.

This work is done in collaboration with Shubhra Sharma of IISER, Mohali and Naresh Rana of National Center for Seismology, New Delhi

(Vinayak Kumar, N. Chauhan, N. Juyal and A.D. Shukla)

Publications

Publications in Journals

Astronomy and Astrophysics

1. Abbott, B. P. et al. including Vadawale, S. V., 2017, *"Multi-messenger Observations of a Binary Neutron Star Merger"*, ApJ, v. 848, pp. 1-59.
2. Ahnen, M.L., Ansoldi, S. and 48 authors including Kaur, N., Sameer, Baliyan, K.S., 2017, *"Multiwavelength observations of a VHE gamma-ray flare from PKS 1510-089 in 2015"*, A&A, v. 603, p. A 29-40.
3. Banerjee, D. P. K., Srivastava, Mudit K., Ashok, N. M., Munari, U., Hambsch, F.-J., Righetti, G. L., Maitan, A., 2018, *"Near-infrared and optical studies of the highly obscured nova V1831 Aquilae (Nova Aquilae 2015)"*, MNRAS, v. 473, p. 1895-1908.
4. Basak, R. including Vadawale, S. V., 2017, *"Surprise in simplicity: an unusual spectral evolution of a single pulse GRB 151006A"*, MNRAS, v. 472, p. 891-903.
5. Bhalerao, V. et al. including Aarthy, E., Mithun, N. P. S., Vadawale, S. V., 2017, *"A tale of two transients: GW 170104 and GRB 170105A"*, ApJ, v. 845, pp. 1-10.
6. Bhalerao, V. et al. including Mithun N. P. S., Vadawale S. V., 2017, *"The cadmium zinc telluride imager on AstroSat"*, JAA, v. 38, p.31.
7. Bhargava, Y. et al. including Mithun, N. P. S., Vadawale, S. V., 2017, *"A precise measurement of the orbital period parameters of Cygnus X-3"*, ApJ, v. 849, pp. 1-7.
8. Bhowmick, A.; Pandey, G.; Joshi, V.; Ashok, N. M., 2017, *"Are DY Persei Stars Cooler Cousins of R Coronae Borealis Stars?"*, ApJ, v, 854, pp. 1-8.
9. Bisht, D., Ganesh, S., Yadav, R.K.S., Durgapal, A., Rangwal, G., 2018, *"Near-infrared study of open clusters Teutsch 10 and Teutsch 25"*, Advances in Space Research, v. 61, p. 571-580.
10. Dewangan, L. K., Baug, T., Ojha, D. K., 2017, *"Hub-filament System in IRAS 05480+2545: Young Stellar Cluster and 6.7 GHz Methanol Maser"*, ApJ, v. 844, pp. 1-11.
11. Dewangan, L. K., Baug, T., Ojha, D. K., Janardhan, P., Devaraj, R., Luna, A., 2017, *"The molecular cloud S242: physical environment and star formation activities"*, ApJ, v. 845, pp. 1-14.
12. Dewangan, L. K., Devaraj, R., Baug, T., Ojha, D. K., 2017, *"Embedded filaments in IRAS 05463+2652: early stage of fragmentation and star formation activities"*, ApJ, v. 848, p. 51.
13. Dewangan, L. K., Devaraj, R., Ojha, D. K., 2018, *"The Embedded Ring-like Feature and Star Formation Activities in G35.673-00.847"*, ApJ, v. 854, pp. 1 - 22.
14. Dewangan, L. K., Ojha, D. K., 2017, *"Observational signatures of cloud-cloud collision in the extended star-forming region S235"*, ApJ, v. 849, pp. 1 - 14
15. Dewangan, L. K., Ojha, D. K., Ninan, J. P., 2018, *"Star Formation in the Sh 2-53 Region Influenced by Accreting Molecular Filaments"*, ApJ, v. 852, pp. 1 - 12.
16. Dewangan, L. K., Ojha, D. K., Zinchenko, I., 2017, *"New insights in the mid-infrared bubble N49 site: a clue of collision of filamentary molecular clouds"*, ApJ, v. 851, pp. 1 - 14.
17. Dias-Oliveira, A. et al., (including Baug, T., Chandrasekhar, T., Ganesh, S. and Jain, J., 2017, *"Study of the Plutino Object (208996) AZ84 from Stellar Occultations: Size, Shape, and Topographic Features"*, AJ, v. 154, p. 13-22.

18. Epili, P., Naik, Sachindra, Jaisawal, G. K., Gupta, Shivangi., 2017, *"Decade long RXTE monitoring observations of Be/X-ray binary pulsar EXO 2030+375"*, MNRAS, v. 472, p. 3455-3466.

19. Evans, A., Banerjee, D. P. K., Gehrz, R. D., Joshi, V., Ashok, N. M. et al (19 authors), 2017, *"Rise and fall of the dust shell of the classical nova V339 Delphini"*, MNRAS, v. 466, p. 4221E.

20. Fouqu, Pascal., Moutou, Claire., Malo, Lison., Martioli, Eder., Lim, Olivia., Rajpurohit, Arvind., Artigau, Etienne., Delfosse, Xavier., Donati, Jean-Franois., Forveille, Thierry., and 6 coauthors., 2018, *"SPIRou Input Catalogue: global properties of 440 M dwarfs observed with ESPaDOnS at CFHT"*, MNRAS, v. 475, p. 1960F.

21. Jaisawal, G. K., Naik, Sachindra., Chenevez, J., 2018, *"Understanding the spectral and timing behavior of a newly discovered transient X-ray pulsar Swift J0243.6+6124"*, MNRAS, v. 474, p. 4432-4437.

22. Janardhan, P., Santosh Vadawale, Bhas Bapat, Subramanian, K. P., Chakrabarty D., Prashant Kumar, Aveek Sarkar, Nandita Srivastava, Satheesh Thampi R., Vipin K. Yadav, Dhanya M. B., Govind G. Nampoothiri, Abhishek J. K., Anil Bhardwaj and Subhalakshmi K., 2017, *"Probing the heliosphere using in-situ payloads on-board Aditya-L1"*, Current Science, v. 113, p. 620-624,.

23. Johansson, J., Goobar, A., Kasliwal, M. M., with Banerjee, D. P. K., Joshi, V...(16 Authors), 2017, *"Spitzer observations of SN 2014J and properties of mid-IR emission in Type Ia supernovae"*, MNRAS, v. 466, p. 3442J.

24. Joshi, V., Banerjee, D. P. K., Srivastava, M., 2017, *"Nova Ophiuchus 2017 as a Probe of 13C Nucleosynthesis and Carbon Monoxide Formation and Destruction in Classical Novae"*, ApJ Letters, v. 851L, p. 30J.

25. Kaur, N, Chandra S., Baliyan, K.S., Sameer and Ganesh, S., 2017, *"Multi-wavelength study of flaring activity in HBL 1ES 1959+650 during 2015-16"*, ApJ, v. 846, p. 158-170.

26. Kaur, N, Sameer, Baliyan, K.S. and Ganesh, S., 2017, *"Optical intra-day variability in 3C 66A: A decade of observations"*, MNRAS, v. 469, p. 2305-2312.

27. Munari, U., Banerjee, D. P. K., 2018, *"Infrared spectroscopy of the remnant of Nova Sco 2014: a symbiotic star with too little circumstellar matter to decelerate the ejecta"*, MNRAS, v. 475, p. 508M.

28. Pal, Main, Dewangan, G. C., Kembhavi, A. K., Misra, R., Naik, Sachindra., 2018, *"Complex Optical/UV and X-ray Variability of the Seyfert 1 galaxy 1H 0419-577"*, MNRAS, v. 473, p. 3584-3597.

29. Pal, Main., Naik, Sachindra., 2018, *"Correlated X-ray/UV/optical emission and short-term variability in a Seyfert 1 galaxy NGC 4593"*, MNRAS, v. 474, p. 5351-5362.

30. Rajpurohit, A. S., Allard, F., Teixeira, G. D. C., Homeier, D., Rajpurohit, S., Mousis, O., 2018, *"Photospheric properties and fundamental parameters of M dwarfs"*, A&A., v. 610A, p.19R.

31. Rao, A. R., Bhattacharya, D., Bhalerao, V. B., Vadawale, S. V., Sreekumar, S., 2017, *"Cadmium Zinc Telluride Imager onboard AstroSat : a multi-faceted hard X-ray instrument"*, Current Science, v. 113, p. 595.

32. Sarkar, A., Vaidya, B., Hazra, S. and Bhattacharyya, J., 2017, *"Simulating Coronal Loop Implosion and Compressible Wave Modes in a Flare Hit Active Region"*, ApJ, v. 851, p. 120-126.

33. Singh V., Wadadekar Y., Ishwara-Chandra C.H., Sirothia S., Sievers J., Beelen A., and Omont A., 2017, *"On the nature of infrared-faint radio sources in the Subaru X-ray Deep and Very Large Array-VIMOS VLT Deep Survey fields"*, MNRAS, v. 470, p. 4956.

34. Vadawale, S. V., Chattopadhyay, T., Mithun, N. P. S., et al., 2018, *"Phase-resolved X-ray polarimetry of the Crab pulsar with the AstroSat CZT Imager"*, Nature Astronomy, v. 2(1), p. 50.

35. Venkata Raman, V., Anandarao, B. G., Janardhan, P., and Pandey, R., 2017, *"An Infrared Photometric and Spectroscopic Study of Post-AGB Stars"*, MNRAS, v. 470, p. 1593-1611.

Solar Physics

36. Dhara, S.K., Belur, R., Kumar, P., Banyal, R.K., Mathew, S.K., Joshi, B., 2017, *"Trigger of Successive Filament Eruptions Observed by SDO and STEREO"*, Solar Physics, v. 292, 145, pp. 1-22.

37. Dumbović, M., Srivastava, N., Rao, Y. K., Vršnak, B., Devos, A., Rodriguez, L., 2017, *"Validation of the CME Geomagnetic Forecast Alerts Under the COMESEP Alert System"*, Solar Physics, v. 292, 96, pp. 1-14.

38. Joshi, B., Thalmann, J. K., Mitra, P. K., Chandra, R., Veronig, A. M., 2017, *"Observational and Model Analysis of a Two-ribbon Flare Possibly Induced by a Neighboring Blowout Jet"*, ApJ, v. 851, 29, pp. 1-14.

39. Kumar, B., Mathur, S., García, R. A., Jiménez, A., 2017, *"On the signatures of flare-induced global waves in the Sun: GOLF and VIRGO observations"*, MNRAS, v. 471, p. 4677-4686.

40. Kumar, S., Bhattacharyya, R., 2017, *"Simulated evolution of three-dimensional magnetic nulls leading to generation of cylindrically-shaped current sheets"*, Physics of Plasmas, v. 24, 064503, pp. 1-5.

41. Kumar, S., Bhattacharyya, R., Dasgupta, B., Janaki, M. S., 2017, *"Chaotic magnetic field lines and spontaneous development of current sheets"*, Physics of Plasmas, v. 24, 082902, pp. 1-12.

42. Louis, R. E., Bayanna, A. R., Socas Navarro, H., 2017, *"Design of an adaptable Stokes polarimeter for exploring chromospheric magnetism"*, Advances in Space Research, v. 60, p. 1547-1556.

43. Mangalam, A., Prasad, A., 2018, *"Topological and statistical properties of nonlinear force-free fields"*, Advances in Space Research, v. 61, p. 738-748.

44. Mathew, S. K., Bayanna, A. R., Tiwary, A. R., Bireddy, R., Venkatakrishnan, P., 2017, *"First Observations from the Multi-Application Solar Telescope (MAST) Narrow-Band Imager"*, Solar Physics, v. 292, 106, pp. 1-25.

45. Mishra, W., Wang, Y., Srivastava, N., Shen, C., 2017, *"Assessing the Nature of Collisions of Coronal Mass Ejections in the Inner Heliosphere"*, The Astrophysical Journal Supplement Series, v. 232, 5, pp. 1-24.

46. Prasad, A., Bhattacharyya, R., Kumar, S., 2017, *"Magnetohydrodynamic Modeling of Solar Coronal Dynamics with an Initial Non-force-free Magnetic Field"*, ApJ, v. 840, 37, pp. 1-12.

47. Sankarasubramanian, K., Sudhakar, M. , Nandi, A., Ramadevi M. C., Adoni, A., Kushwaha, A. Agarwal, A., Dey, A., Joshi, B., et al. (+18 co-authors), 2017, *"X-ray Spectrometers onboard Aditya L-1 for solar flare studies"*, Current Science, v. 113, 4, p. 625-627.

48. Sarkar, R., Srivastava, N., 2018, *"A Comparative Study of the Eruptive and Non-eruptive Flares Produced by the Largest Active Region of Solar Cycle 24"*, Solar Physics, v. 293, 16, pp. 1-21.

49. Srivastava, N., Mishra, W., Chakrabarty, D., 2018, *"Interplanetary and Geomagnetic Consequences of Interacting CMEs of 13 - 14 June 2012"*, Solar Physics, v. 293, 5, pp. 1-12.

50. Tiwary, A. R., Mathew, S. K., Bayanna, A. R., Venkatakrishnan, P., Yadav, R., 2017, *"Imaging Spectropolarimeter for the Multi-Application Solar Telescope at Udaipur Solar Observatory: Characterization of Polarimeter and Preliminary Observations"*, Solar Physics, v. 292, 49, pp. 1-31.

51. Tiwary, A. R., Raja Bayanna, A., Mathew, S. K., 2017, *"Estimation of order parameter of a liquid crystal variable retarder using Haller's approximation"*, Applied Optics, v. 56, p. 4180-4184.

52. Venkatakrishnan, P., Mathew, S. K., Srivastava, N , Bayanna, A. R., Kumar, B., Ramya, B., Jain, N., Saradava, M., 2017, *"The Multi Application Solar Telescope"*, Current Science, v. 113, 4, p. 686-690.

53. Yadav, R., Louis, R. E., Mathew, S. K., 2018, *"Investigating the Relation between Sunspots and Umbral Dots"*, ApJ, v. 855, 8, pp. 1-10.

54. Yadav, R., Mathew, S. K., 2018, *"Physical Properties of Umbral Dots Observed in Sunspots: A Hinode Observation"*, Solar Physics, v. 293, 54, pp. 1-18.

55. Yadav, R., Mathew, S. K., Tiwary, A. R., 2017, *"SPIN: An Inversion Code for the Photospheric Spectral Line"*, Solar Physics, v. 292, 105, pp. 1-16.

56. Yadav, V. K., Srivastava, N., Ghosh, S. S., Srikar, P. T., Subhalakshmi, K., 2018, *"Science objectives of the magnetic field experiment onboard Aditya-L1 spacecraft"*, Advances in Space Research, v. 61, p. 749-758.

Planetary Sciences and PLANEX Program

57. Acharyya,K. and Herbst,E. 2017, *"Gas-grain Fluorine and Chlorine Chemistry in the Interstellar Medium"*, ApJ, v. 850, pp. 1-16.

58. Bhatt,M., Reddy,V., Sanchez,J.A., Schindler,K., Cloutis,E. Mann,P., Corre,L.C., Bhardwaj,A., 2017, *"Composition of Jupiter irregular satellites sheds light on their origin"*, Astronomy and Astrophysics, v. 608, pp. 1-8.

59. Bhatt,M., Wohler,C., Dhingra,D., Thangjam,G., Rommel G. with Bhardwaj, A. and others, 2017, *"Compositional studies of Mare Moscoviense: New perspectives from Chandrayaan-1 VIS-NIR data"*, Icarus, v. 303, pp. 149-165.

60. Das,T.P., Thampi,S.V., Dhanya,M.B. Bhardwaj,A., Ahmed,S.M. and Sridharan, R. 2017, *"Upper limit of helium-4 in the sunlit lunar exosphere during magnetotail passage under low solar wind condition: Result from CHACE aboard MIP in Chandrayaan-1"*, Icarus, v. 297, 189–194.

61. Dhanya,M.B., Bhardwaj,A., Futaana, Y., Barabash,S., Wieser,M., Holmström,M., Wurz,P. 2017, *"New suprathermal proton population around Moon: Observation by SARA on Chandrayaan-1"*, Geophysical Research Letters, v. 44, p. 4540-4548.

62. Gyngard,F. Amari,S., Zinner, E., Marhas,K.K. 2018, *"Correlated silicon and titanium isotopic compositions of presolar SiC grains from the Murchison CM2 chondrite"*, Geochim. Cosmochim. Acta., v.221, p. 145-161.

63. J. P. Pabari, 2017, *"Detection of dust around Mars and its implications"*, Current Science, v. 113, pp.2080-2084.

64. Kohout T.,Haloda J.,Halodov P.,Meier M. M. M.,Maden C.,Busemann H.,Laubenstein M.,Caffee M.W.,Welten K.C.,Hopp J.,Trieloff M.,Mahajan R. R.,Naik S.,Trigo-Rodriguez J.M.,Moyano-Cambero C.E.,Oshtrakh M.I.,Maksimova A.A.,Chukin A.V.,Semionkin V. A.,Karabanalov M.S.,Felner I.,Petrova E. V.,Brusnitsyna E.V.,Grokhovsky V.I.,Yakovlev G.A.,Gritsevich M.,Lyytinen E.,Moilanen J.,Kruglikov N.A. and Ishchenko A.V., 2017, *"Annama H chondrite -Mineralogy, physical properties, cosmic ray exposure, and parent body history"*, Meteoritics & Planetary Science, v.52, p.1525–1541.

65. Lue,C. Futaana,Y., Barabash,S., Wieser,M., Bhardwaj,A., Wurz,P. and Asamura,K. 2017, *"Solar wind scattering from the surface of Mercury: Lessons from the Moon"*, Icarus, v.296, p. 39-48.

66. Mahajan, R.R., Nejia, L.O., Ray, D. and Naik, S., 2018, *"Noble gases, nitrogen, cosmic ray exposure history and mineralogy of Beni M'hira (L6) chondrite, Planet"*, Planetary and Space Science, v.152, p.136-141.

67. Maibam, B., Foley, S., Luguet, A., Jacob, D., Singh Bapin, T., Ray, D., Panda, D., Keppler, R.U., 2017, *"Characterisation of chromites, chromite hosted inclusions of silicates, metal alloys in chromitites from the Indo-Myanmar ophiolite belt of Northeastern India"*, Ore Geol. Rev, v.90, p.260-273.

68. Marhas, K.K. and Sharda,P. 2018, *"Transition elements in supernova presolar grains: condensation vs. Implantation"*, AstroPhysical Journal, v. 853, p.12-27.

69. Mishra, S.K. and Karnam, D.P., 2018, *"Numerical Evaluation of surface modifications at landing site due to spacecraft (soft) landing in the Moon"*, Planetary and Space Science, v. 156 p. 57-61.

70. Mohan,N., Roy,S., Swarup,G., Oberoi,D., Ramanujam, N.M., Raju,C.S., Bhardwaj,A. 2017, *"Radio observation of Venus at meter wavelengths using the GMRT"*, Icarus, v. 297, p. 119-125.

71. Mukundan, V. and Bhardwaj,A. 2017, *"Dayside ionosphere of Titan: Impact on calculated plasma densities due to variations in the model parameters"*, Icarus, v. 299, p. 222–239.

72. Niyogi, A. PatiL, J.K, Patil,S.K. Panda, D. & Munmun Chakarvorty, 2018, *"Magnetic measurements and geochemical characterization of the road-deposited sediments (RDS), Allahabad city, India: impact of climatic perturbations on sediment composition and provenance tracing"*, Journal of Soils and Sediments, v. 18, p. 2581-2595.

73. Pabari, J.P. and Bhalodi, P. J. 2017, *"Estimation of micrometeorites and satellite dust flux surrounding Mars in the light of MAVEN results"*, Icarus, v. 288, pp. 1-9.

74. Panda, D. K., Banerjee, D., Goyal, S. K., Patel, A. R., Shukla, A. D., 2017, *"Development of a Cerium bromide gamma ray spectrometer for space applications"*, Adv. in space Res., v.60, p.1307-1314.

75. Rangwala, N., Colgan,S.W.J., Gal,R.L., Acharyya,K., Huang,X. et al., 2018, *"High Spectral Resolution SOFIA/EXES Observations of C2H2 toward Orion IRc2"*, ApJ, v. 856, pp. 1-12

76. Ray, D. and Shukla, A.D, 2018, *"The Mukundpura meteorite, a new fall of CM chondrite"*, Planetary and Space Science, v. 151, p. 149-154.

77. Ray, D., Mahajan, R.R., Shukla, A.D., Goswami, T. and Chakrabarty, S., 2017, *"Petrography, classification, oxygen isotopes, noble gases and cosmogenic records of Kamargaon (L6) Meteorite: the latest fall in India."*, Meteorit. Planet. Sci., v. 52, p.1744-1753.

78. Ray, D., Shukla, A.D. and Ray, J.S., 2017, *"Early 2017 volcanic activity in Barren: Facts vs hype"*, Current. Science, v.113, p.1657-1659.

79. Ray, D., Upadhyay, D., Misra, S., Newsom, H.E., Ghosh, S, 2017, *"New insights on petrography and geochemistry of impactites from the Lonar crater, India"*, Meteorit Planet Sci., v.52, p.1577-1599.

80. Sinha, R. K., & Vijayan, S, 2017, *"Geomorphic investigation of craters in Alba Mons, Mars: Implications for Late Amazonian glacial activity in the region"*, Planetary and Space Science, 144, 32-48.

81. Sinha, R. K., Vijayan, S., & Bharti, R. R., 2017, *"Study of ice-related flow features around Tanaica Montes, Mars: Implications for late amazonian debris-covered glaciation"*, Icarus, v. 297, p. 217-239.

82. Sinha, R. K.,Vijayan, S.,Shukla, A. D.,Das, P., & Bhattacharya, F., 2018, *"Gullies and debris-flows in Ladakh Himalaya, India: a potential Martian analogue"*, Journal of Geological Society, v. 467.

83. Varun,S., Guleria, R. P. and Ramachandran,S., 2017, *"Global and regional evaluation of a global model simulated AODs with AERONET and MODIS observations"*, Int. J. Climatol, v. 38, pp. 1-21.

84. Vijayan S., and Sinha, R.S. 2017, *"Amazonian fluvial outflow channels in Jovis Tholus region, Mars"*, JGR-Planets, v. 122, p.927-949.

Space and Atmospheric Sciences

85. Arun, S. H., Sharma, S., Chaurasia, S., Vaishnav, R., and Kumar, R., 2018, *"Fog/low clouds detection over the Delhi Earth Station using the Ceilometer and the INSAT-3D/3DR satellite data"*, Int. J. Remote Sens., v. 39, p. 4130-4144.

86. Bagiya, M. S., Sunil, A. S., Chakrabarty, D., and Sunda, S., 2017, *"Salient features of the dayside low latitude ionospheric response to the main phase step-I of the 17 March 2015 geomagnetic storm using IGS TEC maps"*, Adv. Space. Res., v. 60, p. 1827-1837.

87. Bhatt, H., Sharma, S., Trivedi, R., Vats, H.O.,, 2017, *"Variability of fractal dimension of solar radio flux"*, Mon. Not. R. Astron. Soc., v. 475, p. 3117-3120.

88. Bhatt, H., Trivedi, R., Sharma, S. K., an Vats, H. O., 2017, *"Variations in the Solar Coronal Rotation with Altitude-Revisited"*, Sol. Phys., v. 292, p. 1-8.

89. Guharay, A., Batista, P. P., Buriti, R. A., and Schuch, N. J., 2017, *"Signature of the quasi-27-day oscillation in the MLT and its relation with solar irradiance and convection"*, J. Atmos. Sol. Terr. Phys., v. 161, p. 1-7.

90. Hui, D., Chakarabarty, D., Sekar, R., Reeves, G. D., Yoshikawa, A., and Shiokawa, K., 2017, *"Contribution of Storm-Time Substorms to the Prompt Electric Field Disturbances in the Equatorial Ionosphere"*, J. Geophy. Res. Space Phys., v. 122, p. 5568-5578.

91. Jain, C. D., Gadhavi, H. S., Sahu L. K., and Jayaraman, A., 2017, *"Volatile organic compounds (VOCs) in the air, their importance and measurements"*, Earth Sci. India, v. 10(II), p. 1-15.

92. Jain, C. D., Gadhavi, H. S., Wankhede, T., Kallelapu, K., Sudhesh, S., Das, L. N., Pai, R. U., and Jayaraman, A., 2018, *"Spectral Properties of Black Carbon Produced during Biomass Burning Aerosol and Air Quality Research"*, Aerosol and Air Quality Res., v. 18, p. 671-679.

93. Karan, D. K., and Pallamraju, D., 2017, *"Small-scale longitudinal variations in the daytime equatorial thermospheric wave dynamics as inferred from oxygen dayglow emissions"*, J. Geophys. Res. Space Phys., v. 122, p. 6528-6542.

94. Lal, S., Venkataramani, S., Naja, M., Kuniyal, J., Mandal, T., Bhuyan, P., Kumari, K., Tripathi, S., Sarkar, U., Das, T., Swamy, Y., Gopal, K., Gadhavi, H., and Kumar, M., 2017, *"Loss of crop yields in India due to surface ozone: an estimation based on a network of observations"*, Environ. Sci. and Poll. Res., v. 24, p. 20972-20981.

95. Pandey, K., Sekar, R., Anandarao, B. G., Gupta, S. P., and Chakrabarty, D., 2018, *"On the occurrence of afternoon counter electrojet over Indian longitudes during June solstice in solar minimum"*, J. Geophys. Res. Space Phys., v. 123, p. 2204-2214.

96. Pandey, K., Sekar, R., Gupta, S. P., Chakrabarty, D., and Anandarao, B. G., 2017, *"Comparison of quiet time vertical plasma drifts with global empirical models over the Indian sector: Some insights"*, J. Atmos. Sol. Terr. Phys., v. 157-158, p. 42-54.

97. Priyanka, R. S., Jayangondaperumal, R., Pandey, A., Mishra, R. L., Singh, I., Bhushan, R., Srivastava, P., Ramachandran, S., Shah, C., Kedia, S., Sharma, A. K., and Bhat, G. R., 2017, *"Primary surface rupture of the 1950 Tibet-Assam great earthquake along the eastern Himalayan front, India"*, Nature Scientific Reports, v. 7, p. 5433.

98. Rajesh, T. A. and Ramachandran, S., 2017, *"Characteristics and source apportionment of black carbon aerosols over an urban site"*, Environ. Sci. Poll. Res., v. 24, p. 8411-8424.

99. Rajesh, T. A., and Ramachandran, S., 2018, *"Black carbon aerosol mass concentration, absorption and single scattering albedo from single and dual spot aethalometers: Radiative implications"*, J. Aerosol Sci., v. 119, p. 77-90.

100. Rastogi, R. G., Chandra, H., Janardhan, P., and Reinisch, B., 2017, *"Post sunset equatorial spread-F at Kwajalein and interplanetary magnetic field"*, J. Adv. Space Res., v. 60, p. 1708-1715.

101. Rastogi, R. G., Janardhan, P., Chandra, H., Trivedi, N. B., and Erick, V., 2017, *"Effect of solar flare and equatorial electrojet in Eastern Brazil region"*, J. Earth Syst. Sci., v. 126:51, p. 1-8.

102. Rout, D., Chakrabarty, D., Janardhan, P., Sekar, R., Manaiaya, V., and Pandey, K., 2017, *"Solar wind flow angle and geo-effectiveness of corotating interaction regions: First results"*, Geophys. Res. Lett., v. 44, p. 4532-4539.

103. Sahu, L. K., Sheel, V., Kajino, M., Deushi, M., Gunthe, S. S., Sinha, P. R., Yadav, R., Pal, D., Nedelec, P., Thouret, V., and Smit, H. G., 2017, *"Impact of tropical convection and ENSO variability in vertical distributions of CO and O_3 over an urban site of India"*, Climate Dynamics, v. 49, p. 449-469.

104. Sahu, L. K., Tripathi, N., and Yadav, R., 2017, *"Contribution of biogenic and photochemical sources to ambient VOCs during winter to summer transition at a semi-arid urban site in India"*, Environ. Poll., v. 229, p. 595-606.

105. Schultz, M. G., Schröder. S., Lyapina. O., Cooper, O., Galbally, I., Petropavlovskikh, I.,....Gadhavi, H. S.,.... et al.., 2017, *"Tropospheric Ozone Assessment Report: Database and Metrics Data of Global Surface Ozone Observations"*, Elem. Sci. Anth., v. 5, p. 58.

106. Sharma, S., Kumar, P., Jethva, C., Vaishnav, R., and Bencherif, H., 2017, *"Investigations of the middle atmospheric thermal structure and oscillations over sub-tropical regions in the Northern and Southern Hemispheres"*, Climate Dynamics, v. 48, p. 3671-3684.

107. Sharma, S., Kumar, P., Vaishnav, R., Chandra, H., Gadhavi, H., Sridharan, S., and Jayaraman, A., 2017, *"Study of Stratospheric Sudden Warming (SSW) over the tropical and subtropical regions of India using Rayleigh lidar"*, Int. J. Remote Sens, v. 38, p. 4285-4302.

108. Sharma, S., Kumar, P., Vaishnav, R., Jethva, C., and Beig, G., 2017, *"A study of the middle atmospheric thermal structure over western India: Satellite data and comparisons with models"*, Adv. Sp. Res., v. 60, p. 2402-2413.

109. Sharma, S., Kumar, P., Vaishnav, R., Jethva, C., and Bencherif, H., 2018, *"Evaluation of Inter-Hemispheric Characteristics of the Tropopause-Stratopause-Mesopause Over Sub-Tropical Regions"*, Pure Appl. Geophys., v. 175, p. 1123-1137.

110. Sharma, S., Kumar, P., Vaishnav, R., Shukla, K. K., and Phanikumar, D. V., 2018, *"Analysis of total column ozone, water vapour and aerosol optical thickness over Ahmedabad, India"*, Meteorol. Appl., v. 25, p. 33-39.

111. Sharma, S., Vaishnav, R., Shukla, K. K., Lal, S., Chandra, H., and Acharya, Y. B., 2017, *"Rayleigh Lidar observed atmospheric temperature characteristics over a western Indian location: Intercomparison with satellite observations and models"*, European Physical Journal-D, v. 71, p. 187.

112. Singh, R. P., and Pallamraju, D., 2017, *"Near Infrared Imaging Spectrograph (NIRIS) for ground-based mesospheric OH(6-2) and O2(0-1) intensity and temperature measurements"*, J. Earth Sys. Sci., v. 126, pp. 1-17.

113. Yadav, R., Sahu, L. K., Beig, G., Tripathi, N., and Jaaffrey, S. N. A., 2017, *"Ambient particulate matter and carbon monoxide at an urban site of India: Influence of anthropogenic emissions and dust storms"*, Environ. Poll., v. 225, p. 291-303.

Geosciences Division

114. Akhilesh, K., Pappu, S., Rajapara, H, M., Gunnell, Y., Shukla, A.D., and Singhvi, A.K., 2018, *"Early Middle Palaeolithic culture in India around 385–172 ka reframes Out of Africa models"*, Nature, v. 554, p. 97-101.

115. Anand, S.S., Rengarajan, R. and Sarma, V.V.S.S., 2018, *"^{234}Th based carbon export flux along the Indian GEOTRACES GI02 section in the Arabian Sea and the Indian Ocean"*, Global Biogeochem. Cycles, v. 32, p. 417-436.

116. Anand, S.S., Rengarajan, R., Sarma, V. V. S. S., Sudheer, A.K., Bhushan, R., and Singh, S.K., 2017, *"Spatial variability of upper ocean POC export in the Bay of Bengal and the Indian ocean determined using particle-reactive ^{234}Th"*, J. Geophys Res Oceans, v. 122, p.3753 - 3770.

117. Anand, S.S., Rengarajan, R., Shenoy, D., Gauns, M., and Naqvi, S.W.A., 2018, *"POC export fluxes in the Arabian Sea and the Bay of Bengal: A simultaneous ^{234}Th/^{238}U and ^{210}Po/^{210}Pb study"*, Mar. Chem, v. 198, p. 70 - 87.

118. Baker, A.R., Kanakidou, M., Itieri, K.E., Daskalakis, N., Okin, G.S., Myriokefalitakis, S., Dentener , F., Uematsu, M., Sarin, M.M., Duce , R.A., Galloway, J.N., Kenne, W.C., Singh, A., Zamora, L.M., Lamarque, J.F., Hsu, S.C, Rohekar , S.S., and Prospero, J.M., 2017, *"Observation- and model-based estimates of particulate dry nitrogen deposition to the oceans"*, Atmos. Chem. Phys, v. 17, p. 8189-8210.

119. Banerjee, Y., Ghosh, P., Bhushan, R., and Rahul, P., 2017, *"Strong sea forcing and warmer winter during solar minima 2765 yr BP recorded in the growth bands of Crassostrea sp. from the confluence of river Ganges"*, Quat. Int, v. 479, p. 48 - 57.

120. Bhattacharya, F., Shukla, A.D., Patel, R.C., Rastogi, B.K., and Juyal, N., 2017, *"Sedimentology, geochemistry and OSL dating of the alluvial succession in the northern Gujarat alluvial plain (western India) - a record to evaluate the sensitivity of a semiarid fluvial system to the climatic and tectonic forcing since the late Marine Isotopic Stage 3"*, GEOMORPH, v. 297, p.1-19.

121. Bhavya, P.S., Kumar, S., Gupta , G.V.M., Sudharma , K.V., and Sudheesh, V., 2018, *"Spatio-temporal variation in δ^{13}CDIC of a tropical eutrophic estuary (Cochin estuary, India) and adjacent Arabian Sea"*, Cont. Shelf Res, v.153, p.75-85.

122. Bhushan, R., Bikkina, S., Chatterjee, J., Singh, S.P., Goswami, V., Thomas, L.C., and Sudheer, A.K., 2018, *"Evidence for enhanced chlorophyll-a levels in the Bay of Bengal during early north-east monsoon"*, J. Oceanogr. Mar. Sci, v. 9, p.15-23.

123. Bhushan, R., Sat, S.P., Rana, N., Shukla, A.D., Mazumdar, A.S., and Juyal, N., 2018, *"High-resolution millennial and centennial scale Holocene monsoon variability in the Higher Central Himalayas"*, Palaeogeogr. Palaeoclimatol. Palaeoecol, v.489, p. 95-104.

124. Boreddy, S.K.R., Mochizuki, T., Kawamura, K., Srinivas, B. and Sarin, M.M., 2017, *"Homologous series of low molecular weight (C_1-C_{10}) monocarboxylic acids, benzoic acid and hydroxyl acids in fine-mode (PM_{10}) aerosols over the Bay of BengalInfluence of heterogeneity in air masses and formation pathways"*, Atmos. Environ., v. 167, p. 170-180.

125. Chandana, K.R., Bhushan, R., and Jull, A.J.T., 1, *"Evidence of poor bottom water ventilation during LGM in the equatorial Indian Ocean"*, Front Earth Sci, v. 5, p.5-84.

126. Chatterjee, A., and Ray, J.S., 2017, *"Geochemistry of Harappan Potteries from Kalibangan and sediments in the Ghaggar River: Clues for a Dying River"*, Geosci. Front., v. 9, p. 1203-1211.

127. Chatterjee, A., and Ray, J.S., 2017, *"Provenance of the mid-Holocene sediments in the Great Rann of Kachchh, India: Implications for the fluvial landscape of the Harappan Civilization"*, Quat. Int., v. 443, p.177-187.

128. Gautam, I., Ray, J.S., Bhutani, R., Balakrishnan, S., and Dash, J., 2017, *"Role of fractionation correction in accurate determination of $^{142}Nd/^{144}Nd$ by TIMS: a case study of 1.48Ga alkaline rocks from Khariar, India"*, Chem. Geol., v. 466, p.479-490.

129. George, B.G., and Ray, J.S., 2017, *"Provenance of sediments in the Marwar Supergroup, Rajasthan, India: implications for basin evolution and Neoproterozoic global events"*, J.of Asian Earth Sci., v. 147, p. 254-270.

130. Jeelani, Gh., and Deshpande, R.D., 2017, *"Isotope fingerprinting of precipitation associated with western disturbances and Indian Summer Monsoons across the Himalayas"*, J. Earth Sys. Sci., v. 126, pp.1-13.

131. Jeelani, Gh., Shah, R.A., Deshpande, R.D., Fryar, A.E., Perrin, J., and Mukherjee, A., 2017, *"Distinguishing and estimating recharge to karst springs in snow and glacier dominated mountainous basins of the western Himalaya, India"*, J. Hydrol, v. 550, p.239-252.

132. Karkarey, R., Alcoverro, T., Kumar, S., and Arthur, R., 2017, *"Coping with catastrophe: foraging plasticity enables a benthic reef predator to survive in rapidly degrading coral reefs"*, Anim Behav, v.131, p. 13-22.

133. Kothyari, G., Shukla, A.D., and Juyal, N., 2017, *"Reconstruction of Late Quaternary climate and seismicity using fluvial landforms in Pindar River valley"*, Quaternary International, v. 443, p.248-264.

134. Lone, S.A., Jeelani , G., Deshpande, R.D., and Shah, R.A., 2017, *"Evaluating the sensitivity of glacier to climate by using stable water isotopes and remote sensing"*, Environ Earth Sci, v. 76, pp. 1-9.

135. Mukherjee, R., Kumar, S., Muduli, P. R., 2018, *"Spatial variation of nitrogen uptake rates in the largest brackish water lagoon of Asia (Chilika, India)"*, Estuar. Coast. Mar. Sci, IN PRESS.

136. Panda, D.K., Banerjee, D., Goyal, S.K., Patel, A.R. and Shukla, A.D., 2017, *"Development of a Cerium bromide gamma ray spectrometer for space applications"*, Adv. Space Res, v. 60, p.1307-1314.

137. Patel, A., and Rastogi, N., 2018, *"Oxidative potential of ambient fine aerosol over a semi-urban site in the Indo-Gangetic Plain"*, Atmos. Environ, v. 175, p. 127-134.

138. Priyanka, R.S., Jayangonda, P., Bhushan, R., Srivastava, P., Ramachandran, S., Shah, C., Kedia, S., Sharma, A., Bhat, G.R., 2017, *"Primary surface rupture of the 1950 Tibet-Assam great earthquake along the eastern Himalayan front, India"*, Scientific Reports, v. 7, pp. 1 - 12.

139. Sandeep, K., Shankar, R., Anish Kumar, W., Yadava, M.G., Ramesh, R., Jani, R.A., Weijian, Z., and Xuefeng, Lu., 2017, *"A multi-proxy lake sediment record of Indian summer monsoon variability during the Holocene in Southern India"*, Palaeogeogr. Palaeoclimatol. Palaeoecol, v. 476, pp. 1-14.

140. Satish, R.V., Shamjad, P.M., Thamban, N.M., Tripathi, S.N., and Rastogi, N., 2017, *"Temporal Characteristics of Brown Carbon over the Central Indo-Gangetic Plain"*, Environ. Sci. Technol, v. 51, p. 6765-6772.

141. Shamjad, P.M., Satish, R.V., Thamban, N.M., Rastogi, N., and Tripathi, S.N., 2018, *"Absorbing Refractive Index and Direct Radiative Forcing of Atmospheric Brown Carbon Over Gangetic Plain"*, ACS Earth and Space Chemistry, v. 2, p. 31–37.

142. Sharma, S., Shukla, A.D., Bartarya, S.K., Marh, B.S., and Juyal, N., 2017, *"The Holocene floods and their affinity to climatic variability in the western Himalaya, India"*, Geomorphology, v. 290, p. 317-334.

143. Singh, A., Bach, L.T., Fischer, T., Hauss, H., Kiko , R., Paul, A.J., Stange ,P., Vandromme, P., and Riebesell, U., 2017, *"Niche construction by non-diazotrophs for N_2 fixers in the eastern tropical North Atlantic Ocean"*, Geophys. Res. Lett, v. 44, p. 6904–6913.

144. Srivastava, P., Agnihotri, R., Sharma, D., Bhushan, R., and Sawlani, R., 2017, *"8000-year monsoonal record from Himalaya revealing reinforcement of tropical and global climate systems since mid-Holocene"*, Sci. Rep, v. 7, pp. 1-10.

Theoretical and Computational Physics

145. Abbas, G., 2017, *"it A model of spontaneous CP breaking at low scale"*, Phys. Lett. B, v. 773, p. 252-257.

146. Abhishek, A., Mishra, H. and Ghosh, S., 2018, *"Transport coefficients in the Polyakov quark meson coupling model: A relaxation time approximation"*, Phys.Rev. D, v. 97, p. 1-20.

147. Anand, S., Bhatt, J. R., and Pandey, A., 2017, *"Chiral Battery, scaling laws and magnetic fields"*, JCAP, v.1707, pp. 1-13.

148. Anand, S., Chaubal, P., Mazumdar, A. and Mohanty, S., 2017, *"Cosmic viscosity as a remedy for tension between PLANCK and LSS"*, JCAP 1711, v. 11, pp. 1-17.

149. Anand, S., Dey, U. K. and Mohanty, S., 2017, *"Effects of QCD Equation of State on the Stochastic Gravitational Wave Background"*, JCAP, v. 3, pp. 1-10.

150. Ananthanarayan, B., and Rindani, S.D., 2018, *"Inclusive spin-momentum analysis and new physics at a polarized electron-positron collider"*, Phys. J. C, v. 125, pp. 1-17.

151. Ananthanarayan, B., Caprini, I., and Das, D., 2017, *"Electromagnetic charge radius of the pion at high precision"*, Phys. Rev. Lett., v. 119, p. 132002-1 to 132002-5.

152. Arya, R., Dasgupta, A., Goswami, G., Prasad, J. and Rangarajan, R., 2018, *"Revisiting CMB constraints on warm inflation"*, J. Cosmology and Astroparticle Physics, v. 1802, p. 0-23.

153. Arya, R., Mahajan, N. and Rangarajan, R., 2017, *"Gravitino production in a thermal Universe revisited"*, Phys. Lett. B, v. 772, p. 258-264.

154. Atreya, A., Bhatt, J. R. and Mishra., A., 2018, *"Viscous Self Interacting Dark Matter and Cosmic Acceleration"*, JCAP, v. 1802, pp. 1 - 12.

155. Azam, M., Bhatt, J. R. and Sami, M., 2018, *"Many-body aspects of gravity in compact stars"*, Phys.Scripta, v.93, p. 025001.

156. Bandyopadhyay, S., Roy, A. and Angom, D., 2017, *"Dynamics of phase separation in two-species Bose-Einstein condensates with vortices"*, Phys. Rev. A, v. 96, p. 1-9.

157. Bhalla, P., Kumar, P., Das, N., Singh, N.,, 2017, *"Finite frequency Seebeck coefficient of metals: a memory function approach"*, J. Phys. Chem. Solids, v. 109, p. 31.

158. Chakravarty, G. K., Mohanty, S. and Lambiase, G., 2017, *"Testing theories of gravity and supergravity with inflation and observations of the cosmic microwave background"*, Int.J.Mod.Phys., v. 26, p. 1-64.

159. Choubey, S., Goswami, S. and Pramanik, D., 2018, *"A study of invisible neutrino decay at DUNE and its effects on θ_{23} measurement"*, JHEP, v. 1802, p. 055.

160. Choubey, S., Goswami, S., Gupta, C., Lakshmi, S. M. and Thakore, T., 2018, *"Sensitivity to neutrino decay with atmospheric neutrinos at the INO-ICAL detector"*, Phys. Rev. D, v. 97, p. 3, 033005.

161. Das, A., Konar, P. and Thalapillil, A., 2018, *"Jet substructure shedding light on heavy Majorana neutrinos at the LHC"*, JHEP, v. 1802, p. 0-22.

162. Das, D., Hati, C., Kumar G., and Mahajan, N., 2017, *"Scrutinizing R-parity violating interactions in light of $\mathrm{R}_{\mathrm{K}^{(*)}}$ data"*, Phys. Rev. D., v. 96, p. 095033-1 to 095033-8.

163. Deepthi, K. N., Goswami, S. and Nath, N., 2017, *"Can Nonstandard interactions jeopardize the hierarchy sensitivity of DUNE"*, Phys. Rev. D, v. 96, pp. 1 - 6.

164. Deppisch, F. F., Hati, C., Patra, S., Pritimita, P. and Sarkar, U., 2017, *"Neutrinoless double beta decay in left-right symmetric models with a universal seesaw mechanism"*, Phys. Rev. D., v. 97, p. 035005-1 to 035005-9.

165. Dutta, J., Konar, P., Mondal, S., Mukhopadhyaya, B. and Rai, S.K., 2017, *"Search for a compressed supersymmetric spectrum with a light Gravitino"*, JHEP, v. 1709, p. 0-27.

166. Garg, I., Goswami, S., Vishnudath, K.N. and Khan, N., 2017, *"Electroweak vacuum stability in presence of singlet scalar dark matter in TeV scale seesaw models"*, Phys. Rev. D, v. 96, pp. 1 - 17.

167. Goswami, S., Chakravarty, G., Mohanty, S., and Prasanna, A.R., 2017, *"Constraints on cosmological viscosity from GW150914 observation"*, Phys.Rev.D, v. 95, p. 1-6.

168. Hati, C., Patra, S., Reig, M., Valle, J.W.F., and Vaquera-Auaujo, C.A., 2017, *"Towards gauge coupling unification in left-right symmetric $\mathrm{SU}(3)_c \times \mathrm{SU}(3)_{\mathrm{L}} \times \mathrm{SU}(3)_{\mathrm{R}} \times \mathrm{U}(1)_{\mathrm{X}}$ theories"*, Phys. Rev. D., v. 96, p. 015004-1 to 015004-9.

169. Konar, P., Mondal, T. and Swain, A.K., 2017, *"Demystifying the compressed top squark region with kinematic variables"*, Phys. Rev. D, v. 96, pp. 1-6.

170. Kumar, A., Jamal, Y., Chandra, V. and Bhatt, J. R., 2018, *"Collective excitations of a hot anisotropic QCD medium with Bhatnagar-Gross-Krook collisional kernel within an effective description"*, Phys. Rev. D, v. 97, p.034007.

171. Mohapatra, R. K. and Mishra, H., 2017, *"Z(3) metastable states in a Polyakov quark meson model"*, Phys. Rev. D, v. 95, pp. 1-14.

172. Pal, S., Roy, A. and Angom, D., 2017, *"Bifurcations, stability and mode evolution in segregated quasi-2D condensate mixtures"*, J. Phys. B, v. 50, pp. 1-9.

173. Pal, S., Roy, A. and Angom, D., 2018, *"Collective modes in multicomponent condensates with anisotropy"*, J. Phys. B, v. 51, pp. 1-10.

174. Rani, L., Singh, N., 2017, *"Dynamical conductivity of Graphene"*, J. Phys.: cond matt, v. 29, p. 255602.

175. Roy, A., and Angom, D., 2017, *"Finite temperature expansion dynamics of Bose–Einstein condensates in ring traps"*, Phys. Lett. A, v. 381, p. 1-6.

176. Roy, A., and Angom, D., 2017, *"Ramifications of topology and thermal fluctuations in quasi-2D condensates"*, J. Phys. B, v. 50, pp. 1-11.

177. Thakur, L., Haque, N. and Mishra, H., 2017, *"Heavy quarkonium moving in hot and dense deconfined nuclear matter"*, Phys.Rev. D, v. 95, pp. 1-20.

178. Thakur, L., Srivastava, P. K., Kadam, G. P., George, M., and Mishra, H., 2017, *"Shear viscosity η to electrical conductivity σ_{el} ratio for an anisotropic QGP"*, Phys.Rev. D, v. 95, pp. 1-11.

Atomic, Molecular and Optical Physics

179. Aadhi, A. and Samanta, G.K. 2017, *"High power, high repetition rate, tunable broadband mid-IR source based on single-pass optical parametric generation of a femtosecond laser."*, Optics Letters (OSA), v. 42, p. 2886-2889.

180. Aadhi, A. and Samanta, G.K., 2017, *"High-power, high repetition rate, tunable, ultrafast vortex beam in the near-infrared."*, Journal of Optics (IOP), v. 20, pp. 1-7.

181. Aadhi, A. Sharma, V., Singh, R.P. and Samanta, G.K. 2017, *"Continuous-wave, singly resonant parametric oscillator-based mid-infrared optical vortex source."*, Optics Letters (OSA), v. 42, p. 3674-3677.

182. Roy, A., De, S., Arora, B. and Sahoo, B.K. 2017, *"black-body radiation shift, magic and tune-out wavelengths for the 6S-¿5D3/2 clock transition in Yb+."*, J. Phys., v. B 50, pp. 1 - 11.

183. Anwar, A., Vaity, P., Chithrabhanu, P. and Singh, R. P., 2018, *"Direct transfer of pump amplitude to parametric down-converted photons"*, Optics Letters, v. 43, p. 1155-1158.

184. Sahoo, B.K. and Das, B.P. 2017, *"Relativistic coupled-cluster analysis of parity nonconserving amplitudes and related properties of the $6s^2\mathrm{S}_{1/2} - 5d^2\mathrm{D}_{3/2;5/2}$ transitions in 133Cs"*, Mol. Phys., v. 115, p. 2765.

185. Sahoo, B.K. and Kumar, P. 2017, *"Relativistic coupled-cluster theory analysis of unusually large correlation effects in the determination of gj factors in Ca^+"*, Phys. Rev., v. A 96, pp. 1-9.

186. Sahoo, B.K. and Singh, Y., 2017, *"Significance of distinct electron correlation effects in determining the P,T-odd electric dipole moment of 171Yb."*, Phys. Rev., v. A 95, pp. 1-10.

187. Basu, S., Sanyal, P., Sahoo, K., Chauhan, N., Sarkar, A., and Juyal, N., 2017, *"Variation in monsoonal rainfall sources (Arabian Sea and Bay of Bengal) during the late Quaternary: Implications for regional vegetation and fluvial systems"*, Palaeogeography Palaeoclimatology Palaeoecology, v. 491, p. 77-91.

188. Bhushan, R., Sati, S.P., Rana, N., Shukla, A.D., Mazumdar, A.S. and Juyal, N., 2018, *"High-resolution millennial and centennial scale Holocene monsoon variability in the Higher Central Himalayas"*, Palaeogeography Palaeoclimatology Palaeoecology, v. 489, p. 95-104.

189. C.-B. Li, Y. -M. Yu, and Sahoo, B.K. 2018, *"Relativistic coupled-cluster theory analysis of energies, hyperfine structure constants, and dipole polarizabilities of Cd^{+}."*, Phys. Rev., v. 97, pp. 1 - 9.

190. Chauhan, N., and Morthekai, P, 2017, *"Chronology of desert margin in western India using improved luminescence dating protocols"*, Earth Syst. Sci., v. 126, pp. 1 - 26.

191. Chithrabhanu, P., Lal, N., Anwar, A., Reddy, S. G. and Singh, R. P., 2017, *"Quantum information with even and odd states of orbital angular momentum of light"*, Physics Letters A, v. 381, p. 1858-1865.

192. Sahu, D., Minh, Y.C., Lee, Liu, C.F. Das, A., Chakrabarti, S.K., Sivaraman, B., 2018, *"Deuterated Formaldehyde in the Low-Mass Protostar HH_{212}"*, Monthly Notices of the Royal Astronomical Society, v. 475, p. 5322-5329.

193. Kaur, J., Singh, S., Arora, B., and Sahoo, B.K. 2017, *"Annexing magic and tune-out wavelengths to the clock transitions of the alkaline-earth-metal ions."*, Phys. Rev., v. A 95, pp. 1 - 14.

194. Teller, J.T. McGinn, R.A., Rajapara, H.M., Shukla, A.D., and Singhvi, A.K. 2018, *"Optically stimulated luminescence ages from the Lake Agassiz basin in Manitoba"*, Quaternary Research, v. 1, p. 1-16.

195. Akhilesh, K., Pappu, S., Rajapara, H.M., Gunnell, Y., Shukla, A.D. and Singhvi, A.K., 2018, *"Early Middle Palaeolithic culture in India around 385–172 ka reframes Out of Africa models."*, Nature, v. 554, p. 97-101.

196. Kumar, V., Anwar, A. and Singh, R. P., 2018, *"Structuring Stokes correlation functions using vector-vortex beam structures"*, Journal of Optics, v. 20, pp. 1-9.

197. Sharma, L., Sahoo, B. K., Malkar, P. and Srivastava, R. 2018, *"Application of relativistic coupled-cluster theory to electron impact excitations of Mg+ in the plasma environment"*, Eur. Phys. J., v. D 72, pp. 1 - 9.

198. Singh, M., Mondal, S., Sahoo, B. K., and Mishra, T., 2017, *"Quantum phases of constrained dipolar bosons in coupled one-dimensional optical lattices"*, Phys. Rev., v. A 96, pp. 1 - 8.

199. Jabir, M. V. and Samanta, G. K., 2017, *"Robust, high brightness, degenerate entangled photon source at room temperature."*, Scientific Reports (Nature), v. 7, pp. 1 - 7.

200. Jabir, M. V., Chaitanya, N.A., Mathew, M. and Samanta, G. K. 2017, *"Direct transfer of classical non-separable states into hybrid entangled two photon states."*, Scientific Reports (Nature), v. 7, pp. 1 - 7.

201. Chaitanya, N.A., Chaitanya, A., Banerji, J and Samanta, G. K. 2017, *"High power, higher order ultrafast hollow Gaussian beams."*, Applied Physics Letters (AIP), v. 110, pp. 1 - 6.

202. Kumar, P., C.-B. Li, and Sahoo, B. K. 2018, *"Diverse trends of electron correlation effects for properties with different radial and angular factors in an atomic system: A case study in Ca+."*, J. Phys., v. B 51, pp. 1 - 15.

203. Püttner, R. Jänkälä, K., Kushawaha, R.K., Marchenko, T., Goldsztejn, G., Travnikova, O., Guillemin, R. Journel, L., Ismail, I., B Cunha de Miranda, Lago, A.F., Céolin, D., Piancastelli, M.N. and Simon, M. 2017, *"Detailed assignment of normal and resonant Auger spectra of Xe near the L edges"*, Phys. Rev., v. A 96, pp. 1 - 13.

204. Reddy, S. G., Kumar, V., Miyamoto, Y. and Singh, R. P., 2017, *"Scattering of Poincaré beams: polarization speckles"*, Optics Express, v. 25, p. 19886-19893.

205. Pavithraa, S. Sahu, D., Seth, G., J. -I. Lo, Raja Sekhar, B. N., Cheng, B. -M. Das, A., Mason, N.J. and Sivaraman, B. 2017, *"SH stretching vibration of propanethiol ice - a signature for its identification in the interstellar icy mantles"*, Astrophysics and Space Science, v. 362, p. 126.

206. Pavithraa, S., Lo, J. -I., Rahul, K., Raja Sekhar, B. N. Cheng, B.-M. Mason, N. J. and Sivaraman, B. 2018, *"Vacuum ultraviolet photoabsorption of prime ice analogs of Pluto and Charon"*, Spectrochimica Acta Part A: Molecular and Biomolecular Spectroscopy, v. 190, p. 172-176.

207. Yu, Y.-M. and Sahoo, B.K. 2017, *"Estimation of blackbody - radiation Shift due to Stark Effect for the Microwave 113Cd+ Ion Clock."*, Phys. Rev., v. A 96, pp. 1 - 5.

Library & Information Services

208. Alam, M. N and Shukla, A., 2018, *"Mapping of Research on Planetary Systems (PS) in India"*, International Journal of Library, Information, Networks and Knowledge (IJLINK), v. 2, p. 89-102.

209. Pandey P., 2018, *"Growth of Remote Sensing and GIS in India."*, Journal of Remote Sensing & GIS, v. 9, p. 8–14.

Publications

Publications in Proceedings of Conference/ Symposia/ Workshops

Astronomy and Astrophysics

1. Chandra Sunil, Singh, K.P., Baliyan, K.S., 2017, *"Multiwavelength flares and magnetic field in blazars: a case study of IBL S5 0716+714"*, Proc. IAU, New frontiers in black hole astrophysics, Vol.12, p. 203-206.

Planetary Sciences and PLANEX Program

2. Bhatt,M., C. Woehler, N. Srivastava, V. V. Shevchenko, A. A. Berezhnoy, A. Grumpe, A. Bhardwaj, 2018, *"Regolith Alteration Processes at Reiner Gamma Shed Light on the Formation of Lunar Swirls"*, Lunar & Planetary Sci. Conf., Houston, USA, p. 1765.
3. Chandan Kumar,K Durga Prasad,Sanjeev Kumar, P Thirupathaiah and S A Haider, 2017, *"An Improved Retarding Potential Analyzer (RPA) For Future Mars Missions"*, AOGS 2017 Singapore, PS05-13-A021.
4. Ghosh, J., Arora, G., and Basu Sarbadhikari, A, 2018, *"Lunar Magnetic Field Anomaly - Global Distribution and Possible Origin"*, LPSC, Houston,USA, 1972.
5. Goyal S. K., Naik, A. P., Mithun, N. P. S., Vadawale, S. V., Tiwari, N. K., Chattopadhyay, T., Nagrani, N., Madhavi, S., Ladiya, T., Patel, A. R., Shanmugam, M. Adalja, H. L. Patel, V. R., Ubale, G. P, 2017, *"Design and development of position sensitive detector for hard X-ray using SiPM and new generation scintillators"*, Proc. SPIE 10392, Hard X-ray, Gamma-ray, and neutron detector physics XIX, 1039205.
6. A. D. Jadav, J. P. Pabari, and D. G. Kamdar, 2017, *"Design of signal processing module for an impact ionization dust detector"*, International Conference on Intelligent Systems and Signal Processing , Vallabh Vidyanagar, SPCE06.
7. K Durga Prasad, Chandan Kumar, Sanjeev Kumar and S A Haider, 2017, *"An improved Langmuir Probe for future Mars Missions"*, AOGS, Singapore, PS5-12.
8. K. Durga Prasad, Vinai K. Rai and S.V.S. Murty, 2017, *"Thermophysical behavior of lunar analogues under simulated lunar environment"*, 47th Lunar and Planetary Science Conference, #1414.
9. K. K. Marhas and R. K. Mishra, 2018, *"The vanguard of irradiation: the fourth element"*, 49th LPSC ,Houston, #1646.
10. Mahajan R. R., Basu Sarbadhikari A., and Sisodia M. S., 2017, *"Piplia Kalan eucrite: noble gases, nitrogen and cosmic ray exposure history"*, 80th Annual Meeting of the Meteoritical Society, #6083.
11. R. K. Mishra, K. K. Marhas and M. Trieloff, 2018, *"$^{26\mathrm{A}}l - ^{26\mathrm{M}}g$ isotope systematics in Leoville CAIs and Chainpur chondrule"*, 49th LPSC, Houston, #1633.
12. R.K. Mishra and K.K. Marhas, 2017, *"Discerning a general formation scenario of Hibonite-pyroxene spherules from petrographic and mineralogical study of a pristine object in Allan Hills 77307 (CO3.03)"*, 48th LPSC , Houston.
13. Rajiv. R. Bharti and I. B. Smith, 2018, *"Investigating Multiple Lava Flows near Mangala Fossa with SHARAD"*, 49th LPSC ,Houston, USA,1550.
14. A. Basu Sarbadhikari, J. Ghosh, and Narendranath, S, 2018, *"Alkali-rich rocks at and near tycho crater of the Moon"*, 49th, PLSC. Houston ,USA, 1980.
15. Basu Sarbadhikari A. , Mahajan R. R., Das P., Chakraborty S., Babu E. V. S. S. K., Vijaya Kumar T., and Sisodia M. S., 2017, *"New constraints of the petrogenesis of piplia kalan eucrite"*, 80th Annual Meeting of the Meteoritical Society, #6207.
16. Sanjeev Mishra, Chandan Kumar, Durga Prasad, 2017, *"Numerical Evaluation of Sensor for Electric Field and Plasma*

Measurements in Upper Martian Ionosphere", AOGS 2017 Singapore.

17. Sharda P. and Marhas K.K., 2017, *"Temperature based implantation and concentration profiles of trace elements in presolar SiC type X grain"*, Goldschmidt 2017, Paris.

Geosciences Division

18. Banerji, U.S., Bhushan, R., and Jull, A.J.T., 2017, *"Evidences of Roman Warm Period and Dark Ages of Cold Period from the active mudflats of the western Indian coast: major climatic event of first millennium"*, Oral presentation at OSICON 2017, NCESS, Trivandrum.
19. Banerji, U.S., Bhushan, R., and Jull, A.J.T.,, 2017, *"Evidences of Global Climatic Events for Last Two Millennia and their Forcing Factors from Active Mudflats of Western India"*, Oral presentation at Goldschmidt Conference 2017, Paris, France, v. 228.
20. Bhushan, R., Yadava, M.G., Shah, M.S., Raj, H., 2017, *"New 1 MeV AMS Laboratory (PRL-AURiS) at Physical Research Laboratory (PRL), Ahmedabad, India for the measurement of* ^{14}C, ^{10}Be *and* ^{26}Al*"*, In Proceedings of the XIVth International Conference on Accelerator Mass Spectrometry held at Ottawa, Canada.
21. Damodararao, K, Singh, S.K, Bhushan, R., Rengarajan, R., and Rai, V.K., 2017, *"Dynamics of Hf Isotopic Compositions in the Indian Ocean Waters"*, Oral presentation at Goldschmidt Conference 2017, Paris, France, Goldschmidt Abstracts, v.827.
22. Raj, H., Banerji, U S., Shah, C., and Bhushan, R., 2017, *"Age depth model comparison of radiocarbon based sedimentation rates from the Northern Andaman Sea"*, In proceedings of the Geochronology workshop at Inter University Accelerator Centre, New Delhi.
23. Raj, H., Banerji, U.S., Shah, C., and Bhushan, R., 2018, *"Corals from Lakshadweep Island: High Resolution Proxy Records of Past Climate Over Northern Indian Ocean"*, Oral presentation at National Seminar on 'Dynamics of Surface and Subsurface Geological Processes', Pondicherry University, Pondicherry, p. 122.
24. Ramesh, R. and Singh, A., 2017, *"Applications of Stable Nitrogen and Carbon Isotopes in Oceanography"*, Indian Association of Nuclear Chemists and Allied Scientists (IANCAS) Bulletin, v. 16, p.51-57.
25. Ray, D., Ghosh, S., and Shukla, A. D., 2017, *"The Katol (L6-7): A unique chondrite with evidences of shock induced melting and post-shock annealing"*, EPSC2017, Sept17-22, RIGA Latvia.#399.
26. Ray, J S., 2017, *"Bitter Springs* $\delta^{13}C$ *anomaly in the Vindhyan Supergroup, Rajasthan, India"*, Proceedings of National Seminar on Dynamics of surface and subsurface geological processes, Pondicherry University, p. 135.
27. Rengarajan, R., Subha Anand, S., Bhushan, R., and Singh, S.K., 2017, *"Spatial Distribution of POC Export Flux Estimated Using 234Th/238U Disequilibrium along the GEOTRACES GI03 Section"*, Goldschimdt Conference, p. 3320.
28. Shah, C., Banerji, U.S., Bhushan, R., and Shah, N.K., 2017, *"Geochemical characteristics and productivity changes in the sediment core of the Arabian Sea of last 115 years"*, Oral presentation at OSICON 2017, NCESS, Trivandrum.
29. Shah, M.S., Bhushan, R., Saxena, A., and Prajapati, N,D., 2018, *"A proposed automated instrument to analyse coral reef sample (Spectral Luminescence Scanner)"*, paper presented at "2017 IEEE, International Conference on Intelligent Computing, Instrumentation and Control Technologies" IEEE Xplore.
30. Shukla, A.D., and Ray, D., 2017, *"Integrated Scanning Electron Microscopy-Micro Raman spectrometer (SEM Raman): future tool for planetary exploration"*, EPSC2017, September 17-22, 2017, RIGA Latvia.#183.
31. Singh, A., Su, D., Kurten, A., Cedras, B., Todinanahary, R., Raes, G., Fernandes, E., Kumar, M.N., and Senkondo, E, 2017, *"An IIOE-2 Capacity Building Initiative - The Indian Ocean Early Career Scientist Network"*, IAPSO-IAMAS-IAGA Assembly in Cape Town, South Africa, 27 Aug – 1 Sep 2017.Newsletter.
32. Subha Anand ,S., Rengarajan, R., 2017, *"234Th and 210Po-210Pb based Carbon export flux along the Indian GEOTRACES GI02 section in the Arabian Sea and the Indian Ocean"*, Goldschimdt Conference, p. 3812.

Theoretical and Computational Physics

33. Goswami, S., 2017, *"The Status of INO"*, Neutrino 2016, London, UK, v. 888, p. 1-012025.
34. Konar, P. and Swain, A.K, 2017, *"Mass restricting variables in semi-invisible production at the LHC"*, Pramana, v. 89, p. 1-5.
35. Mishra, H. and Abhishek, A., 2017, *"Transport Coefficients in Polyakov Quark Meson Model: a quasi particle approach"*, Proceedings of Science (PoS), Critical point and onset of deconfinement, Wang Center, StoneBrook, USA, Aug. 2017.
36. Mishra, H., Dev, P. and Kadam, G. P., 2017, *"Estimating Transport Coefficients In Hot And Dense Quark Matter"*, Proceedings of Science (PoS), International Conference on Nuclear Physics 2017, Adelaide, Australia, v. 336, p. 1-9. PoS, CPOD 17, 080, 2018, v. 080, p. 1-14.

Atomic, Molecular and Optical Physics

37. A. Roy, S. De, B. Arora and B. K. Sahoo, 2017, *"Polarizabilities and Magic Wavelengths of 171Yb+ clock transition 6S-¿5D3/2"*, Joint Conference of the European Frequency and Time Forum and IEEE International Frequency Control Symposium July 9 – 13, 2017 Micropolis Conference Center Besançon, France, p. 753-757.
38. A Chaitanya, A. C. Nellikka, J. Banerji, and G. K. Samanta, 2017, *"Nonlinear Interaction of Ultrafast Hollow Gaussian Beams."*, Frontiers in Optics, v. JTu3A, p. 96.
39. A. C. Nellikka, M. V. Jabir, J. Banerji, and G. K. Samanta, 2017, *"Nonlinear Interaction of Oppositely Charged Vortices Generating Hollow Gaussian Beams."*, CLEO: QELS Fundamental Science, v. FW1D, p. 2.
40. Anwar, A., Vaity, P., Chithrabhanu, P. and Singh, R. P., 2017, *"Revealing pump amplitude in parametric down converted photons"*, Fourth International Conference on Optical Angular Momentum (ICOAM 17) September 18-22, Anacapri, Italy, P1.03., P1.03.

41. Ekta Patel, Rajesh K Kushawaha, Hardik Mewada and Umang Soni, 2017, *"Developing a multi-plates velocity map imaging spectrometer for 3D velocity vector imaging of electrons and ions"*, 2017 Nirma University International Conference on Engineering (NUiCONE), p. 1-5.

42. Kumar, V. and Singh, R.P., 2017, *"Correlation singularities in vector speckle fields"*, 13th International Conference on Correlation Optics 2017, September 11-15, Chernivtsi, Ukrain,, v. S2.07.

43. Kumar, V., Piccirillo, B., Reddy, S. G. and Singh, R. P., 2017, *"Polarization correlation singularities in vector speckle field"*, Fourth International Conference on Optical Angular Momentum (ICOAM 17) September 18-22, Anacapri, Italy,, P1.22.

44. Lal, N., Anwar, A., Perumangatt, C. and Singh, R.P., 2017, *"Intensity correlations of twisted photons generated by spontaneous parametric down-conversion"*, Frontiers in Optics 2017, September 18-21, Washington DC, U.S.A., v. JW4A, p. 13.

45. M. V. Jabir, A. C. Nellikka, and G. K. Samanta, 2017, *"Generation of hybrid entangled two photon state using classical non-separable state of the pump beam."*, Laser Science, v. JW4A, p. 29.

46. M. V. Jabir, and G. K. Samanta, 2017, *"Robust, bright entangled photon source based on type-0, non-collinear phase matching in periodically poled crystal."*, Frontiers in Optics, v. JW4A, p. 30.

47. Reddy S.S., K.R. Nagabhushana, N. Chauhan, and F. Singh, 2017, *"TL/OSL properties of beta irradiated* Al_2O_3 *Nanophosphor synthesized by microwave combustion method"*, D.G. Kuberkar, N.A. Shah (Eds.), AIP Conf. Proc., Rajkot, Gujarat, India doi:10.1063/1.4982129, p. 40045.

48. Srinivas, P., Perumangatt, C., Pidishety, S., Srinivasan, B. and Singh, R. P., 2017, *"Investigation of self-healing property of composite vector vortex beams"*, CLEO: QELS Fundamental Science, 2017, May 14-19, San Jose, California, USA, v. FW1D, p. 8.

49. U. Ablikim, C. Bomme, E. Savelyev, H. Xiong, R. Obaid4, B. Kaderiya, S. Augustin, K. Schnorr5, I. Dumitriu, R. Bilodeau, D. Kilcoyne, V. Kumarappan, R. K. Kushawaha, F. Ziaee, T. Osipov, A. Rudenko, N. Berrah and D. Rolles, 2017, *"Studying Molecular Structure and Dynamics via Coulomb Explosion Imaging with X-rays and Ultrafast Laser Pulses"*, IOP Conf. Series: Journal of Physics, v. 875, p. 032026.

50. V. Sharma, A. Aadhi, and G. K. Samanta, 2017, *"Direct generation of tunable optical vortex dipole beams using a Gaussian beam pumped optical parametric oscillator."*, Frontiers in Optics, v. FW2B, p. 2.

51. V. Sharma, A. Aadhi, N. A. Chaitanya, and G. K. Samanta, 2017, *"Multi-GHz femtosecond Airy beam radiation in higher-harmonic fractional cavity OPO."*, CLEO: Science and Innovations, v. JTh2A, p. 90.

Publications

Books Edited / Review Articles / Other Publications

Books Edited

1. Fischer, C.J., Abbas, G. and Ananthanarayan, B.2018, *"it Perturbative Expansions in QCD Improved by Conformal Mappings of the Borel Plane"*, Perturbation Theory: Advances in Research and Applications, Nova Science Publishers, p. 211-254

Review Articles

1. Ray, J.S.,2017, *"Principles of Radiometric Dating by K. Gopalan,"*, Current Science,, v. 114, p. 397-398.
2. Goswami, S. and Ahmed, S. 2017, *" Physics Potential of the ICAL detector at the India-based Neutrino Observatory (INO)"*, Pramana, v. 88, p.5.
3. Ramesh, R., Borgaonkar, H., Band, S. and Yadava, M.G2017, *"Proxy climatic records of past monsoon, in(M.N. Rajeevan and S. Nayak, eds.) Observed climate variability and Change over the Indian region,"*, Springer, p.271-284.
4. Srivastava, N.2018, *"Young volcanism on the Moon"*, Encyclopedia of Lunar Science, Springer, v.ISBN: 978-3-319¬05546-6.

PRL Technical Notes

5. T. A. Rajesh and S. Ramachandran, 2018, "Data analysis and visualization software package for SKYRAD.PACK V4.2", PRL Technical Note, PRL-TN-2018-111.
6. T. A. Rajesh, S. Ramachandran, P. Malaidevan, Vishnu K. Dhaker, J. T. Vinchhi, Mitesh B. Bhavsar and T. K. Sunilkumar, 2017, "Laboratory simulation of atmospheric transmission", PRL Technical Note, PRL-TN-2017-110.

Various Events, and Outreach Activities at PRL

Foundation Day Celebration at PRL – 11 November 2017

PRL celebrated its Seventieth Foundation Day on Saturday, the 11 November 2017 and honoured Dr. K. Kasturirangan with Shri Hari Om Ashram Prerit Senior Scientist Award for the year 2016 which was tenth of the series since its inception in 1998 and Dr. Durgesh Tripathi was conferred with the Buti Foundation Award for the year 2017 which was sixth of the series since its beginning in 2007. The award ceremony was organized at the K. R. Ramanathan Auditorium, Physical Research Laboratory, Ahmedabad.

Dr. Anil Bhardwaj, Director, PRL, presented the awards in the presence of distinguished guests from various institutions in Ahmedabad, invited representatives from the Hari Om Ashram Trust, Nadiad, Buti Foundation, New Delhi, Dr. Vikram A. Sarabhai's family, and staff members of PRL.

Dr. K. Kasturirangan, Chairman, National Education Policy, Chairman, Karnataka Knowledge Commission, an Honorary Distinguished Advisor, Indian Space Research Organisation, an Emeritus Professor at the National Institute of Advanced Studies and former Chairman of ISRO has been awarded the Hari Om Ashram Prerit Senior Scientist Award for the year 2016 for his outstanding lifetime contributions in the Space Sciences and Technology and its impact on national development.

Dr. Kasturirangan delivered the award lecture on 'Vistas of Astrophysics and Planetary Science Research- The Indian Perspective'. He discussed about the major astrophysical facilities currently available for research by the Indian scientific community in different electromagnetic wavelength bands. Further, he also give a brief description of some of the planned ambitious facilities such as Indian Neutrino Observatory. One more aspect of the talk was the level of India's participation in the establishment of some of the major astrophysical observatories elsewhere in the world such as Thirty Metre Telescope promoted by USA and Square Kilometre Array promoted by Australia and South Africa.

Celebration of 70^{th} Foundation Day of PRL, Ahmedabad.

The Buti Foundation Award for the year 2017 is given to Dr. Durgesh Tripathi of the Inter-University Centre for Astronomy and Astrophysics, Pune, India. Dr. Tripathi was given the Buti Foundation Award in recognition of his work in the area of Space and Plasma Physics, especially for his fundamental contributions to Solar Plasma Physics. On this occasion Dr. Tripathi presented his work on heating and maintaining the Solar Coronal Plasma to a Million Degree.

Activities on the promotion of Basic Sciences

Celebration of World Space Week - 9 October 2017

A day-long celebration of World Space Week was held on 9^{th} October 2017 at PRL. On this occasion around 160 students and teachers various schools visited both the campuses of PRL in Ahmedabad. The celebration included some lectures followed by interactions of students with PRL scientists and laboratory visits. Both, PRL faculty and students/PDFs, participated in this celebration with lots of enthusiasm and interest. The programme was coordinated by the Outreach committee. The students were extremely happy at the end of the programme and shared their feedback with outreach committee members. Some students told that the information they received from PRL on specialized research such as Space Sciences, Planetary Sciences, Cosmology etc. was a unique learning experience for them.

Celebration of World Space Week, 9th October 2017.

National Science Day (NSD) 2018 celebrations

As has been the practice for several years, a day-long celebration was held on 24^{th} February 2018 at PRL, Ahmedabad to mark the National Science Day. The celebrations aim to attract young minds and motivate them to take up science as one of their career options. National Science Day is also observed to spread the message of the importance of science and its application among the people and to accelerate the pace of development among them.

Nearly 150 students were selected for participation on the basis of a screening test conducted at Ahmed-abad, Gandhinagar, Vallabh Vidyanagar, Vadodara, Bharuch, Surat, Valsad, Porbandar, Rajkot, Bhuj, Pal-anpur, Bhavnagar and Patan on 7^{th} January 2018. The selected students were requested to prepare one poster each on the following themes and many interesting and novel ideas were presented in the post-ers.

Poster Themes were:

1. Theme 1: Atmospheric Pollution: Causes and Effects
2. Theme 2: Microbes: Enemy or Friend.

Two popular talks one on “C. V. Raman and his effects”, and the other on “Unraveling the gravitational wave universe: dawn of a new astronomy” were arranged for the teachers and students. There was also a session of interaction with scientists in which students and teachers had asked questions related to their queries in science.

Every year PRL awards five scholarships sponsored by Aruna Lal Endowment Fund, created by late Prof. Devendra Lal, former Director of PRL. Based on the performance in the screening test a few students were selected for an interview leading to the five Aruna Lal Endowment Fund Scholarships. This scholarship was instituted to encourage science among high school students. The scholarship comprises a cash award of ₹ 10,000 and a citation. This year’s winners of Aruna Lal Scholarship are;

1. Mr. Samyak Bharwad, Maharaja Agrasen Vidyalaya, Ahmedabad
2. Mr. Aditya Trivedi, Delhi Public School, Bopal, Ahmedabad
3. Mr. Raj P. Mehta, Anandalaya, Anand
4. Mr. Riju Dutta, Anandalaya, Anand
5. Mr. Abhishek Kodinariya, Premier Schools, Rajkot

The programme ended with the felicitation of the Aruna Lal scholarship winners (05), screening test toppers (14) and winners of the poster competition (12).

Most students were accompanied by their teachers and parents. Teachers and students had good interaction with PRL scientists and the judges of the poster competitions throughout the day.

PRL had also organized a science exhibition displaying the exhibits of some of the research activities being pursued at PRL also exhibits of some fundamental science topics.

Open House Science Exhibition

PRL organised an “Open house Science Exhibition” during 26-27 February 2018 at PRL that coincided with National Science Day celebrations. In this exhibition live experiments, live laboratory measurements, dynamic models, path breaking in-house built equipment, rare specimens of terrestrial and extra-terrestrial material, together with info-graphics on current research trends were exhibited. In addition, information on fire and elevator safety were also exhibited. A live exhibit of glass blowing attracted the visitors. PRL research scholars also had a career counseling booth where in visitors, especially young students and their teachers/parents interacted with lot of interest. An exhibit on ”Swachha Bharat” containing items prepared by various PRL sections along with ”swachhata pledge selfie point” was an unique exhibit this year. The objective of this exhibition was to reach out to students, teachers, researchers and a common man with interesting and exciting exhibits. Around 3000 people including kids and young school/college/university students visited PRL during this exhibition.

Glimpses of NSD and Open house science exhibition.

PRL has been organizing popular lectures by eminent scientists open to the public. In this series the following popular lectures were organized during the this year.

- "A Brief History of Light", Prof. Majid Ebrahim-Zadeh, The Institute of Photonic Sciences (ICFO), Spain.
- "The Mysterious Magnetic Personality of our Sun", popular lecture under aegis of 21st National Conference on Atomic, Molecular and Optical Physics, hosted by PRL, Ahmedabad, Prof. Arnab Rai Choudhuri, IISc, Bangalore.

NSD celebrations at Udaipur Solar Observatory, Udaipur:

The National Science Day (NSD) was celebrated at the Udaipur Solar Observatory on 14th February, 2018. The NSD organizing team of Udaipur Solar Observatory (USO) staff targeted toward a proactive participation of school students in the celebration. A total of eleven schools participated, where each school was represented by two students of class XI and an accompanying teacher.

For a direct involvement of students in the NSD celebration, the schools were requested in advance to submit an essay (in Hindi or English) on the topic "Solar Physics" for an essay competition. The schools: Vidya bhawan Senior Secondary School, Maharana Mewar Public School and Delhi Public School stood first, second, and third. Each of them was awarded a certificate of appreciation along with science books as prizes.

The NSD program also had active participation from the USO and PRL members. The participants were welcomed by Prof. Nandita Srivastava who gave a talk on the importance of National Science Day and highlighted the recent achievements of ISRO. The students and post-doctoral fellows also participated actively. Mr. Ranadeep Sarkar gave an introduction to the Solar Physics. A team of students led by Dr. Avijeet Prasad conducted a hands-on session using various astronomy kits like sun dials, start clocks and clinometers while Ms. Sushree Sangeeta Nayak gave a presentation featuring Indian women in science. Dr. Bhushit Vaishnav from PRL shared his views on "Science as a career".

The school students gave oral presentations on the topic "Importance of Science and Technology in Social Development" — of which, the first three were rewarded with books and certificates. The three winners are; Ryan International School, Delhi Public School and Maharana Mewar Public school in descending order of merit. The program was concluded by formally thanking all the participants for their support and interest. Special thanks are also due to Ms. Arpita Agrawal and Mr. Akshay Kumar Suthar for their effort to make the celebration successful.

To popularize astronomy, a night-sky-watch session— using the 14 inch telescope at USO—was organized for the participants in the evening session, which was enthusiastically received.

Glimpses of NSD celebrations at Udaipur Solar Observatory.

Glimpses of Outreach activities by Udaipur Solar Observatory.

Night sky-watch program at Udaipur Solar Observatory

Two night sky-watch events were organised by the Outreach Committee at the Udaipur Solar Observatory using the on-campus 14-inch telescope. The Post-docs and PhD students showed the night-sky to the visitors with the telescope.

1. The first event was conducted for the USO staff and their family members on 22nd January 2018. The session began around 7 pm and continued till 9.30 pm. The session was attended by around 30-40 people which involved observations of the Moon and various Messier objects like Andromeda galaxy, double stars, Orion nebula, globular- and open-clusters.
2. The second event was conducted as part of the National Science Day celebration on 14th February, 2018. This was attended by around 20-30 students and their accompanying teachers. The students were first given a brief overview of the night sky, highlighting the important night-sky objects followed by a hands-on session on using astronomy kits. The night-sky objects shown were similar to the first event. The session was well received with lots of discussions and interesting questions from the students.

Outreach Activity: Visits to the island observatory and GONG instrument site

In the year 2017-2018, the Outreach Committee of USO organized several visits of groups of students, mainly from Colleges. These student groups visited the Multi-Application Solar Telescope (MAST) located on the island in the Fatehsagar lake and also visited the Global oscillation Network Group (GONG) site in the office campus. The visits were organised on the basis of the requests received from various colleges in India. These include, Punjab University, Chandigarh, IIT Bombay Astronomy Amateur Club, VP & RPTP Science College, Vallabh Vidyanagar, Sangam University, Bhilwara. In addition students from various Science and Engineering Colleges of Udaipur also visited USO.

Like previous years, this year too, the selected winners of Astronomy Competition held for school students by Aryabhat Foundation, Bhopal, were sent to USO on an educational trip.

In total, USO team reached out to approximately 500 students by engaging in showing the solar telescopes and also the night–sky. This number also includes few enthusiastic residents of Udaipur city.

PRL Student chapter

PRL student chapter was formed on 15 June 2015. Currently the chapter has 25 PhD student members from different divisions of PRL. Although the PRL student chapter started with the vision of popularizing optics and photonics among the school and college students through hands on experiments, however, with time the chapter has expanded its scientific portfolio by incorporating hands on experiments from other branches of science. So far the PRL student chapter have devised more than 50 hands on basic experiments to explain many phenomena in our daily life. The major activists of the student chapter during 2017-2018 are as follows.

Student's conference:

PRL student chapter organized its annual conference named as Students' Conference in Optics and Photonics (SCOP), for the professional development of the PhD students, during 1-2 September 2017. This is a two days' conference, organized by the students and participated by the students and post-doctoral fellows from different parts of India. In SCOP-2017, we had 45 students and post-doctoral fellows from 25 different Institutes/Universities and 20 in-house participants. To broaden the perspective of the participants, the conference hosted few invited speakers from different Institutes of India working on different fields including planetary science, atmospheric science and biology, and a plenary talk by an eminent scientist from ICFO, Barcelona, Spain. Due to this annual conference, the M.Sc., PhD and postdoctoral students from different parts of India get the opportunity to visit PRL with full funding and share their research and build networking among themselves. The details of SCOP-2017 can be found using the webpage, ~(https://www.prl.res.in/ prlosachap/SCOP2017/index.html). In its second year, the conference has already started getting appreciation from different parts of the research community.

Visiting remote school

Eight volunteers of PRL student chapter visited a small tribal school, Government Primary School, Kajavas, Poshina, Gujarat on 10^{th} February, 2018. It was a middle school (up to standard 8) situated in a remote village along the Gujarat-Rajasthan interstate border. The students were from relatively poor families, but the school was equipped with mid-day meal system. Though the school was situated in an interior village area, the roads leading to the school was in good shape. Our student chapter members demonstrated 14 hands on experiments over 3 hours to around 400 students. The students were encouraged to try the experiments by themselves. Despite the challenges like poor infrastructure, lack of advanced study materials and the remote location of the school, the students have attended all the demonstrations and learnt whatever bits and pieces they could understand. At the end of the day, all the volunteers felt happy and privileged for their visit to small underprivileged primary school and meet those vibrant young future scientists. The chapter members realized the importance of the outreach activities in such remote schools and would like to conduct their outreach programs in such under exposed, remote schools throughout Gujarat. This will not only help those students to develop an interest towards science, but also help the chapter members to grow as a better individual.

Demonstration during NSD and open house activity of PRL Like previous years, our student chapter demonstrated their hands-on experiments to the students participated in the National Science Day (NSD) and open house activities organized by PRL during 24-27 February 2017.

Demonstration in LD Engineering college, Ahmedabad LD Engineering College, Ahmedabad invited PRL student chapter members to demonstrate hands-on experiments in their Science fest. Members to PRL student chapter demonstrated hands-on experiments to the participants of the Science fest organized by LD Engineer College on 24^{th}th March 2017.

Participants of SCOP 2017 held during 1-2 September 2017, in Physical Research Laboratory.

SWACHHTA PAKHWADA CELEBRATION-2018

PRL organized Swachhata Pakhwada for the period from 01.02.2018–15.02.2018. A brief of activities undertaken are as below:

Emphasize and sensitization of staff towards weeding out of Old records and Cleanliness of work area reiterating to adopt environment conservation by green initiative and plantation of trees in more number in all Office/Residential premises, discarding use of plastic bags/water bottle(s), usage of paper and stationery pragmatically in office taking steps towards green footprint/initiative. Beyond Economic Repair instruments may be identified for disposal following the due procedures and particularly handling of hazardous and e-waste discard in periodic intervals.

- Mass Swachhata Pledge by Officials on inauguration and concluding day of the Pakhwada including at Mount Abu and Udaipur Campuses.
- Health, hygiene & sanitation awareness camp at Gulbai Tekra (slum area), Ambawadi for the benefit of around 300 residents. The identified slum area lacks basic facilities pertaining to hygiene, health and sanitation and accordingly ideal for this intervention to create awareness.
- Mass Tree Plantation in which PRL Officials took initiative and planted trees within the main campus of PRL. Around 100 saplings were planted by the employees. "Mass Tree Plantation" was organized in PRL resident colony at Vikram Nagar Ambli-Bopal Road. The activity is planned in

coordination with Local Residents Welfare Association. PRL Staff members, Faculty and Children have participated in the event. Enthusiasm and excitement of the youth was center of attraction.

- Public Afforestation program in which students of Kendriya Vidyalaya SAC, Girls Polytechnic/Ambawadi and Sri Sri Ravishankar Vidya Mandir/Satellite, were invited to plant trees, along the PRL Boundary Wall outside.
- In order to spread awareness amongst officials, an online-cum offline Swacchta quiz competition amongst Faculty/Staff members was organized on various Swachhta-related topic. The questions were based on Swachhta Bharat Abhiyan, waste management, cleanliness and sanitation, Energy Conservation and so on so forth.
- Inter-Divisional Competition "Best Out of the Waste" in order to promote innovation and spread awareness regarding use/re-use of various waste materials generated in Office, such as Plastic Bottles, Newspapers, stationary etc., thereby leading to reduction in waste materials.
- "Swachhta /Cleanliness Drive" was undertaken at PRL main Campus. The Officials decided to make the Drive opposite to the PRL Campus, wherein a lot of plastic waste is thrown by travelers and passersby. Around 60 staff members participated in the Swachhta Drive. Cleanliness and sanitation drive carried out at USO/PRL island Observatory campus in similar manner.
- As part of Social outreach activities on Swachhta Pakhwada celebration, PRL Staff members held a Walkathon, involving a 1-KM walk from PRL to Gujarat University and back. This activity was also covered by local News reporter of Prashar Bharti, DD Girnar and is also available on $http://youtu.be/\mathrm{Z}25f_yh3uz\mathrm{Q}$
- On 15.02.2018, the Closing Ceremony was conducted that started with the Mass pledge once again taken by PRL Officials in the spirit of the very first day of Pakhwada. PRL arranged an interactive Guest lecture by Dr. Shilpa Sutariya, District Health Officer of Ahmedabad, on the subject "Health and Hygiene – Government initiatives and our contributions". Thereafter Prize Distributions were conducted for the Internal Competitions by the Director, PRL.
- To spread an awareness in students about the Swacchta, Cleanliness, health, hygiene, sanitation and scientific outlook, PRL Scientists delivered lecture to school students as a part of outreach on National Science Day celebrations.

Initiatives under progress approved during the Pakhwada

Installation of Vermi Compost Plant

LED-based Solar Lighting

Rejuvenation of Water Harvest Facilities

To rework on water harvest pits located in various campuses and to revamp before onset of monsoon to tap rain water and avoid stagnation of water to control vector borne diseases.

Vigilance Awareness Week 2017

Vigilance Awareness Week was celebrated in PRL during 30th October to 4th November 2017. During Vigilance Awareness Week celebration, different types of activities were conducted within organization.

Vigilance Awareness Pledge was undertaken by PRL staff members on 30.10.2017. An awareness lecture on "My Vision – Corruption free India" was arranged on 31.10.2017 and the lecture was delivered by Shri C P Zunzuwadia, Former Deputy Secretary, Gujarat Vigilance Commission.

To encourage participation of one and all in celebration of vigilance awareness week, an Essay Writing Competition (English/Hindi) on "My Vision – Corruption Free India" was conducted in PRL on 02.11.2017.

To spread awareness, interactive lecture was delivered by Shri Sangeet Kumar Mishra, Senior Administrative Officer, Space Application Centre, Ahmedabad on 02.11.2017 on the subject "Vigilance Machinery of the Government & Vigilance Awareness in Administration". Participation of a Faculty, Staff and Students in large number has made this event successful.

The banners and various pamphlets with regard to Vigilance Awareness were displayed at prime location of Physical Research Laboratory, Ahmedabad. Integrity pledge is also affixed permanently at a few places for staff and also suppliers/visitors sensitizing vigilance and integrity at work place.

Celebration of International Yoga Day at PRL

International Day of Yoga was celebrated in PRL on 21^{st} June 2017. Shri Yogeshbhai, a renowned Yoga Instructors in Ahmedabad was invited to lead the practice/demonstration sessions. There were about 60 participants and their family members attended the practice session. All had participated enthusiastically. The session was attended by our Director who encouraged staff members to actively participate and practice Yoga and encouraged the event with his presence. Yoga Session was enriched by learning – Flexibility Exercises, Yogasans, Pranayama and Meditation etc. Similar Yoga Sessions were also held at our Udaipur Solar Observatory (USO), Udaipur and Infrared Observatory at Mt. Abu.

Celebration of Ambedkar Jayanti at PRL

The 126^{th} Birth Anniversary of Dr. Babasaheb Bhimrao Ambedkar was celebrated in Physical Research Laboratory on 14^{th} April, 2017. The programme commenced with lighting of lamp and offering floral tributes to Babasaheb's photograph. The Director, PRL recalled the significant contributions of Babasaheb towards shaping up of today's India. He opined that unless life of people in villages and remotest parts of our Country are improved, the real vision of our forefathers may not see reality. The changes in our social set up towards equality and education would be the real tribute to the views of Bharat Ratna Dr. Babasaheb Ambedkar.

Glimpses of various events and activities by PRL.

Internal Complaints Committee

PRL is an institution committed to gender equality, women's rights and empowerment. PRL has a firm zero tolerance stance towards any form of sexual harassment. PRL firmly believes that a sense of security at the workplace will improve women's participation in Scientific work, resulting in their empowerment and inclusive growth.

In pursuance of the Sexual Harassment of Women at Workplace (Prevention, Prohibition and Redressal) Act 2013 and the Rules framed under the Act, PRL set up an Internal Complaints Committee in 2010. The committee consists of 7 members from the administrative as well as scientific areas and includes an external expert as mandated under rules. Since inception, the PRL Internal Complaints Committee has been meeting at regular intervals to discuss and plan activities as well as strategies to make sure that the workplace is a zero tolerance. The Committee has organized several awareness seminars and talks on gender sensitization for PRL employees Every year, the committee celebrates International Women's day by inviting prominent thought-leaders to deliver lectures on women empowerment and also distributes souvenirs to its female employees. The Committee organizes formal and informal interactive sessions with women employees to understand their concerns. The ICC at PRL makes sure that the policy is communicated to all PRL Women employees and display details of the dedicated officers on all its notice boards. A webpage on Internal Complaints Committee has been set up on the PRL website to disseminate information. Internal Complaints Committee members are also deputed to attend workshops on prevention of sexual harassment of women at workplace from time to time.

For the period April, 2017 to March, 2018, no complaints have been received by the ICC.

Workshop on Reservation in Services For Central Government Employees

A Workshop on "Reservation in Services for Central Government Employees" was held at PRL, during 01-02, February, 2018. Total 103 PRL permanent Staff Members were nominated from Director-PRL for taking participation in these two days programme. Amongst 103 participants, Total 54 PRL-Employees were from Reserved Categories and other employees nominated from Administrative and Scientific Areas. Members of Faculty from Institute of Secretariat & Training Management (ISTM), New Delhi have conducted in-house training programme covering aspects of constitutional provision in reservation, case studies on reservation issues, Role and functions of Liaison officer, Laws of disabilities and so on so forth. The Liaison Officers Shri H.R. Vaghela (For OBC) and Dr. A.D.K. Singh (For SC/ST/PWD/Ex-serviceman) were instrumental in organising the workshop. PRL employees from Reserved class segment, in particular, and Scientific and Administrative personnel, in general, immensely benefited from the Workshop.

Capacity Building Programmes

PLANEX Programme

A new initiative by Indian Space Research Organization for beginning a program of dedicated Space missions in Planetary and Space Sciences opened new opportunities for scientists and technologists within India to embark upon a new era of Planetary Exploration. In this context, the Advisory Committee on Space (ADCOS) suggested back in 2001 that a comprehensive national program on Planetary Sciences be taken up as a thrust area of research in the country. A plan was prepared and submitted to ISRO, followed by reviews and a formal approval from ISRO to begin a program on Planetary Science and Exploration (PLANEX) with the Physical Research Laboratory being the nodal point. The objectives of the PLANEX Program comprised (i) carrying out research on areas of Planetary Sciences and encourage young students to participate in Planetary Science research, (ii) provide discussion forum for Planetary Exploration Missions of ISRO for science objectives, payload design and data analysis, and (iii) provide facilities for research in Planetary Sciences at other academic institutions/universities. To realize the above objectives, the PLANEX Program began supporting projects being undertaken at various institutions and Universities within India. Many new research groups have taken up planetary science projects on studies of meteorites, impact craters, spectral reflectance, laboratory studies of lunar analogues, analysis of data from planetary missions and planetary instrumentation. Presently, 10 projects are being supported by ISRO over 2015-2018 under the PLANEX Program.

The Annual PLANEX Project Review Meeting was held in the Physical Research Laboratory, Ahmedabad on June 26, 2017. Eleven Principal Investigators associated with PLANEX projects attended the review meeting and made presentations on their projects. The DDU Nadiad PLANEX project has completed three years, and closed last year, whereas the remaining 10 projects are projected to continue until 2018-19. A 10-member review committee attended the review meeting to evaluate the progress made and provide suggestions to improve the quality of the PLANEX Program. The presentations made by PIs during the meetings were generally of a high level. PLANEX PIs have also presented their work in international and national conferences and several peer-reviewed publications have resulted from their work over the last year.

RESPOND Programme

PRL administers the Indian Space Research Organization (ISRO) RESPOND to provide funding to academia in India for conducting research and development activities related to Space Science, particularly in the fields of Astronomy and Astrophysics, the Physics of Earth's atmosphere/ionosphere, Solar Physics, Space Weather, and Space Plasma Physics. The main aim of the RESPOND programme is to encourage quality research in areas of relevance to the Indian space programme.

The typical duration of a RESPOND research proposal is 3 years. The proposal grant generally includes funding for at least one JRF leading to his/her PhD degree. The RESPOND programme at PRL mainly supports space sciences research in university, college and national institutes. The main deliverables of the RESPOND programme at PRL have been publication of research papers in international and national refereed journals, developing trained scientists and PhD theses of JRFs. The proposers also seek funding for augmenting computational facilities; occasionally the RESPOND grant is also utilised to set up a new laboratory facility for research at the university or institute.

During the 2017-2018, PRL received about 22 proposals, out of which 3 have been approved, 12 are at different stages of review and recommendation process. Few proposals were redirected to other ISRO centres for review and few were not selected. Some of these new proposals are aimed at scientific investigations based on observations of ISRO's astronomy satellite, i.e. ASTROSAT. A few proposals in the upcoming field of Astrochemistry have also been

received. Many projects aimed at providing theoretical modeling support to various problems in Space physics, Astrophysics and Earth Sciences have been received at PRL.

The total number of ongoing projects as of March, 2018 is 15. The recipients of project funding through RESPOND, mainly include researchers from Universities/Colleges, national research institutes, and also from IITs. Apart from Space Sciences related proposals, PRL is also mentoring the student team of Thiagarajar college of Engineering for the RESPOND project on “Multi-Factor Authentication Add-on For OpenVPN” as part of Smart India Hackathon-2017.

UN Course on Space and Atmospheric Science

A nine-month Post-Graduate Diploma Course in Space and Atmospheric Science is conducted every alternate year at Physical Research Laboratory (PRL), Ahmedabad under the auspices of Center for Space Science and Technology Education in Asia and the Pacific (CSSTEAP). CSSTEAP has headquarters in Dehradun and is affiliated to the United Nations. So far 10 courses have been conducted and 109 participants from 16 countries in the Asia-Pacific region have benefited. In suitable cases this course leads to an M.Tech. degree on fulfillment of the requirements of the Andhra University.

Official Language promotion at PRL

Activities on the Promotion of Official Language

- A two-day Inter-Centre Hindi Technical Seminar was organized in PRL on April 21-22, 2017 whose title was “Role of Space Science and Technology in the progress of India”. In this Seminar around 58 papers were presented by different scientists from various Centres/Units of Department of Space.
- Hindi Patrika “Vikram” was released on June 30, 2017.
- Departmental Inspection of Official Language Inspection of USO, Udaipur was done on 24.06.2017.
- PRL Hindi section staff members participated in the Hindi Technical Seminar held in Space Applications Center on July 7, 2017.
- PRL representative attended the first half-yearly TOLIC meeting organized in Gujarat Vidyapeeth on August 07, 2017. First prize was awarded to PRL staff member Smt. Amee Patel for Online Hindi Competition. PRL also contributed to the content for the magazine that was released by TOLIC. Senior Hindi Officer, Shri RS Gupta was felicitated with Seva Samman – A Lifetime Achievement Award by TOLIC, Ahmedabad.
- The PRL website is also updated in Hindi from time to time.
- Hindi Pakhwada was celebrated in P.R.L. during September 14-28, 2017. The highlights of the celebration included debates, extempore, word quiz, typing, Hindi essay and self-written poetry competition, Kavi Sammelan etc. This time video calling facility was initiated for the first time during the Hindi Pakhwada so as to enable staff members of other outstation PRL premises to attend the same without travelling from one state to another.
- On September 27, 2017 under “Swachhta hi Sewa” mission, banners regarding cleanliness were prepared in Hindi and displayed at different places.
- An Outreach activity to motivate school children in Science was conducted on October 09, 2017 wherein scientific lectures in Hindi were delivered by senior faculty members of PRL.
- Translation of P.R.L. Annual Report was done in October 2017.
- An Orientation program for Hindi Officials and staff was organized by Department of Space in ISTRAC, Lucknow on 10th November 2017 which was attended by Senior Translator & Hindi Typist. This program is regarding the propagation of Hindi and its progress.
- Departmental Inspection of Official Language Inspection of IRO-PRL, Mount Abu was done on 15th November, 2017.
- According to the Directives of DOS different days were celebrated which were marked with Hindi Nibandh Competition organized on Vigilance Awareness Week in November, 2017.
- In every quarter PRL OLIC meetings are organized to review the progress of Hindi and to fulfill the targets of correspondence. Throughout the year OLIC quarterly meetings were organized on 25.05.2017, 29.08.2017, 01.12.2017 and 17.03.2018 in different campuses of PRL in Ahmedabad, Thaltej, Udaipur and Mount Abu. In this, data related to correspondence and official language activities from all sections are sought and compiled. In particular, the emphasis is on the achievement of target in correspondence.
- Hindi Workshops are also organized alongside OLIC meetings, in which the staff members of different sections deliver talk related to their work.
- Departmental Inspection of Official Language of APEP Aluva was done by Hindi Officer. In-house inspection of all sections of PRL was completed by March.
- A Hindi Nibandh competition and a popular talk was organized in PRL on 10th January, 2017 on the occasion of Vishwa Hindi Diwas.
- The December issue of Hindi Patrika “Vikram” was released on Republic Day.
- PRL participated in the second half-yearly TOLIC meeting held in NID on February 07, 2018. PRL staff member Smt. Amee Patel won First prize for Nibandh Pratiyogita organized by TOLIC.
- National Science Day question paper was prepared in bilingual, also support was given to faculty members in Hindi talk.
- Outreach booklet was published in bilingual.

Facilities and Services

Computer Centre

Computational Services Group (CSG)

The Computational Services Group (CSG) is responsible for providing services/facilities like Networking (Internet, Local Area Network, Wifi, SPACENET), High performance Computing, E-mail, Web, DNS, Proxy, VPN, Centralized Printing, DHCP, Video Conference, software development and maintenance. Following services/facilities are added/upgraded/provided during the year 2017-2018.

[A] Web Site/Page

1. Quiz Competition – Hindi Pakhwada

PRL celebrates Hindi Pakhwada every year in the month of September. During year 2017, Hindi Pakhwada was celebrated from 14th September 2017 to 28th September 2017 in PRL. During the Pakhwada programme various quiz competitions were planned where all the PRL employees could participate. However, every year, the employees at Mount Abu and Udaipur Solar Observatory, Udaipur, have to travel to PRL Main Campus, Ahmedabad to participate in the various competitions like 'Aashubhashan', 'Kavita Path', 'Hamara Karya' etc.. Further, those employees were unable to view the same ongoing competition at PRL. To encourage participation from both the remote centres of PRL, we implemented web based Video Calling facilities using NextCloud. Due to this feature, all the employees from Mount Abu and Udaipur could participate and view the Hindi Pakhwada programme.

During the Hindi Pakhwada, PRL also organizes Hindi Typing Speed Test. To encourage all the PRL's employees to participate in Hindi Typing Speed Test, we developed a web based application where employees can login through their PRL's email username and password and participate in the Hindi Typing Test. This application allows user to login and type the given paragraph within prescribed time only. It also calculates Hindi Typing Speed in Words per Minute and accuracy of typing. The result is also generated immediately. We had received overwhelming response from the employees and total 70 employees participated in the competition.

2. Online MCQ Competition – Swachhta Pakhwada

The Swachhta Pakhwada programmewas celebrated in PRL. To spread awareness about Swachhtaamongst the employees, an online Multiple Choice Question (MCQ) quiz was organized. An online webbased application was developed by Computational Services Group (CSG) where employees can login through their PRL's email username and password and participate in the Swachhta Quiz. We received huge participation from PRL employees where total 120 employees have participated.

[B] Scientific Network Licenses software

Computational Services Group (CSG) manages centralized network licenses of various scientific software like Mathematica, Matlab, IDL, Maple, Sigmaplot and many others. CSG has procured latest version of gridMathematica with 15 users' network concurrent licenses for parallel computations. CSG has procured latest version of Matlab R2017a with 20 concurrent network user licenses along with 2 concurrent network users for different toolboxes of Matlab. CSG has also upgraded the Sigmplot software version 13 to version 14. All details are available on Intranet site ofComputational Services Group (CSG).

[C] Internet and Intranet

1. Upgradation of network link between Thaltej and Main Campus
The point-to-point network connectivity between Thaltej campus and

Main Campus was operational over 100 Mbps dedicated Optical Fiber Cable (OFC) provided by Bharat Sanchar Nigam Limited (BSNL). This bandwidth between main campus and thaltej campus has been upgraded to 5 Gbps for efficient virtualization data synchronization, Internet Access and Access of PRL IT services from Thaltej Internet Gateway. Due to varying technological availability of feature and its usage, a lot of efforts were put to configure and enable 5 Gbps link using port truncking at switch level.

2. Separate Internet Connectivity at Thaltej Campus

The Thaltej campus hosts the PRL's near DR site setup since Dec-2015 with existing hardware. A dedicated separate 1 Gbps Internet connectivity over Optical Fiber Cable (OFC) from Bharat Sanchar Nigam Limited (BSNL) was commissioned to restore the PRL's IT services from Thaltej campus in case of any disaster event at Main campus. A separate secure proxy/gateway server is configured and running at Thaltej campus which can allow PRL users to browse Internet over 1 Gbps Thaltej link if Internet link of main campus is not available due to any reasons. Currently it is in testing phase. At present, all the Video Conference through thaltej campus is taking place using Thaltej Campus Internet connectivity. This is also a redundant failsafe facility for Main campus VC.

3. Local Area Network (LAN) Expansion to newly come up scientific projects

Over the period many scientific facilities have come up in Thaltej campus of PRL and they require extension of Endpoint LAN connectivity for their Laboratory and experiments. LAN connectivity provision to all such new facilities was carried out for various locations by means of Ethernet cable extension or Fiber cable lying like New Dispensary Building at Transit accommodation, Thaltej campus, Terahertz Project building, LAN points augmentation work in Thaltej planex building for newly come up LA-ICPMS and Astrochemistry labs.

4. Network Switches Up-gradation

Recently, Computational Services Group (CSG) has replaced PRL's majority of Network switches with latest technology based IPv6 compatible network switches, These switches provides full power PoE support and many security features. All the network switches are secured as per industry standard best security practices like removed default IP address and Username-Password of the switch, disabled non-required services, enable switch management from specific IP Addresses, access of switch over secure channel like SSH, HTTPS and restriction to usage of unauthorized IP Address, eliminate issue of IP Address conflict, prevent usage of server IP Address in client machines within PRL-LAN.

[D] SPACENET

SPACENET is a Close User Group (CUG) network of DOS/ISRO Centers/Units. This network is used for accessing Intranet sites of other DOS/ISRO Centers/Units.

To strengthen the security of SPACENET network, IPTABLES based firewall and SQUID proxy server has been installed at gateway level to comply with DOS/ISRO IT Security policy. Also, New IP Address Scheme has been developed for this new secure SPACENET Network. Installation and commissioning of new dedicated infrastructure for SPACENET Network in PRL Main campus has been completed. This work includes laying OFC, installing LAN Rack and fixing Lan I/O in rooms at different places in PRL. Using this New Infrastructure, SPACENET Connectivity is now operational at Multistory Building and Administration Building.

[E] Participation in the National Science Day/Outreach Activities

Computational Services Group (CSG) prepared Beowulf Cluster using Raspberry Pi in order to familiarize the students and the visitors with "High Performance Computing". It is often puzzled by the people about How HPC works! To create the Beowulf Cluster, we used four Raspberry Pi, out of which, one used as Master Node and rest three as client nodes. All the RPi were interconnected through small computer network. To share a single job among all the RPi, Message Passing Interface (MPI) was used. Students/Visitors were demonstrated time taken by the job, if being run on single node or on all the nodes of the Beowulf Cluster. This simple Beowulf Cluster helped students/visitors to understand working mechanism of HPC. Students/Visitors were also encouraged to prepare such low cost HPC at home. The methodology to prepare such HPC was also shared with the students and visitors and same is available in PRL's website at location: (`https://www.prl.res.in/prl-eng/hpc_knowledge_base`)

Library & Information Services

During 2017-18, three hundred and four (304) scientific, 43 general books, 90 hindi books and 50 CDs/DVDs were added in the Main, Thaltej and USO libraries. Subscription of eleven journals has been added to the existing library collection of 185 journals. During this period, number of visitors, visiting the library was 5702 and number of documents issued and returned were 1704 and 1598 respectively. Forty two (42) book grant requests were processed to assist the students this year. Number of photocopies made, in house were 41176 and by outside agency were 81431.

PRL Library continues to have access to full-text databases like AGU Digital Library, GSA Archive, Nature archive (access from 1987), PROLA, Science Archive, SPIE and IEEE Digital Library. During 2017-18 Proquest Dissertation and Thesis (PQDT) has been subscribed for PRL students and scientists. As no library can be completely self-sufficient, the Library also provides document delivery service through ILL. The number of document delivery requests for articles fulfilled by PRL Library was 145 and that of requests of PRL staff fulfilled by other libraries was 39. The Library homepage gives access to the digital content subscribed by PRL as well as the open access content. Primarily, it gives links to 185 online journals out of the 196 journals subscribed by the library. The PRL library also subscribes to 'Discovery Tool' which searches a topic through all the journals simultaneously with filters like full-text and 'peer reviewed'. Library also carries out similarity check for students using the Ithenticate tool as it is becoming mandatory for students to carry out the similarity / originality check before submitting the thesis and most of the journals carry out the originality check during peer review. During this period Library also bought the Digital Notice Board software (I-Display) which is used to disseminate information about PRL activities like division seminars, colloquium, public talks, images of events like Republic Day celebration, Women's Day celebration, etc. In addition, PRL in

news, list of recent publications of PRL scientists, new books added to the library collection are also displayed in 3 campuses simultaneously through the LAN. Mt Abu campus will be linked soon.

The PRL Library maintains an institutional repository which consists of journal articles published by the PRL authors from 1990 to present and is also linked through the Library homepage. About 4300 articles by PRL authors are now part of the repository. All the PRL theses from 1952 onwards (404) are now available full text for PRL users. All the Technical Notes since 1977, published by PRL have been digitized (110) and are available full text for PRL users. Two hundred and seventy (270) e-books can be accessed through the library homepage (http://www.prl.res.in/ library). The Library has taken up the digitization of the photographs archive. Scanning of the photographs of 250 albums is completed. Giving the captions and metadata for each photograph for easy retrieval has been done for 145 albums using the digital library software – Greenstone Digital Library (GSDL).

Book exhibition organized by the Library in November 2017

Workshop

WORKSHOP

Workshop facilities at Main Campus as well as newly equipped Workshop facility at Thaltej Campus has been providing excellent supports for fabricating various precision parts required in scientific experimental setups and payload activities. It has also rendered the supports in carried out complex assemblies and mechanical works. Some of the work carried out during 2017-2018 are listed below

1. **Fabrication activities Carried out by PRL workshop for Chandrayaan-2 payloads**

   (a) **Realisation of Lead filled SS container with internal Al layer for APXS payload of Chandrayaan-2**

   For storage and transportation of Assembly of Cm-244 radioactive sources used in APXS payload of chandrayaan-2 Payload, Two Containers are fabricated from SS with lead linings.

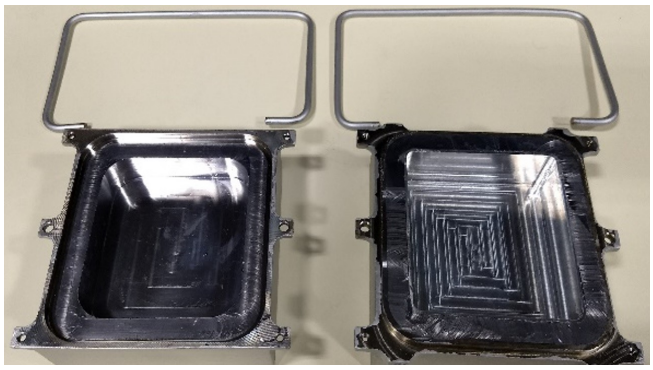

Figure No.:1 Internal Detail of Storage and Transportation Container.

(b) **Realisation of Glove Box Assembly and associated Fixtures for APXS payload of Chandrayaan-2** Glove box chamber is realised to assemble Cm-244 sources. This chamber is fabricated from SS with lead lining and lead gloves are attached for accessibility and lead glass is provided for vison while assembly. Several fixtures are also fabricated for facilitating the assembly of radioactive sources.

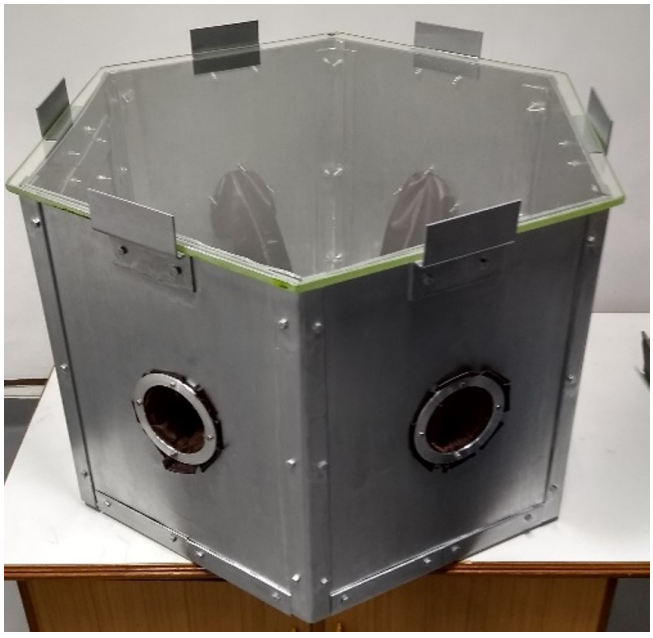

Figure No.:2 Glove Box Chamber.

(c) **Realisation of Test setup for testing and calibration of QM and FM model of APXS payload of Chandrayaan-2**

Various fixtures i.e., calibration source holder with push fit locknut, dummy locknuts for Source Holder Assembly, mounting fixtures etc., are fabricated as well as modified for custom requirement to carrying out testing and calibration of APXS EM, QM and FM with different target materials.

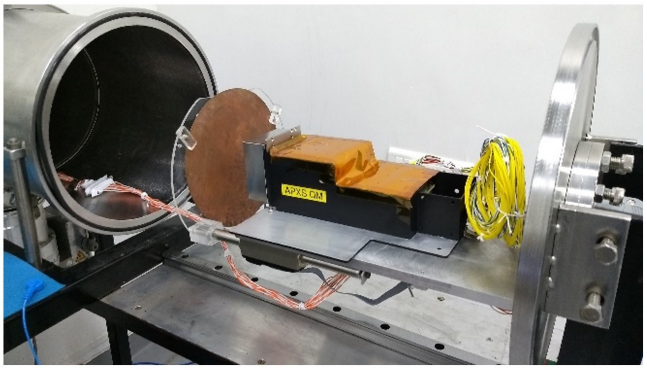

Figure No.: 3 Calibration Setup of APXS QM.

(d) **Realisation of Test setup for testing and calibration of QM and FM model of XSM payload of Chandrayaan-2**

For Carrying out Testing and Calibration of EM, QM and FM of XSM payload onboard Chandrayaan-2 Orbiter, Various test fixture and Parts i.e, Gun support structure, Pipe support blocks, lead lined enclosure for X-Ray gun and various fixtures for mounting XSM package etc., were fabricated.

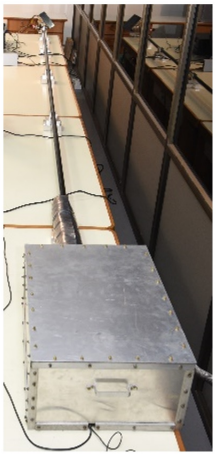

(a)

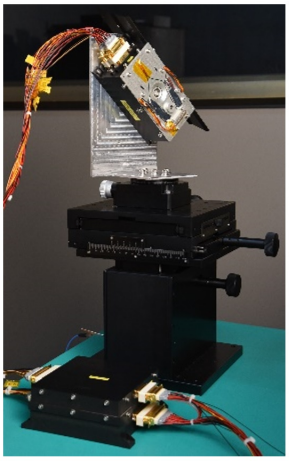

(b)

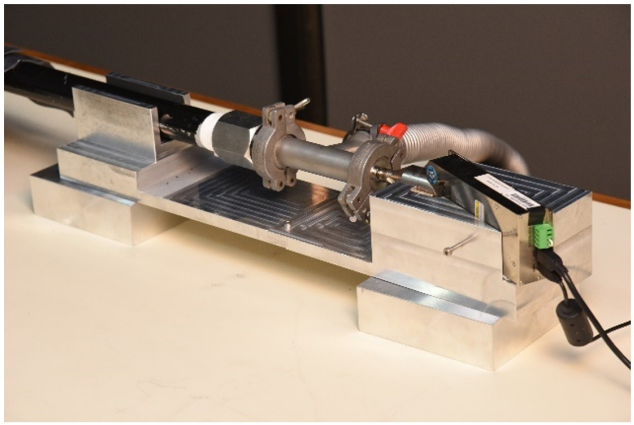

(c)

Figure No.:4(ab).
Figure No.: 4 (a) XSM Calibration set-up, (b) XSM Mounting Fixture (c) X-Ray Gun Mounting Fixture.

(e) **Realisation of PCB Fabrication Fixtures and Payload Handling Fixtures for Chandrayaan-2**

For populating PCBs of QM, FM and FM of XSM and APXS payload of Chanrayaan-2 mission fixtures ware realised in order to easy handling and testing while soldering components to respective PCBs as well as ETLS testing of entire payloads.

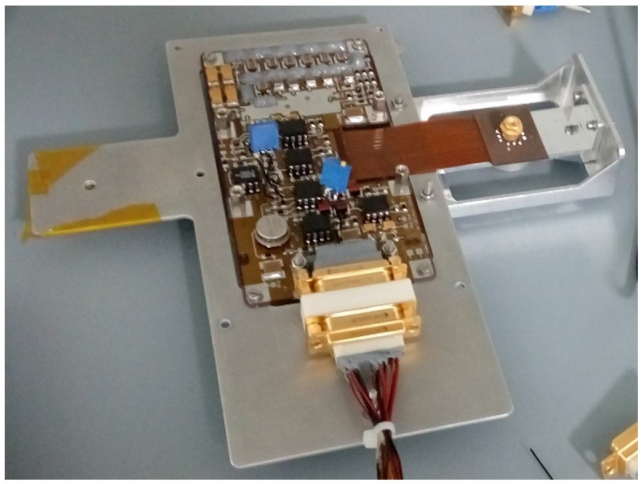

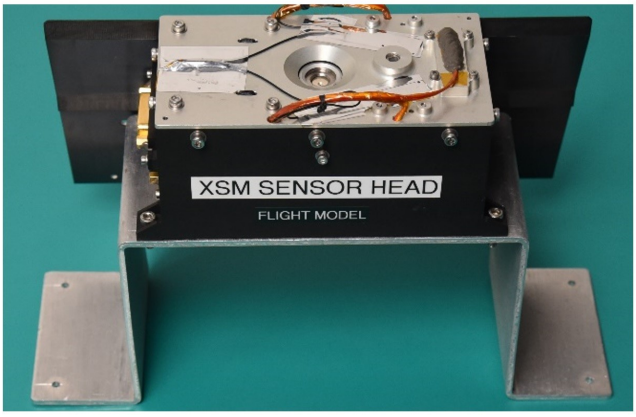

Figure No.:5 (a) PCB Fabrication Fixture.
Figure No.: 5(b) Payload Handling Fixture.

(f) **ChaSTE Payload Probe**

The ChaSTE payload onboard Chandrayaan-2 Lander is an experiment to derive the thermal conductivity and diffusivity of the top 10 cm of the lunar soil. It contains a probe which has 10 RTD sensors along its body. The probe is 40 cm long and is made of Cyanate Ester material. In PRL we hav fabricated in workshop from Teflon material.

(g) **Lunar Simulation Chamber Extension**

Simpex Lab houses a lunar simulation chamber which is used to simulate a lunar surface in the lab. The chamber was extended to accommodate the ChaSTE payload probe by 30 cm in height. This extension of chamber is under testing presently and will be used for calibration of the FM Model of the ChaSTE payload.

(h) **Fabrication of magnet assembly of STEPS of ASPEX payload of ADITYA-L1**

Parts for modified magnet assembly are fabricated for further testing and evaluating of EM of ASPEX payload

of ADITYA-L1 mission.

Figure No.: 6 (a) Magnet Assembly of Rectangular Detector.
Figure No.: 6 (b) Magnet Assembly of Circular Detector.

2. **Fabrication and Assembly of Opto-mechanical Component of MFOSC-P**

In the continuum of last year while developing of MFOSC-P (Mount Abu Faint Object Spectrograph and Camera Pathfinder) instrument following are some major opto-mechanical components are fabricated in PRL workshop.

(a) **Development and assembly of version-2 of Collimator Cage road system:**

In this version a new concept of lens mount barrel is introduced. Barrel has a tolerance/precision of $\pm$ 25 micron in which lens mounts are to be fitted. This much accuracy is required to obtain desired optical alignment of the instrument. Here are some images for the assembly done in workshop.

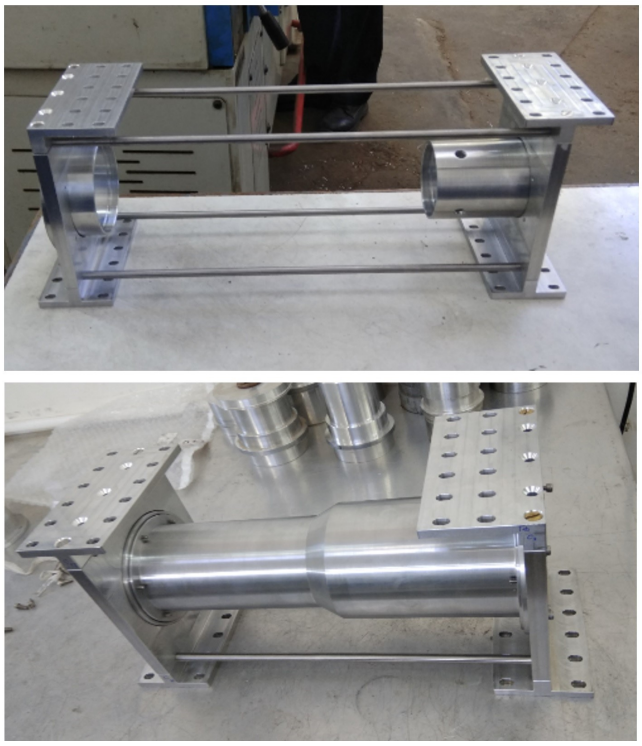

Figure No.: 7(a) Collimator Cage rod system version-1.
Figure No.: 7(b) Collimator Cage rod system version-2.

(b) **Development and assembly of version-2 of Camera Cage road system:**

In this version two highly precise i.e. tolerance of $\pm$ 25 micron barrels are fabricated in workshop which are required to maintain the optical alignment of MFOSCP. Below are some images for assembly of cage system.

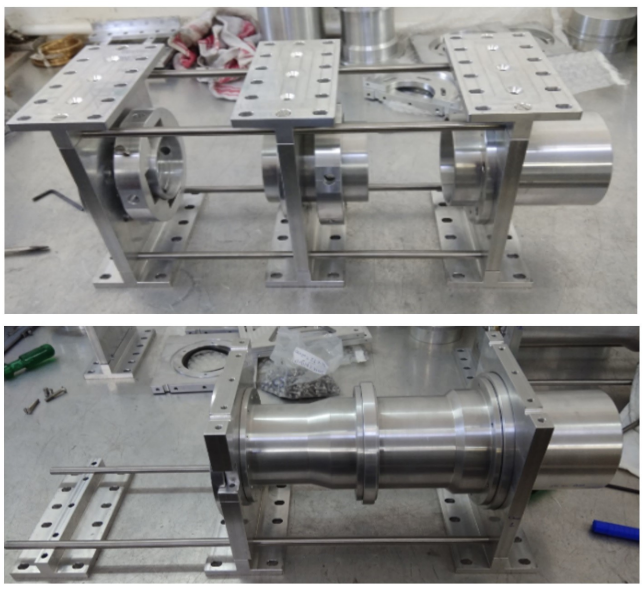

Figure No.: 8(a) Camera Cage rod system version-1.
Figure No.: 8(b) Camera Cage rod system version-2.

(c) **Development and assembly of Calibration Unit of MFOSC-P.**

For the calibration purpose, calibration unit had been

fabricated and assembled in workshop. This unit basically contain an integrating sphere mount along with some lenses and mirror mount. Below are some picture for the same.

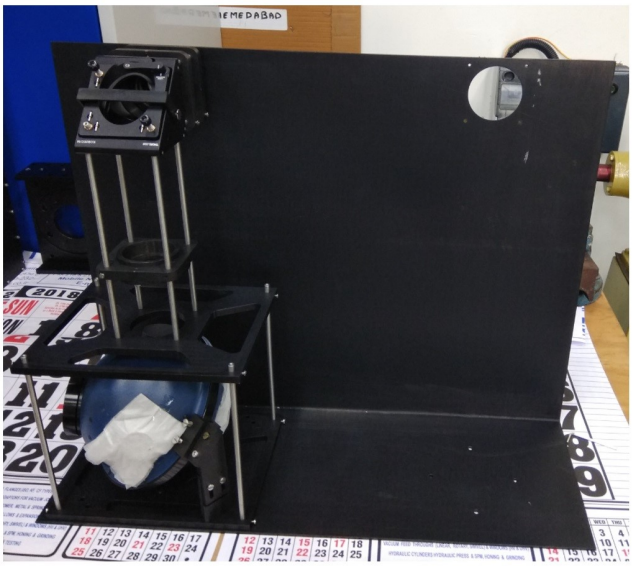

Figure No.: 9(a) Calibration Unit.
Figure No.: 9(b) Calibration Unit Assembly Testing.

(d) **Fabrication of Auto Guider Unit**

For the guiding of telescope an Auto Guider unit for the instrument has been developing with in the PRL workshop. System has the provision for mounting of 45 degree mirror, guiding CCD with is to be rotated via stepper motor around the telescopic beam using the gears the Fabrication of system is under process.

(e) **Assembly Testing of MFOSC-P mechanical components (without Optics) in Thaltej Workshop.**

Assembly and integration of MFOSC-P instrument without optics is an ongoing activity in Thaltej workshop. PRL fabricated opto-mechanical subsystem like calibration fold mirror mount, collimator cage rod system, motorized filter wheel mount, motorized grating box, camera cage rod system etc. are to be mounted on MFOSC-P chassis. While assembling the instrument some necessary holder and clamps are also fabricated.

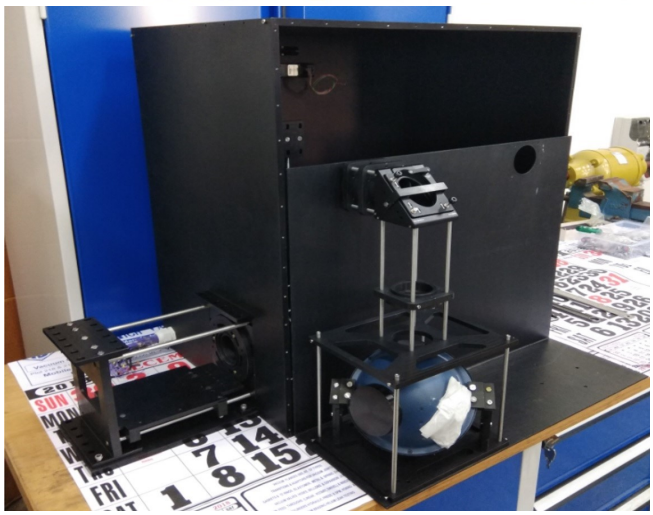

Figure No.: 10(a) MFOSC-P Assembly in Thaltej Workshop.
Figure No.: 10(b) MFOSC-P Assembly in Thaltej Workshop.

3. **Other New Developments and Mechanical supports**

(a) **Retarding Potential Analyser**

Retarding Potential Analyzer is an instrument used to measure plasma parameters such as number density

and temperature. It uses multi-layer grids which are biased at different voltages. The outermost grid is biased at negative voltage for acquiring ions and positive for acquiring electrons. The plasma particles pass through the different grids based on their charge and fall on a collector plate. The particles hitting the collector results in generation of current. This current with respect to the applied bias results in a characteristic curve. This curve helps in deriving major scientific information related to the plasma.

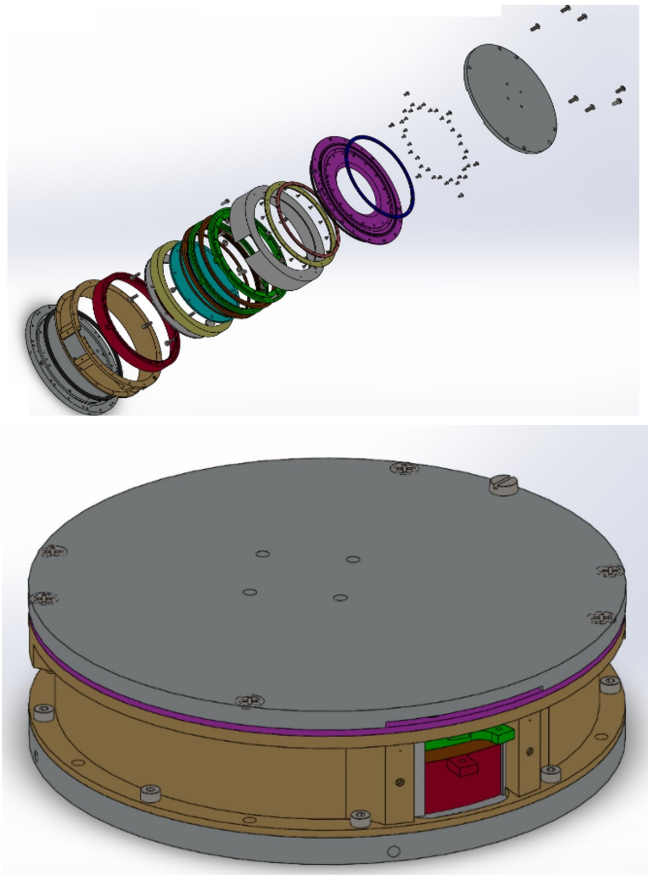

Figure No.: 11(a) Exploded View of RPA.
Figure No.: 11(b) Retarding Potential Analyser (RPA).

There are Total 22 parts of Retarding Potential Analyser (RPA). Each part of RPA was designed in Solid Works Mechanical Software. After designing of all parts, Assembly and Simulation were checked in software. Assembly of RPA was required very much accuracy and precision in designing because all parts are inserted one or another part of Retarding Potential Analyser.

(b) **Langmuir Probe and Electric Field Experiment**

The Langmuir probe and Electric filed probe experiment aims at measuring electron density and electric field in the Martian atmosphere. The experiment has a spherical conductor (diameter 2.5 cm) as a probe which is positively biased to attract the electrons. These electrons fall on the conductor and results in a current. It includes a precise electronics to measure the feeble currents and other processing and bias electronics. EF experiment houses two probes (diameter 5 cm) to measure the electric filed in the Martian atmosphere.

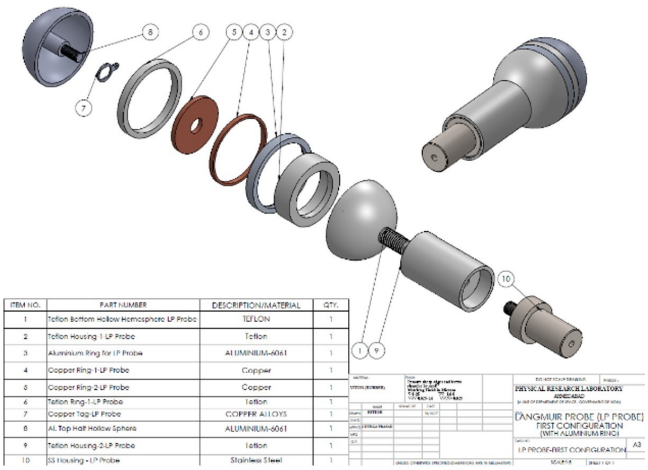

ITEM NO.	PART NUMBER	DESCRIPTION/MATERIAL	QTY.
1	Teflon Bottom Hollow Hemosphere LP Probe	TEFLON	1
2	Teflon Housing 1 LP Probe	Teflon	1
3	Aluminium Ring for LP Probe	ALUMINIUM-6061	1
4	Copper Ring 1 LP Probe	Copper	1
5	Copper Ring 2 LP Probe	Copper	1
6	Teflon Ring-1 LP Probe	Teflon	1
7	Copper Top LP Probe	COPPER ALLOYS	1
8	AL Top Half Hollow Sphere	ALUMINIUM-6061	1
9	Teflon Housing-2 LP Probe	Teflon	1
10	SS Housing - LP Probe	Stainless Steel	1

PHYSICAL RESEARCH LABORATORY AHMEDABAD

LANGMUIR PROBE (LP PROBE) FIRST CONFIGURATION (WITH ALUMINIUM RING)

LP PROBE-FIRST CONFIGURATION

Figure No: 12 (a) Langmuir Probe.
Figure No: 12 (b) Electrical Field Prob.

The design of Langmuir Probe and Electric Field Probe was being made in workshop. For Langmuir Probe, two configurations have been designed, one with Al. ring and another without Al. Ring. The design of each parts of Electric Field Probe also requires precision and accuracy because all parts are assembled to gather and make a final assembly. The material for LP and EF Probes is Aluminum-6061.

(c) **Stainless Steel Piping Structure for AMS Chiller**

AMS has large size electromagnets that require continuous cooling by chilled water. Two chillers have been installed outside the laboratory building. A plumbing line was designed to make a common connection to two chiller systems with suitable cocks and pressure gauzes.

Honorary Fellows

A. Hewish

J. E. Blamont

K. Kasturirangan

P. J. Crutzen

U. R. Rao [Deceased 24.07.2017]

Honorary Faculty

A. Ambastha
Sr. Professor (Retd.)

A. Singal
Retd. Associate Prof.

A. K. Singhvi
FNA, FASc, FNASc, FTWAS
J.C. Bose & Raja Rammanna Fellow

A. R. Prasanna
Sr. Professor (Retd.)

A. S. Joshipura
FNA, FASc, FNASc
J.C. Bose & Raja Rammanna Fellow

B. G. Anand Rao
Sr. Professor (Retd.)

H. Chandra
Retd. Prof.

J. Banerji
Course Director, CSSTEAP

J. N. Goswami
FNA, FASc, FNASc, FTWAS
J.C. Bose Fellow

K.P. Subramanian
Honorary Scientist - B

K.S. Baliyan
Retd. Prof.

M. M. Sarin
FNA, FASc, FNASc
J.C. Bose Fellow & INSA Sr. Scientist

N. Bhandari
FNA, FASc, FNASc, INSA Honorary Scientist

N. Juyal
Retd. Scientist SF

R. Rengarajan
Project I/C POCEF, MoES

R. Sridharan
FASc, FNASc, NASI Senior Scientist

Shyam Lal
FNA, FASc, FNASc
J.C. Bose Fellow & INSA Sr. Scientist

S.D. Rindani
FNASc & J.C.Bose Fellow

U. C. Joshi
Retd. Prof.

V. K. B. Kota
Sr. Professor (Retd.)

Y. B. Acharya
Retd. Engineer SG

PRL Faculty

Sr. No.	Name	Designation	Specialization	Academic Qualification
1	Bhardwaj A. $FNA,\ FASc,\ FNASc$	Director	Planetary & Space Science	Ph.D., IIT, BHU (1992)
2	Acharyya K.	Reader	Astrochemistry	Ph.D., University of Calcutta (2008)
3	Banerjee D.	Professor	Thermoluminescence & Planetary Physics	Ph.D., PRL, Gujarat Univ. (1997)
4	Banerjee S. B.	Scientist - SF	Experimental Molecular Physics	Ph.D., Saurashtra Univ. (2011)
5	Basu Sarbadhikari A.	Scientist-SE	Petrology & Geochemistry	Ph.D., IIT, Kharagpur (2006)
6	Bhatt J. R.	Professor	Astrophysics	Ph.D., IPR, M.S. Univ. (1992)
7	Bhattacharyya R.	Associate Professor	Plasma Physics	Ph.D., Jadavpur Univ. (2006)
8	Bhushan R.	Scientist-SG	Oceanography and Paleoclimatology	Ph.D., PRL, M.S. Univ. (2009)
9	Chakrabarty A.	Professor	Extra-solar planets, Star Formation & Instrumentation	Ph.D., PRL, Gujarat Univ. (1999)
10	Chakrabarty D.	Associate Professor	Space Weather	Ph.D., PRL, M.L.S Univ.(2008)
11	Chauhan N.	Scientist-SD	Luminescence Dating and Luminescence Dosimetry	Ph.D. Gujarat University (2012)
12	Deshpande R. D.	Scientist-SG	Application of Environmental Tracers in Hydrology	Ph.D., PRL, M.S. Univ. (2007)
13	Dewangan. L. K.	Scientist-SD	Astrophysics	Ph.D., Gujarat Univ. (2011)

Sr. No.	Name	Designation	Specialization	Academic Qualification
14	Ganesh S.	Scientist-SF	Milky Way, Comets, AGN, Astronomical polarimetry	Ph.D., PRL, Gujarat Univ. (2010))
15	Gadhavi H.	Scientist-SE	Atmospheric Physics	Ph.D., PRL, Gujarat Univ. (2006))
16	Goswami S.	Professor	High Energy Physics	Ph.D., Calcutta Univ. (1998)
17	Guharay A.	Reader	Atmospheric Physics	Ph.D., Kumaun Univ. (2010)
18	Haider S.A. $FASc,\ FNA,\ FNASc$	Senior Professor	Planetary and Cometary Atmospheres	Ph.D., Banaras Univ. (1984)
19	Janardhan P.	Senior Professor	Solar Radio Astronomy & Space Weather	Ph.D., PRL, Gujarat Univ. (1991)
20	Joshi B.	Associate Professor	Solar Physics, Astronomy	Ph.D., ARIES, Kumaun Univ. (2007)
21	Joshi V.	Scientist-SD	Observational Astronomy	Ph.D, Gujarat Univ. (2013)
22	Juyal N.	Scientist-SF	Quaternary Geology & Paleoclimate	Ph.D., PRL, M.S. Univ. of Baroda (2004)
23	Kushawaha R. K.	Scientist-SD	Atomic Physics	Ph.D., PRL, M.L.S. Univ. (2009)
24	Konar P.	Associate Professor	Particle Physics	Ph.D.,HRI, Allahabad Univ. (2005)
25	Kumar B.	Reader	Solar Physics	Ph.D., PRL, M.L.S Univ. (2007)
26	Kumar S.	Associate Professor	Aquatic and Terrestrial Biogeochemistry	Ph.D., PRL, M.S. Univ. of Baroda (2004)
27	Mahajan N.	Associate Professor	Particle Physics	Ph.D., Delhi Univ.(2004)
28	Marhas K. K.	Associate Professor	Solar System studies	Ph.D., PRL, D.A.V.V Indore (2001)
29	Mathew S. K.	Professor	Solar Magnetic & Velocity Fields	Ph.D., PRL, Gujarat Univ. (1999)
30	Mishra H.	Professor	Strong Interaction Physics & Nuclear Astrophysics	Ph.D., IOP, Utkal Univ. (1994)
31	Mohanty S.	Senior Professor	Astroparticle Physics	Ph.D., Wisconsin Univ. (1989)
32	Naik S.	Associate Professor	High Energy Astrophysics, X-ray Binaries	Ph.D., TIFR, Bombay Univ. (2003)
33	Pallamraju D.	Professor	Space Weather and Atmospheric coupling processes	Ph.D., PRL, D.A.V.V Indore (1997)
34	Rai V.	Associate Professor	Stable Isotope Cosmochemistry	Ph.D., PRL, M.S Univ. of Baroda (2001)
35	Rajpurohit A. S.	Scientist-SD	Astronomy & Astrophysics	Ph.D., Uni. de Franche-Comté, France (2013)
36	Ramachandran S.	Professor	Aerosols, Radiation & Chemistry-Climate Interactions	Ph.D., PRL, M.S Univ. of Baroda (1996)
37	Rangarajan R.	Professor	Particle Physics & Cosmology	Ph.D., Univ. of California, Santa Barbara (1994)

Sr. No.	Name	Designation	Specialization	Academic Qualification
38	Rastogi N.	Associate Professor	Atmospheric & Aerosol Chemistry	Ph.D., PRL, M.L.S Univ. (2005)
39	Ray J. S.	Professor	Isotope Geochemistry	Ph.D., PRL, M.S Univ. of Baroda (1998)
40	Ray D.	Scientist-SE	Marine Geology & Igneous Petrology	Ph.D., Jadavpur Univ. (2009)
41	Sahoo B. K.	Associate Professor	Atomic Physics	Ph.D., IIA, Mangalore Univ. (2006)
42	Sahu L. K.	Associate Professor	Atmospheric Science, Trace gases	Ph.D., PRL, M.L.S.Univ. (2005)
43	Samanta G. K.	Reader	Laser and Nonlinear optics	Ph.D., Universitat Politecnica de Catalunya Uni., Barcelona (2009)
44	Sarkar A.	Reader	MHD simulation & Solar Physics	Ph.D, University of Goettingen, Germany (2005)
45	Sharma S. K.	Associate Professor	Middle Atmosphere & Long Term Atmospheric Changes	Ph.D., PRL, Gujarat Univ. (2010)
46	Sheel V.	Associate Professor	Modelling of Lower Atmosphere	Ph.D., PRL, Gujarat Univ. (1996)
47	Shukla A. D.	Scientist-SE	Geochemistry & Cosmochemistry	Ph.D., PRL, M.S. Univ. (2012)
48	Singh A.	Reader	Ocean Biogeochemistry	Ph.D, MLSU Udaipur (2011)
49	Singh A. D.	Professor	Atomic Physics	Ph.D., IIA, Bangalore Univ. (1998)
50	Singh N.	Associate Professor	Theoretical condensed matter and Statistical Physics	Ph.D., RRI, Bangaluru (2006)
51	Singh R. P.	Professor	Laser Physics	Ph.D., J.N.U., New Delhi. (1994)
52	Singh S. K.	Professor	Isotope Geochemistry	Ph.D., PRL, M.S. Univ. of Baroda (1999)
53	Singh V.	Scientist-SD	Active Galactic Nuclei and evolution of galaxies	Ph.D., Calicut University (2011)
54	Sivaraman B.	Reader	Low Temperature Astrochemistry	Ph.D., The Open University, UK (2008)
55	Srivastava M.	Reader	Astronomical Instrumentation	Ph.D., Univ. of Pune (2012)
56	Srivastava Nandita	Professor	Solar Physics	Ph.D., PRL, Ravi Shankar Shukla Univ. (1994)
57	Srivastava Neeraj	Scientist SE	Planetary Remote Sensing	Ph.D., PRL, IIT, Roorkee. (2014)
58	Vadawale S. V.	Associate Professor	High Energy Astrophysics and X-Ray Spectroscopy	Ph.D., TIFR, Bombay Univ. (2003)
59	Vijayan S.	Scientist-SD	Planetary Remote Sensing	Ph.D., Anna Univ. Chennai (2013)

Sr. No.	Name	Designation	Specialization	Academic Qualification
60	Yadava M. G.	Scientist-SG	Palaeoclimate, Radiocarbon dating and stable isotopes	Ph.D., PRL, DAVV, Indore (2003)
61	Mahirale V.K.	Engineer-SG	Civil Engg.	B.E., D.A.V.V., Indore (1982)
62	Adalja H.L.	Scientist/Engineer-SD	Mechanical Engineering	BE, CU Shah College of Engineering & Technology (2007)
63	Adhyaru P. R.	Engineer-SF	Development of electronic sub systems for spectrometry	B.E., Gujarat Uni., (1991)
64	Bharti R.R.	Scientist/Engineer-SD	Computer Science,	M.Sc., M. D. University (2003)
65	Bhavsar K.J.	Engineer-SE	Electrical Systems	B.E., Gujarat Uni. (1995)
66	Bayanna A. R.	Scientist-SE	Optical instrumentation & Solar Physics	Ph.D., PRL, MLSU-Udaipur (2015)
67	Bireddy R.	Scientist/Engineer-SD	Electronics & Communication	B.Tech., JNTU, Hyderabad (2012)
68	Dixit V.	Scientist/Engineer-SD	Scientific Computing,	M.Sc., University of Heidelberg,
69	Durga Prasad Karanam	Scientist/Engineer-SD	Planetary Surface Science & Instrumentation	Ph.D., PRL, Pondicherry Univ. (2018)
70	Goyal S.K.	Scientist/Engineer-SD	Electrical Engineering	B.E. (Electrical), Gujarat University (2002)
71	Jain N.	Scientist/Engineer-SD	Elect.& Comm. Engg.	A.M.I.E. Institution of Engineers (2002)
72	Jani R. A.	Scientist-SE	Paleoclimate and Application of Stable Isotopes in Hydrology	M.Sc., Gujarat Uni. (1988)
73	Kumar P.	Scientist/Engineer-SD	Laser matter interactions, Spectroscopy & Payload development	B.Tach., IIST (2011)
74	Mahajan R.R.	Scientist-SE	Noble gas isotopes, Meteorites	M. Sc. North Maharashtra Uni. Jalgaon (1994) M. Tech., D.A.V.V., Indore (1997)
75	Mehta D.	Scientist/Engineer-SD	Web Applications Development & Security	M.Tech, Karnataka state Open Univ. (2013)
76	Manke A.A.	Scientist/Engineer-SD	Computer Science	ALCCS, IETE (2013)
77	Mishra H.D.	Scientist/Engineer-SD	Computer Science and Applications	M.C.A., GJ Univ. of S& T (2003)
78	Nishtha A.	Librarian-SE	Library & Information Sciences	Ph. D., M. S. Uni. of Baroda (2012)
79	Pabari J. P.	Engineer-SE	Planetary and Interplanetary Dust	Ph.D., PRL, IIT Bombay (2011)
80	Padhya V.K.	Scientist/Engineer-SD	Computer Science	M.Tech, Karnataka State Open Univ. (2013)

Sr. No.	Name	Designation	Specialization	Academic Qualification
81	Parmar V.M.	Scientist/Engineer-SD	Electrical Engineering	B.E. (Electrical), Gujarat Uni. (2002)
82	Rajesh T. A.	Scientist-SE	Aerosol characterization and instrumentation	M.Sc., RDVV, Jabalpur (1998)
83	Rao D. K.	Scientist-SF	Isotope Studies of Methane	M.Sc., Andhra Uni. (1979)
84	Raval J.	Engineer-SE	IT/Cyber Security, Linux System Administration, Network Administration	M.Tech., Allahabad Agricultural Institute (2006)
85	Panda D.	Scientist-SE	Nuclear Instrumentation & Remote Sensing	M.Sc., Berhempur Uni. (1998)
86	Patel A.R.	Scientist/Engineer-SD	FPGA, Payload hardware design and testing	ME, LD College of Engineering, (2010)
87	Shah A. B.	Engineer-SG	Design and Development of Scientific instrumentation	B.E., Gujarat Univ. (1984)
88	Shah M.	Scientist/Engineer-SD	Automation, Robotics, Payload development & FPGA	MSc, Illinois Inst. of Tech., Chicago (2015)
89	Shah R. R.	Engineer-SG	Instrumentation & Control, Data Acquisition, Telescope	B.E., M.B.A.
90	Shanmugam M.	Engineer-SE	Space instrumentation, Semiconductor detectors and ASICs	Ph.D., PRL, D. D. Uni. (2016)
91	Shrivastava A.	Scientist/Engineer-SD	Cyber Security, Computer Networking and System Administration	M.Sc., MDS University (1998)
92	Singh R. P.	Scientist-SE	Mesosphere and Lower Thermosphere	M.Sc. (1998)
93	Sinha R.K.	Scientist/Engineer-SD	Planetary remote sensing, Glaciology & Impact Cratering	M.Tech., SRM Univ. (2011)
94	Sudheer A. K.	Scientist-SE	Chemistry	M.Sc., Calicut Uni. (1995)
95	Sarvaiya T.N. A.	Scientist/Engineer-SE	IT Security Virtualization, Sys. Adm. & Networking	M.S, BITS Pilani (2014)
96	Ubale G. P.	Engineer-SF	Design,Development,Production, Planning and Control of mechanical systems	B.E. (1987)
97	Vaghela H. R.	Engineer-SE	Mechanical Engineering and Finance	B.E. (1996), M.B.A. (2002)
98	Vaishnav B.G.	Scientist/Engineer-SD	Atomic & Molecular Physics	PhD Sardar Patel University (2008)
99	Venkataraman V.	Scientist-SE	Infrared studies of evolved stars	Ph.D., PRL, MLSU, Udaipur (2015)
100	Venkataramani S.	Scientist-SF	Atmospheric Physics	M.Sc., Uni. of Madras (1986)
101	Wairagade S.	Engineer-SE	Civil Engg.	B.E., Nagpur Univ. (1993)

Audited Statement of Accounts

7th Floor, Heritage Chambers
B/h. Bikanerwala, Off S.M. Road,
Nr. Azad Society, Nehru Nagar, Ahmedabad-380 015.
Phone : (B) 079 - 2647 2000 E mail : contact@mmsco.in
Website : www.mmsco.in

MUKESH M. SHAH & CO.
CHARTERED ACCOUNTANTS
AHMEDABAD . MUMBAI . BANGALORE

AUDITORS' REPORT

To

The Trustees

Physical Research Laboratory

1. We have audited the accompanying Financial Statements of the Physical Research Laboratory situated at Navrangpura, Ahmedabad having Registration No. E/1371 Ahmedabad for the year ended 31st March, 2018, which comprises the Balance Sheet as at 31st March, 2018, the Income & Expenditure Account for the year then ended and a summary of significant accounting policies and Notes forming part of accounts.

2. Management is responsible for the preparation of these financial statements that give a true and fair view of the financial position and financial performance of Physical Research Laboratory. This responsibility includes the design, implementation and maintenance of internal control relevant to the preparation and presentation of the financial statements that give a true and fair view and are free from material misstatement, whether due to fraud or error.

3. Our responsibility is to express an opinion on these financial statements based on our audit. We conducted our audit in accordance with the Standards on Auditing issued by the Institute of Chartered Accountants of India. Those Standards require that we comply with ethical requirements and plan and perform the audit to obtain reasonable assurance about whether the financial statements are free from material misstatement.

   An audit involves performing procedures to obtain audit evidence about the amounts and disclosures in the financial statements. The procedures selected depend on the Auditor's judgment, including the assessment of the risks of material misstatement of the financial statements, whether due to fraud or error. In making those risk assessments, the auditor considers internal control relevant to the management's preparation and presentation of the financial statements that give a true and fair view in order to design audit procedures of the entity's internal control. An audit also includes evaluating the appropriateness of accounting policies used and the reasonableness of the accounting estimates made by the Management, as well as evaluating the overall presentation of the financial statements.

4. We believe that the audit evidence we have obtained is sufficient and appropriate to provide a basis for our audit opinion.

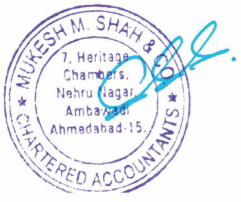

7th Floor, Heritage Chambers
B/h. Bikanerwala, Off S.M. Road,
Nr. Azad Society, Nehru Nagar, Ahmedabad-380 015.
Phone : (B) 079 - 2647 2000 E mail : contact@mmsco.in
Website : www.mmsco.in

MUKESH M. SHAH & CO.
CHARTERED ACCOUNTANTS
AHMEDABAD . MUMBAI . BANGALORE

5. We report that:

i. As informed to us, value of movable and immovable assets as per physical verification last carried out in the financial year 2013-14, are subject to reconciliation with books of accounts including fixed assets. The loss which may arise due to non-making reconciliation between value of Fixed Assets (Movable) as per physical verification and value as disclosed in the books of Fixed Assets is not provided for.
Further loss/gain which may arise on providing depreciation on WDV of each individual asset instead of providing depreciation on WDV of block of assets, which is not worked out and ascertained.

ii. The Trust has as required by the Prudent accounting policy not considered grants for the purpose of capital expenditure either while calculating depreciation or by way of amortization of grants to Income and Expenditure account. Except the grants Received during the year for specific purpose for Creation of Capital Assets. Cumulative Depreciation of ₹. 1,78,27,96,964/- is not charged to the Income & Expenditure account, however as per the consistent policy adopted by the Trust, the same is written off against the Corpus Fund.

iii. None of the assets including Buildings of the trust except Vehicles are insured. Non-Insurance of Building is in violation of Rule 65 of The Bombay Public Trust (Gujarat) Rules, 1961.
However, the policy adopted by PRL is in confirmation with the provision of Department's [Department of Space, Government of India] 'Book of Financial powers' as clarified vide letter No.28011/1/2014-V dated January 3, 2014.

iv. As informed to us the balances either Debit or Credit, stated under various advances to staff, deposits, receivables, advances to others and those under sundry creditors are subject to confirmation and reconciliation if any.

v. The balances of various external projects being managed by the Trust are subject to confirmation, and are appended as Annexure 1 to the Notes of Accounts.

6. **Subject to the matters stated in Para No. 5,** in our opinion and to the best of our information and according to the explanation given to us, the financial statements give a true and fair view in conformity with the accounting principles generally accepted in India:

MUKESH M. SHAH & CO. 7, Heritage Chambers, Nehru Nagar, Ambawadi, Ahmedabad-15. CHARTERED ACCOUNTANTS

7th Floor, Heritage Chambers
B/h. Bikanerwala, Off S.M. Road,
Nr. Azad Society, Nehru Nagar, Ahmedabad-380 015.
Phone : (B) 079 - 2647 2000 E mail : contact@mmsco.in
Website : www.mmsco.in

MUKESH M. SHAH & CO.
CHARTERED ACCOUNTANTS
AHMEDABAD . MUMBAI . BANGALORE

a) in the case of the Balance Sheet, of the state of affairs of the Trust as at March 31, 2018.

b) in the case of the Income and Expenditure Account, of the Income for the year ended on that date;

7. We further report that:

a. Except for sanction and release of Grant for creating Capital Assets during the Finance Year **2013-14,** for other Capital Assets i.e., Fixed Assets are being purchased from the balances held from the grants (without having any specific directions) received by the Trust for the year prior to the current financial year.

b. As informed to us, the Trust has provided depreciation on its fixed assets for the first time in F.Y. 2008-2009 calculating retrospectively with effect from F.Y. 2001-2002, by estimating the same at 90% of opening Book Value of Fixed Assets for F.Y. 2001-2002. Then onwards for the subsequent additions and on the carried forward balances, depreciation is provided on the opening balance of fixed assets at the rates as prescribed under the Income Tax Act, 1961 by way of the written down value method. The Trust does not provide any depreciation on any additions / deletions in assets during the year.

c. The value of stores and medicines is taken as certified by the Management.

d. Reliance has been placed on Management for allocation of expenses amongst various external as well as internal projects including imprest at USO Udaipur and IFO Mt. Abu on account of the same being technical in nature. The expenses incurred are classified as capital or revenue by the Management as per policies and practices.

e. The accounts are maintained regularly and in accordance with the provision of the Bombay Public Trust Act, 1951 and the Bombay Public Trust (Gujarat) Rules, 1961.

f. Receipts and disbursements are properly and correctly shown in the accounts.

g. The cash balance and the vouchers were in the custody of the Accounts Officer on the date of audit and were in agreement with the accounts.

h. The books, deeds, accounts, vouchers and other documents and records required for the purpose of Audit were produced before us.

i. The registers of stock and inventories are certified by the Trustee, is maintained and updated on regular basis. However, register of movable and immovable

MUKESH M. SHAH & CO. 7, Heritage Chambers, Nehru Nagar, Ambawadi Ahmedabad-15. CHARTERED ACCOUNTANTS

7th Floor, Heritage Chambers
B/h. Bikanerwala, Off S.M. Road,
Nr. Azad Society, Nehru Nagar, Ahmedabad-380 015.
Phone : (B) 079 - 2647 2000 E mail : contact@mmsco.in
Website : www.mmsco.in

properties is required to be reconciled with balances as stated in Financial Statements.

j. The Registrar Shri Chavali V.R.G. Deekshitulu and the Head Accounts & Internal Financial Adviser Smt. P Sudha appeared before us and furnished the necessary information required by us.

k. No property or fund of the Trust was applied for any objects or purposes other than for the objects or purposes of the trust.

l. During the year under review there was no write off to Income & Expenditure account.

m. Tenders were invited for repairs or construction for the expenditure exceeding Rs.5000/-.

n. No money of the public trust has been invested contrary to the provisions of Section 35 of the Bombay Public Trust Act, 1951.

o. No alienations of immovable property are noticed in contrary to the provision of Section 36 of the Bombay Public Trust Act, 1951.

p. In view of the notification no. 51/2009 dated 25.06.2009 as issued by The Central Government, the Income of the Trust is eligible for exemption under Income tax law and hence no provision for income tax has been made in the books of accounts.

For Mukesh M Shah & Co.
Chartered Accountants
Firm Regn. No.106625W

MUKESH M. SHAH & CO. 7, Heritage Chambers, Nehru Nagar, Ambawadi Ahmedabad-15. CHARTERED ACCOUNTANTS

CA Suvrat S Shah
Partner
Membership No.102651
Place: Ahmedabad
Date: 20/09/2018

PHYSICAL RESEARCH LABORATORY

Ahmedabad - 380 009

[Trust Regn. No. E/1371/Ahmedabad]

BALANCE SHEET as at 31st March, 2018

[Vide Schedule - VIII, Rule 17(1) of The Bombay Public Trust (Gujarat) Rules, 1961]

FUNDS & LIABILITIES	₹.	₹.	PROPERTY & ASSETS	₹.	₹.
TRUST FUND CORPUS			IMMOVABLE PROPERTIES		
Grant and contribution	4,63,02,83,135			39,60,52,191	
			Less : Depreciation	14,59,27,867	25,01,24,324
Less : Depreciation	1,78,27,96,964	2,84,74,86,171	MOVABLE PROPERTIES		
			Equipments, Furniture & Fixtures,		
OTHER EARMARKED FUNDS	1,05,63,079		Dead Stock,Vehicles,Books & Journals	3,21,86,88,823	
		1,05,63,079		1,63,68,69,097	
			Less : Depreciation		1,58,18,19,726
RESERVE FUND			INVESTMENTS [AT COST]		
Depreciation Fund	-				36,20,56,173
Any Other Fund	-	-			
			Stock of Stores [At cost]	7,02,899	
LOANS (SECURED OR UNSECURED)			Stock of Medicine [at cost]	54,262	
From Trustees	-		(As per inventory certified		
From Others	-	-	by the management)		7,57,161
			ADVANCES (SECURED)		
PROJECTS BALANCES [GRANTS]	4,21,36,499		Staff members		
		4,21,36,499	Vehicle/Computer Advance (Including		
			accrued interest Rs. 34,943)	3,79,078	
CURRENT LIABILITIES			House Building Advance	1,02,597	4,81,675
For Expenses	1,04,19,769		CASH & BANK BALANCES		21,36,42,189
For Materials & Contracts	2,66,14,542				
Miscellaneous Liabilities	4,28,18,648				
Other Deposits	2,05,50,322				
New Pension Scheme	13,26,959		ADVANCES (UNSECURED)		
CHSS Retired Subscription	40,78,927	10,58,09,168			
			To Employees (including Rs.1,15,304.00	71,58,684	
			More than one year and considered		
			doubtful)		

MUKESH M. SHAH & CO. CHARTERED ACCOUNTANTS 1, Heritage Chambers, Nehru Nagar, Ambawadi Ahmedabad-15

PHYSICAL RESEARCH LABORATORY

Ahmedabad - 380 009

[Trust Regn. No. E/1371/Ahmedabad]

BALANCE SHEET as at 31st March, 2018

[Vide Schedule - VIII, Rule 17(1) of The Bombay Public Trust (Gujarat) Rules, 1961]

FUNDS & LIABILITIES	₹.	₹.	PROPERTY & ASSETS	₹.	₹.
INCOME & EXPENDITURE ACCOUNT			To Contractors & Suppliers	60,34,94,624	
Balance as per last Balance Sheet	6,32,67,390		To Others	3,13,24,207	64,19,77,515
Less : Excess Income over Expenditure for the year	1,09,53,123	7,42,20,513	(including Rs.11059384 as Deposit)		
			ADVANCES (For CIVIL WORKS)		
			To Civil Engineering Division, DOS	55,20,044	
			To Civil Engineering SAC	1,34,69,632	1,89,89,676
			RECEIVABLES		
			Customs Duty Receivable	61,12,187	
			Forex Claim Receivable	1,93,974	
			SBI - ATM Rent Receivable	30,000	
			Block Grant Receivable	70,000	
			Interest Receivables on FDR	39,60,831	1,03,66,992
TOTAL ₹. ->		3,08,02,15,431	TOTAL ₹. ->		3,08,02,15,431

As per our report of even date
Mukesh M. Shah & Co.,
Chartered Accountants
(F.R.N.: 106625W)

MUKESH M. SHAH & CO. ★ 7, Heritage Chambers, Nehru Nagar, Ambawadi Ahmedabad-15. ★ CHARTERED ACCOUNTANTS

CA Suvrat S Shah
Partner
Membership No. 102651

Ahmedabad
Date : 20/09/2018

For, Physical Research Laboratory

Kartikeya V Sarabhai
Trustee
P R L Council

Sanjay S. Lalbhai
Trustee
P R L Council

Ahmedabad
Date : 20/09/2018

PHYSICAL RESEARCH LABORATORY

Ahmedabad - 380 009

[Trust Regn. No. E/1371/Ahmedabad]

INCOME & EXPENDITURE ACCOUNT For the Year ended on 31st March, 2018

[Vide Schedule - IX, Rule 17(1) of The Bombay Public Trust (Gujarat) Rules, 1961]

EXPENDITURE	₹.	₹.	INCOME	₹.	₹.
EXPENDITURE IN RESPECT OF PROPERTIES			RENT (Realised) :		1,638,227
Rates, Taxes & Cesses	3,939,910				
Repairs & Maintenance	22,924,746		**INTEREST (Accrued/Realised) :**		
			On Vehicle/Computer Advance	61,514	
Salaries	-		On Interest (Miscellaneous)	8,812	
Insurance	-		On Interest (NPS Fund)	-	
Depreciation	-		On Bank FDs	21,836,440	21,906,766
Other Expenses	-	26,864,656			
ESTABLISHMENT EXPENSES :					
Remuneration (in case of a Math to the Head of a Math, including his household expenses if any.)		-			
LEGAL EXPENSES :		381,154	**GRANTS**		1,180,090,000
AUDIT FEES :			**INCOME FROM OTHER SOURCES :**		
Statutory Audit Fees		177,000			
Certification Fees		40,120	Miscellaneous Income		
Contribution and fees :	-		(Sale of unserviceable/obselete articles, discarded assets, Insurance Claim)	1,357,167	
AMOUNT WRITTEN OFF :			Income : Miscellaneous	44,084	
(a) Bad Debts & Store	-		(Loss of ID Cards,RTI fee,)		1,401,251
(b) Loan Scholarship	-				
(c) Irrecoverable Rent	-				
(d) Other items	-	-			
(e) Irrecoverable Project Balance	-				

MUKESH M. SHAH & CO. CHARTERED ACCOUNTANTS 7, Heritage Chambers, Nehru Nagar, Ambawadi Ahmedabad-15.

PHYSICAL RESEARCH LABORATORY

Ahmedabad - 380 009

[Trust Regn. No. E/1371/Ahmedabad]

INCOME & EXPENDITURE ACCOUNT For the Year ended on 31st March, 2018

[Vide Schedule - IX, Rule 17(1) of The Bombay Public Trust (Gujarat) Rules, 1961]

EXPENDITURE	₹.	₹.	INCOME	₹.	₹.
			Prior Period Income		
			Other Income (Vehicle, Housing Adv. Int.)	-	
			Other Income (CISF Recovery)	-	-
EXPENDITURE ON OBJECTS OF TRUST :					
Educational & Research		1,155,011,059			
Prior period Expenses		11,609,132			
Excess Income Over Expenditure during the Year : 2017-18		10,953,123			-
	TOTAL ₹	**1,205,036,244**		TOTAL ₹	**1,205,036,244**

As per our report of even date
Mukesh M. Shah & Co.,
Chartered Accountants
(F.R.N.: 106625W)

MUKESH M. SHAH & CO. CHARTERED ACCOUNTANTS 7, Heritage Chambers, Nehru Nagar, Ambawadi Ahmedabad-15.

CA Suvrat S Shah
Partner
Membership No. 102651

Ahmedabad
Date : 20/09/2018

For, Physical Research Laboratory

Kartikeya V Sarabhai
Trustee
P R L Council

Sanjay S. Lalbhai
Trustee
P R L Council

Ahmedabad
Date : 20/09/2018

PHYSICAL RESEARCH LABORATORY
NAVARANGPURA, AHMEDABAD – 380 009

SIGNIFICANT ACCOUNTING POLICIES & NOTES FORMING PART OF ACCOUNTS FOR FINANCIAL YEAR 2017-2018

A. CONSTITUTION

Physical Research Laboratory (PRL) is a Trust registered under The Bombay Public Trust Act, 1950 and engaged in basic sciences research. PRL has not been carrying out any commercial activity.

B. SIGNIFICANT ACCOUNTING POLICY

1. ACCOUNTING METHOD

The trust has been following mercantile system of accounting *except* for the expenditure on retirement benefits since 01.04.2011 as per the recommendations of Comptroller and Auditor General of India and directions of the Department of Space vide letter dated 11.03.2002.

2. RECOGNITION OF INCOME AND EXPENDITURES

In view of specific direction from the donor for the utilization of the `Grant in Aid – Salaries' and ` Grant in Aid General' grants, entire grant is credited to Income & Expenditure Account. The expenditure is also met against the respective object head. The Grant in aid received during the financial year towards any capital component is taken to Corpus Fund for creation of specific Assets to the Balance Sheet; since objective head: Grants for creation of Capital Assets' and acquisition of assets thereto; shown separately in the books of accounts.

3. Fixed Assets

i. Fixed Assets are stated at historical cost of acquisition less accumulated depreciation.

ii. The assets to the extent identified by the Management for disposal are written off against its corpus till 31.03.2010, the amount realized from the sale of such Assets are credited to the Income & Expenditure Account. During the year under review the trust has not written off any assets. However, amount realized from the sale of such assets identified by the Management

MUKESH M. SHAH & CO. CHARTERED ACCOUNTANTS 7, Heritage Chambers, Nehru Nagar, Ambawadi Ahmedabad-15

for disposal has been credited to Income & Expenditure account under the head Miscellaneous Income.

The original cost less depreciation of the Assets sold/discarded is not deducted from the value of Assets and hence the value of Assets is overstated to that extent. Consequently, the profit or loss on disposal of Assets is not accounted.

iii. Books, periodicals and journals including digital journals are capitalized and the same are shown under Movable assets.

iv. Fixed Assets including Equipments are valued at costs which are physically verified by an outside agency appointed by the Management and the same are subject to reconciliation with the Fixed Assets Register. Physical verification of Moveable Assets & Equipments was carried out by a firm of Chartered Accountants up to the year 2013-14. Reconciliation of Fixed Assets physically available with the value as disclosed in the Books of Accounts is not done and consequently loss which would arise due to difference in such values will be provided on ascertaining such loss. Depreciation on such Assets of Immovable and Moveable nature is worked out on the gross value of Assets less accumulated depreciation. Depreciation on individual WDV of each asset is not worked out.

4. Depreciation

i. The trust has worked out depreciation on its fixed assets for the first time in F.Y. 2008-2009 calculating retrospectively with effect from F.Y. 2001-2002, by estimating the same at 90% of opening Book Value of Fixed Assets for F.Y. 2001-2002. Then for the subsequent additions and on the carried forward balances, depreciation is provided on the opening balance of fixed assets at the rates as prescribed under the Income Tax Act, 1961 by way of written down value method. The trust does not work out any depreciation on any additions / deletions in assets during the year.

5. Investments

The trust consistently classifies Fixed Deposits under the head Investments. The fixed deposits are maintained in the custody of Accounts Officer and are physically verified by the Management or its authorized representative(s) periodically.

MUKESH M. SHAH & CO. 7, Heritage Chambers, Nehru Nagar, Ambawadi Ahmadabad-15. CHARTERED ACCOUNTANTS

Surplus out of grants, those of endowment funds are maintained by way of Fixed Deposits and Savings Bank Accounts with Scheduled Banks.

6. Inventories

The stock of consumables and medicines are valued at cost which are physically verified by the Management and reconciled with the Stores records.

The stores item purchased and issued immediately to the department are treated as consumed.

7. Retirement Benefits

Retirement Benefits which include Gratuity, Leave Encashment and Pension are treated as payable in the year in which the retirement of employees takes place.

8. Foreign Currency Transactions

Foreign currency transactions are recorded at the exchange rate prevailing as on the date of the payment. Foreign Exchange fluctuation gain or loss is not booked for the payments outstanding as on 31st March, 2018.

C. Notes to Accounts

1 The trust has not quantified contingent liability in view of impending cases in various Courts.

2 In view of the notification no. 51/2009 dated 25.06.2009 as issued by The Central Government, the income of the trust is eligible for exemption under Income tax Law and hence no provision for income tax has been made in the books of account.

3 Expenditure incurred upto 2014-15 of ₹.13,26,99,700/- on additions/alterations to existing Buildings has not been appropriated to the respective building, but all such expenses have been clubbed under a separate head "Civil works, Additions, Alteration and Extension" shown in the Balance Sheet.

MUKESH M. SHAH & CO.
7, Heritage Chambers, Nehru Nagar, Ambawadi Ahmedabad-15.
CHARTERED ACCOUNTANTS

4 The Depreciation is not charged to the Income & Expenditure account, but it is shown as a deduction from Gross value of Fixed Assets and deduction from Corpus fund in the Balance Sheet. However, no accounting entries are passed for giving effect of such depreciation. The amount of such depreciation for the year current is ₹ 19,75,78,151/- and accumulated balance as on 31st March, 2018 is ₹ 178,27,96,964/-.

5 The registers of stock and inventories are certified by the trustee, maintained and updated on regular basis. Register of stocks for movable properties is maintained for Assets acquired from 01.04.2004 (FY2004-05) which requires to be reconciled with balances as stated in Financial Statements, by making adjustments/ writing off untraceable items. However, register of immovable properties is required to be maintained including adjustment of expenditure stated in Para 3 above.

6 The retirement benefits payable to employees are recognized in the year in which retirement of employees takes place. However, the trust has obtained Actuarial valuation report for the accrued liabilities on account of retirement benefits. Accordingly, the liability is as under:

[As per actuarial valuations as on 31st March, 2018]:

Gratuity	: ₹.	13,42,40,331
Half Pay Leave encashment	: ₹.	1,47,85,680
Earned Leave encashment	: ₹.	11,13,17,115
Pension	: ₹.	2,72,52,41,203
Total	**: ₹.**	**2,98,55,84,329**

However, provision for the same is not made in the books of accounts.

7 Balances stated either Debit or Credit under various advances to staff, deposits, receivables, advances to others and those under sundry creditors are subject to confirmation and reconciliation.

8 Project Leader Imprest comprising of cash and bank balance maintained by the project leader on account of the Trust, is stated under Cash and bank balance.

9 The rental agreement with State Bank of India not firmed up as on date hence rent receivable is not recognized.

MUKESH M. SHAH & CO. CHARTERED ACCOUNTANTS 7, Heritage Chambers, Nehru Nagar, Ambawadi Ahmedabad-15.

10 Advance includes ₹. 61,12,187/- of customs duty receivable for which claim was rejected by the Customs Department and on further appeal made by the management, The Commissioner of Customs (Appeals-II) Mumbai passed order in favour of Trust. The Department went into further appeal, which the Customs, Excise & Service Tax Appellate Tribunal, West Zonal Bench – Mumbai dismissed vide order No. S/93425/16/CB and A/93426/16/CB dated 27.06.2016. The customs filed a petition in honorable High Court of Bombay hence, no provision is made in the books of accounts.

11 A Fire took place in Seminar Hall Building in the year 2011-12 wherein furniture, electrical and Air-condition fixtures and fittings were destroyed. The original cost of item destroyed had not been identified and quantified and hence loss on account of this fire could not be written off.

12 The trust had initiated the new pension scheme as per Government guidelines. Some employees who had left the services hence their individual accounts could not be opened and data/funds could not be transferred to NPS Trust Fund due to lack of guidelines in this regard by PFDRA, New Delhi. The non-transfer of such subscriptions to the NPS trust fund account of PFDRA, balance held by PRL during the current financial year are invested in fixed deposits. The fund of such subscribers returned on formulation of exit policy under NPS.

13 No fraud on or by the trust has been reported or recorded.

14 The trust is consistently not charging common institutional overheads on external projects.

15 The broad classification of expenses incurred and balances of Endowment / Earmarked funds adopted by the management construed as for the purpose of attainment of its objectives.

16 Transactions recorded in the books of accounts are supported by documentary evidences where such documentary evidence is not available; the entries in books of accounts have been taken as relied upon as authenticated by the Management.

MUKESH M. SHAH & CO. CHARTERED ACCOUNTANTS 7, Heritage Chambers, Nehru Nagar, Ambawadi Ahmedabad-15.

17 The accounting for external projects managed by the Trust against specific mandate and funds received on reimbursement basis are segregated with effect from 01.04.2013 and separate books of accounts and bank balances have been maintained. The activities are carried out as per mandate [directions] from the donor agencies and expenditures are met from the funds received from such donor agencies and interest earned from such unspent balance deposited in the bank account. The details of unspent grant of each donor agency and the bank balances are appended as per ***Annexe- 1*** to the notes to accounts.

18 The trust has not received any gifts or donations in kind or equipment on loan basis during the year under review as reported by the Management.

19 The current Liabilities include a balance amounting to ₹.27,36,045 in Gift under Will and its Codicil of Late Dr.Devendra Radhekrishna Lal Bank Savings bank account: Pension, NRI and PPF accounts shown in PRL's bank account. In addition, a Bungalow located in 20 Jayantilal Park, Makarba, Ahmedabad is also to be received under WILL for which application was made to the concerned revenue authorities on 09 May 2013. The property is transferred in the name of Council including power and municipal tax records. The transactions shall be accounted for on getting valuations by an approved valuer for the said property in favour of Physical Research Laboratory, Ahmedabad.

20 The loss due to carry forward deficit of ₹.1,64,31,122/- of PRL Employees Provident Fund shall be accounted for on getting approval from Department of Space/Ministry of Finance for permission to write off and one time grant to be met the deficit. The grant amount as projected in the budget estimates amounting to ₹.1,69,00,000/- and claimed, funds have been received and kept as a separate TDR/FDR including Interest of ₹ 25,44,730/- pending decision/approval in this regard by the Government. The Grant amount of Rs. 1,69,00,000/- received was erroneously credited to the grant income in the Income & Expenditure Account for the financial year 2015-16 which is now transferred to liability account by debiting to PF Contribution expenses for this year and shown under Current Liability.

MUKESH M. SHAH & CO. CHARTERED ACCOUNTANTS 7, Heritage Chambers, Nehru Nagar, Ambawadi Ahmedabad-15.

21 The commitments for Purchase, both local and foreign and Works as at 31/03/2018 are as below :

Purchase Commitment:

Consumables	: ₹.	10,64,37,073
Equipments	: ₹.	5,19,54,230

Stores Commitment:

Consumables	: ₹	1,31,99,671
Equipment	: ₹	2,11,64,708

Works Commitment:

Repairs and Maintenance	: ₹	Nil
Capital works	: ₹	Nil

22 The following accounts heads include certain old outstanding debit (for more than one year) and credit balances (for more than one year) which need to be reconciled, adjusted or written off, as per Generally Accepted Accounting Principles (GAAP) by the management:

Accounts Head	Debit Balances		Credit Balances	
	No. of Accounts	Amounts (₹)	No. of Accounts	Amounts (₹)
Suppliers and Contractors	71	1,84,53,383	68	93,62,590
Travelling Advance	78	4,74,673	125	4,99,546
Staff Advance	59	87,238	41	1,26,828

Mukesh M. Shah & Co.
Chartered Accountants
(F.R.N.: 106625W)

MUKESH M. SHAH & CO. 7, Heritage Chambers, Nehru Nagar, Ambawadi Ahmedabad-15. CHARTERED ACCOUNTANTS

CA Suvrat S Shah
Partner
Membership No.102651

For Physical Research Laboratory

Kartikeya V Sarabhai
Trustee

Sanjay S. Lalbhai
Trustee

Place: Ahmedabad
Dated: 20/09/2018

PHYSICAL RESEARCH LABORATORY Ahmedabad- 380009

Annexe-1 to Note to Accounts - Project Balances [Liabilities] and Bank balances and other Assets.

2017-18

Account	Opening Balance of Grant as per Books	Additions		Deduction	Project Closed & balance Amount refunded	Closing Balance	Bank Balances
		Grants Received	Interest	Exp. During the year			
2108 DOS PLANT SCIENCE GRANT	10,67,283	68,34,000	1,35,416	37,63,589	-	42,73,110	42,74,213
4900 ISROGBP AABB GRANT	82,05,197	-	3,32,237	-	-	85,37,434	85,37,434
5400 CSSTE AP M. TECH SAS-9 GRANT	1,02,504	18,28,773	25,653	18,81,603	-	75,327	7,01,481
7100 ISRO MLLIT GRANT	74,463	-	2,832	-	-	77,295	77,295
7300 ISRO GBP-PRCCD/QMPPMR GRANT	28,15,994	-	1,13,220	-	-	29,29,214	29,00,519
7360 ISROGBP MCNC Fund	42,02,903	-	1,80,974	37,96,876	-	5,87,001	43,71,989
7350 ISROGBP PRS Fund	23,56,324	-	2,03,716	2,61,533	-	22,98,507	23,76,206
7460 ISRO GBP ARFI Grant	1,35,494	-	7,843	-	-	1,43,337	1,13,432
7870 MoES TEI in Indian Ocean Fund -SKS	1,85,48,178	-	6,65,204	45,31,393	-	1,46,81,989	1,24,48,409
7880 DST SDR - JC Bose Fellowship Grant	10,56,631	9,00,000	59,211	5,60,747	-	14,55,095	14,62,410
7891 ASJ - JC Bose Fellowship Grant	8,45,337	-	33,486	25,410	-	8,53,413	8,53,413
7901 DSL - JC Bose Fellowship Grant	9,96,055	-	35,378	88,079	9,07,976	35,378	35,378
7910 JNG - JC Bose Fellowship Grant	2,58,099	-	14,570	5,25,404	-	(2,52,735)	(56,542)
7920 AKS - JC Bose Fellowship Grant	7,72,271	-	25,177	3,14,151	-	4,83,297	4,53,166
7940 MMS -JC Bose Fellowship Grant	11,18,720	-	38,832	4,24,019	-	7,33,533	7,33,533
7950 NASI - Fellowship Grant	3,01,471	1,58,529	10,386	3,60,000	-	1,10,386	1,28,386
7956 SERB-Women Excellence Award Grant - KKM	-1,35,547	-	68	-	-	(1,35,479)	5,040
8450 Planex Chandrayaan II Payload Grant	99,49,830	-	3,97,965	-	-	1,03,47,795	1,02,21,999
8460 PLANEX - Ch-2 Devl/Experimental Fund	1,15,42,309	-	4,70,704	1,696	-	1,20,11,317	1,20,11,317
8470 Ch2 XSM Fund	1,72,19,817	-	7,16,057	33,73,767	-	1,45,62,107	1,45,45,875
8480 Ch2 APXS Fund	3,56,43,315	-	17,55,662	44,284	-	3,73,54,693	3,32,70,338
8570 MoES Annamox in NLAS Fund	7,37,392	-	28,038	-	-	7,65,430	7,65,430
8580 MoES POCEF from UAS-BoB Fund	-7,51,560	-	20	0	-	(7,51,540)	552
8590 MoES- TEINIO from UAS-BoB Fund	-65,535	-	1,443	1,90,315	-	(2,54,407)	2,481
8645 Grant from LEOS for SPROC facility at PRL(Mt. ABU)	-60,224	9,92,407	6,492	4,73,039	-	4,65,636	6,48,020
9101 ISRO AT-CTM GRANT	1,93,70,870	3,02,00,000.00	8,68,090	3,02,00,000	-	2,02,38,960	2,02,47,552
9100 ISRO GBP TCG Grant	85,14,894	-	3,48,631	36,75,607	-	51,87,918	67,05,833
9760 SAC_Study of Moon and Mars Analogues Fund	4,67,586	-	18,016	3,18,577	-	1,67,025	2,13,181
3217 INSA Grant/fellowship-MMS	41,410	4,18,590	2,280	4,09,882	-	52,398	1,40,016
7970 DST-INSPIRE Grant DBS	7,05,468	-	27,750	-	-	7,33,218	7,37,218
8481 ASPEX Projects Fund	99,30,543	7,90,00,000	30,51,962	55,45,397	-	8,64,37,108	8,59,56,229
8586 INSA Grant/Fellowship-DSL	96,377	3,58,426	3,983	4,39,989	-	18,797	18,821
9200 Raja Ramana Fellowship-AKS-Grant	1,58,744	-	2,469	1,20,000	-	41,213	41,213
9220 NAM S&T RTF-DCS Scheme Grant	1,65,903	-	2,503	1,27,279	-	41,127	41,127
7990 SAH - JC Bose Fellowship Grant	4,61,607	-	4,885	11,12,770	-	(6,46,278)	18,980
9210 Raja Ramana Fellowship- ASJ- Grant	2,59,770	-	3,998	2,40,000	-	23,768	23,768
8000 Onset of Solar Flares - Indo - Austrian Project	-	4,56,500	7,090	2,21,954	-	2,41,636	2,41,636
8010 DST-INSPIRE Grant DSR	-	19,00,000	4,008	0	-	19,04,008	19,04,008
SUB- TOTAL (A) ₹	**15,71,09,893**	**12,30,47,225**	**96,06,249**	**6,30,27,360**	**9,07,976**	**22,58,28,031**	**22,71,71,356**

MUKESH M. SHAH & CO. ★ CHARTERED ACCOUNTANTS ★
7, Heritage Chambers, Nehru Nagar, Ambawadi Ahmedabad-15.

2017-18

Account	Opening Balance	Additions		Deduction	Project Closed & balance Amount refunded	Closing Balance	Bank Balances
		Grants Received	Interest	Exp. During the year			
Receivable From PRL							
ISRO GBP ARFI	34,481	-	-	-	-	34,481	
ISRO GBP PRCCD/QMPPR	33,695	-	-	-	-	33,695	
ISROGBP PRS (MGY)	1,55,062	-	-	-	-	1,55,062	
DST JC BOSE FELLOWSJIP DSL	12,050	-	-	-	-	12,050	
CH2 APXS	40,75,156	-	-	44,284	-	40,30,872	
ASPEX - ADITYA L1	-	-	-	-	-	5,14,889	
MoES TEI in Indian Ocean [SKS]	41,54,868	-	-	24,51,115	-	17,03,753	
LEOS/SPROC	4,00,000	4,00,000	-	-	-	-	
SUB- TOTAL (1) ₹	88,65,312	4,00,000	-	24,95,399	-	64,84,802	-
Payable to PRL							
CH2 XSM	11,68,541	8,08,117	-	20,07,587		(30,929)	
CSSTE-AP Dehradun	-	-	-	-	-	(6,62,145)	
DST JC Bose Fellowship - JNG		-	-	-	-	(2,21,213)	
DST JC Bose Fellowship - SAH	-	-	-	-	-	(6,65,258)	
DST JC Bose Fellowship - SDR	-	-	-	-	-	(7,315)	
ISROGBP MCNC [957]	(1,77,240)	-	-	36,30,079	-	(38,07,319)	
ISROGBP PRS (MGY)	28,772	-	-	2,61,533	-	(2,32,761)	
SB WEA KMK	(2,35,756)	-	-	-	-	(2,35,756)	
MoES- TEINIO from UAS-BoB (Dr.Ravi Bhushan)	(1,48,440)	-	-	1,90,315	-	(3,38,755)	
SAC_Study of Moon & Mars Analogues Fund	-	-	-	-	-	(46,156)	
ISRO GBP TCG	(3,524)			15,56,080		(15,59,604)	
MoES POCEF from UAS-BoB	(2,64,114)	-	-	-	-	(2,64,114)	
SUB- TOTAL (2) ₹	3,68,239.00	8,85,277.00	-	76,32,764.00	-	(80,71,325.00)	
Net Payable to PRL [1-2] (B) ₹	(84,97,073.00)					(15,86,523.00)	
Liability							
Liability for expenses						9,958	
IT on Contractor and Prof. Services & LWS-3208/3270/3277						2,31,714	
Electricity Charges						6,000	
Misc. Liability - Labour Welfare & Proj control account						50,157	
Security Deposits- M/s HEC Infra Projects						4,56,686	
Advance to staff & cliam receivable						-	9,97,713
SUB- TOTAL (C) ₹	99,70,029	25,70,554	-	2,02,56,326	-	7,54,515	9,97,713
Capital Expenditure							
Project Grant received for acquisation of Capital Asset						-	
Assets acquired from the Capital Grant for Projects							-
SUB- TOTAL (D) ₹						-	-
GRAND TOTAL (A+B+C+D) ₹	15,85,82,849	12,56,17,779	96,06,249	7,96,53,607	9,07,976	22,81,69,069	22,81,69,069

MUKESH M. SHAH & CO. CHARTERED ACCOUNTANTS 7, Heritage Chambers, Nehru Nagar, Ambawadi Ahmedabad-15.




पी.आर.एल. में गतिविधियां
Events at PRL

















पी.आर.एल. में गतिविधियां
Events at PRL






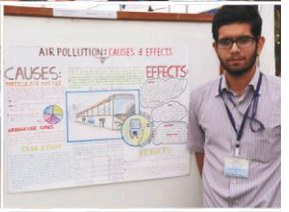











पी.आर.एल. में गतिविधियां
Events at PRL
Narendra Modi
Following
Immensely proud of our scientists, who created history by discovering a sub-Saturn size planet 600 light years away from the Earth. Congratulations to them. The discovery puts India among select countries. isro.gov.in /discovery-of-s ...
PRL RESERVED CLASS EMPLOYEES ASSOCIATION
भौतिक अनुसंधान प्रयोगशाला, अहमदाबाद
हिन्दी पखवाड़ा समारोह

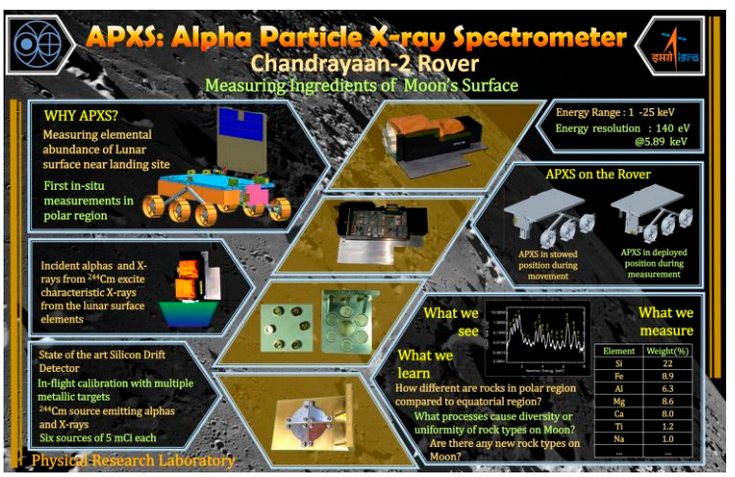

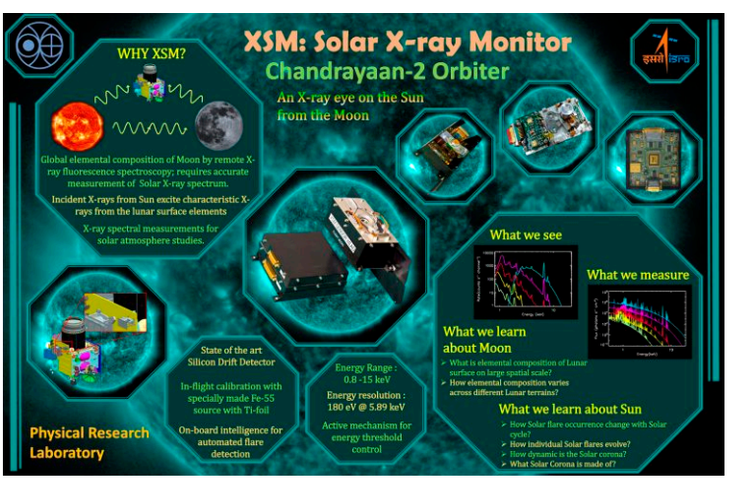

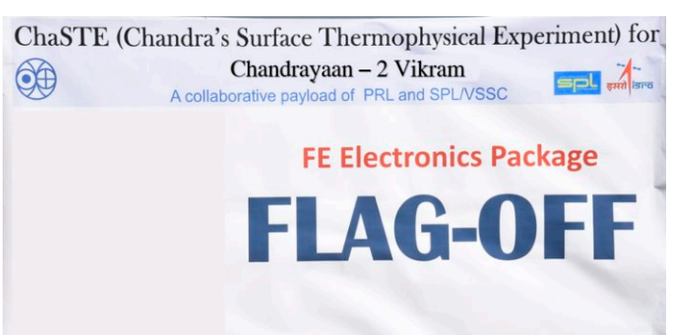

"Scientists who have relied on the experimental method and the powerful tool of observation, have a particularly valuable contribution to make in providing education through the acquisition of insights by experience rather than by hearing or reading."

-Dr. Vikram A. Sarabhai